This electronic thesis or dissertation has been downloaded from the King's Research Portal at https://kclpure.kcl.ac.uk/portal/

A Mesenchymal Stem Cell (MSC) Niche in Mouse Incisor

Wang, Longlong

Awarding institution:
King's College London

The copyright of this thesis rests with the author and no quotation from it or information derived from it may be published without proper acknowledgement.

END USER LICENCE AGREEMENT

Unless another licence is stated on the immediately following page this work is licensed under a Creative Commons Attribution-NonCommercial-NoDerivatives 4.0 International licence. https://creativecommons.org/licenses/by-nc-nd/4.0/

You are free to copy, distribute and transmit the work

Under the following conditions:

- Attribution: You must attribute the work in the manner specified by the author (but not in any way that suggests that they endorse you or your use of the work).
- Non Commercial: You may not use this work for commercial purposes.
- No Derivative Works - You may not alter, transform, or build upon this work.

Any of these conditions can be waived if you receive permission from the author. Your fair dealings and other rights are in no way affected by the above.

Take down policy

If you believe that this document breaches copyright please contact librarypure@kcl.ac.uk providing details, and we will remove access to the work immediately and investigate your claim.

Download date: 30. Dec. 2024

A Mesenchymal Stem Cell (MSC) Niche in Mouse Incisor

Longlong Wang

A Thesis Submitted for the Degree of Doctor of Philosophy at the University of London

2015

Department of Craniofacial Development and Stem Cell Biology
Dental Institute

King's College London

Abstract

Mesenchymal stem cells (MSCs) are heterogeneous cell populations that are identified by their *in vitro* characteristics while their biological properties and *in vivo* identities are often less understood. Different from human teeth, mouse incisors grow and erupt continuously throughout their lives and compensate for daily abrasions with the existence of stem cells. However, the precise location of the mesenchymal stem cells (MSCs) in the incisor is unclear. Generally, the MSCs in the mouse incisor are believed to be located in the mesenchyme close to the epithelium cervical loops, since the growth and differentiation of the incisor always initiates at the apical end and extends towards the incisal end.

The utilization of label-retaining experiments and transgenic reporter mouse lines has enabled further understanding of the less established identities and properties of dental pulp stem cells *in vivo*. The work described in this thesis demonstrates that the mesenchymal stem cell niche located at the apical end of mouse incisor contains three distinct but connected cell populations: 1) a slow cycling cell population containing Thy-1+ cells essential for tooth dental pulp and odontoblast formation 2) a *Ring1/Bcor*-associated fast cycling cell population crucial for maintaining tissue growth and homeostasis of epithelium stem cells in labial cervical loop 3) a quiescent long-term cell population marked by Flamingo homologue Celsr1 might respond to generate new stem cells when the stem cells become depleted.

Acknowledgements

I would like to express my sincere gratitude to my supervisor, **Professor Paul Sharpe**, for his patience, vast knowledge, practical suggestions and help for the project. I am highly grateful to my second supervisor, **Professor Agi Grigoriadis** for his kind assistance throughout my study.

I am immensely grateful for **Zhengwen An** for her detailed and constructive comments in the preparation of this thesis. I also wish to thank **Yvonne Peng** for her valuable feedback during the writing of this thesis. Special thanks go to **Christopher Healy** for providing technical support throughout my work in CFD. Sincere thanks go to **Val Yianni, Liu Yang** and **Babb Rebecca f**or their help in writing my thesis, as well as their continuous support and encouragement throughout my PhD project.

A word of gratitude is extended to all former and current CFD2 members: **Tian Yu, Atsushi, Miko, Katsu, Mona, Doris, Maja, Jifan** and many more people in CFD; all of them have taken part in my inquires at various stages/times. Special thanks go to **Simone** and **Lucyene** from Brazil for being such wonderful companions in laboratory and coffee time as well. My warm thanks are also extended to **Angela, Rebecca, Alex** and **Martin** for their kind assistance whenever I needed it.

I am forever indebted to my parents for their patience and constant support throughout my study abroad in the UK.

The financial support from **KING'S COLLEGE LONDON** is also gratefully acknowledged.

Table of contents

List of Figures

List of Tables

List of Abbreviations

aa	Amino acid
am	Ameloblasts
Alk5	Activin A receptor type II-like kinase
APC	Allophycocyanin
ASCs	Adult stem cells
BCIP	5-Bromo-4-chloro-3-indolyl-phosphate
Bcl-6	B-cell CLL/lymphoma 6
Bcor	Bcl-6 interacting corepressor
BMMSCs	Bone marrow-derived mesenchymal stem cells
BMPs	Bone morphogenetic proteins
BrdU	5-bromo-2'-deoxyuridine
CldU	Chlorodeoxyuridine
CL	Cervical Loop
c-Myc	C-myc myelocytomatosis viral oncogene homolog
CNC	Cranial neural crest
CNPase	Cyclic nucleotide 3'phosphohydrolase
CNS	Central nervous system
Crabp-1	Cellular Retinoid Acid Binding Protein-1
DAB	3,3'-Diaminobenzidine tetrahydrochloride
DTT	DL-Dithiothreitol

de	Dentin
DEPC	Diethyl pyrocarbonate
df	Dental follicle
DFPCs	Dental follicle progenitor stem cells
DIG	Digoxigenin
Dil	1,1'-dioctadecyl-3,3,3',3'-tetramethylindocarbocyanine perchlorate
Dkk1	Dicckopf-related protein 1
DMSO	Dimethyl sulfoxide
dp	Dental pulp
DPBS	Dulbecco's Phosphate Buffered Saline
DPSCs	Dental pulp stem cells
DSCs	Dental stem cells
Dspp	Dentin sialophosphoprotein
EDTA	Ethylenediaminetetraacetic acid
EdU	5-ethynyl-2'-deoxyuridine
eGFP	Enhanced Green Fluorescent Protein
ena	Enamel
eo	Enamel organ
ER	Estrogen Receptor
ERM	Epithelial cell rests of Mallassez
ES	Embryonic Stem cells
FACS	Fluorescence activated cell sorting

FBS	Fetal Bovine Serum
FGFs	Fibroblast growth factors
FITC	FluoresceinIsothiocyanate
FM	Follicle mesenchyme
GAD	Glutamic acid decarboxylase
GFAP	Glial fibrillary acidic protein
GFP	Green fluorescent protein
Gli	Glioblastoma
H&E	Hematoxylin and eosin
HERS	Hertwig's epithelial root sheath
ICH	Immunohistochemistry
IDE	Inner dental epithelium
IdU	Iododeoxyuridine
IL	Interleukin
iPS	Induced pluripotent stem cells
ISCT	International Society for Cellular Therapy
ISH	In situ hybridization
Klf4	Krueppel-like factor 4
LB	Luria-Bertani
LRC	Label-retaining cells
Micro-CT	Micro Computerised Tomography
MSCs	Mesenchymal stem cells

NBT	4-Nitro blue tetrazolium chloride
NF	Neurofilament
NFM	Neurofilament-M
NG2	Neural/Glial Antigen 2
NSCs	Neural stem cells
O/N	Overnight
O.C.T	O.C.T. compound
OCT3/4	Octamer-binding transcription factor ¾
od	Odontoblast
ODE	Outer dental epithelium
oe	Oral epithelium
OFCD	Oculofaciocardiodental
OHT	4-hydroxy tamoxifen
OPT	Optical Projection Tomography
Pax9	Paired box gene 9
PBS	Phosphate buffered saline
PcG	Polycomb group
PCGFs	Polycomb group RING fingers
PDGERβ	Platelet-derived growth factor receptor-beta
PDL	Periodontal ligament
PDLSCs	Periodontal ligament stem cells
PE	Phycoerythrin

PFA	Paraformaldehyde
PH3	Phospho-Histone H3
PM	Papilla mesenchyme
PN	Postnatal
PRC	Polycomb Repressive Complex
Ptc-1	Patched-1
R26	Rosa26
Rcf	Relative centrifugal force
RLT	RNeasyLysis buffer
RYBP	Ring1 YY1-binding protein
SCAP	Stem cells from apical papilla
SDS	Sodium dodecyl sulphate
SHED	Stem cells from human exfoliated deciduous teeth
Shh	Sonic hedgehog
Smo	Smoothened
Sox2	SRY (sex determining region Y) -box 2
SR	stellate reticulum
SRY	Sex determining region Y
SSEA-3	Specific embryonic antigen-3
TA	Transit amplifying
TEA	Triethanolamine
TGF-β	Transforming growth factorß

THN	tetrahydronaphthalene
αSMA	Alpha-smooth muscle actin

Chapter 1 : Introduction

1.1 Stem cells

As a repair system in the body and means of replenishing tissues, stem cells are an undifferentiated cell type, distinguished by their ability to self-propagate and differentiate into other cell types. In both murine and human research, two types of stem cells have been defined according to the stages of their development. Embryonic stem (ES) cells are isolated from the blastocyst stage of early mammalian embryos; multiple studies (Evans and Kaufman, 1981, Martin, 1981, Thomson et al., 1998) have characterised the ability of these cells to differentiate into any cell type *in vivo.* Adult stem cells (ASCs), also known as somatic stem cells, are distributed throughout the body to replenish damaged tissue and facilitate regeneration. More recently, however, a novel class of stem cells "Induced" pluripotent stem (iPS) has been described (Takahashi and Yamanaka, 2006, Takahashi et al., 2007). iPS are derived from differentiated cells which have been transformed into an ES-like cell line by expressing four transcription factor genes encoding octamer-binding transcription factor 3/4 (Oct3/4); SRY (sex determining region Y) -box 2 (Sox2); Krueppel-like factor 4 (Klf 4); and c-mycmyelocytomatosis viral oncogene homolog (c-Myc). Stem cells can be grouped into five types, depending upon their potential to differentiate into a given lineage. Totipotent cells are capable of dividing and forming various differentiated cells; a zygote is an example of a totipotent cell that can develop into a

new organism. Pluripotent stem cells have the ability to differentiate into all cell types of the three germ layers, i.e., the ectoderm (nervous system and epidermis), mesoderm (connective tissue, muscle, bone and circulatory systems), or endoderm (respiratory and digestive tracts). Stem cells that demonstrate a selective pattern of differentiation toward few lineages are termed multipotent cells; an example is hematopoietic stem cells, which can develop into various types of blood cells such as monocytes or lymphocytes. Oligopotent stem cells are also able to differentiate into certain cell types of specific lineages, such as lymphoid stem cells that can form B and T cells, or other blood cell types. Finally, unipotent stem cells can only differentiate into one particular cell type (Fig. 1.1, Fig. 1.2).

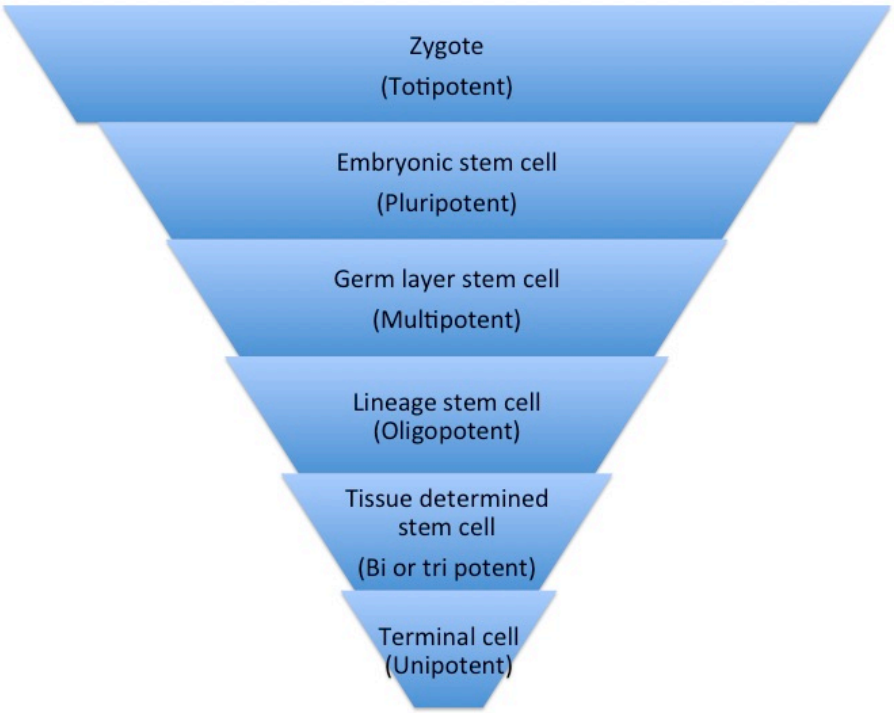

Fig 1. 1: Stem cell hierarchy during the differentiation process.

Differentiation potential decreases and specialisation increases at each stage of the differentiation process.

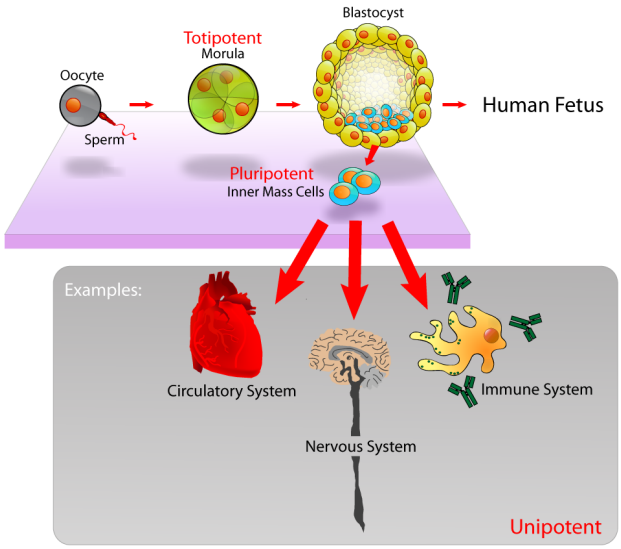

Fig 1. 2: Schematic of stem cell differentiation potential.

Pluripotent stem cells derived from blastocyst inner mass cells can differentiate into all three germ layers. Adapted from (Jones et al., 2007).

1.1.1 Embryonic stem (ES) cells

First described by Evans and Kaufman in 1981, ES cells originate in the inner cell mass of the blastocyst stage of early mammalian embryos (Evans and Kaufman, 1981). Although variations in growth characteristics, doubling time, cell surface markers, signaling pathways and cultivation conditions are observed across different species, all ES cells are pluripotent (Yamanaka et al., 2008). In mice, ES cells can give rise to a fully viable embryo, with all cell types represented. Produced at the blastocyst embryonic stage (achieved at 4-5 days post-fertilisation) that consists of between 50 and 150 cells, human ES cells are distinguished by their unrestricted scope for *in vitro* proliferation and differentiation. ES cell lines have been reported to propagate all other embryonic multipotent and unipotent stem cells, thus giving rise to

all three embryonic germ layers (Wobus and Boheler, 2005). Certain safety concerns, however, such as immunocompatibility and potential tumourigenicity as well as complex ethical and legal issues have significantly restricted the further application of ES cells (Salibian et al., 2013).

1.1.2 Adult stem cells (ASCs)

Isolated from differentiated cells in an adult tissue or organ, ASCs are undifferentiated cells that can self-renew and further differentiate to produce all of the cell types of the tissue of origin. Regeneration of damaged tissues and the replenishment of cells to maintain cell quantity, along with their differentiation into several distinct cell types, appear to be the major functions of adult stem cells in human tissues. Given that they are derived from adult tissues and possess the ability to differentiate into multiple cell types, ASCs can be applied to research purposes without the ethical and technical limitations related to ES cells. Researchers have documented multiple sources of ASCs, including stromal cells from adult skin and bone marrow and adipose tissue-derived stem cells from fat sources (Al-Nbaheen et al., 2013). As demonstrated by a study in 2013, ASCs are readily isolated from adult tissues and their ability to differentiate into more than one cell type along with the potential they offer for autologous stem cell donation has rendered ASCs an important factor in regenerative medicine (Salibian et al., 2013). Although they circumvent many of the limitations of ES cell research, ASCs develop into a narrow range of cell types and are thus restricted by the cell lineage from which they derive.

1.1.3 Induced pluripotent stem (iPS) cells

As described by Takahashi et al. (2006, 2007), ASCs can, under *in vitro* reprogramming, produce iPS cells. The introduction into ASCs of four key transcription factors Oct3/4, Sox2, Klf 4 and c-Myc, causes the cells to reprogram themselves into pluripotent stem cells. Initially described in murine cell lines, a similar transformation was performed in human fibroblasts using the retroviral delivery of Oct3/4, Sox2, Klf4 and c-Myc, the first instance of the production of iPS cells from adult human cells (Yamanaka, 2007). A similar outcome was subsequently obtained by the use of lentiviral transduction to deliver Oct4, Nanog, Sox2 and Lin28 (Yu et al., 2007). The production of iPS cells circumvents the need for embryonic destruction, given that they are isolated from developed tissue sources. Furthermore, iPS cells are derived from individual adult tissues and therefore offer the opportunity for application to personalized therapies. As argued by several researchers, however, the application of iPS cells for therapeutic transplantation purposes is limited by the use of retroviruses in their production, given the risk of mutations being inserted in the target cell. Furthermore, several of the reprogramming factors utilised in the process are oncogenes with an inherent potential tumourigenicity. However, the unrestricted availability of autologous cells holds great potential for future therapeutic transplants without the risk of immune rejection (Marion et al., 2009, Selvaraj et al., 2010).

1.1.4 Mesenchymal stem cells (MSCs)

Initially isolated from bone marrow, as ASCs, MSCs are clonal, plastic-adherent and capable of *in vivo* differentiation into cell types such as osteoblasts, adipocytes and chondrocytes (Friedenstein, 1976). Other tissues are also viable sources of MSCs, such as cord blood (Erices et al., 2000), peripheral blood (Zvaifler et al., 2000), adipose tissue (Zuk et al., 2002), amniotic fluid (In 't Anker et al., 2003), compact bone (Guo et al., 2006), articular cartilage (Dowthwaite et al., 2004), foetal tissue (Miao et al., 2006) and lung tissue (Sinclair et al., 2013). The term, 'MSCs' is therefore no longer appropriate, given the range of tissue types from which these cells have since been isolated. Although these cells types continue to be referred to as MSCs, 'multipotent stromal cells' is a more accurate description. The "International Society for Cellular Therapy" (ISCT) has proposed a set of minimal criteria in order to define MSCs. Firstly, MSCs must be plastic-adherent with a fibroblast-like morphology when maintained in standard culture conditions. Secondly, MSCs must express CD105, CD73 and CD90, but not CD45, CD34, CD14 or CD11b, CD79a or CD19 and HLA-DR surface molecules. Finally, MSCs must be capable of differentiating to osteoblasts, adipocytes and chondroblasts *in vitro* (Dominici et al., 2006).

MSCs' multipotency has been well described in the literature, with research describing the differentiation of these cells into cell types such as osteoblasts, adipocytes, chondrocytes and myocytes. Neuron-like cells have also been shown to derive from MSCs, but further research is required to verify the functionality of these

differentiated cells (Jiang et al., 2002, Birbrair et al., 2011). This multipotency exists alongside the ability of MSCs to replenish their population. Variations in the levels of differentiation of cultures MSCs have been observed between individuals and the process has also been shown to depend on the method used to initiate the differentiation process. Further work is required to determine whether these variations derive from differences in progenitor cell levels, or from variations in the inherent capacity for differentiation displayed by a specific progenitor.

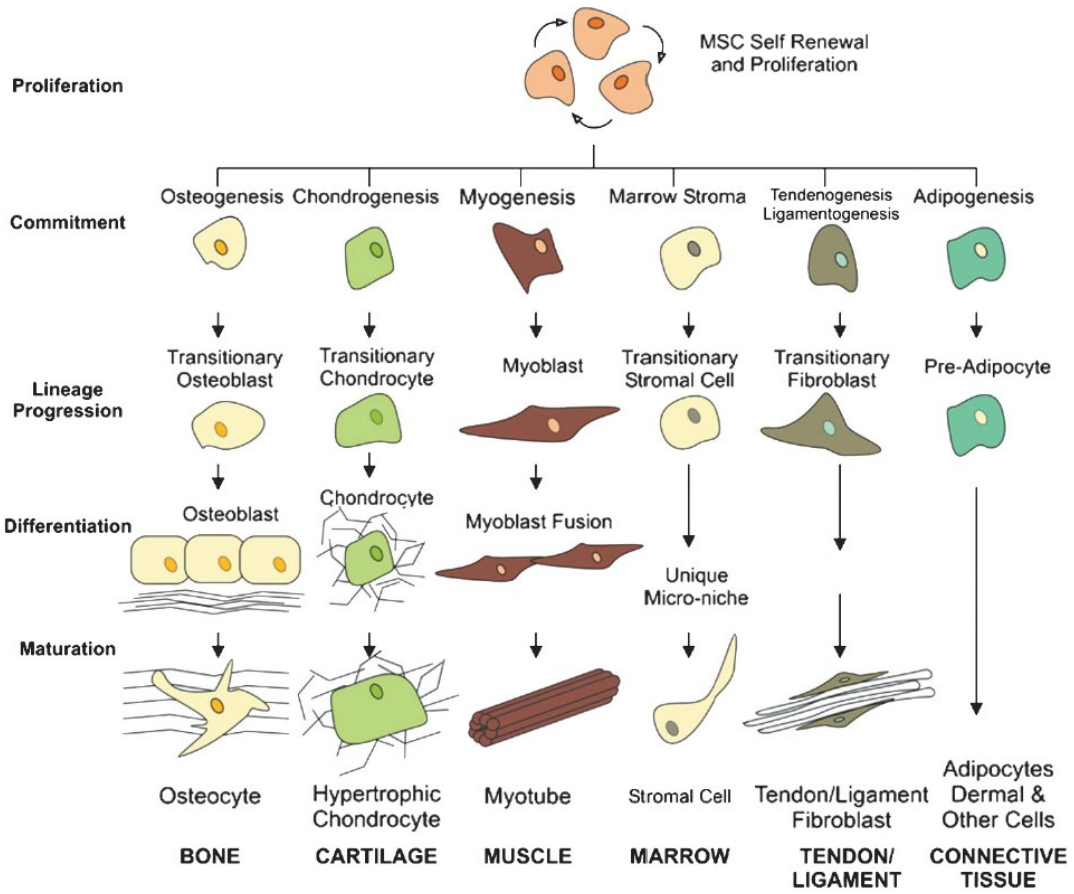

Fig 1. 3: Schematic of MSC differentiation.

Mesenchymal stem cell can differentiate into osteoblasts, chondrocytes, myocytes, marrow stroma cells and tendogenesis cells, which subsequently form bone, cartilage, muscle, marrow and tendon (Firth and Yuan, 2012).

The therapeutic use of MSCs for transplantation benefits from the lack of allogeneic rejection observed in both human and animal studies. This observation can be attributed to three factors, as demonstrated by co-culture experiments *in vitro*. Firstly, MSCs often lack MHC-II and co-stimulatory molecule expression. Secondly, MSCs are capable of indirectly inhibiting T cell responses through modulation of dendritic cells and directly by suppressing the natural killer cell response in addition to the activity of CD8+ and CD4+ T cells. Finally, a study has shown that MSCs produce immunosuppressive conditions through the local upregulation of prostaglandin and interleukin-10 production, in addition to the production of indoleamine 2, 3, dioxygenase which suppresses immune responses by depleting local tryptophan (Ryan et al., 2005). This research also demonstrated that the activity of local inflammatory factors such as interferon-gamma can contribute to the immunomodulatory function of MSCs. However, research on the potential mechanisms by which MSCs exert their immunosuppressive effects is largely restricted to *in vitro* studies; further evidence *in vivo* is thus required.

1.2 Adult stem cell niches

ASCs serving as a reservoir of new cells for tissue growth and repair are located among differentiated cells but maintained in 'niches' (Schofield, 1978). Stem cells within these dynamic microenvironments are capable of balancing homeostasis between quiescent and active states of differentiation (Greco and Guo, 2010, Voog and Jones, 2010). Unnecessary proliferation of stem cells is prevented when ASCs are

maintained within niches and the cells themselves are also protected from depletion. An essential component of the stem cell niche is stem cell. However, the presence alone of stem cells is not the only factor required when characterising niches as demonstrated in 2006, both anatomic and functional components are required in a stem cell niche (Scadden, 2006). Well-characterised niches have been shown to exist in locations such as the bone marrow, small intestinal crypts and hair follicle bulges (Kordes and Haussinger, 2013). These tissues are all characterized by substantial cell turnover, facilitating the detection of stem cell activity due to the continuous supply of cells. In studies on the mouse incisor, the permanent proliferating cells of the tooth organ indicate the presence of stem cells. Murine dental pulp has been shown to contain two forms of stem cells, epithelial stem cells that differentiate to ameloblasts (enamel producing cells) and MSCs that give rise to odontoblasts (dentine forming cells) (Seidel et al., 2010).

1.3 Dental stem cells (DSCs)

DSCs from the tooth, one of the many types of ASCs, have potential in applications such as tissue engineering and regenerative medicine as a result of their capacity for multipotent differentiation. There are two main benefits of using DSCs over other types of ASCs. Firstly, DSCs are more readily available in that they can be obtained in routine clinical practice from both permanent (Gronthos et al., 2000, Arthur et al., 2009) and human exfoliated deciduous teeth (SHEDs) (Miura et al., 2003). They are easily cultivated and can be stored without adverse functional effects (Papaccio et al.,

2006). Secondly, the neural crest cells, responsible for producing neurons, contribute a large portion of a tooth (including dental pulp) (Huang et al., 2008a, Chai et al., 2000) and give rise to DSCs; the DSCs have a potential to form neurons. This suggestes a possible therapeutic use of DSCs in neurodegenerative disorders such as Alzheimer's disease, Parkinson's disease and amyotrophic lateral sclerosis (Kanafi et al., 2014). To date, researchers have described several types of stem cells identified in the tooth, such as dental pulp stem cells (DPSCs) (Gronthos et al., 2000), stem cells from human exfoliated deciduous tooth (SHEDs) (Miura et al., 2003), periodontal ligament stem cells (PDLSCs) (Seo et al., 2004), dental follicle progenitor stem cells (DFPCs) (Morsczeck et al., 2005) and stem cells derived from the apical papilla (SCAPs) (Sonoyama et al., 2008).

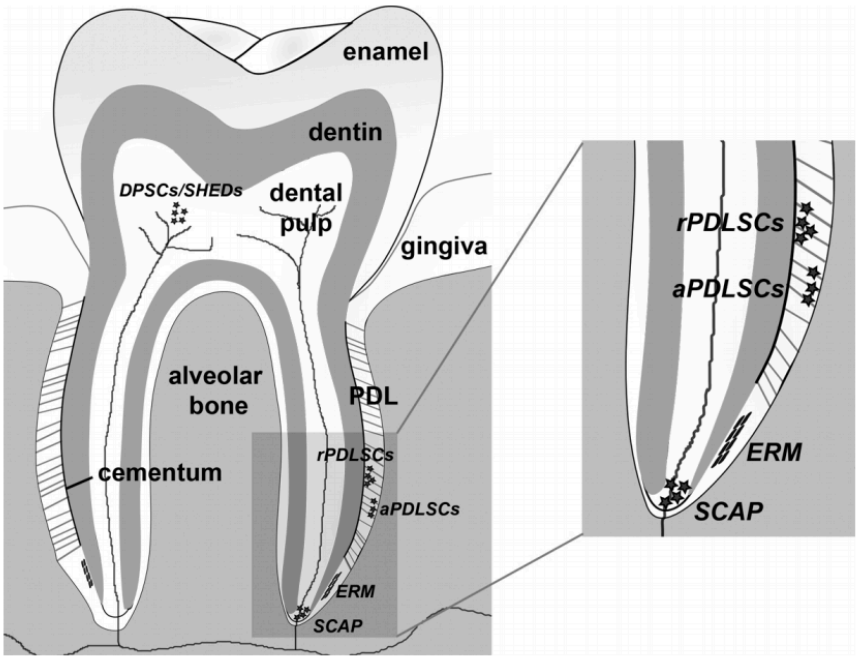

Fig 1. 4: Stem cell niches located in the adult human tooth.

Abbreviations: aPDLSCs, alveolar periodontal ligament stem cells; DPSCs, dental pulp stem cells; ERM, epithelial cell rests of Mallassez; PDL, periodontal ligament; rPDLSCs, root periodontal ligament stem cells; SCAP, stem cells from the apical papilla; SHEDs, stem cells from human exfoliated deciduous teeth. Adapted from'Horizons in Clinical Nanomediciine' (Mitsiadis, 2009).

Table 1.1: Properties of human dental mesenchymal stem cells

Cell Source	Abbreviation	Diffrentiation Potential *in vitro*	*in vivo*	Markers
Dental pulp	DPSC	myogenic odontogenic adipogenic chondrogenic osteogenic neurogenic	muscles teeth bone heart dentin-pulp-like complex	STRO-1 CD146 CD44
Exfoliated deciduous teeth	SHED	neurogenic odontogenic myogenic adipogenic osteogenic chondrogenic	bone dentin teeth	STRO-1 CD146
Root apical papilla	SCAP	odontogenic adipogenic	dentin	STRO-1 CD146 CD44 CD24
Periodontal ligament	PDLSC	adipogenic osteogenic chondrogenic cementogenic	cementum PDL-like-tissues	STRO-1 CD146 CD44
Dental follicle	DFSC	cementogenic cementum osteogenic	PDL	STRO-1 CD44 BMPR-IA BMPR-IB BMPR-II

Adapted from 'Horizons in Clinical Nanomediciine' (Mitsiadis, 2009)

1.3.1 Stem cells from exfoliated deciduous teeth (SHEDs)

As described by Miura et al (2003), exfoliated deciduous dental pulp is a source of multipotent stem cells. SHEDs can be isolated from dental pulp explants or tissue digestion. Multiple neural and glial markers, such as nestin, βIII tubulin, Glutamic acid decarboxylase (GAD), Neuron-specific nuclear-binding protein (NeuN), glial fibrillary acidic protein (GFAP), Neurofilament-M (NFM) and Cyclic nucleotide 3' phosphohydrolase (CNPase), are expressed by SHEDs, along with STRO-1 and CD146 surface molecules, a feature shared with DPSCs (Gronthos et al., 2000; Miura et al., 2003). Other researchers have demonstrated that SHEDs express additional markers, including Oct4, CD13, CD29, CD44, CD73, CD90, CD105 and CD166 (Huang et al., 2009, Pivoriuunas et al., 2010). SHEDs display a greater rate of proliferation than DPSCs, albeit a reduced ability to form dentin-pulp complexes and capable of forming bone and dentin, as demonstrated by work *in vivo* (Miura et al., 2003). Specific assays have revealed the capacity of SHEDs to differentiate into multiple cell types *in vivo* such as odontoblasts, osteoblasts, adipocytes, neural cells, myocytes and chondrogenic myocytes (Miura et al., 2003, Wang et al., 2010). Furthermore, SHEDs cultured into biodegradable scaffolds and subsequently transplanted into immunodeficient mice gave rise to a dental pulp-like tissue, indicating the potential of SHEDs to differentiate *in vivo* into odontoblast-like cells. SHEDs can also produce large quantities of bone tissue as well as endothelial-like cells, as shown by several researchers (Arthur et al., 2009, Daltoe et al., 2014).

1.3.2 Stem cells from the apical papilla (SCAP)

The root apical papillae are soft tissues found at the apex of the developing permanent tooth and are a source of SCAP. It contains fewer cellular and vascular elements than dental pulp, but its cells proliferate 2-3 times faster (Sonoyama et al., 2008). Stem cells from the apical papilla have shown an increased rate of proliferation and telomerase activity than DPSCs. A study has demonstrated the increased expression of markers of MSC and 'stemness' within *in vivo* cultures of apical papillae cells, along with increased levels of differentiation inhibitors and CD90 (Ruparel et al., 2013). In addition to CD24, which is expressed only in SCAPs, both DPSCs and SCAPs express the three MSC surface markers STRO-1, CD146 and CD44 (Sonoyama et al., 2008). In addition to root formation, a study has reported that SCAPs can function as precursors for odontoblasts, neural cells, adipocytes and dentin-like tissue, as well as reacting to neurogenic stimuli to express nestin, neurofilament and other markers of neurogenesis (Huang et al., 2008b). Other studies have shown that hypoxia evokes the upregulation of genes specific to neuronal differentiation and augmente the neuronal differentiation of SCAP in the presence of exogenous differentiation stimuli (Vanacker et al., 2014).

1.3.3 Periodontal ligaments stem cells (PDLSCs)

Located near the periodontal tooth ligament, PDLSCs are a subset of MSCs with the ability to differentiate into functional cementoblasts following transplantation into immunocompromised mice. This gives rise to cementum- and periodontal ligament-like structures as well as collagen fibres within the cementum-like tissue.

These properties of PDLSCs infer a capacity for *in vivo* replenishment of the cementum and PDL (Seo et al., 2004, Mrozik et al., 2010). Sensitive to specific external stimuli within a neurotrophic culture medium, PDLSCs can give rise to neural cells as well as other cell types such as osteoblasts, chondrocytes and adipocytes (Kadar et al., 2009, Gay et al., 2007, Kim et al., 2012). Notably, PDLSCs can be discerned from MSCs of the bone marrow by their specific expression of apolipoprotein D, major histocompatibility complex-DR-alpha (MHC-DR α) and major histocompatibility complex-DR-beta (MHC-DR β) (Fujita et al., 2007). Recently, a specific gene for F-spondin that indicates an early stage dental follicular cell type with clonogenic potential has been proposed as a marker for PDLSC, along with the absence of tenascin-N, a gene indicative of terminally differentiated periodontal ligament cells (Nishida et al., 2007).

1.3.4 Stem cells derived from the dental follicle (DF)

Dental follicle precursor cells, or DFPCs, are derived from the dental follicle, a sac containing the developing tooth which is instrumental in tooth development (Cahill and Marks, 1980). Expressing the likely markers of stem cells, Nestin and Notch-1 in the follicular sacs of human third molars, DFPCs also display increased attachment *in vitro* in addition to the capacity to give rise to cell types such as osteoblasts, cementoblasts, chondrocytes and adipocytes (Morsczeck et al., 2005, Yao et al., 2008). In a study whereby bovine DFSCs were transplanted into immunocompromised mice, the development of cementoblasts was observed, as was the production of a PDL-like

tissue in similar *in vivo* studies using murine DFSCs and severe combined immunodeficient (SCID) mice (Handa et al., 2002, Yokoi et al., 2007). The capability of DFPCs to produce cementum and periodontal ligament was demonstrated in a study in co-cultures with Hertwig epithelial root sheath cells (Bai et al., 2011). A study has shown that DFPCs express the mesenchymal cell marker vimentin, as well as overexpressing IFF-2 transcripts, a feature that distinguishes DFPCs from BMSCs (Morsczeck et al., 2010). This cell type is also distinct from SHEDs and other dental stem cells in cell morphologies and stem cell marker expression patterns under standard cell culture conditions. For example, different patterns in expression of neural cell markers, such as microtubule-associated protein 2, are observed between DFPCs and SHEDs when cultured in serum-replacement medium. In addition, SHED and DFPCs have different neural differentiation potentials. Furthermore, unlike SHEDs, the stem cell marker Pax6 is not expressed by DFPCs (Morsczeck et al., 2010).

1.4 Dental pulp tissue

The central cavity of the tooth contains a soft fibrous connective tissue, dental pulp. The pulp continues through the length of the tooth as far as the root. The blood vessels and nerves of the dental pulp access the tooth where the root canal and the periodontium meet, at the apical foramen. Surrounded by dentine for structural support and protection from the microbial rich environment of the mouth, dental pulp contains elements of all connective tissues, namely cellular, vascular, neuronal and

matrix components containing fibrous components collagen type I, II and non-fibrous components (Nanci, 2007). Within the dental pulp chamber, dentin-producing odontoblasts are capable of depositing dentin matrix to form a continuous dentin layer, which encloses the dental pulp during tooth development. Outside of the chamber, enamel, the hardest tissue in the human body, covers the dentin at the crown. Cementum and periodontal ligament fibres support and connect the tooth to the alveolar bones (Fig. 1.5).

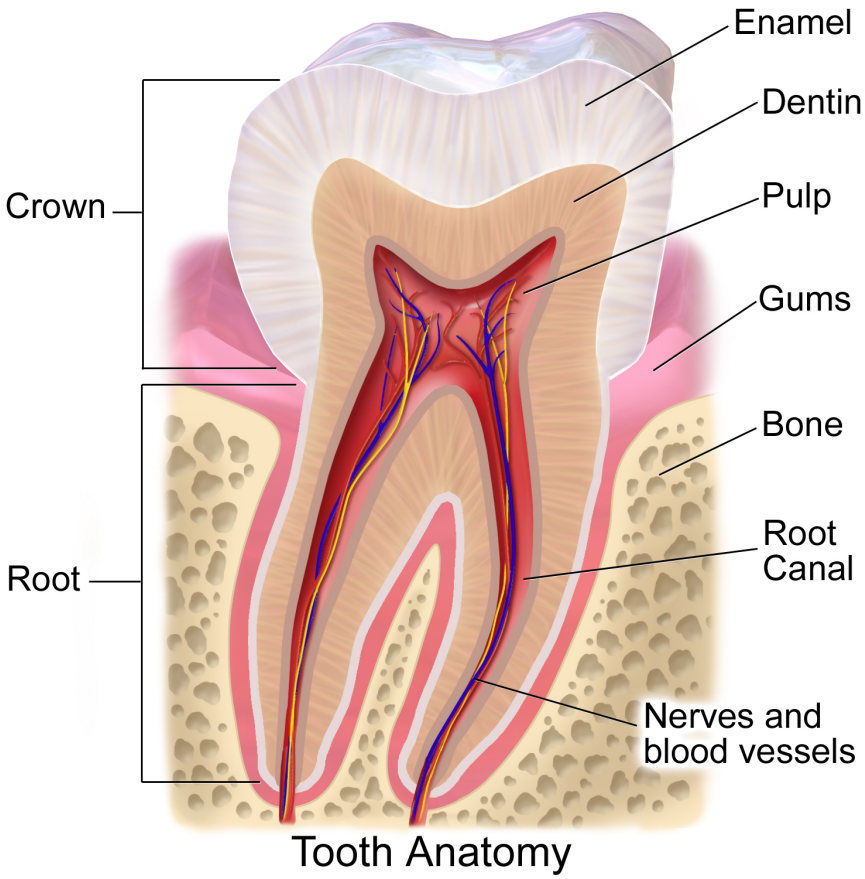

Fig 1. 5: Schematic drawing of the typical structures of the tooth.

Dental pulp tissue resides in the central cavity, enclosed by a continuous dentin layer produced by odontoblasts. Enamel covers the crown section of the dentin layer, while cementum covers the root dentin. Adapted from: Blausen.com, "Blausen gallery 2014"

1.4.1 Dental pulp formation during tooth development

In common with many other organs, tooth development initiates from interactions between the epithelium and mesenchyme. As demonstrated in studies, tooth development occurs in a process of sequential and reciprocal interactions between the ecto-mesenchyme of the cranial neural crest (CNC) and the epithelium of the mouth, following the migration of CNC cells into the appropriate structures of the head and neck (Chai et al., 2000, Jernvall and Thesleff, 2000). Figure 1.6 shows the various stages of tooth development, each denoted by the resulting shape of the dental epithelium at that specific stage. This process initiates morphologically at the tooth-forming site with the thickening of oral epithelium. Then leads to invagination into the adjacent mesenchymal layer (the E11.5 stage observed in murine models), whose cells condense to give rise to an epithelial "bud", at stages E12.5 to E13.5. The E14 stage is characterised by the formation of a "cap", produced by dental pulp and odontoblasts following the expansion of the epithelium and it's surrounding of the condensed mesenchyme-dental papilla (Neubuser et al., 1997). Several researchers, have described the generation of the dental follicle or sac from the proliferation of the outermost cells of the dental papilla and cells adjacent to the epithelial dental compartment (Tucker and Sharpe, 2004). The cementum, periodontal ligament, alveolar bone and other tooth-supporting tissues are subsequently generated by the dental follicle. Studies also detailed the E16 stage, whereby differentiation takes place along the epithelium-mesenchymal interface of the bell-shaped tooth as odontoblasts (which produce dentin) are generated from the mesenchyme and ameloblasts (which

produce enamel) are produced by the epithelium. The dental root is formed by the apical growth of Hertwig's epithelial root sheath (HERS), a bi-layered sheath produced by the cervical epithelium, in parallel with the production of enamel and dentin to complete the formation of the crown. This process is followed by the eruption of the tooth to the point of the oral occlusal plane.

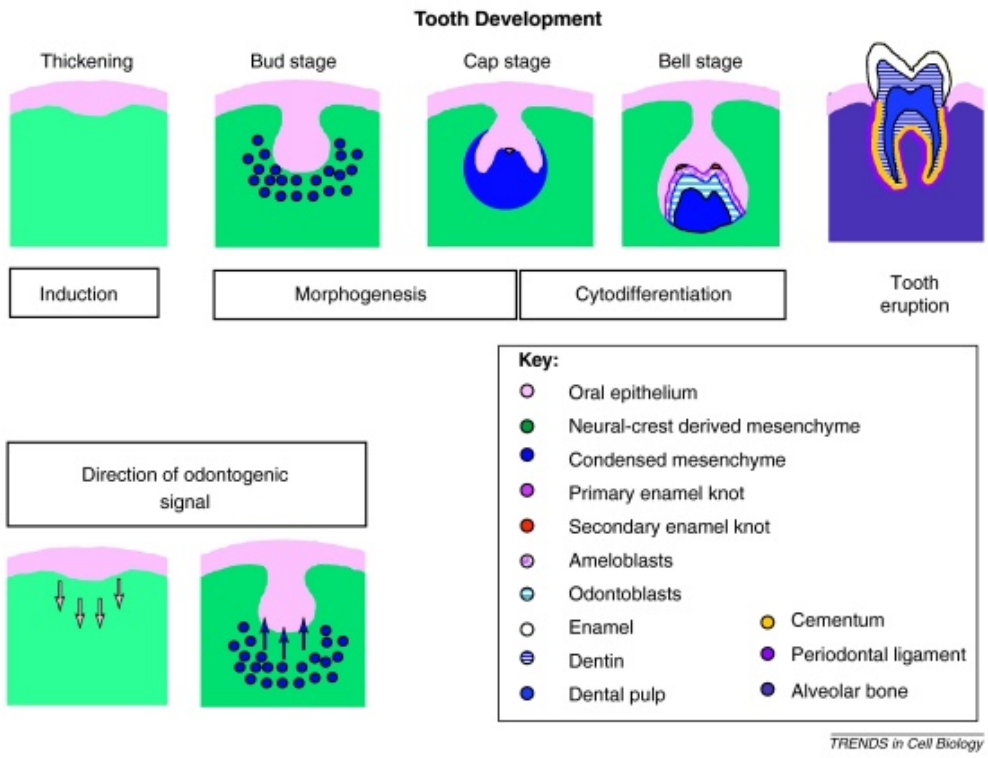

Fig 1. 6: The key stages of tooth development. Adapted from (Volponi et al., 2010)

1.4.2 Dental pulp in continuously growing rodent incisors

Humans and rodents share many similarities in tooth organ formation and patterning, although humans possess more complex tooth types and two sets of dentitions while the mouse incisor exhibits continuous growth at the apical end throughout the

animal's lifetime. Mouse incisor development commences later than that of molars (Neubuser et al., 1997) through identical development stages except in the cap stage (E14.5) where the incisor rotates and develops horizontally along the proximo-distal axis of the mandible (Fig. 1.7, A). The labial cervical loop is formed at E16, the bell stage and is a specific element of the epithelial compartment produced when the labial epithelium lengthens to a greater degree than the lingual epithelium due to the generation of differentiated ameloblasts (Tucker and Sharpe, 2004). Previously demonstrated as self-renewing due to the subset of epithelial stem cells it contains (which lead to the continuous production of enamel through differentiation to ameloblasts), the labial cervical loop also consists of stellate reticulum (SR) cells enclosed by an epithelial layer (Harada et al., 1999). A further difference between molar and incisor germs is that, from the late bell stage (E19.5), the incisor germs continue to grow without forming roots (Harada et al., 2002). In rodents, incisors lack obvious crowns or roots, but exhibit two specific surfaces as shown in Fig. 1.7, B and C, the labial side and the lingual side, with the former covered by enamel produced by ameloblasts (Ohshima et al., 2005).

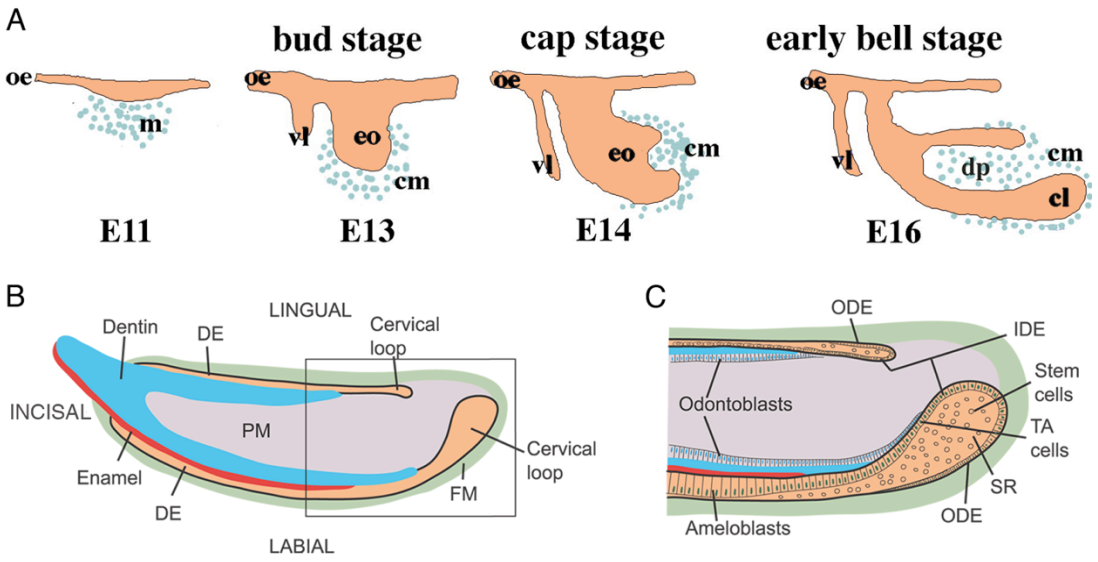

Fig 1. 7: Structure and development of the murine incisor.

A: stages of development of the mouse incisor tooth germ. B: basic structure of the well-formed mouse incisor. C: inset of B displaying individual cell types within the mouse incisor. Stem cells are located within the stellate reticulum (SR). Colour coding: enamel (red), dentin (blue), epithelium (orange), dental mesenchyme (light blue dots) and follicular mesenchyme (green). Abbreviations: cl, cervical loop, cm, condensed mesenchyme, dp, dental papilla, eo, enamel organ, m, molar, oe, oral epithelium, p, pulp, vl, vestibular lamina, DE, dental epithelium, FM, follicle mesenchyme, IDE, inner dental epithelium, ODE, outer dental epithelium, PM, papilla mesenchyme, SR, stellate reticulum, TA, transit amplifying. Adapted from (Harada et al., 2002; Wang et al., 2007).

1.4.3 Stem cells within the mouse incisor

The observation that cells of the rodent incisor proliferate throughout the animal's lifetime is indicative of the presence of stem cells. In contrast to cells located adjacent to the incisal region, Studies have demonstrated the rapid division of cells located in the incisor apex and the apical-to-incisal direction of differentiation that occurs across a gradient (Smith and Warshawsky, 1975). Researchers subsequently showed that the apex of the incisor contains enamel- and dentine-producing stem cells, while a study in murine dental pulp indicated that enamel was generated by ameloblasts, arising from epithelial stem cells, while dentine was produced by odontoblasts, produced through the differentiation of mesenchymal stem cells (Harada et al., 1999, Seidel et al., 2010).

1.4.4 Epithelial stem cells in the cervical loop

The mesenchymal layer of dental pulp is enclosed by lingual and labial side epithelia in the form of an elongated cylinder, as illustrated in studies on the rodent incisor (Thesleff et al., 2007). Given that the lingual epithelia does not give rise to ameloblasts, enamel is not produced on the lingual surface of the incisor, unlike the labial side where it is secreted by ameloblasts derived from epithelial stem cells (Harada et al., 1999).

Label retention assays such as those utilising BrdU (5-bromo-2'-deoxyuridine) can be used to confirm the presence of stem cells within the cervical loop of the labium. This analogue of thymidine is taken up by the genome during cell division and subsequently diluted. The degree of dilution is dependent on the number of cell divisions, with actively cycling cells labeled following a short exposure to BrdU. Cells that divide slowly will require a longer period of exposure. Previous studies demonstrated that cervical loop cells with a low rate of division (slow cycling), termed label-retaining cells (LRCs), retained the label after the assay was completed while fast cycling cells diluted the BrdU label, thus indicating the presence of LRCs within the labial cervical loop (Harada et al., 1999). Other researchers have endorsed the existence of stem cells within the cervical loop through studies identifying the co-location of important regulatory molecules that mediate the maintenance and proliferation of stem cells and TA cells (Harada et al., 2002, Mitsiadis et al., 2007, Lapthanasupkul et al., 2012).

1.4.5 Perivascular and non-perivascular mesenchymal stem cell niche

Previous studies have suggested the existence of a perivascular niche (pericytes) in the mouse incisor mesenchymal tissue through Cre-mediated genetic lineage tracing of pericytes during tooth development. In their study, *NG2 Cre* mice were crossed with *Rosa26 (R26R)* reporter mice. The result was that odontoblasts were produced *in vivo* by pericyte differentiation during the growth of incisors and also following damage. Of the resulting odontoblasts, however, it was shown that only 15% were derived from pericytes, indicating the existence of another source of MSCs within murine incisor mesenchyme. In order to identify responses to tooth damage within the various regions of the incisor pulp, a Dil-labeling assay was performed which labeled cells quiescent in the absence of damage in the cervical area but which subsequently migrated to the region of damage within 48 hours. This indicates the existence of a specific subset of mesenchymal stem cells localized to the mouse incisor cervix (Fig. 1.8). Further research is required, however, in order to determine the exact location of this subset (Feng et al., 2011).

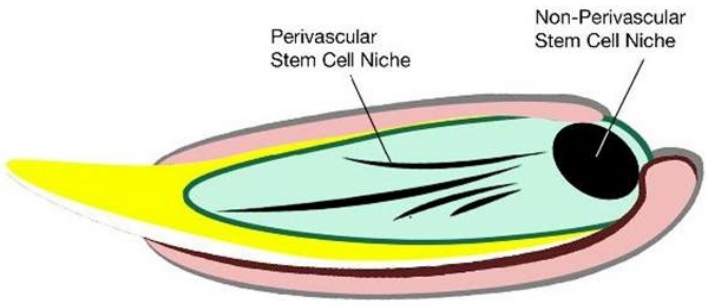

Fig 1. 8: The populations of mesenchymal stem cells located within the dental pulp.

Pericytes are found in a perivascular location while mesenchymal stem cells are believed to be localized to the apical terminus of the mesenchyme (Feng et al., 2011).

1.5 Markers for MSCs

Among the best-characterised type of ASC, MSCs were first identified in bone marrow and later in multiple tissue types, displaying a high degree of plasticity. MSCs can be extracted, cultured and used in *ex vivo* research with relative ease, rendering them suitable candidates for therapeutic use (Beyer Nardi and da Silva Meirelles, 2006). However, the recent identification of heterogeneous populations within MSCs with varying degrees of 'stemness' and their subsequent isolation through plastic adherence culture methods has led to a more complex definition of MSCs (Lv et al., 2014). Somewhat obscure physical, phenotypic and functional characteristics of MSCs are used in their identification at present, thus the minimal criteria of MSCs is not met when isolating cells by cloning on a specific cell surface marker. Nonetheless, cell surface markers with individual patterns of expression in MSCs derived from various tissues have been proposed, such as STRO-1, SSEA-4, CD271 and CD146. However, specific markers associated with the stem cell nature of MSCs await identification.

1.6 Thy-1

Thymocyte differentiation antigen (Thy-1 or CD90), a known MSC marker, has been investigated in several tissues, including liver (Petersen et al., 1998), BM (Mayani and Lansdorp, 1994), epidermis (Nakamura et al., 2006), pericytes (Shi et al., 2008), neural and osteoprogenitor cells (Nakamura et al., 2010, Locatelli et al., 2003). In the

previous study of mouse incisor MSCs, the expression of Thy-1 was noticed by our research group. Thus, Thy-1 may be a candidate mesenchymal stem cell marker of the dental pulp stem cells. Further analysis is required, however, to determine the role of cells expressing Thy-1.

Thy-1 is a heavily glycosylated 25–37 kDa conserved-cell surface protein anchored in glycophosphatidylinositol (GPI) (Almqvist and Carlsson, 1988). It was the first T cell marker identified during the characterisation of heterologous antisera against murine leukaemia cells and was shown to be located to thymocytes, T lymphocytes and neuronal cells (Reif and Allen, 1964). Thy-1 exists in many species, in 1982, a study detailed the conservation of Thy-1 throughout the evolution of vertebrates and selected invertebrates, with homologues demonstrated in squid, frogs, chickens, mice, rats, dogs and humans (Williams and Gagnon, 1982). In rodent, Thy-1 core protein has 111-112 Amino acid (aa) and was shown to contain three N-glycosylated sites. In humans, Thy-1 protein contains only two N-glycosylated sites (Almqvist and Carlsson, 1988) and is initially translated as a 161 and 162 aa pro-form (Seki et al., 1985).

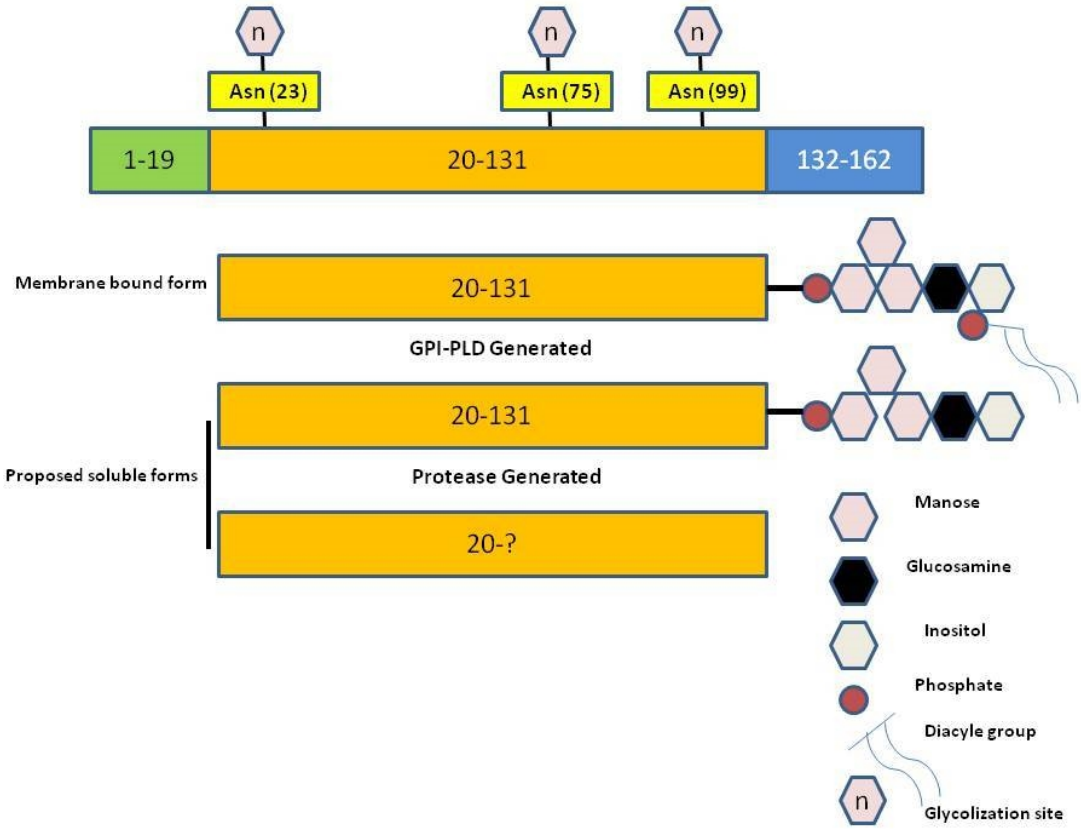

Fig 1. 9: The Thy-1 molecule and its proposed soluble forms in mice.

Thy-1 is first generated in a 161 aa pro form. The initial 19 aa signal peptide is removed and the terminal 31 aa is replaced with a GPI anchor, thus producing the mature form anchored to the outer leaflet of the cell membrane through the diacyl group of the GPI anchor. N-linked glycosylation sites represent conserved, glycosylated asparagine residues within murine Thy-1. Soluble Thy-1 is generated either by cleavage of the GPI anchor by GPI-PLD, or by unspecified proteases acting at undetermined sites of cleavage (Bradley et al., 2009).

1.6.1 Thy-1 expression

Murine Thy-1 is located to thymocytes, peripheral T cells, myoblasts, epidermal cells and keratinocytes, while the human form has been described in endothelial and smooth muscle cells, CD34+ bone marrow cells, umbilical cord blood, cardiac fibroblasts and haemopoietic cells derived from foetal liver (Reif and Allen, 1964; Nakamura et al., 2006). Study also demonstrated the localization of Thy-1 to certain brain cells and fibroblasts in most types of vertebrates (Pont, 1987). In addition, Thy-1 is strongly expressed in rat nervous tissue, among other locations, study

showed that Thy-1 levels rise by almost 100-fold in the development of the early postnatal brain. Of note, cells previous lacking Thy-1 expression can subsequently produce high levels of the protein, with the reverse also observed. These developmental changes can take place in spatially- or temporally-defined periods of maturation (Morris, 1985).

1.6.2 Functions of Thy-1

Despite the existence of a large body of research on Thy-1, the function of Thy-1 has not yet been fully elucidated. At present, the functions of Thy-1 mainly include the following aspects: cognition, T-cell activation, neurite outgrowth, apoptosis, tumour suppression, inflammation and fibrosis (Abeysinghe et al., 2003, Rege and Hagood, 2006).

1.6.3 Thy-1 as a stem cell marker

Thy-1 has been well-established, along with other markers, as a surface marker for many MSC types. For example, researchers have inferred that the detection of early markers of stem cells, such as Nanog, Oct-3/4 and SSEA-3, is indicative of stem cell potential along with stem/progenitor characteristics suggested by the co-location of CD90/Thy1, CD105, CD49, CD81, nestin, CD146, STRO-1 and other mesenchymal stem cell markers in a subpopulation of labial minor salivary gland cells (Andreadis et al., 2014). Thy-1 can also be considered a murine marker of hematopoietic stem cells as proved by its widespread use for this purpose (Petersen et al., 1998). Fibroblasts and myofibroblasts, plus certain blood progenitor cells of normal rat liver, typically

express Thy-1 and a minor subset of Thy-1-positive endogenous mesenchymal-epithelial cells has been recently identified within mature rat livers, functioning as hepatic stem cells or progenitors (Liu et al., 2015). Furthermore, a study in rodents has demonstrated the existence of Thy-1 expressing progenitors forming hepatocytes or cholangiocytes (Masson et al., 2006). In addition, a study suggested that Thy-1 may be a marker for keratinocyte stem cells as Thy-1 was capable of identifying enriched populations of human keratinocytes stem cells (Nakamura et al., 2006). It can thus be seen that the stem cell marker functionality of Thy-1 is widely described, but of additional research interest.

1.7 Flamingo

Flamingo, as a member of the adhesion-G protein-coupled receptors (GPCR) family of proteins, was originally identified in *Drosophila*. In humans and rodents, three Flamingo gene orthologs had been discovered, namely, CELSR1–3 and Celsr1–3 (Tepass et al., 2000, Vincent et al., 2000, Wu and Maniatis, 2000). These Celsr proteins have nine N-terminal cadherin repeats, followed by six EGF-like domains, seven putative trans-membrane segments and an intracellular C-terminus. Previous studies on Flamingo have centered on two main functions: regulate dendritic field deployment and planar cell polarity (Usui et al., 1999). In *Drosophila*, Flamingo can regulate dendrite branch elongation and prevent the dendritic trees of adjacent sensory neurons from having overlap of dendritic arbors (Kimura et al., 2006). In a study in mammalian, researchers found CELSR2 is involved in the regulation of dendrite

growth. CELSR2 expression reduced can lead to simplification of dendrites of pyramidal neurons in cortical cultures and purkinje neurons in cerebellar cultures (Shima et al., 2004). Another important function of Flamingo is the regulation of planar cell polarity. In the *Drosophila* wing, Flamingo localized at cell–cell boundaries, the absence of Flamingo can lead to distorted planar polarity. Studies showed that before morphological polarization of wing cells along the proximal-distal (P-D) axis, Flamingo is re-distributed predominantly to proximal and distal cell edges suggesting that cells acquire the P-D polarity by way of the boundary localization of Flamingo (Usui et al., 1999). Similarly, in mice, Celsr1 protein is required for the normal polarized position of kinocilia to one side of hair cells of the inner ear (Curtin et al., 2003). In addition, a new function of Flamingo in maintaining quiescent cells has been identified in a study of HSC niche. The study showed that noncanonical Wnt signaling member Flamingo regulates Frizzle family receptor Fz8 distribution at the interface between HSCs and N-cadherin+ osteoblasts in the HSC niche. N-cadherin+ osteoblasts predominantly express noncanonical Wnt ligands and inhibitors of canonical Wnt signaling under homeostasis. Under stress, noncanonical Wnt signaling is attenuated and canonical Wnt signaling is enhanced in activation of HSCs. These results demonstrated that noncanonical Wnt signaling maintains quiescent long-term HSCs through Flamingo and Fz8 interaction in the niche (Sugimura et al., 2012).

1.8 Polycomb Group (PcG) proteins

PcG proteins were initially shown to repress *Hox* genes in *Drosophila melanogaster* (Cao et al., 2002). Mutations of these proteins in flies result in the homeotic transformation of one body segment into the identity of another. Aside from a role in the control of body plan and segmentation, studies also revealed several crucial roles of PcG proteins in the maintenance of embryonic and adult stem cells, cell proliferation, oncogenesis, genomic imprinting and X-chromosome inactivation (Valk-Lingbeek et al., 2004). In mammalians, two distinct PcG complexes, Polycomb Repressive Complex (PRC) 1 and 2, have been well-characterised (Ku et al., 2008). Mammalian PRC1 consists of orthologs of *Drosophila* Polycomb (Cbx2, Cbx4, Cbx6, Cbx7 and Cbx8), Posterior sex combs (Mel18, Bmi1, Nspc1/Pcgf1 and MBLR), dRing (Ring1a and Ring1b) and Polyhomeotics (Phc1, Phc2 and Phc3), while core PRC2 was shown to consist of Suz12, Eed, Ezh1 and Ezh2 (Schwartz and Pirrotta, 2007, Ringrose and Paro, 2004). Studies have demonstrated the importance of PRC1 to the stability of gene repression through its inhibition of nucleosome remodelling. Furthermore, a study has shown the key role of Ring1a and Ring1b of PRC1 in terms of the E3 ubiquitin ligase activity for histone H2A displayed (de Napoles et al., 2004). In a recent study in murine incisor stem cells, researchers described the expression of Bmi1 of PRC1, the deletion of which gave rise to fewer stem cells, disrupted gene expression and impaired production of enamel. Transcriptional profiling further demonstrated that *Hox* genes' expressions were typically inhibited by Bmi1 in adults, with functional assays revealing the maintenance of the undifferentiated state of stem

cells through Bmi1-mediated repression of *Hox* genes (Biehs et al., 2013). The roles of PRC2 include gene repression and as a histone methyltransferase that specifically methylates lysine 27 of histone H3 (H3K27) in nucleosomes (Schwartz and Pirrotta, 2007).

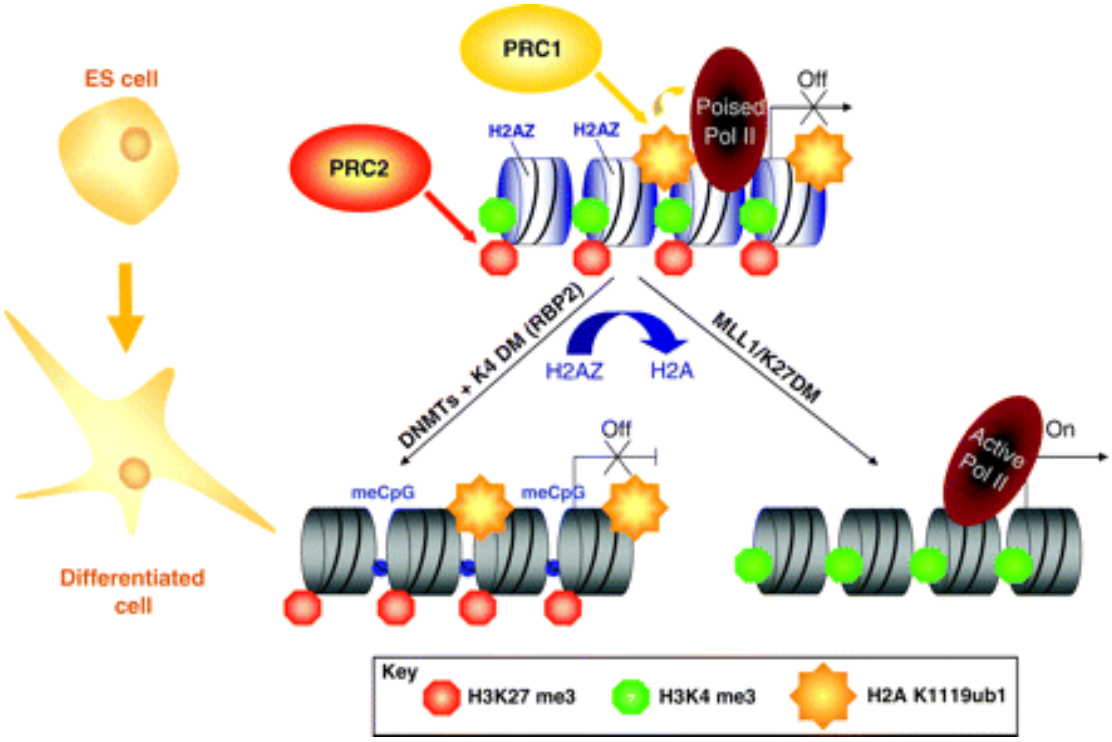

Fig 1. 10: The resolution of bivalent chromatin domains during differentiation of ES cells.

In ES cells, histone H3K27me3 and H3K4me3 mark several key developmental regulators, bound by a non-processive form of RNA polymerase II (poised pol II). PRC1-mediated ubiquitylation of histone H2A on lysine 119 (H2AK119ub1) maintains RNA pol II in a poised configuration. Several silent key developmental regulators are marked by the histone variant H2AZ, which may further protect these genes from DNA methylation and stable silencing. Upon differentiation of ES cells, activated bivalent genes are relieved from the repressive H3K27me3 mark and H2AZ is redistributed to a different set of highly active genes. Histone methyltransferase MLL1 is required for the resolution of specific bivalent domains, potentially by the recruitment of H3K27-specific demethylases (K27DM). Conversely, bivalent genes that remain inactive in differentiated cells lose the active H3K4me3 mark through the activity of K4-specific histone demethylases (K4DM), such as RBP2. The replacement of H2AZ by H2A may lead to CpG island methylation (meCpG, blue circles), causing stable gene silencing (Ku et al., 2008).

1.9 PRC1 complex and stem cells

The PRC1 family can be further divided into at least six groups based on the identity of the PCGF subunit according to the specific polycomb group ring finger protein (PCGF) subunit (Gao et al., 2012). PCGF1, for example, is found in PRC 1.1, along with Bcor and Ring proteins, both of which have been shown to play a critical role in the suppression of regulators of development and maintenance of the undifferentiated state of ES cells (Wamstad et al., 2008). Results from studies in mice lacking Ring1b expression indicated that Ring1b might affect the differentiation potential of neural stem cells (NSCs) to neurons and glia. In foetal NSCs, Ring1b-deficiency has been shown to cause premature neuronal differentiation. In addition, *Ring1b* gene mutation leads to enhanced neuronal differentiation and reduced gliogenesis by modulating the temporal specification of developing neural progenitors (Roman-Trufero et al., 2009). A recent study in mice demonstrated that the 3T3-L1 pre-adipocyte differentiation was inhibited by anti-adipogenic Fbxl10 in a Ring1b knockdown model, suggesting that adipogenesis is inhibited through the repressing of key genes such as *Pparg* by Fbxl10 via a non-canonical PRC1 complex pathway (Inagaki et al., 2014). Ring1b inactivation in adult stem and primitive progenitor cells within the hematopoietic compartment leads to proliferative alterations rather than differentiation proposing a critical role for Ring1b in modulating hematopoietic cell turnover by inhibiting the proliferation of stem cells while stimulating proliferation of their mature progeny (Cales et al., 2008). Bcor has also been reported to regulate mesenchymal stem cell function by epigenetic mechanisms (Fan et al., 2009). *Bcor* mutation increased MSCs

proliferation and osteo-dentinogenic capacity in cells derived from the dental pulp tissue of an oculofaciocardiodental (OFCD) patient. Although the precise mechanisms remain unclear, this preliminary data suggest that members of the PRC1 complex have a crucial role in the maintenance of DPSC lineage in both humans and mice.

1.10 Hypothesis and aims of the research project

Data suggest that MSCs residing in different organs show a high degree of similarity, however, certain properties or characteristics may be modified due to functional and/or signaling differences in the tissue-specific micro-environments. Therefore, the analysis of the microenvironment in which MSCs are located is particularly important in understanding their properties and behaviour.

Hypothesis: Unlike human teeth, murine incisors constantly erupt and grow throughout the animal's lifetime in order to mitigate for regular wear, a process in which stem cells within the incisors play an important role. Given the previous research of mouse incisors we assume a MSCs niche is located at the apical end of mouse incisor.

Aims: As dental pulp mesenchymal stem cells have been mostly studied based on their *in vitro* characteristics and their *in vivo* characteristics are not well understood. This project seeks to determine the location of the MSC niche and, subsequently, of stem cells within the murine incisor while determining the gene profile specific to these cells, thus contributing to an increased *in vivo* understanding of dental pulp stem cells and their micro-environments.

Chapter 2 : Method and Techniques

2.1 Tissue processing

2.1.1 Reagents and solutions

Paraformaldehyde PFA (4%)	Sigma, P6148
DEPC (Diethyl pyrocarbonate)	Sigma, D5758
Formic acid, 98%	Fisher, F/1850/PB17
EDTA (Ethylenediaminetetraacetic acid)	VWR, 20302.293
Ethanol	VWR, 101077Y
Methanol	Fisher, M/4056/PB17
Histoclear	National Diagnostics, HS-202
1,2,3,4-Tetrahydronaphthalene	SIGMA, 429325
Ultraplast Polyisobutylene Histological Wax	Solmedia, WAX060
Erhlich's Haematoxylin	Solemedia, HST003
Eosin, aqueous solution (0.5%)	Riedel-de Haën, 32617
DePex	BDH, 360294H
BrdU	Sigma, B5002
CldU	Sigma, C6891
IdU	Sigma, I7125
EdU	Invitrogen, A10044
Tamoxifen	Sigma, T5648
Corn oil	Sigma, C8267

2.1.2 Obtaining mouse tissues

The UK Home Office approved all the animal experiments. Unless otherwise stated, colonies of wild type and transgenic mice were maintained and carried out breeding by Mr. Alex Huhn. The cross and design of mice were performed by myself according to experiment demands. As in this project, the *Cre/loxP* site-specific recombination system was used as an important tool to investigate cell fates and gene functions. A $pCAG^{CreERT2}$ mouse line purchased from Jackson's lab was used to provide ubiquitous expression of Cre under a strong synthetic promoter CAG that is frequently used to drive high levels of gene expression in mammalian expression. Beside, Thy-1 Cre mouse line with Thy-1 promoter was purchased to enable Cre expression in all Thy-1 expressing cells. In addition, two reporter mouse lines: mT/mG double-fluorescent reporter mouse line (*R26R mT/mG*) and a 4-colour reporter mouse line (*R26R-Confetti*) were purchased to provide reporter genes. Moreover, a *R26::Cre ERT2* mouse line purchased from Jackson's lab was used to cross the $Ring1a^{-/-}$ $Ring1b^{fl/fl}$ mice to accomplish conditional inactivation of *Ring1b in vivo.* Furthermore, $Bcor^{fl/+}$*;Pax3Cre* and $Bcor^{fl/y}$*;Pax3Cre* adult tissues which Cre was driven by Pax3 promoter in neural crest were provided by Dr. Vivian Bardwell. All mouse lines are listed in the Table 2.1.

The *Thy-1 Cre* and *Cre-ERT2* transgenic mice lines were maintained as heterozygotes. Mice carrying these transgenes were identified by performing a genotyping polymerase chain reaction (PCR) that amplified a *Cre* and *Cre-ERT2* product by myself. *Thy-1Cre; R26R-Confetti* and *Thy-1Cre; R26R mT/mG* were made and confirmed by PCR (Access RT-PCR System Promega, A1250).

Table 2.1: Mouse lines used in this project

Mouse line1	Mouse line2	Compound mouse line
pCAG^{CreERT2} (from Jackson's lab)	*R26R mT/mG* (from Jackson's lab)	*pCAG*^{CreERT2}*; R26R mT/mG*
Thy-1Cre (from Jackson's lab)	*R26R mT/mG* (from Jackson's lab)	*Thy-1Cre; R26R mT/mG*
	R26R-Confetti (from Jackson's lab)	*Thy-1Cre;R26R-Confetti*
Ring1a$^{-/-}$*;Ring1b*$^{fl/fl}$ generated as described previously (Cales et al., 2008)	*R26::Cre ERT2* (from Jackson's lab)	*Ring1a*$^{-/-}$*;Ring1b*$^{fl/fl}$*; R26::Cre ERT2*
Bcor$^{fl/+}$*;Pax3Cre* provided by Dr. Vivian Bardwell		*Bcor*$^{fl/+}$*; Pax3Cre*

Vaginal plugs were checked using a probe the following day after male and female mice mated overnight (O/N). The day on which the vaginal plug was discovered was used to determine the embryonic stage and was designated as embryonic day 0.5 (E0.5). Home office schedule one specification was followed during the collection of embryonic and neonatal tissues. Cervical dislocation and CO_2 suffocation was used to sacrifice mice. Mice mandibular and maxillary were collected in ice-cold 1x PBS. For postnatal pups, the day on which pups were born was designated as postnatal day 0 (PN0). Pups and adult mice were sacrificed by cervical dislocation or CO_2 suffocation followed by decapitation. After excess blood was blotted on a tissue paper, pup heads were collected in ice-cold 1x PBS.

2.1.3 Nucleosides administration

Nucleosides, such as BrdU, CldU, IdU and EdU are thymidine analogues that are incorporated into the newly synthesized DNA of S-phase cells. Therefore, detection of nucleosides can be used to reflect cell division by specific antibodies against BrdU,

CldU, IdU and EdU. To detect rapid cell division, per 1kg body weight, 200 mg BrdU (10 mg/ml BrdU stock in 0.9% saline) was administrated intraperitoneally to CD1 PN5 and adult mice. Mice were subsequently sacrificed shortly at time points of 2 hours, 8 hours and 16 hours after the injection and processed through histology and ICH analysis. To detect slow cycling cells, a different nucleoside-administrating strategy was performed. CD1 mice continuously received freshly prepared 1mg/ml BrdU in water by oral administration for 3 weeks. The BrdU solution was protected from light and changed every other day. The mice were then culled after a washout period for 1 day, 8 days, 16 days, 32 days and 64 days respectively. The BrdU labeling would be retained and detected only in slow cycling cells. To label the fast cycling cells and slow cycling cells on one sample section, two rounds of nucleosides labeling were subsequently performed. In the first round, IdU was used to label slow cycling cells, IdU was given to CD1 mice continuously by drinking water for 3 weeks (10 mg/ml) in double distill water, followed by a 32 day washout period, then mice received a single dose CldU injection (200mg/kg body weight) to label fast cycling cells, they were then culled and analyzed the next day. To label fast/slow cycling cells for flow cytometry analysis PN5 CD1 pups were continually given EdU injections (3.3 μg per g body weight) for 3 weeks and washed out for another 3 weeks before collection.

2.1.4 Tamoxifen administration

For *pCAG*^{ERT2Cre};*R26R mT/mG* double transgenic mice, PN2 pups were given a single low dose intraperitoneal injection of 2 μg tamoxifen (10 mg/ml in corn oil) to randomly activate the Cre-expression to produce eGFP fluorescence. Following tamoxifen administration, the pups were then sacrificed by cervical dislocation 3 weeks later and the teeth were carefully dissected out and stained by ICH to visualize the eGFP expression. For the high dose tamoxifen injection group, three high doses tamoxifen

injections (67 µg/g body weight, 10 mg/ml in corn oil solution) were given to the *pCAG*^{ERT2Cre}*;R26R mT/mG* double transgenic mice every 2 days to activate the Cre-expression in all the cells to produce eGFP fluorescence. The mice were then sacrificed by cervical dislocation 1, 2 and 3 weeks later to dissect teeth for ICH and analysis.

To accomplish conditional inactivation of *Ring1*b *in vivo*, *Ring1a* $^{-/-}$*; Ring1b*$^{fl/fl}$*; R26::CreERT2* mice were generated. Conditional deletion of *Ring1b* was carried out at the desired stage of postnatal life by 4-hydroxy tamoxifen (OHT) treatment (40 mg/kg body weight). *Ring1a* $^{-/-}$*; Ring1b*$^{cko/cko}$ mice were obtained by injecting OHT at PN9 and PN13 to inactivate Ring1b. The *Ring1a* $^{-/-}$*;Ring1b*$^{cko/cko}$ mice were sacrificed at PN17. The efficiency of tamoxifen-induced Cre expression to delete *Ring1b* was confirmed by *in situ* hybridization (ISH) of PN17 incisors.

2.1.5 Tissue fixation, decalcification and dehydration

Mouse mandibles and maxillae were dissected in cold 1x nuclease-free PBS and fixed up to 2 days in 4% paraformaldehyde (PFA) at 4ºC according to age. For E15.5 or older embryonic heads, fixation was about 4-12 hours. For adult head, the fixation time was prolonged to 2 days. Mouse tissues older than E16.5 need to be decalcified in 4.3% or 12.5% EDTA pH8.0 containing 1% PFA for 1-3 weeks at room temperature on a shaker, depending on the developmental stages of the embryos/mice. Adult mouse tissues were decalcified for 3-6 weeks with Morse's Solution (10% sodium citrate and 22.5% formic acid) or 4-8 weeks with 10% EDTA pH8.0 at room temperature on a shaker. All decalcifying solutions were freshly prepared and changed every day. Tissues were thoroughly washed with 1x nuclease-free PBS to eliminate residual PFA and decalcified solution and then dehydrated in ascending ethanol solutions (30%, 50%, 70%, 85%, 95%

and 100%) after fixation and decalcification. The duration of each step was determined by the size and age of the sample, as listed in the Table 2.2 below.

Table 2.2: Dehydration time in ethanol according to the specimen

Sample	Ascending Ethanol Solutions
Embryo head (E11.5 or earlier)	30 minutes per change
Embryo head (E12.5- E16.5)	2-4 hours per change
Embryo head (E16.5- E18.5)	4-8 hours per change
Postnatal 1-10 days	O/N per change
Adult mouse jaw	24 hours per change

2.1.6 Paraffin embedding

After final dehydration in 100% ethanol the tissues were incubated in several changes of histoclear. Tissue samples were incubated in a histoclear: paraffin mix (in 1:1 ratio) at 60°C up to 1 hour, following by several consecutive wax changes to allow the replacement of ethanol by paraffin wax. The detailed duration of each step for different tissues is specified in Table 2.3. After the long incubation period in paraffin wax, whole jaws were embedded in a specific orientation (frontal or sagittal) using metal moulds. Paraffin wax blocks were stored at room temperature until sectioning.

Table 2.3: Duration of each embedding step according to the developmental stage of mouse jaws

Tissues	Histoclear	Histoclear: Wax (1:1)	Wax	Vacuum Embedding
E11.5 or earlier (Head)	30 minutes x 2	30 minutes	1 hour x 3	N/A
E12.5-E16.5 (Head)	20 minutes x 6	30 minutes	1 hour x 5	30 minutes – 1 hour
E16.5-E18.5 (Head)	30 minutes x 6	30 minutes	1 hour x 5 + O/N	1 hour
Postnatal 1-10 days	1 hour x 5	30 minutes	1 hour x 5 + O/N	1 hour
Postnatal/Adult (Jaw)	1 hour x 6 + O/N	1 hour	1-2 hours x 5 + O/N	1 hour

2.1.7 O.C.T. compound (O.C.T) embedding for frozen sectioning

After fixation in 4% PFA according to developmental stages, samples were washed in 1x PBS 3 times for 5 minutes each to remove residuary PFA. Tissue samples were then incubated in 30% surcrose dissolved in 1x PBS at 4°C O/N up to 24 hours and samples were subsequently, transferred to surcrose: O.C.T mix (in 1:1 ratio) for 12 to 24 hours at room temperature before immersion in O.C.T solution at room temperature O/N to 24 hours to allow tissues be filled with O.C.T. Samples were then placed in the bottom of a plastic mold at a specific orientation (frontal or sagittal) and immersed in the O.C.T. These moulds containing samples and O.C.T were placed on the dry ice to solidify the O.C.T. The O.C.T block containing samples were kept in -20°C until sectioning.

2.1.8 Tissue sectioning

Paraffin wax blocks were sectioned using a microtome (Leica RM2245). The samples were sectioned to produce wax ribbons of 5-8 µm in thickness. Consecutive sections

were then mounted serially on glass slides (SuperFrost®Plus, VWR™) for the next step of analysis.

O.C.T embedded PN5 mouse incisors were sectioned using a cryostat (Bright Instrument Ltd). While O.C.T embedded adult incisors were sectioned using an alternative (Huntingdon England) with a blade specialized for sectioning hard tissues. The samples were sectioned to produce sections of 12-30 µm in thickness. Sections were mounted on glass slides (SuperFrost®Plus, VWR™) and stored at -20°C until staining and further analysis.

2.1.9 Haematoxylin and Eosin staining (H&E) for histology analysis

H&E staining was used to assess tissue and cell morphology. Cell nuclei were stained blue by haematoxylin, while eosin stained the cytoplasm, connective tissue and other extracellular substances pink or red. Paraffin sections were de-paraffinised with two 10 minutes histoclear washes and rehydrated through a graded series of ethanol washes (100%, 90%, 70% and 50%) for 2 minutes each. Sections were washed in distilled water for 10 minutes and submerged in Erhlich's haematoxylin for 10 minutes. The samples were washed to remove excess haematoxylin under running water for 10 minutes. Prior to differentiation, sections were rinsed in distilled water and submerged in acid alcohol (0.5% HCl 35% alcohol) for 15 seconds. Subsequently, the sections were stained with 0.5% aqueous eosin for 2 minutes and washed in distilled water after dehydration and through a series of two minutes ethanol washes (70%, 90% and two 100%). Sections were air-dried for up to 1 hour before being coverslipped with DePex in a fume hood. To visualize cell morphology, sections were viewed in a light-field using a Zeiss microscope (Axioskope 2 plus) and captured with an AxioCam HRC (Zeiss) and Axiovision software.

2.2 Staining for β-galactosidase (LacZ) activity

2.2.1 Reagents and solutions

Trizma® base (Tris base)	Sigma, T1503
Glutaraldehyde	MERCK, 104239025
Sodium deoxycholate	Sigma, D6750
IGEPAL CA-630 (NP-40)	Sigma, I3021
Potassium ferrocyanide ($K_4[Fe(CN)_6]$)	BDH, 102054F
Potassium ferricyanide ($K_3[Fe(CN)_6]$)	BDH, 102044D
Magnesium chloride ($MgCl_2$)	Fisher, BP214-500
5-bromo-4-chloro-3-indolyl-β-D-galactopyranoside (X-Gal)	Fermentas, R0404
Phosphate buffered saline (PBS)	Fisher, BP-665-1
Methanol	Fisher, M/4056/PB17
Propan-2-ol (isopropanol)	Acors Organics, 389710025
1,2,3,4 -Tetrahydronaphthalene	Sigma, 429325
Eosin, Alcoholic Solution (in Ethanol)	
Eosin Y disodium salt (0.25%)	Riedel-de Haën, 32617
21% Distilled H_2O	
0.5% ml Glacial Acetic Acid	VWR, 20104.334
Nuclear Fast Red (in H_20)	
Nuclear Fast Red (0.2%)	Sigma, 60700
Aluminum potassium sulphate (10%)	Fisher, A/2400/53
O.C.T. compound	BDH, 361306E
Sucrose	Sigma, S0389

2.2.2 Whole mount β-galactosidase staining

Transgenic mice carrying a LacZ reporter were processed through the LacZ staining protocol. Samples were carefully dissected in cold 1x PBS. Postnatal teeth were carefully dissected from the mandibles and maxillae to allow better penetration of the fixative and the staining solution. Dissected tissues were immediately placed in fixative solution (0.4% PFA and 0.2% glutaraldehyde in PBS) at room temperature. The fixation time varied depending on the tissue (Table 2.4).

Table 2.4: Fixation time for X-gal staining

Sample Stage	Incubation Time
E14.5	30 minutes
Postnatal PN5	4 hours
Adult	O/N

The fixed tissue was then washed in 1x PBS and incubated with X-gal staining solution (Table 2.5) at 37ºC in the dark. Adequate reaction colour (blue) usually developed after approximately 24-48 hours after initial incubation. Samples were washed 3 times in 1x PBS for 10 minutes each or longer and then re-fixed in 4% PFA for at least one hour at room temperature for histological processing.

Table 2.5: Components of LacZ staining solution

Components	Concentration
Tris HCl pH 7.3	10 mM
Sodium deoxycholate	0.005%
IGEPAL	0.01%
$K_3Fe(CN)_6$	5 mM
$K_4Fe(CN)_6$	5 mM
$MgCl_2$	2 mM
X-Gal	0.8 mg/ml
1x PBS	Up to final volume

2.2.3 Processing X-gal stained tissues for sectioning

After re-fixation, postnatal samples were decalcified 4-8 weeks with 10% EDTA pH 8.0 at room temperature on a shaker. Samples were dehydrated through a graded series of methanol solutions (30%, 50%, 70%, 85%, 95% and 100%) to minimise de-staining. The duration for each wash step was dependant on the age of the sample (Table 2.6).

Table 2.6: Methanol dehydration time for X-gal stained sample (per step)

Sample Stage	Incubation Time
E14.5	30 minutes
PN5	60 minutes
Adult	3 hours

Following dehydration in 100% methanol, the samples were incubated in isopropanol for 15 minutes twice and then they were placed in tetrahydronaphthalene (THN) at room temperature until saturated and moved to 60ºC for 15 minutes. Subsequently samples were placed in a 1:1 mixture of THN: paraffin wax at 60ºC for 15 minutes. In

the end, samples were washed at least four times (each wash lasting 1 hour) in paraffin wax at 60°C before embedding. Wax embedded samples were sectioned and mounted.

2.2.4 Counterstaining of X-gal stained sections

To stain the nuclei, X-gal stained sections were counterstained using eosin to allow the identification of unstained structures. Sections were de-paraffinised in histoclear for 10 minutes twice and dehydrated briefly in descending ethanol solutions (100%, 90% and 70%) for 2 minutes each. After incubation with alcoholic eosin (0.25%) for 30 seconds-2 minutes, slides were washed with 95% ethanol to get rid of access staining. Sections were then dehydrated in 100% ethanol for 2 minutes twice and rinsed in distilled H_2O for 2 minutes. The slides were air-dried and then coverslipped with DePex.

To stain the cytoplasm, X-gal stained samples were counterstained with Nuclear Fast Red that stains nuclei pink to red and cytoplasm pale pink. Slides were similarly de-paraffinised and then briefly rehydrated in descending ethanol solutions (100%, 90%, 70%, 50% and 30%) for 1 minute each and in distilled water for 2 minutes. Slides were then immersed in 0.2% nuclear fast red solution for 30 seconds to 2 minutes and rinsed in distilled water until no excess staining was evident. Slides were dehydrated in a series of ascending ethanol solutions (70% and 90%) for 1 minute each and in 100% ethanol for 1 minute twice. Slides were left at room temperature to air dry and coverslipped using DePex in a fume hood.

2.3 Immunohistochemistry (ICH)

2.3.1 Reagents and solutions

Blocking Buffer (1% BSA and 10% FBS in 1x PBS)

Albumin from bovine serum, BSA (1%)	Sigma, A4919
FBS (10%)	Sigma, F7524
Hydrochloric acid (HCl)	VWR, 20252.244
Trizma® base (Tris base)	Sigma, T1503
Citric Acid	Sigma, C7129
Vectastain Elite ABC Kit	Vector Labs, PK-6101
DAB Peroxidase Substrate Kit	Vector, SK-4100
Hematoxylin solution according to Delafield (Counterstain)	Fluka, 03971
VECTASHIELD Mounting Medium with DAPI	Vector, H1200
O.C.T. compound	BDH, 361306E
PBST (2% Tween20 in PBS)	

2.3.2 ICH on section

Paraffin sections were de-paraffinised in histoclear for 20 minutes twice and rehydrated through decreasing concentrations of ethanol solutions (100%, 95%, 90%, 70% and 50%) for 5 minutes each followed by washing in 1x PBS. After rehydration, permeabilization, antigen retrieval was carried out depending on the primary antibodies used (Table 2.7). For the antigen retrieval, both heat-based method and proteinase K method were applied in the pre-experiment. Based on pre-experiment results, heat-based antigen retrieval was selected as it showed the best result. Heat-based antigen retrieval was performed by microwaving slides twice in a 0.1M Tris-HCl pH9.5 solution for 10 minutes. After antigen retrieval, the sections were thoroughly washed in PBST (2% Tween20 in PBS) 3 times for 5 minutes each and then incubated with blocking buffer (5% FBS 1% BSA in 1x PBS) for 1 hour at room temperature. Primary antibodies were applied to samples in a pre-optimised dilution in 1% BSA and incubated for 3 hours at

room temperature or O/N at 4ºC in a humidified chamber. Frozen sections were washed in 1x PBS for 20 minutes twice before being incubated with blocking buffer (5% FBS 1% BSA in 1xPBS); then incubated with primary antibodies. Before applying secondary antibodies (Table 2.8) in pre-optimized dilutions, slides were thoroughly washed 3 times in PBST for at least 5 minutes per wash to remove the unbound primary antibodies. The secondary incubation was performed inside a humidified chamber for 1 hour at room temperature.

For fluorescence-conjugated secondary antibodies, sections were washed 3 times in PBST solution for at least 5 minutes each before mounted with VECTASHIELD DAPI fluorescence mounting medium. Fluorescent images were acquired using Nikon's Fluorescence Microscope H600L or confocal microscopy (Leica Sp5 AOBS) equipped with the following lenses: 103 (HCX PL APO CS NA0.40) dry objective; 203 (HCX PL FLUOTAR L NA0.40) dry objective; 403 (HCX PL APO NA0.85) dry objective; and 633 (HCX PL APO NA1.30) glycerol objective. The imaging of the confocal stack was done with the z-axis shift of 7 mm for every step.

For biotin conjugated secondary antibodies, sections were additionally immersed twice in 3% H_2O_2 in methanol for 5 minutes each prior to primary antibody incubation to block endogenous peroxidase. To visualize antibodies, the samples were incubated in ABC solution (Vectastain kit) for 1 hour at room temperature and then washed in PBST. In the end, the colour reaction (brown) was developed by DAB Peroxidase Substrate Kit following the manufacturer's instructions. The sections were then counterstained for 45 seconds to 2 minutes in diluted Delafield's hematoxylin (1:4), which leaves nuclei stained with a contrasting pale blue colour. The sections were gradually dehydrated and mounted with cover slips using DePex mounting medium as previously described. Sections were viewed in a light-field using a Zeiss microscope (Axioskope 2 plus) and captured with an AxioCam HRC (Zeiss) using Axiovision software.

Table 2.7: Optimised dilution and antigen retrieval for each primary antibody

Primary Antibody	Dilution	Antigen Retrieval	Manufacturer
Anti-BrdU antibody (Rat monoclonal, reactive against CldU)	1:500	Heat-based	Abcam, ab6326
Anti-BrdU antibody [IIB5] (Mouse monoclonal, reactive against IdU)	1:100	Heat-based	Abcam, ab8152
Anti-Phospho-Histone H3 antibody (Rabbit polyclonal)	1:500	Heat-based	Millipore, 06-570
Anti-GFP antibody (reactive against eGFP) (Chicken polyclonal)	1:500	Heat-based	Abcam, ab13970
Anti-GFP antibody (reactive against eGFP) (Rabbit polyclonal)	1:500	Heat-based	Abcam, ab6556
Anti-Thy-1 (CD90)-FITC conjugated antibody (Mouse monoclonal)	1:100	N/A	Abcam, 62009
Anti-Pax9 antibody (Rabbit polyclonal)	1:100	N/A	*
Anti-Neurofilament antibody (Mouse monoclonal)	1:1000	N/A	Abcam, 24574
Anti-Celsr1 antibody (Rabbit polyclonal)	1:100	N/A	Millipore, ABT1119
Anti-Cre antibody (Rabbit polyclonal)	1:200	N/A	Novagen, 69050-3
Anti-Ring2 / Ring1b / RNF2 antibody	1:500	N/A	Abcam, ab3832

* Anti-Pax9 (Rabbit polyclonal) was kindly provided by Professor Heiko Peters

Table 2.8: Optimised dilution for each secondary antibody

Secondary Antibody	Dilution	Manufacturer
Biotinylated goat anti-rabbit antibody	1:200	Vector, BA-1000
Biotinylated rabbit anti-rat IgG antibody	1:200	Vector, BA-4001
Donkey-anti rat IgG (H+L) antibody Alexa Fluor 594, A21209	1:200	Life technologies
Donkey-anti rabbit IgG (H+L) antibody Alexa Fluor 594, A21207	1:200	Life technologies
Goat-anti rabbit IgG (H+L) antibody Alexa Fluor 660, A21073	1:200	Life technologies
Goat-anti chicken IgG (H+L) antibody Alexa Fluor 488, A11039	1:200	Life technologies
Goat-anti mouse IgG (H+L) antibody Alexa Fluor 488, A11017	1:200	Life technologies
Goat-anti rabbit IgG (H+L) antibody Alexa Fluor 594, A11072	1:200	Life technologies
Goat-anti mouse IgG (H+L) antibody Alexa Fluor 594, A11020	1:200	Life technologies
Goat-anti mouse IgG (H+L) antibody 647 Alexa Fluor, A21235	1:200	Life technologies
Rabbit-anti mouse IgG (H+L) antibody Alexa Fluor, 488 A21204	1:200	Life technologies
Rabbit-anti mouse IgG (H+L) antibody Alexa Fluor, 546 A11060	1:200	Life technologies

2.4 *In situ* hybridization (ISH)

2.4.1 Reagents and solutions

DH5α™ Competent cells (Subcloning Efficiency)	Invitrogen, 18265-017
Luria-Bertani (LB) broth	
1% NaCl	BDH, 102415K
1% Tryptone	Oxoid, LP0042
0.5% Yeast Extract	Oxoid, LP0021
Luria-Bertani (LB) agar	
1% Tryptone	Oxoid, LP0042
1% NaCl	BDH, 102415K
0.5% Yeast Extract	Oxoid, LP0042
1.5% Agar	Oxoid, LP0011
Ampicillin Sodium Salts (50 mg/ml)	Sigma, A9518
Fast Plasmid®Mini	Eppendorf AG, 955150601
QIAGEN Plasmid Maxi Kit	QIAGEN, 12163
QIAquick® Gel Extraction Kit	QIAGEN, 28706
Restriction enzymes and buffers	Promega
Polymerase enzymes	Promega
DIG RNA labeling Mix (10x)	Roche, 11277073910
SigmaSpin™Post-Reaction Clean-Up Column	Sigma, 5059
DL-Dithiothreitol (DTT)	MP Biomedicals, 100597
Triton® X-100 (Iso-Octylphenoxypolyethoxyethanol)	BDH, 306324N
Tween-20	Sigma, P7949
IGEPAL CA-630	Sigma, I3021
Proteinase K	Sigma, P2308

Glycine	Sigma, G7403
Formamide	Merck, K36952408
tRNA (RNA from yeast)	Roche, 109223
Blocking Reagent	Roche, 11096176001
Heparin lithium salt, (Porcine Interstinal mucosa)	Sigma, H08078
CHAPS	Sigma, C3023
SDS (Sodium dodecyl sulfate)	Severn, 30-33-50
Anti-Digoxigenin-AP Fab fragments	Roche, 11093274910
NBT (4-Nitro blue tetrazolium chloride)	Roche, 11383213001
BCIP (5-Bromo-4-chloro-3-indolyl-phosphate)	Roche, 11383221001
Polyvinyl alcohol	BDH, 297914D
TEA (Triethanolamine)	BDH, 103704U
Acetic anhydride	BDH, 100022M
50x Denhardt's	
1% (w/v) Ficoll 400	Sigma, F4375
1% (w/v) Polyvinylpyrrolidone	BDH, 436032C
1% (w/v) Bovine Serum Albumin	Sigma, A9647
50% Dextran sulphate	Chemicon, 0702051849

2.4.2 Transformation of plasmid DNA to competent *E. Coli* cells

Approximately 1.0 µg of plasmid DNA were carefully added to 50 µl gently thawed *E.coli* DH5α competent cells. The mixture was then gently placed on ice for 30 minutes to allow the DNA to be adherent to the bacterial cell. The bacteria were then heat shocked by incubation for 60 seconds in a water bath at 42ºC, followed by a 2 minutes' incubation on ice. 450 µl of Luria-Bertani-medium (LB-medium) was added to the mixture and then incubated at 37ºC for 1 hour. 100 µl of the mixture was streaked on a LB-agar plate containing 100 µg/ml ampicillin. The plates were left at room

temperature for 10 minutes and then inverted before incubating O/N at 37ºC. The next day a single clone was used to inoculate LB-medium for maxiprep plasmid isolation.

2.4.3 Plasmid amplification and isolation

A single *E.coli* colony was selected from a LB-agar plate and inoculated into either 4 ml (mini-preparation) or 250 ml (maxi-preparation) of LB-medium with the addition of a plasmid specific antibiotic. The LB-medium containing the plasmid DNA was incubated with agitation at 37°C O/N. A small quantity of plasmid DNA was isolated using Fast Plasmid® Mini Kit following manufacturer instructions (mini-preparation). Large quantities of plasmid DNA was isolated and purified using DNA purification columns from QIAGEN Plasmid Maxi Kit following manufacturer's instructions (maxi-preparation).

2.4.4 DNA quantification

Plasmid DNA concentration was measured by spectrophotometer (BioPhotomer, Eppendorf AG, 22331) measuring absorbance at a 1:100 dilution of the DNA samples at 260 nm.

2.4.5 DNA template preparation for synthesis of anti-sense probes

2.4.5.1 Linearization of plasmid DNA

To make the anti-sense probes, 20 µg of plasmid DNA containing a specific gene sequence was digested using an appropriate restriction enzyme (Table 2.9) in the reaction mixture listed below (Table 2.10). The reaction was incubated at 37ºC for 2 hours. 1 µl of linearized DNA product (corresponding to 400 ng of linearized DNA) and an equivalent quantity of unlinearized DNA were then loaded onto a 1% agarose gel to confirm the completion of the digestion.

Table 2.9: Details for plasmids used for making anti-sense probe

Gene	Vector	Size of insert	Digestion Enzyme	Polymerase Enzyme	Manufacturer
Alk5	Psk Bluescript	0.551kb	BamH1	T3	Source bioscience
BCor	pT7T3-Pac	1.6 kb	XhoI	T3	Source bioscience
Dkk-1	pSport1	2 kb	Kpn1	Sp6	Source bioscience
Thy-1	pCMV-SPORT 6	2.3 kb	Kpn1	T7	Source bioscience
Ring1	PT7T3D-Pac1	1.5 kb	Pac1	T7	Source bioscience
Shh	pBluescript	2.6 kb	EcoR1	T7	Source bioscience
Gli-1	Bluescript	1.7 kb	Not1	T3	Source bioscience
Ptc-1	pBluescript	1 kb	BamH1	T3	Source bioscience
Celsr1	pBluescript	0.7 kb	EcoR1	T3	Source bioscience

All plasmids were confirmed by DNA sequencing; anti-sense probes were confirmed by checking sizes on agarose gel and peoforming ISH on positive tissues according to journal articles.

Table 2.10: Reagents for linearizing plasmid DNA (per reaction)

Reagents	Volume
Bovine serum albumin (10 µg/µl)	0.5 µl
Plasmid DNA (Table 2.9)	20 µg
Restriction enzyme	2 U/ µg plasmid DNA
10x Buffer	5 µl
Nuclease-free H2O	Up to final volume (50 µl)

2.4.5.2 Purification of linearized plasmid DNA

A QIAquick Gel Extraction Kit was used to purify linearized plasmid DNA following manufacturer instructions once complete digestion was confirmed by running the whole digested DNA on an agarose gel.

2.4.5.3 Synthesis of DIG-labeled RNA probes (DIG-RNA) by *in vitro* transcription

Anti-sense RNA probes were synthesized from each linearized plasmid by adding reagents as outlined in Table 2.11. The reagents were mixed well and incubated at 37ºC with 1µl of the specific polymerase for one hour and then another 1µl of polymerase was added for a further hour. 1µl of the transcribed DNA was used to run on a gel to confirm the production of RNA after the reaction. 2 µl of RNase free DNase was then added to the mixture and incubated at 37ºC for 20 minutes to eliminate the DNA template. Following the DNase treatment, a SigmaSpin™Post-Reaction Clean-Up Column was used to purify the synthesised RNA following manufacturer instructions. The RNA probes were collected and stored at -80ºC for future use.

Table 2.11: Reagents to transcribe a DIG-labeled RNA probe (per reaction)

Reagents	Volume
5x transcription buffer	8 µl
100 mM DTT	4 µl
RNasin (40 U/µl)	1 µl
Linearised plasmid DNA	1 µg
DIG RNA labeling mix	2 µl
Polymerase enzyme (20U /µl)	1 µl
Nuclease-free H_2O	Up to final volume (40 µl)

2.4.6 DIG Whole mount ISH

2.4.6.1 Sample preparation of dig whole mount ISH

PN5 incisors were carefully dissected in cold 1x DEPC PBS and were then fixed in 4% PFA at 4ºC O/N. The fixed teeth were decalcified in 4% EDTA for 5 days at room temperature on a shaker. After decalcification, the tooth samples were thoroughly washed with ice-cold PBST (0.1% Triton X-100 in 1x DEPC PBS) for 5 minutes three times to eliminate residual EDTA. The samples were then dehydrated in a graded methanol series diluted in PBST (25%, 50%, 75%, 90% and 100%), for 30 minutes in each solution and stored at -20ºC until use.

2.4.6.2 Pre-treatment and hybridization of whole tooth samples

Whole tooth samples were rehydrated in a 75%, 50% and 25% methanol/PBT series and washed in PBT for 5 minutes three times at room temperature. The teeth were treated with detergent mix for 3x 20 minutes to permeabilize the tissues. The samples were then refixed in 4% PFA for 20 minutes and washed for 5 minutes three times in PBT at room temperature. Whole teeth were then briefly rinsed in a 1:1 mixture of hybridization solution (Table 2.12) and PBT and followed an immersion in the pre-warmed

hybridization solution at room temperature until they sank. The teeth were then incubated with pre-warmed hybridization solution at 65ºC for at least 1 hour. In hybridization step, the teeth were incubated with pre-warmed hybridization solution containing 0.1 µg of DIG-labeled RNA probe per ml of hybridization solution with gentle rocking at 65ºC O/N.

Table 2. 12: Hybridization solution (for whole mount ISH)

Components	Volume
Formamide	5 ml
20X SSC (3 M NaCl 0.3 M sodium citrate, pH 4.5)	2.5 ml
Blocking Reagent (10 %)	2 ml
10 mg/ml tRNA	1 ml
0.5 M EDTA, pH 8	100 µl
50 µg/µl Heparin	10 µl
10 % Triton X-100	10 µl
10 % CHAPS	100 µl

2.4.6.3 Post-hybridization washes and detection of the probes

After the hybridization step, unbound probe was re-collected and the samples were washed with pre-warmed washing solution (50% formamide, 1x SSC pH 4.5 and 0.1% Tween 20) four times for 30 minutes at 65ºC on a rocking plate. The samples were then briefly rinsed in a 1:1 mixture of washing solution and MABT solution (100 mM maleic acid pH 7.5, 150 mM NaCl and 0.1% Tween 20) at 65ºC, followed by three washes of MABT for 5 minutes each and then another two 30 minute washes at room temperature. Next the teeth were blocked with 2% blocking reagent in MAB (100 mM maleic acid, pH 7.5 and 150 mM NaCl) for 1 hour at room temperature and then with 2% blocking

reagent and 20% sheep serum in MAB for another 2 hours at room temperature. The probe was detected by incubating the samples O/N at 4ºC with alkaline phosphatase (AP)-conjugated anti-DIG antibody in a 1/2000 dilution of MAB with 2% blocking buffer and 20% sheep serum. The following day, the samples were washed six times in MABT for 1 hour each at room temperature and washed O/N at 4ºC in MABT on a shaker.

Before the colour development step, the teeth samples were immersed in freshly made NTMT solution (100 mM Tris-HCl pH 9.5, 50 mM $MgCl_2$, 100 mM NaCl and 0.1% Triton X-100) for 10 minutes four times at room temperature. The samples were then incubated in the dark with 1 µl/ml 4-Nitro blue tetrazolium chloride (NBT) and 1 µl/ml 5-Bromo-4-chloro-3-indolyl-phosphate (BCIP) in NTMT at room temperature with gentle shaking. Colour precipitates (bluish-purple) were produced at the sites of the target RNA by chemical reaction of NBT and BCIP substrates with alkaline phosphatase. The progress of the reaction was monitored periodically and the reaction was stopped by washing with NTMT and PBT for 10 minutes each. The whole teeth were then fixed and placed in PBT O/N at 4ºC, photographed directly using Leica. DFC300 FX microscope for whole mount or Zeiss Axioskop2 plus microscope for vibratom sections.

2.4.6.4 Vibratome sectioning

Before vibratome sectioning (Leica VT 1000S), fixed samples were rinsed briefly in 1x PBS and then embedded in the desired orientation in pre-warmed 20% gelatin by using plastic disposable moulds. The gelatin blocks were solidified O/N at 4ºC before they were fixed and then kept in 4% PFA for a week. Subsequently, gelatin blocks containing the sample were fixed onto a metal block holder with super glue for sectioning. Sections (50 µm thick) were collected from 1x PBS bath with a brush and

transferred to slides. The slides were mounted with coverslips using an aqueous mounting reagent. The mounted slides were cleaned to remove excess mounting agent before taking photographs using a Zeiss Axioscop microscope.

2.4.7 DIG-section ISH

2.4.7.1 Pre-treatment and hybridization of tissue on sections

All the solutions used in the experiment were DEPC-treated and autoclaved. RNase-free glassware, slide racks and metal spatulas were wrapped up in foil and baked O/N at 180ºC. The slides bearing paraffin sections were firstly de-paraffinised twice with histoclear for 10-15 minutes each, followed by rehydration through a graded ethanol solutions: 100% (2 minutes twice), 95% (2 minutes twice), 70% (2 minutes twice) and 1x PBS (10 minutes twice). Next, to permeabilise the tissues the sections were incubated in 10 µg/ml Proteinase K in 1x PBS at 37ºC for 10 minutes. The sections were then incubated in 2 mg/ml glycine in 1x PBS at room temperature for 10 minutes to block the protease and rinsed with 1x PBS for 5 minutes followed by a re-fixation in 4% PFA for 20 minutes at room temperature. Sections were acetylated for 10 minutes in a solution (25 ul acetic anhydride 10 ml 0.1 M Triethanolamine). At the end, the sections were finally washed with 1x PBS for 5 minutes three times before hybridization to remove the remaining positive charges in the tissue.

To perform hybridization, the sections were incubated in pre-warmed hybridization solution (Table 2.13) and placed horizontally on glass rods in chambers with tissue towels soaked in 50% formamide and 5x SSC at room temperature for 1 hour. Approximately 25 ng/ml of DIG-labeled RNA probe in hybridization solution was denatured by heating at 90 ºC for 3 minutes immediately followed by 3-minute incubation on ice before being applied it to the slides. About 200 µl of probe diluted in hybridization solution was applied to each slide and covered with a glass coverslip. The

chambers were sealed with cling film to maintain humidity in the box. The incubation was performed at 70ºC O/N in a hybridization oven.

Table 2.13: Hybridization solution (for DIG-section ISH)

Components	Volume
Formamide	5 ml
1 M Tris-HCl pH 7.6	0.5 ml
10 mg/ml tRNA	1 ml
50x Denhardt's solution	1 ml
50% Dextran sulphate	5 ml
5 M NaCl	6 ml
10 % SDS	1.25 ml
0.5 M EDTA, pH 8	100 µl
Nuclease-free H_2O	1.25 ml

2.4.7.2 Post-hybridization washes and signal detection

To visualize the signal, firstly, the cover slips were removed by dipping in pre-warmed 5x SSC solution after hybridization. Then sections were washed in 2x SSC solution with gentle rocking at 70ºC for 1 hour to remove unbound probes. Next the slides were equilibrated in TBS buffer (100mM Tris-HCl and 150mM NaCl) at room temperature for 5 minutes. Secondly, the sections were blocked with 0.01% blocking reagent in TBS for 1 hour at room temperature and then incubated in a 1: 5000 dilution of an anti-DIG antibody coupled with alkaline phosphatase in TBS blocking buffer O/N at 4ºC. Lastly, on the following day, the sections were washed in TBS 5 minutes three times followed by incubation in freshly made NTMT solution for 5 minutes at room temperature. The colour of the signal (bluish purple) was developed in the dark at room temperature by

incubating the sections with 2.5 µl/ml NBT and 1.7 µl/ml BCIP in a basic solution (50% Polyvinylalcohol, 100 mM Tris-HCl pH 9.5, 100 mM NaCl, 5mM $MgCl_2$ and 0.1% Tween20). When a strong purple colour was achieved in the tissue the reaction was stopped by rinsing slides in the NTMT solution and 1x PBS for twice each. The slides were air-dried and mounted with cover slips using a DePex mounting medium and photographed afterwards as pre-described.

2.5 Optical projection tomography (OPT)

2.5.1 Reagents and solutions

Agarose, low gelling temperature	Sigma, A9414-100G
Folded filter papers	Whatman
Benzyle Benzoate	Sigma, W213810
Magnetic moulds	Bioptonic
Bioptonic scanner 3001	Bioptonic

2.5.2 Method

After ISH, the teeth samples were washed 3 times for 5 minutes each in PBS and embedded in supporting blocks of 1% low-melting point agarose. This agrose block afterward was attached on a magnetic mount with a cyanoacrylate adhesive (super glue) and trimmed with a sharp blade to give a smooth surface with many facets, leaving a few millimetres of agarose around the teeth samples. The agarose blocks containing samples were dehydrated in 4 changes of 100% methanol each for half a day. Samples turned opaque after dehydration and were subsequently placed in a histological 'BABB' (a mixture of 2 parts of benzyl benzoate to 1 part benzyl alcohol) for a few hours to make them transparent that optically match the refractive index of cell membranes. In the last step before scanning, the scanning microscope was aligned using the alignment

pin. Then the samples stuck to the mount were inverted and attached by magnetism to the rotating plate above the cuvette in the OPT microscope. In the end, the scanning was controlled using Skyscan scanner software.

2.6 Micro computerised tomography (Micro-CT) analysis

Adult mouse heads were fixed for 1 day and washed in 1x PBS for 3 times to remove fixation solution and then scanned using a GE Locus SP micro-CT scanner by Dr. Christopher Healy. Briefly, mouse heads were immobilised using ultrasound gel and cotton gauze and scanned to produce 14 μm voxel size volumes. After scanning, Microview software programme (GE) was used for visualisation and analysis. In this study, the two-dimensional (2D) images were obtained from micro-CT cross-sectional images parallel to the long axis of the mouse teeth. The three-dimensional (3D) reconstructions were obtained by creating three-dimensional isosurfaces of the mouse teeth.

2.7 Cytospin

Mouse cells were obtained from the dental pulp tissue of mouse incisor and resuspended in 2% BSA. A single chamber cytospin device was assembled according to the Cytospin instruction manual. 0.2 ml of diluted cell suspension was applied into the chamber and centrifuged slide at a setting of 6 (20g) for 6 minutes, then the slide was immediately fixed in 4% PFA for 5 minutes and for immunostaining.

2.8 Cell culture

2.8.1 Reagents and solutions

Dulbecco's Phosphate Buffered Saline (DPBS)	Sigma, D1408
Trypsin-EDTA solution	Sigma, T4049
Culture dish (center-well organ culture dish)	Falcon, 353037
MF-Millipore membrane (0.1 μm)	Millipore, VCWP02500
0.4-μm cell culture membranes	Becton Dickinson, 35–3090
Alpha MEM Eagle w/ UGln1 and nucleosides	Lonza-BE02-002F
L-Glutamine	Sigma, G7513
Fetal bovine serum (FBS)	Sigma, F7524
Penicillin-Streptomycin solution	Sigma, P0781
Dimethyl sulfoxide (DMSO)	Sigma, D8418

2.8.2 Method

Cells were collected immediately after the mice used in the experiment were sacrificed. Using sterilized instruments, both upper and lower incisors were dissected out from the jaws by gently removing the mucosa and the bone shell covering them. The dental pulp was then removed from the incisors by pressing it gently with a curved needle in sterilized PBS. The dental pulps were kept on ice during operation. Subsequently the dental pulp tissue was cut into small pieces using a sharp sterilized blade and digested by TypleE for 15-30 minutes in a small tube at 37°C. After checking the completion of digestion, the reaction is stopped by adding FBS. Cell suspension then centrifuged at 1200 (rcf) for 5 minutes at 4ºC to get the cell pellet which was then resuspended in medium and went for filter, cells were centrifuged at 1200 (rcf) for 5 min at 4ºC again to get the cell pellet and re-suspended in an adequate amount of medium to undergo cell

counting before being transferred to a 6 well culture plate (100,000 per well) in CO_2 incubator at 37°C. This passage was defined as passage 0 and later passages were named accordingly. The culture medium was then changed twice a week. The cells were passaged and trypsinized by Trypsin/EDTA once the cultured cells reach 70% confluency. All medium was removed and cell monolayer was washed with sterilized PBS X 3. 1-5 ml Trypsin was added to digest cells for 5-8 minutes at 37°C. When cells were half detached, an equal amount of medium containing serum was added to stop the effect of Trypsin. Cell suspensions were centrifuged at 1200 (rcf) for 5 minutes at 4ºC to get the cell pellet. Next the cell pellet was suspended in an adequate amount of medium and cells were re-plated a split ratio 1:2.

2.9 Flow cytometry

2.9.1 Reagents and solutions

Blocking buffer

Fetal Bovine Serum (FBS)	Lonza, DE14-801F

2.9.2 Method

For fresh tissue samples, the collection of cells was the same as the cell culture described above. Cells were re-suspended in medium and went for staining according to the following protocol:

The cell pellet was re-suspended in FACS blocking buffer at a density of $5x10^3$ cells/ml, 0.5 µg of conjugated antibodies or primary antibodies (Table 2.14) was added to cell suspension and incubated in dark at 4˚C for 30 minutes. Then the antibody was washed off using the blocking buffer and centrifuged at 1200 (rcf) for 5 minutes at 4ºC to get the cell pellet. For the un-conjugated antibodies, the cell pellet was re-suspended again

in blocking buffer and the secondary antibody (0.5-1.0 µg) was added to the cells and incubated for the same time and conditions for primary antibody. Then the secondary antibody was washed three times using the blocking buffer and centrifuged as mentioned to get the cell pellet. Subsequently, the cell pellet was re-suspended in 4% PFA for 10-15 minutes at room temperature then washed with PBS and centrifuged to get the cell pellet which was re-suspended and kept in 1x PBS until acquisition and analysis. FACs data was acquired using BD FACSCanto II flow cytometer and analyzed using BD FACSDiva version 6.1.3. Each flow cytometry analysis was replicated three times.

Table 2.14: Antibodies and their optimal dilution used in flow cytometry

Gene	Dilution	Gene Localization	Manufacturer
Anti-Thy-1 (CD90)- FITC conjugated antibody (Mouse monoclonal)	1:2000	Cell Surface	Abcam
Anti-Ring1b antibody (Rabbit polyclonal)	1:2000	Nucleus	Abcam
Mouse IgG2bk isotype control FITC	1:2000	Cell Surface	Abcam
Anti-EdU antibody (Mouse monoclonal)	1:2000	Nucleus	Abcam
Anti-GFP antibody (Rabbit polyclonal)	1:2000	Cell Surface	Abcam
DAPI (4',6-Diamidino-2-Phenylindole, Dihydrochloride)	1:10000	Nucleus	Life technologies

2.10 Microarray samples preparation

For fresh tissue, dental pulp cells were collected immediately after the mice used in the

experiment were sacrificed. The dental pulp tissues were collected as described above. RNA was extracted using RNeasy mini kit (Qiagen) according to the manufacturer's instructions. For cells from fluorescence activated cell sorting (FACs), cells were homogenized in a denaturating buffer (RNeasyLysis buffer, RLT) that contains guanidine thiocyanate, which instantly inactivates RNases to ensure the purification of intact RNA. 70% Ethanol was then added to provide appropriate binding conditions to the silica-based membranes of the spin columns. RNA Wash buffer (RW1) and RNA pre-elution buffer (RPE) were then added to the columns, which were then spun in the microcentrifuge at 10,000 rpm. RNA was eventually eluted in 20-50 µl of RNase-free water and sent for analysis. (GeneChip® Mouse Genome 430 2.0 Array Affymetrix, Inc. Santa Clara, CA, USA). Microarry results were followed up with qPCR.

2.11 Real-time quantitative PCR

2.11.1 RNA extraction

Dental pulp tissue was obtained as described above. Then total RNA was isolated from dental pulp tissues by using RNeasy micro Kit (Qiagen) following the manufacturer's recommended protocol.

2.11.2 cDNA synthesis

cDNA were made by using the reverse transcription system (promega) as Table 2.15 shows. RNA, primer and RNase free water were added to a 1.5 ml tube up to 14 µl then incubated on a heat block for 5 minutes at 70˚C and put on ice for another 5 minutes. The leftover solution was prepared at the same time and mixed with the previous solution briefly. The whole reaction was incubated at room temperature for 10 minutes and then transferred to a 50˚C heat block for 50 minutes. Synthesized cDNA was then

applied for real-time PCR. The rest of the cDNA can be kept at -20˚C for long-term storage.

Table 2.15: Reagents used for cDNA synthesis (25µl)

Components	Volume
RNA	1 mg
Primer (Random primer)	2 µl
RNase free water	Up to14 µl
5x Reaction Buffer (MMLV-RT)	5 µl
Dntp (10mM)	1.25 µl
MMLV RT	1 µl
RNase free water	3.75 µl

2.11.3 Result analysis

Analysis of the qPCR results was performed by the standard curve method, house-keeping gene GAPDH was used for normalization as previous studies have shown its constant expression in the dental pulp tissue. Distilled water was always used as a negative control, 5 ng of cDNA per reaction was used to detect the expression levels of interested genes. Table 2.16 shows the qPCR program. Primers are listed in table 2.17.

Table 2.16: Program of qPCR

Cycle	Temperature	Duration
Deactivation	95˚C	10 minutes
*Denaturation	95˚C	15 seconds
*Annealing	60˚C	30 seconds
*Extention	72˚C	30 seconds

*Step repeated in 40 cycles in order

Table 2.17: Sequence of the primers

Gene	Left	Right
Ring1b	L agccgagactcgccatatt	R ctgcacagcctgagacattt
Thy1	L gaaaactgcgggcttcag	R ccaagagttccgacttggat
BcoR	L gaactgtatgcagattccagtca	R actgtcctcttgtaatccttcca
GDF11	L acagacctggctgtcacctc	R actcgaagctccatgaaagg
ALK5	L cagctcctcatcgtgttgg	R cagaggtggcagaaacactg
Ctnna2	L ggagctccaatcgggagt	R gctgcctggatgagtgatg
DKK1	L ccgggaactactgcaaaaat	R ccaaggttttcaatgatgctt
Jagged1	L gaggcgtcctctgaaaaaca	R acccaagccactgttaagaca
Jagged2	L tcctcctgctgctttgtgat	R ttgcagggctgaaagacac
Notch1	L ctggaccccatggacatc	R aggatgactgcacacattgc
Notch2	L tgcctgtttgacaactttgagt	R gtggtctgcacagtatttgtcat
Notch3	L agctgggtcctgaggtgat	R agacagagccggttgtcaat
Notch4	L ggacctgcttgcaaccttc	R cctcacagagcctcccttc
Dll1	L gggacagaggggagaagatg	R cacaccctggcagacagat
Dll4	L aggtgccacttcggttacac	R gggagagcaaatggctgata
Furin	L ctgaggaggccttctttcg	R cctgaggcccagacaaag
Jak2	L aagattgccaaggccaga	R tgttgttccagcactctgtca
Egfr	L ttggaatcaattttacaccgaat	R gttcccacacagtgacacca
Stat3	L ggaaataacggtgaaggtgct	R catgtcaaacgtgagcgact
Tcf3	L cgcagaccaaactgctcat	R gggttcaggttgcgttctc
Wdr12	L gctgaagttgcggaccttagta	R ggaaatcaaactcgacatgct

Chapter 3 : Characterisation of the Dental Pulp MSC Niche in the Continuously-Growing Mouse Incisor

3.1 Introduction

In rodents such as mice, the incisors are able to grow throughout the animals life. The continous growth of their incisors needs to be maintained by a reservoir of stem cells to form epithelial ameloblasts and mesenchymal odontoblasts (Harada et al., 1999, Feng et al., 2011). Studies have shown dental pulp pericytes in the mouse incisor contributing to the incisor growth and repair along with the well-studied ameloblast forming epithelial stem cells in the cervical loop (Feng et al., 2011). However, this contibution is limited. Thus, besides pericytes, there may be other stem cell population(s) in the dental pulp mesenchymal tissue. However the precise location (stem cell niche) of these stem cells and their identity are yet unknown.

Interestingly, molecular techniques have provided clues about the stem cell niche and identified potential markers for dental stem cells (Harada et al., 1999). One of the important characteristics of stem cells in adult tissues is that adult stem cells (slow cycling cells) divide infrequently to preserve their long-term proliferation potential. However, some adult stem cells must also be able to continually produce progeny (fast cycling or transit-amplifying cells, TA cells) that rapidly differentiate in organ development and after injury (Fig. 3.1). Thus, nucleotide chase experiments allow us to identify the location of the mouse incisor mesenchymal stem cell niche by labeling fast and slow cycling cells through thymidine analogue labeling strategy.

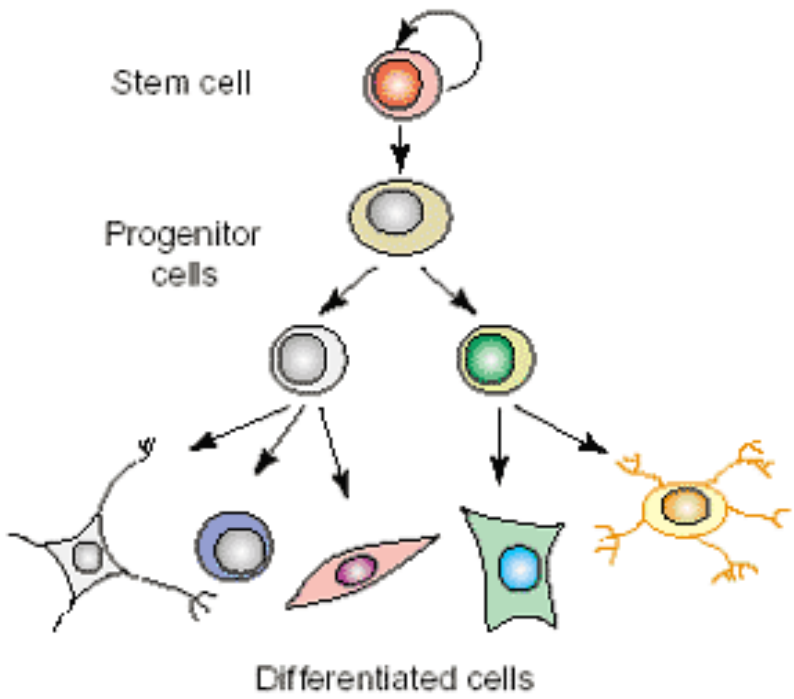

Fig 3. 1: Asymmetric differentiation of adult stem cells.

As adult stem cells proliferate in the stem cell niche, both stem cells themselves and progenitor daughter cells are produced. Stem cells are able to keep existing at a low proliferate rate to maintain a stable size of stem cell population in tissue while progenitor cells proliferate quickly and further differentiate into different types of cells needed in the tissue and organ (Diaz-Flores et al., 2006).

BrdU is a thymidine analogue that can be incorporated into the newly synthesized DNA of replicating cells (during the S phase of the cell cycle), thus BrdU labeled cells can be used to reflect cell proliferation in the mouse incisor dental pulp tissue. By short exposure to BrdU (single pulse injection to mouse), fast cycling cells can be identified as they are more easily to be labeled with BrdU. Unlike fast cycling cells with a high proliferation rate, the slow cycling cells divide infrequently for stem cells maintenance. Only after long exposure to BrdU (consecutive BrdU injection to mice) can slow cycling cells be labeled as well as all other dental pulp cells. After a long “wash time” slow cycling cells can be identified since all other cells have quickly diluted their BrdU labeling over many cell divisions. By performing these BrdU labeling experiments, the locations of fast cycling cells and slow cycling cells can be identified, respectively. Inspired by the BrdU incorporation method, sequential incorporation of different

thymidine analogues (CldU and IdU) into adult mice incisors was developed to better elucidate the locations of the slow and fast cell populations during mouse incisor growth. Consequently, slow cycling cells labeled with IdU and fast cycling cells labeled with CldU can be detected by immunofluoresent staining in the same incisor sample and provide a clue regarding the location of MSC niche in mouse incisor dental pulp tissue.

Furthermore, for long-term maintanance of stem cells in adult tissue, a population of long-term "quiescent" cells is required to maintain stem cell population (Haug et al., 2008). Once stem cells are required they can provide a source for new stem cells to avoid stem cell depletion. Thus, identification of the location of these long-term quiescent cells in a mouse incisor would add more information about the location of MSC niche. To detect the existence of quiescent cells in the mouse incisor, a thymidine analogues label-retaining experiment is the best choice. However, the quiescent cells hardly divide after tissue formation, thus, a strategy to label tooth cells in the embryonic stage when tissue formation begins by giving consecutive IdU to mice from E10.5 before embryo tooth germs begin forming until birth was developed. By this way we were able to identify quiescent cells in the mouse incisor after a long wash time for all other cells to dilute labeling. In addition, a recent research in hematopoietic stem cells (HSCs) has identified a group of long-term quiescent cells that expressing noncanonical Wnt signaling member Flamingo exist in a specialized niche in adult bone marrow tissue (Sugimura et al., 2012). This finding provides a possibility to identify quiescent cells in mouse incisor by investigating Flamingo expressing cells.

Lastly, MSCs in the mouse incisor proliferate and differentiate into the dentin forming odontoblasts. The investigation of cell fate is of importance to identify stem cell population. The *Cre/loxP* site-specific recombination system has emerged as an important tool to trace cell fate by conditionally controlling reporter gene activation or inactivation in almost any tissue of the mouse. In the *Cre-loxP* system, Cre recombinase

is expressed under the control of a tissue- or a cell-specific promoter in one mouse line (Feil et al., 2009). In the following study, to add inducibility to *Cre-loxP* system, a CreERT2 recombinase was developed. This CreER recombinase can be activated by the synthetic estrogen receptor ligand tamoxifen, therefore allowing for external temporal control of Cre activity. When that line was crossed with a second mouse line carrying a reporter gene that is flanked by a *loxP-STOP-loxP* (‘‘floxed’’ STOP) sequence, progeny animals expressing both constructs were made. In these progeny animals, external tamoxifen enable Cre to excise the STOP sequence to produce reporter. Tracing these reporters durting organ development and growth, researchers are able to investigate cell fate of certain cell type.

In our study, an mT/mG double-fluorescent reporter mouse line (*R26R mT/mG*) was used to provide reporter gene. This mouse line has a membrane-targeted tdTomato/ membrane-targeted eGFP system in which tdTomato is expressed before a Cre-mediated recombination event whereas eGFP is expressed after the event (Muzumdar et al., 2007). Thus, mating with a $pCAG^{ERT2}$ *Cre* mouse line that can activate Cre in all cells by external tamoxifen, progeny $pCAG^{ERT2Cre}$*; R26R mT/mG* mice enable temporal control of the fluorescence gene expression by converting membrane-targeted tandem dimer Tomato (mT) to membrane-targeted green fluorescent protein (mG) (Fig. 3.2).

pCAG^{ERT2cre} mice X Rosa26$^{mT/mG}$ mice

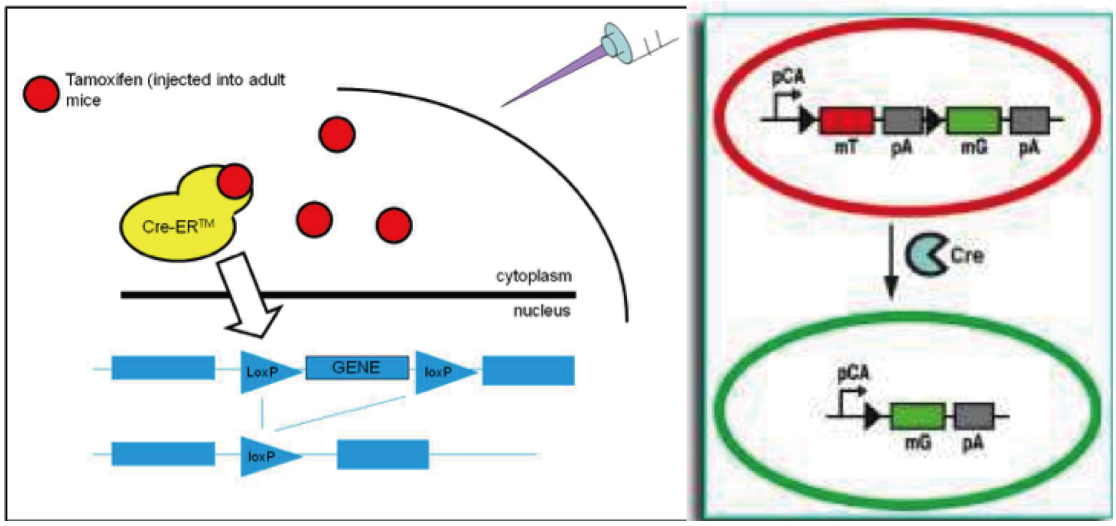

Fig 3. 2: Effect of Tamoxifen when injected into inducible *pCAG^{ERT2Cre}; R26R mT/mG* mice.

With a Tamoxifen injection, CreER is translocated into the nucleus where recombination occurs between *Cre* and *Loxp* sites leading to the expression of membrane-targeted green fluorescent protein instead of the expression of tandem dimer Tomato without Cre.

In summary, in order to better understand the properties of MSCs and their role in the growth of the mouse incisor, clear identification of the MSC populations and the microenvironment in which they exist is obligatory. Thus, the aim of this chapter is to identify slow cycling, fast cycling as well as long-term quiescent cell populations to characterise the potential MSC niche area and stem cell populations in the mouse incisor mesenchymal tissue, using several different approaches.

3.2 Results

3.2.1 Identification of fast and slow cycling cells localization in mouse dental pulp

To locate the fast and slow cycling cells, BrdU chase experiments were performed on adult CD1 mice. Mice were divided into two groups: single BrdU injection group and constant BrdU injection group. In the single pulse BrdU injected group, mice (n=3) were collected each time 2, 8, 24 hours after BrdU injection. The ICH results showed that after 2 hours chase time, the labeled cells were located in the area adjacent to the cervical loop (Representive picture, Fig. 3.3 B), while after 8 hours, labeled cells were more dispersed (Fig. 3.3 C). 24 hours later, more BrdU labeled cells were found in the apical end except a vacancy between cervical loops (Fig. 3.3 D). These results suggested the fast cycling cells were located in the area adjacent to the cervical loop. In the constant BrdU injection group, 3 weeks after BrdU injection, mice (n=3) were collected and examined at two time points each time from 1 day to 64 days. The detection of BrdU showed that 1 day after BrdU incorporation, almost all the cells in the mouse incisor were labeled with BrdU (Fig. 3.3 E), while 2 days after BrdU injection, cells located adjacent to the cervical loop have lost BrdU labeling, which suggested a high proliferation rate of these cells (Fig. 3.3 F). 32 days and 64 days later, BrdU labeling was continously reduced and only existed in the area between cervical loops (Fig. 3.3 G, H), which suggested a slow cycling cell population in this area. Taken together, results using BrdU incorporation confirmed that two cell populations with different proliferation rates exist in the apical end of the mouse incisor, with the slow cycling cells being located in the area between cervical loops and fast cycling cells being located more distantly (Fig. 3.4). All experiments were repeated 3 times under the same conditions.

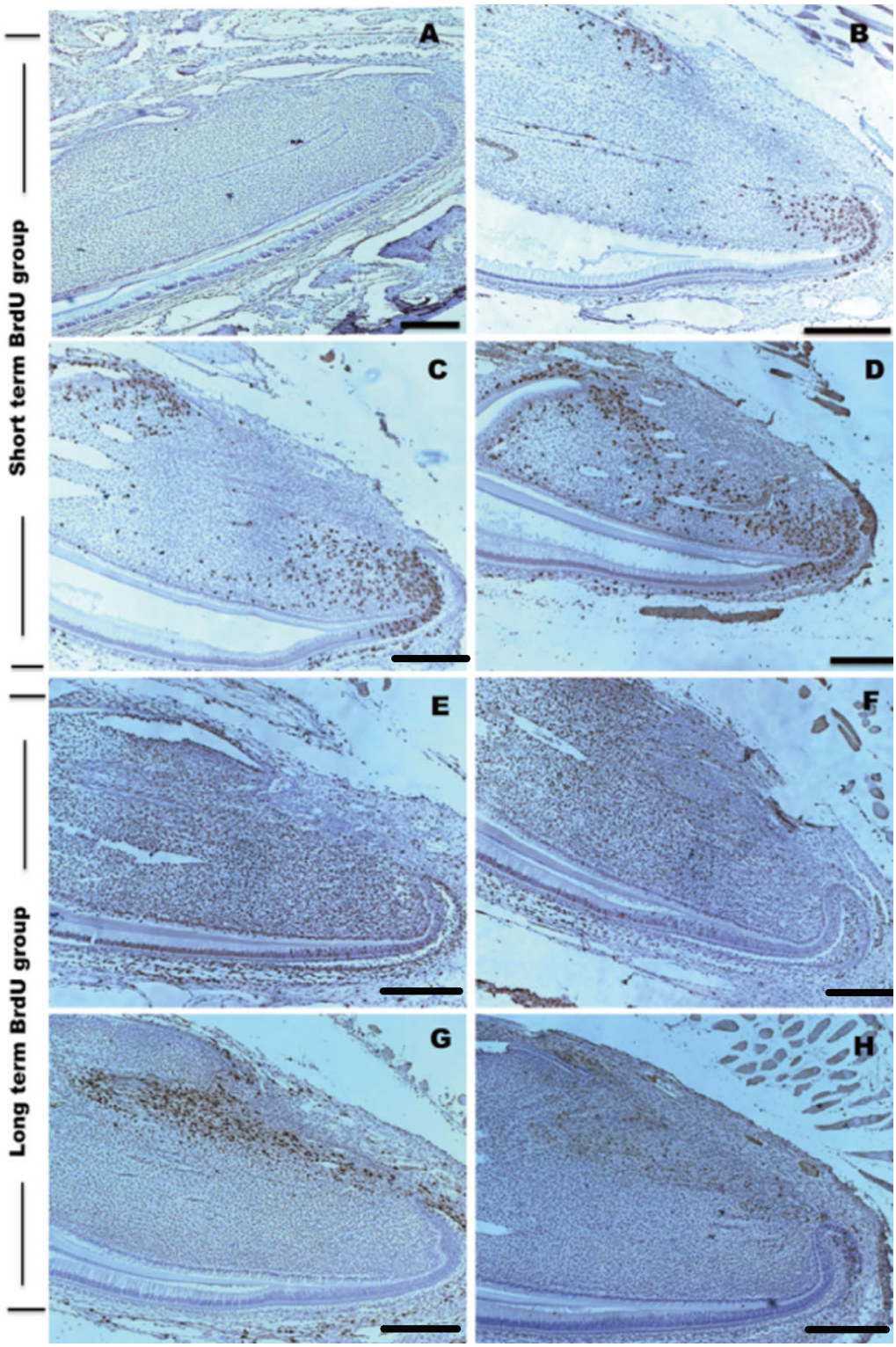

Fig 3.3: BrdU chase experiments in mouse incisor dental pulp.

(A-D) Short term BrdU chase experiments: (A) Control group, before BrdU injection. (B) 2 hours after BrdU injection, labeled cells were located in the area close to the cervical loop. (C) 8 hours after BrdU injection, more labeled cells produced. ((D) 24 hours after BrdU injection, BrdU labeled cells were more dispersed in the apical end of mouse incisor. (E-H) Long-term BrdU injection results: (E) 1 day after 3 weeks BrdU injection, all the cells were labeled. (F) 2 days after 3 weeks BrdU injection, cells in the area next to the cervical loop firstly lost their labeling. (G) 32 days after 3 weeks BrdU injection, labeled cells only were located in the area between two cervical loops. (H) 64 days after 3 weeks BrdU injection, more cells lost their labeling. All samples from different mouse showed similar results. Scale bars = 500 µm in (A, D). Scale bars =750 µm in (B C, E, F, G, H).

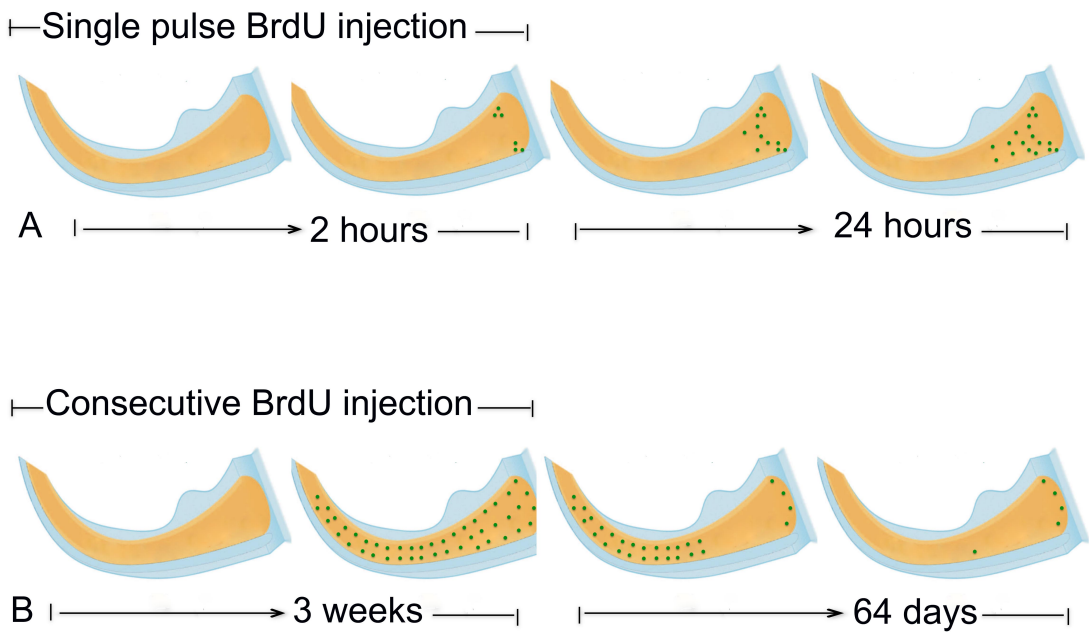

Fig 3. 4: Schematic diagram of BrdU incorporation and chase experiments in mouse incisor.

(A) Short term BrdU chase experiment: Single pulse BrdU was injected to mice, BrdU incorporation was chased from 2 hours after BrdU injection to 24 hours after. BrdU labeling cells were located in the area close to the cervical loop. (B) Long-term BrdU chase experiment: Consecutive BrdU was injected to mice, BrdU incorporation was chased from 1 day after BrdU injection to 64 days after. BrdU labeling was first seen in all the dental pulp cells. 1 day after consecutive BrdU injection, cells in the area close to the cervical loop firstly lost their labeling. 64 days after consecutive BrdU injection, only cells in the area between cervical loops still had their labeling.

To better elucidate the locations of the slow and fast cell population during mouse incisor growth, IdU was administered to mice (n=5) for 3 weeks to allow all the dental pulp cells including slow cycling cells labeled by IdU. After 30 days "wash time" when all other cells except slow cycling cells have lost their labeling, single pulse CldU was given to these mice to label the fast cycling cells, then mice were sacrified to examine both slow cycling cells labeled with IdU and fast cycling cells labeled with CldU in the incisor dental pulp tissue. The results of IdU and CldU double incorporation showed a similar pattern detected by the BrdU chase experiments in all 5 mice: slow cycling cells were mainly in the area between two cervical loops of the mouse incisor while fast cycling cells disperse more distally. (Fig. 3.5 A). Co-incorporation of IdU and CldU (Fig. 3.5 A', A'') was also observed in some cells suggested that the slow cycling cells at the point of transition into fast cycling cells. To further confirm that the cells close to

the cervical loop area were fast cycling cells, cell proliferation was analyzed using immunostaining with a PH3 antibody that detects cells undergoing mitosis. Immunostaining showed that the locations of mitotically active cells (Fig. 3.5 B) were consistent with the BrdU labeling of fast cycling cells (Fig. 3.5 C), thereby confirming a mitotically active area of cells distal to the slow cycling cells.

Taken together, these experiments showed that a special niche that consisting of slow cycling cells (stem cells) and a fast cycling cell (TA cells) was located in the apical end of mouse incisor.

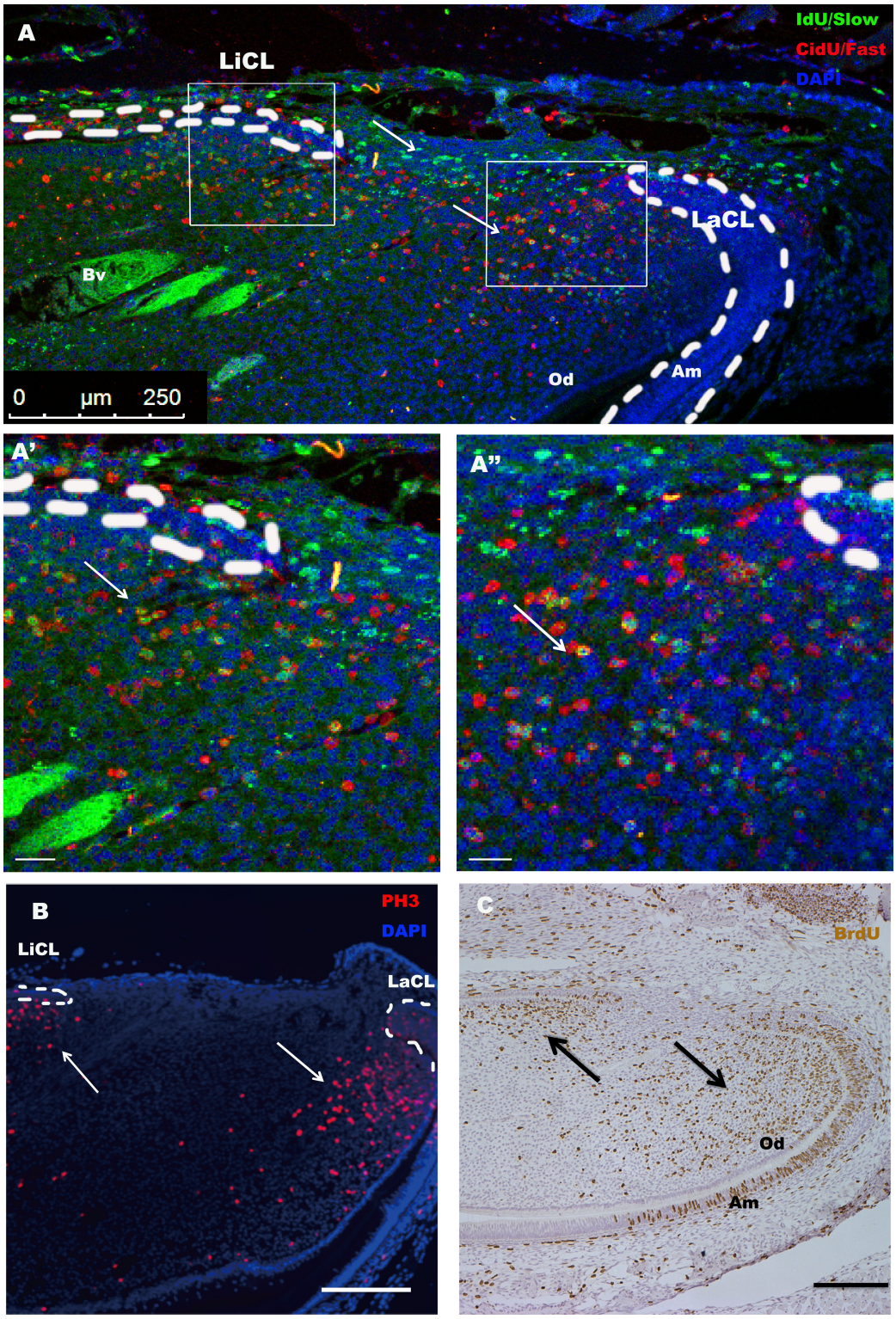

Fig 3. 5: Immunostaining results of fast and slow cycling cells.

(A) Slow cycling cells (IdU+, green) were detected in the dental pulp mesenchymal tissue between cervical loops while the fast cycling cells (CldU+, red) were located more distally. (A', A'') High magnification of dashed area in (A) showed the co-localization of IdU and CldU in some cells (arrows) were located between IdU+ and CldU+ cells boundary at the apical end of mouse incisor. (B) PH3+ cells (mitotic cells) showed the same location pattern as fast cycling cells in the development of mouse incisor. (C) BrdU labeling indicated that highly proliferative cells were located predominantly in the dental mesenchyme near labial and lingual cervical loops and in also the TA cells of the dental epithelium. Abbreviation: BV, blood vessel; OD, odontoblast; Am, ameloblast; LiCL: lingual cervical loop; LaCL, labial cervical loop. Scale bars=25 µm in (A', A''). Scale bar = 150 µm in (B). Scale bar =250 µm in (C).

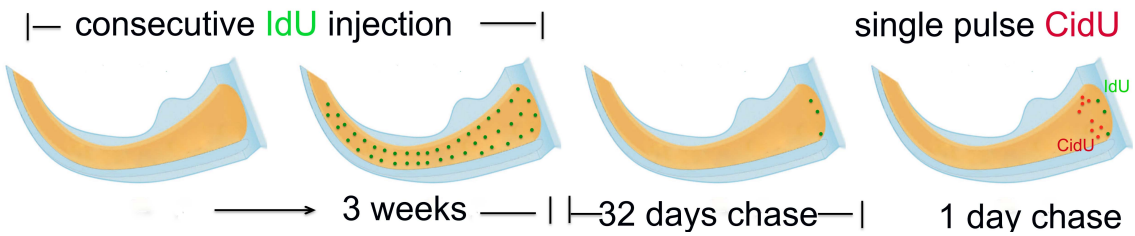

Fig 3. 6: Schematic diagram of IdU and CldU incorporation and chase experiments in mouse incisor.

Consecutive IdU was injected to mice for 3 weeks to label all dental pulp cells, after 32 days wash time, only slow cycling cells still kept IdU labeling, then single pulse CldU was injected to mice. 1 day after CldU injection, mice were collected and examined, showing dual labeling of CldU and IdU in the mouse incisors.

Furthermore, experiments showed that the label-retaining cells (LRCs) were detected in several areas in the mouse incisor after a 32 day chase period, including the cervical loop, apical end mesenchyme and pericytes (Fig. 3.7 A). In the labial cervical loop, a well-studied stem cell niche, LRCs were detected in the labial cervical loop among the stellate reticulum cells, close to the basal epithelium (Fig. 3.7 B'). In addition, LRCs were also detected in the outer enamel epithelia that give rise to enamel producing cells, ameloblasts (Fig. 3.7 B'), suggesting LRCs in our experiments were epithelium stem cells. In the mesenchymal tissue, a subset of LRCs were detected in the middle of the dental pulp rich in blood vessels (Fig. 3.7 C, C'). Here a stem cell niche harboring pericytes that differentiate into specialised odontoblasts during tooth growth and in response to damage *in vivo* has been reported (Feng et al., 2011). Another LRC population was detected in the area between the cervical loops (Fig. 3.7 B, B'') that suggested a potential MSCs source in this area contributing to the development and growth of the mouse incisor.

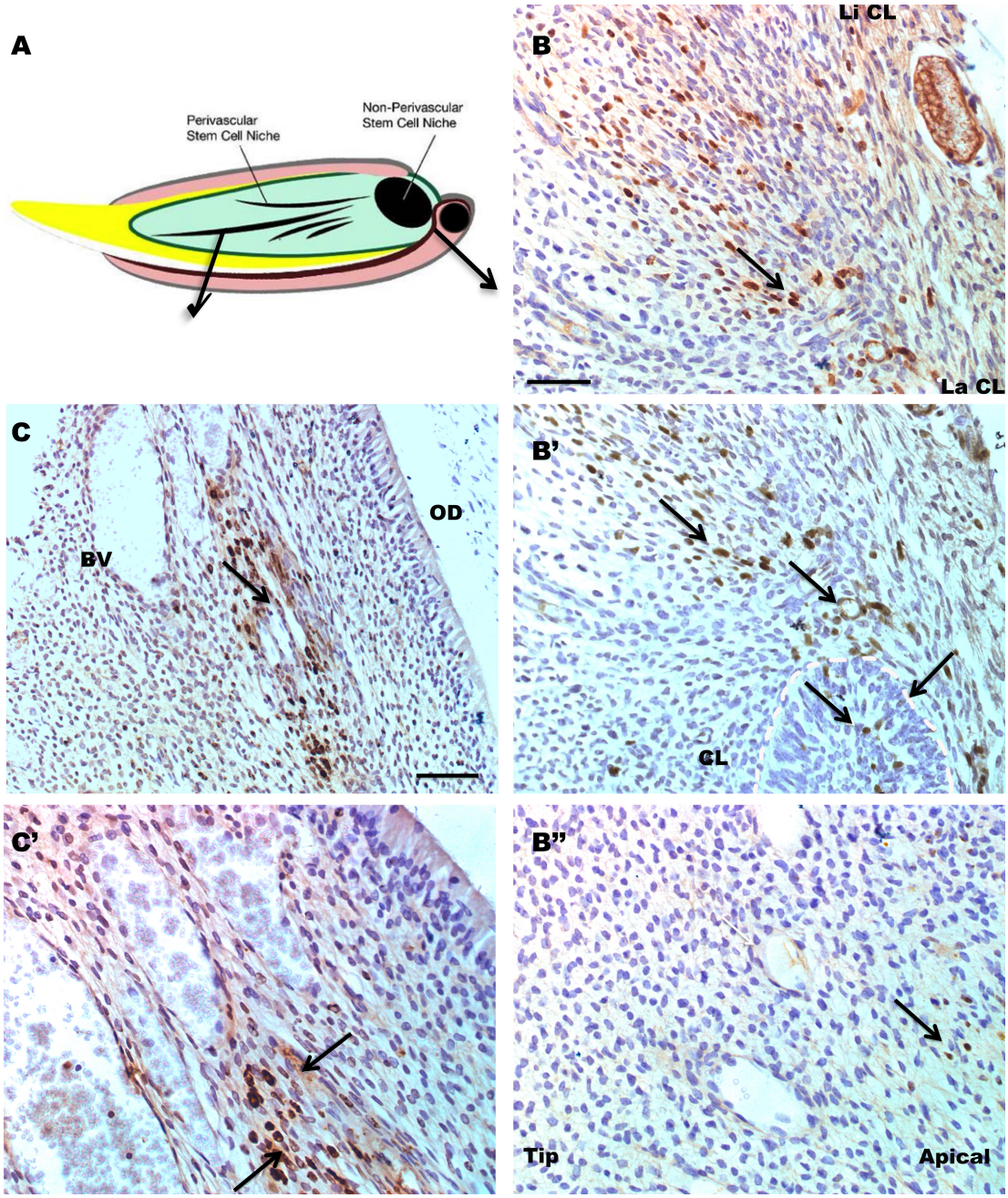

Fig 3. 7: Slow cycling cells/LRCs in mouse incisor dental pulp.

(A) Schematic of stem cells populations in the dental pulp: perivascular stem cell niche, epithelium stem cell niche (labial cervical loop) and the putative mesenchymal stem cells niche at the apical end of mouse incisor dental pulp (Feng et al., 2011). Accordingly, arrows in (B-C) show LRCs in these stem cell niches respectively. Arrows in (B, B', B'') showed LRCs were located in the labial cervical loop and close mesenchymal tissue; Arrows in (C, C') showed LRCs were located in the perivascular area close to blood vessel (BV). Abbreviation: OD, odontoblasts; CL, cervical loop; LiCL, lingual cervical loop; LaCL, labial cervical loop. Scale bars= 50 µm in (B, B', B'' and C'). Scale bar = 100 µm in (C).

3.2.2 Analysis of fast cycling cells and slow cycling cells

To further analyze the fast cycling and slow cycling cell populations, adult incisor dental pulp cells were collected and analyzed by flow cytometry following EdU

labeling. EdU is a replacement of BrdU that allows the use of mild conditions to access the DNA incorporation without requiring DNA denaturation (typically using HCl, heat, or digestion with DNase). In our study, the incisor pulp cells of 6 adult mice were collected and analyzed. This experiment were repeated 3 times. EdU+ (LRCs) cells from 42 days after long-term EdU injection were considered as slow cycling cells (stem cells) while EdU+ cells from 24 hours after a single EdU injection were considered as fast cycling cells (TA cells) in the mouse incisors. Flow cytometry analysis results showed that approximately 17.8±2.1% pulp cells were EdU+ from the fast cycling cell group while only 4.3±1.5% incisor dental pulp cells were EdU+ / LRC cells (Fig. 3.8). This suggested a small number of slow cycling cells and a relatively larger number of fast cycling cells in mouse incisor dental pulp tissue. More importantly, the numbers of fast cycling cells and slow cycling cells were correlated with the results of immunostaining on sections. Approximately 20% pulp cells were fast cycling cells while 5% pulp cells were slow cycling cells. Cells that neither slow cycling cells nor fast cycling cells (approximately 75%) were considered as descendants of fast cycling cells which contributed to the growth of whole dental pulp tissue.

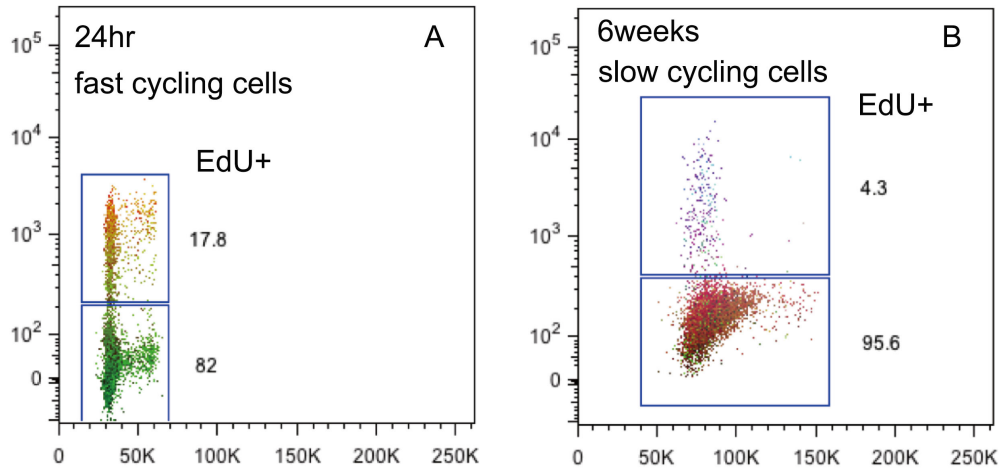

Fig 3. 8: FACS analysis of fast cycling cells and slow cycling cells in the mouse incisor dental pulp.

17.8% EdU+ pulp cells were detected in fast cycling cells group (A) in comparison to 4.3% EdU+ cells in slow cycling cell group (B).

3.2.3 Identification of quiescent cell localized in the mouse dental pulp

To identify these specialized quiescent cells in the mouse incisor, a quiescent cell marker in HSCs niche, Celsr1, was investigated in incisor dental pulp tissue. ISH was used to detect Celsr1 mRNA expression in PN5 mouse incisor, result showed that Celsr1 mRNA was expressed in the outer region of the incisor mesenchyme between two cervical loops. Immunostaining results further confirmed that result: a small number of flamingo homolog Celsr1+ cells were located in the outer region of the incisor dental pulp mesenchyme adjacent to the dental follicle. In addition, to detect the existence of quiescent cells in the mouse incisor, two rounds of label-retaining experiments were performed. Howerer, different incorportation strategies need to be used to label the quiescent cells since these quiescent cells hardly divide after tissue formation but can be only labeled in the embryonic stage when tissue formation initiates. Thus, consecutive IdU was given to mice (n=10) from E10.5 before embryo tooth germs began forming until birth; consecutive CldU was administrated to the pups until PN30, followed by a 30 day wash prior to sacrifice to label the slow cycling cells. Immunostaining results of IdU and CldU labeling also revealed that a very small number of quiescent cells (IdU+) proximal to the slow cycling cells (CldU+) were located in the outer region of the incisor dental pulp where Celsr1+ cells located (Fig. 3.9). Taken together, these results suggested the existence of a quiescent cell population in the apical end of mouse incisor mesenchymal tissue.

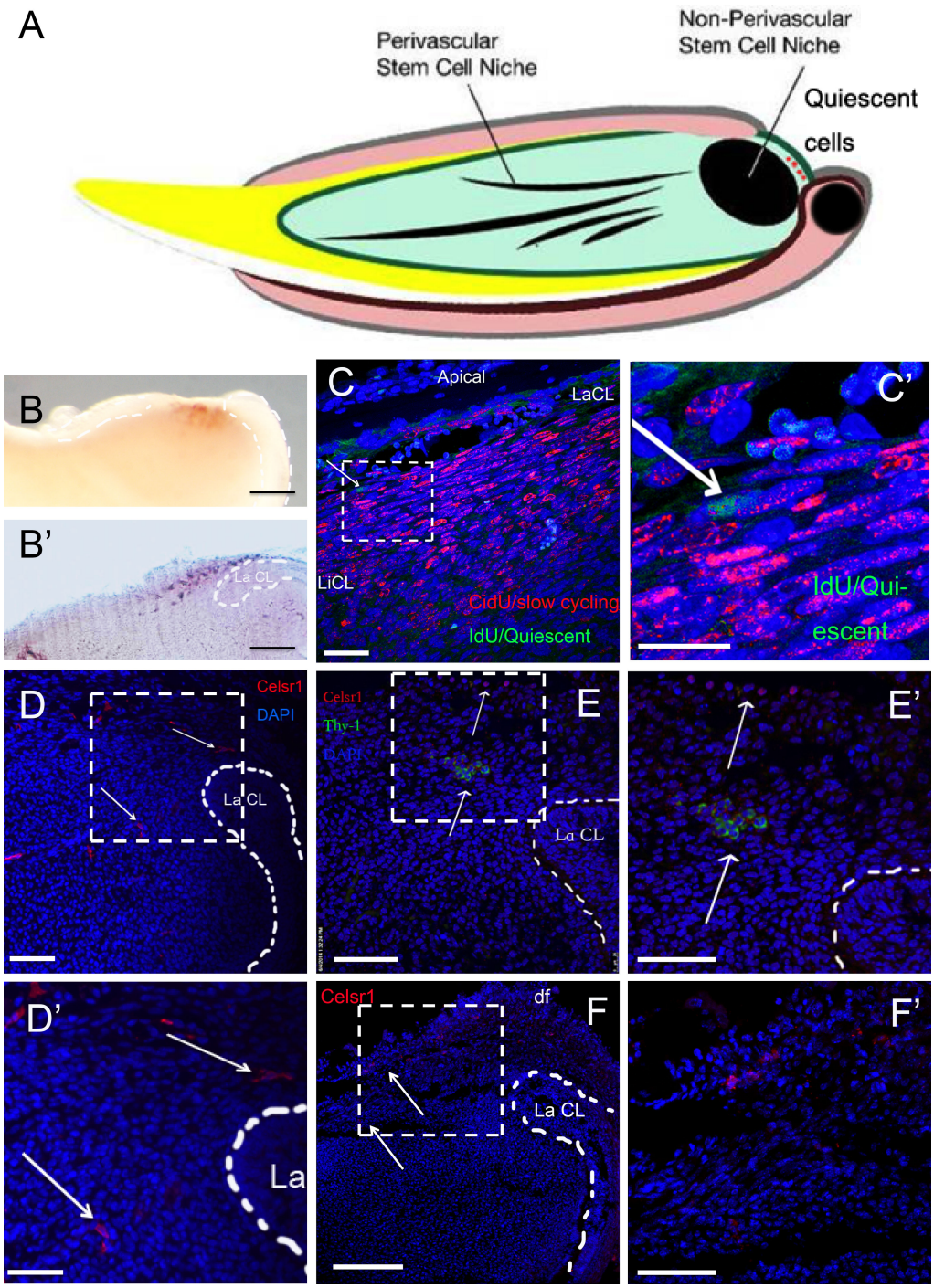

Fig 3. 9: Location of quiescent cells in the mouse incisor dental pulp.

(A) Diagram of quiescent cell location. (B, B') whole mount ISH in PN5 incisor and ISH on section showed that Celsr1 was detected in the area between cervical loops. (C) Arrow show quiescence cells (IdU, green) were located on the approximal of slow cycling cells (CldU, red) which are mainly concentrated on the area between cervical loops. (C') High magnification of dashed box in (C). (D, D') Arrows showed immunostaining of Celsr1: Celsr1+ cells were observed in the apical end of mouse incisor dental pulp. (E) Arrows show Celsr1+ cells (red) and Thy-1+ cells (green) in incisor dental pulp tissue. (E') High magnification of dashed box in (E'). (F, F') Arrows show Celsr1 + staining in dental pulp mesenchymal cells adjacented to dental follicle. Antibody was checked on bone morrow as positive control and no signal was detected in negative control (result is not shown). Abbreviation: df, dental follicle, LaCL, labial cervical loop. Scale bar in B and F, indicates 500µm. Scale bar = 100 µm in (B, D, E,E',F'). Scale bar =25 µm in (C). Scale bar=10 µm in (C'). Scale bar=50 µm in (D').

3.2.4 Investigation of prospective stem cells and their role in the development of mouse incisors

To locate and trace the stem cell population, a *pCAG*^{ERT2Cre}*; R26R mT/mG* mouse line was generated in our study. In this mouse line, all cells including dental pulp cells can express GFP upon tamoxifen injection. Once all the cells are GFP+ and all non- stem pulp cells are lost at the tip as mouse incisors grow continuously, only stem cells will retain and keep producing TA cells. Thus after a period of time that is long enough for a complete repopulation of the tooth pulp and odontoblasts all GFP+ cells will be stem cell derived. In our study, mice (n=12) were divided into 2 groups (6 in high dose tamoxifen group and 6 in low tamoxifen group). Experiments were repeated 3 times under the same condition. Results showed that 3 days after high dose tamoxifen adminstration which was enough to activate Cre/loxP system in all the cells, all dental pulp cells were GFP+ including odontoblasts and ameloblasts in all samples (Fig. 3.10 B). This result confirmed the effectiveness of ubiquitous *pCAG*^{ERT2}*Cre* and that all dental pulp cells can be activated under the control of *pCAG*^{ERT2} Cre. While rather interestingly, after 3 weeks chase time, when most pulp cells have migrated out the incisor, a larger number of cells in the mouse incisor dental pulp still contained GFP (Fig. 3.10 C). These cells formed a large cell stream starting from apical end to the middle of incisor suggested the existence of stem cell population at the apical end of mouse incisor keep producing TA cells. However, this cell stream could consist of several stem cell progeny populations. How an individual stem cell evolves in the growth of mouse incisor is still not clear. Thus, in our low tamoxifen group, a low dose of tamoxifen was given to *pCAG*^{ERT2Cre}*; R26R mT/mG* mice to activate GFP expression to identify individual stem cell and its progeny populations. Low dose tamoxifen is not enough to activate Cre recombination in all the incisor dental pulp cells, but can randomly activate dental pulp cells to express GFP. If an individual stem cell was

activated among dental pulp cells, when all other pulp cells have been lost from the tip, only this stem cell will stay and produce TA cells with GFP expression. Thus, a stem cell and its progeny cell population would be identified in the mouse incisor. Our results from low dose tamoxifen group showed that most of our samples that received low dose tamoxifen adminstrations show GFP expression on random cells as we expected. In these samples, GFP was randomly expressed by individual cells in dental pulp tissue 3 days after the adminstration of tamoxifen (Fig. 3.10 D). 1 week after the low dose tamoxifen adminstration, cell clones and streams were observed in some of our samples (Fig. 3.10 E, E', Fig. 3.11). These cells have migrated to the middle of incisor which confirmed the effectiveness of our incisor model, however, unfortunately they were no MSCs in these samples. Luckily, in one of our samples, a very small GFP+ cell clone was found located at the apical end of the mouse incisor mesenchyme 3 weeks after tamoxifen adminstration suggesting the existence of individual GFP-producing cells that keep proliferating and giving rise to dental pulp cells at the apical end of mouse incisor. This mesenchymal cell clone contained about 20 cells that contribute to the formation of odontoblasts (Fig. 3.10 F, F''). If this clone was from a single stem cell, they need roughly 4 rounds of cell division to reach this number that may present a pattern of how a single mesenchymal stem cell behaves and contributes to the formation of odontoblasts in the mouse incisor dental pulp. In addition, a GFP+ cell clone was found in the epithelium close to the epithelium stem cell niche cervical loop (Fig. 3.10 F'), suggesting the effectiveness of *pCAG*^{ERT2Cre}*; R26R mT/mG* mice in detecting stem cell progeny. In summary, the study in *pCAG*^{ERT2Cre}*; R26R mT/mG* mice suggested the existence of prospective stem cells at the apical end and individual stem cell and their progency can be followed in the mouse incisors.

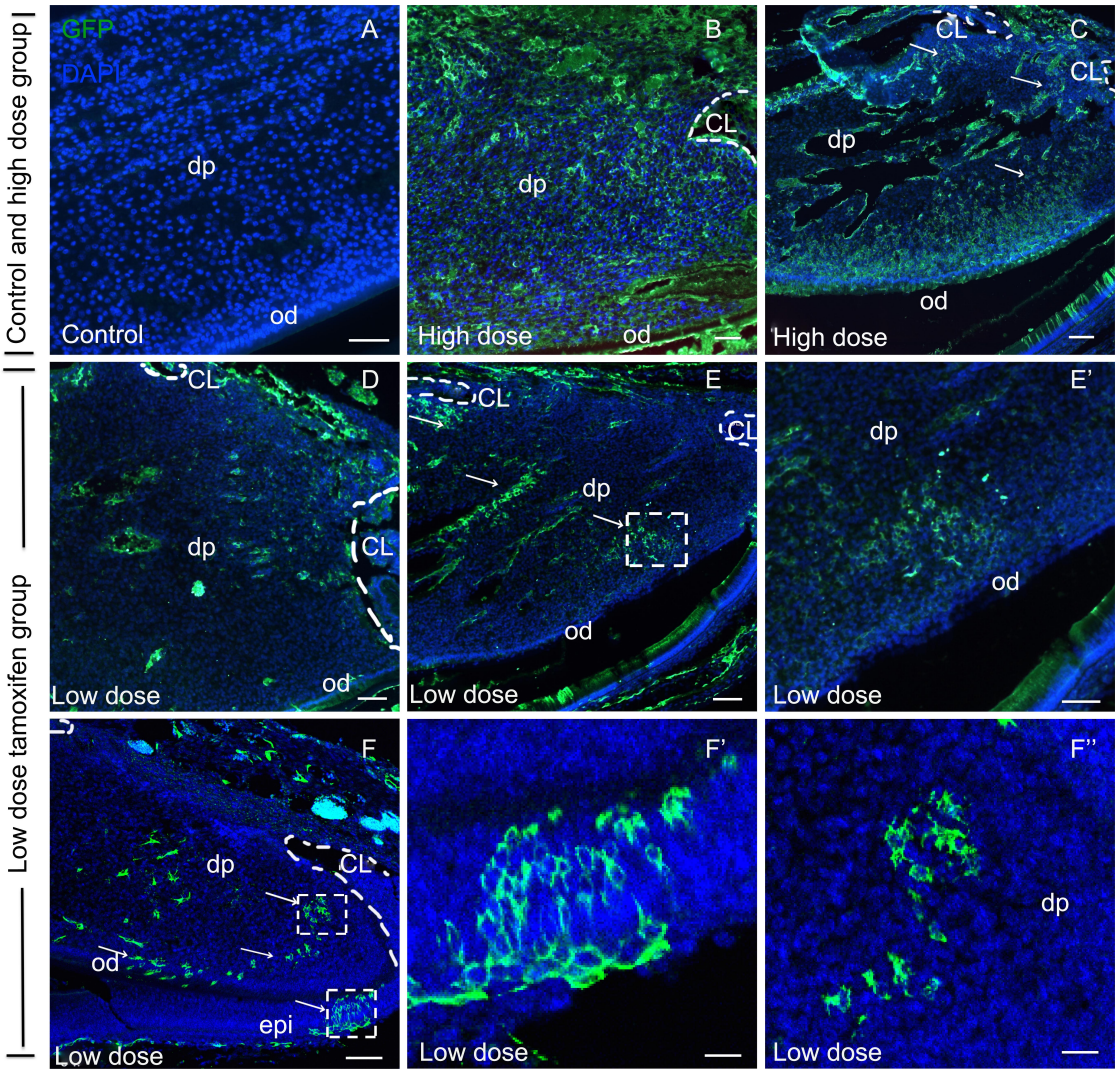

Fig 3. 10: Label perspective stem cells and their progeny population in *pCAG^{ERT2Cre}; R26R mT/mG* mouse mandibular incisors (sagittal sections).

(A) Control group, no GFP was expressed in *pCAG^{ERT2Cre}; R26R mT/mG* mice mandibular incisor without tamoxifen administration. (B-E) High dose tamoxifen group: (B) All dental pulp cells were GFP+ 3 days after consecutive high dose tamoxifen injection. (C) Large numbers of dental pulp cells were still GFP+, these cells formed cell stream and gave rise to odontoblasts. (D-F) Low dose tamoxifen group: (D) Few cells were GFP+ 3 days after low dose tamoxifen was given into *pCAG^{ERT2Cre}; R26R mT/mG* adult mice; these labeled cells distributed randomly to the whole dental pulp, no cell clone was observed. (E) Three GFP+ cell streams were observed in the incisor dental pulp 1 week after low dose tamoxifen was given into *pCAG^{ERT2Cre}; R26R mT/mG* adult mice. (E') High magnification of dashed area in (E). (F) GFP+ cell clone was detected 3 weeks after low dose tamoxifen injection. Cells from mesenchymal clone and cells from epithelia clone were detected. (F', F'') High magnification of dashed area in C. Abbreviation: dp, dental pulp cells; od, odontoblasts; am, ameloblasts; epi, epithelia. Scale bar =250 µm in (A, B, C, D, E, F), Scale bar =100 µm in (E'), Scale bar =50 µm in (F', F'').

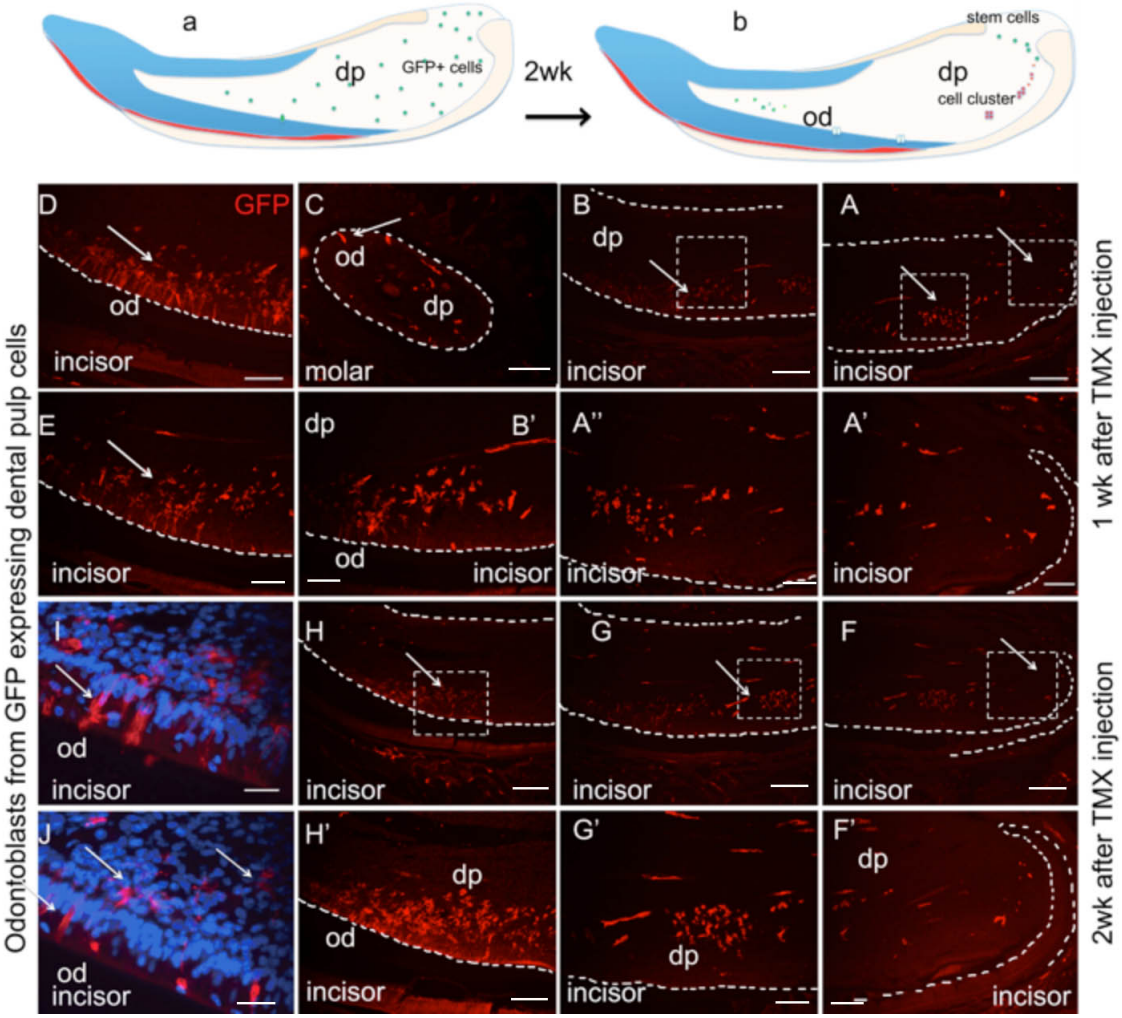

Fig 3. 11: Label perspective stem cells and their progeny population in *pCAG^{ERT2Cre}; R26R mT/mG* mice mandibular incisor (low dose tamoxifen group, Sagital sections).

(a,b): Demonstration of random labeled cells and their fate. (A-C) 1 week after low dose tamoxifen injection: (A) Few cells were detected in the area between cervical loops, however, a cell cluster in the middle of dental pulp tissue was detected (B). (C) Individual odontoblasts cell was observed but no cell cluster was seen in molar. (A'-C') High magnification of dashed area in A and B. (F-H) 2 weeks after low dose tamoxifen injection, few cells existed in the apical end, cell cluster was observed in the middle of pulp. (F'-H') High magnification of dashed area in F-H. (D, E, I, J) High magnification of odontoblasts. Abbreviation: dp, dental pulp cells; od, odontoblasts. Scale bar =100 µm in (A, B, F, G, H). Scale bar =50 µm in (D, E, A'-B', F'-H'). Scale bar =10 µm in (I, J).

3.3 Discussion

3.3.1 Identification of slow and fast cycling cell populations at the apical end of mouse incisors

In adult mice, stem cells reside in specialized physical locations known as niches (Schofield, 1978), which constitutes a three-dimensional microenvironment containing mesenchymal cells, extracellular matrix, molecule signaling and stem cells (Ohlstein et al., 2004). In mouse incisors, extensive studies have been carried out to identify the labial side cervical loop region as a stem cell niche containing an epithelial stem cell population for continuous renewal of dental epithelial components during incisor growth (Harada et al., 1999, Harada et al., 2002). A BrdU incorporation experiment was successfully used to identify LRCs in the cervical loop as stem cells. However, in the incisor dental mesenchyme, the identity of stem cells and stem cell niche are still not well characterized, although MSCs are generally believed to be located in the apical end mesenchyme. Thus, simialr BrdU incorporation experiments described in our study identified a slow cycling stem cell population in the dental pulp mesenchyme region between two cervical loops and a fast cycling cell population distant to this, presenting a specialize region (presumably a stem cell niche) located in the apical end of mouse incisor. Sequential incorporation of different thymidine analogues (CldU and IdU) into incisors of adult mice further confirmed the locations of these two cell populations corresponding to one of the important characteristics of adult stem cells, namely stem cells that divide infrequently to preserve their long-term proliferation potential (slow cycling cells) and their daughter cells (fast cycling or TA cells) which are able to continually produce progeny that rapidly differentiate in organ growth (Diaz-Flores et al., 2006). Besides mouse incisor, slow cycling cells (LRC) in the salivary glands and mouse brain tissue were all found to be stem cells (Furutachi et al., 2015, Zhang et al.,

2014) .In summary, these samilar results in the mesenchyme campare to well studied epithelial stem cell niche strongly suggested a MSC niche is located at the apical end of mouse incisor.

The average eruption rate of the mouse incisor is 365 μm/d, thus, it replaces itself approximately 5-6 weeks (Coady et al., 1967). In our BrdU labeling experiment, several time points were selected. The results showed that 32 days after BrdU injection, most pulp cells at the apical end have renewed. Thus, cells that still retained BrdU labeling were roughly defined as slow cycling cells. In the flow cyctometry analysis, pulp cells were collected and analyzed 6 weeks after EdU injection to allow the repopulation of the whole tooth. The results showed that approximately 5% cells still kept EdU labeling which was consistent with the number of BrdU labeling cells from immunostaining of sections. However, both the numbers of BrdU+ cells from flow cytometry results and the immunostaining results were very crude. The exact number of labeling cells needs to be quantitated in the future. Regarding fast cycling cells, as early as 2 hours after BrdU injection, pulp cells close to the cervical loop were labeled with BrdU suggesting cells in this area were undergoing cell division. In the flow cytometry analysis, 24 hours after EdU injection, 2 rounds of cell cycling were noticed, thus, those cells with EdU before 24 hours were roughly considered to be fast cycling cells. Similarly, the number of fast cycling cells was crude. This needs to be quantitated in the future. However, although our nucleoside labeling experiments did not give exact numbers of fast cycling cells and slow cycling cells, the results successfully presented two cell populations with different proliferation rates and identified their locations which provided a basis for future study.

The identification of slow cycling stem cells and fast cycling cells in the mouse incisor provided an opportunity to study the connection of stem cells and TA cells and how they support the mesenchymal component. The differences in gene expression between

stem cells and TA cells need to be addressed further in future studies. Similarly, how stem cells and TA cells were regulated in the stem cell niche was not clear. This MSC niche micro-environment regulation needs further study. Studies in other organs have provided some clues. For example, evidence from hair follicles showed that emerging TA cells constitute a signaling center that orchestrates tissue growth. Whereas primed stem cells generate TA cells, quiescent stem cells only proliferate after TA cells form and begin expressing Sonic Hedgehog (Shh). Without Shh from TA cells there is not sufficient input from quiescent stem cell generation and the TA cell pool wanes. TA cells are independent of autocrine Shh, but if they can not produce Shh, replenishment of primed stem cells for the next hair cycle is compromised, delaying regeneration and eventually leading to regeneration failure. This finding unveiled TA cells as transient but indispensable integrators of stem cell niche components (Hsu et al., 2014).

3.3.2 Identification of quiescent cells of mouse incisor

Mouse incisors grow continuously throughout their lives. This growth requires stem cells in the mouse incisors to keep providing daughter cells. To prevent these stem cells from depletion, a long-term quiescent cell population is needed. Evidence from adult mice showed that for long-term maintenance of HSCs in bone marrow, a subset of stem cells is kept in long-term quiescence in a specialized niche. Thus, the identification of quiescent cells in the mouse incisor can provide more information of stem cell niche together with the locations of slow cycling cells and fast cycling cells. According to our BrdU labeling experiments, dental pulp cells can be labeled soon after BrdU administration, thus, consecutive IdU given to mice from E10.5 until birth was able to label all tooth germ cells including rarely dividing quiescent cells. As a result, a small number of quiescent cells were identified proximal to the slow cycling cells in the incisor. Unfortunately, technical restriction made it difficult to perform an exact

quantitative analysis, however, this result still described a special area consisting of different cell populations with different proliferation rates further verified our hypothesis that a MSC niche exists at the apical end of mouse incisor. In addition, a study in the HSC niche showed that Flamingo, a protein in noncanonical Wnt signaling, is expressed in and functionally maintains quiescent long-term HSCs (Sugimura et al., 2012). Whether these Flamingo expressing cells exist in the mouse incisor was investigated. ICH and ISH results showed that Celsr1, a homolog of Flamingo expressed in a few cells at the same area of quiescent cell of the apical end of mouse incisor further confirming that a quiescent cell population existed in the mouse incisor. However, due to limited number of these quiescent cells (4-5 per sample), isolation and analysis of these cells has not been successfully performed, more work needs to be done in the future.

3.3.3 Investigation of prospective stem cells of mouse incisor

It remains unclear how MSCs proliferate and differentiate to odontoblasts during the continuous incisor growth. Stem cell studies showed that adult stem cells divide infrequently to preserve their long-term proliferation potential. Yet, TA cells rapidly differentiate in organ development to provide specialized cells. In our genetic lineage tracing experiments with *pCAG*^{ERT2Cre}*; R26R mT/mG* mice, a group of cells were observed in the apical end mesenchyme contributed to the formation of a patch of odontoblasts, it was reasonable to propose that these labeled cells were a stem cell clone which contributed to the formation of odontoblasts. This result further confirmed our hypothesis that incisor MSCs are located in apical end of mouse incisor and contribute to the formation of dental pulp tissue including odontoblasts. In addition, our result also presented a very small cell cluster consisting of approximiately 20 cells in the apical end of mouse incisor. If these cells were from a single stem cell, there were

approximately 4 rounds of cell division before them gave rise to form patch of odontoblasts. However, how stem cell and TA cell act in the stem cell/TA cell production was still unclear in this single colour labeling system. The cell clusters and streams observed in *pCAG*^{ERT2Cre}*; R26R mT/mG* mouse incisors might be formed by different stem cell progeny cells. Questions such as if stem cells are next to each other and how many stem cells stay together cannot be answered due to a lack of evidence. Thus, a new four colour labeling transgenic mouse *pCAG*^{ERT2Cre}*; R26R-Confetti* are expected to identify single stem cell clone and it's progeny in the mouse incisors in future studies.

3.4 Conclusions

In the continuously growing mouse incisor, three cell populations existed in the apical end: slow cycling cells, fast cycling cells and quiescent cells. The slow cycling cells mainly approached the area between the two cervical loops at the apical end of mouse incisor while fast cycling cells were located distally. Furthermore, co-localization of IdU and CldU was also detected in some cells suggesting that these were slow cycling cells in transition to fast cycling cells which supports the theory that adult stem cells hardly divide but produce TA cells. These TA cells divide very fast giving rise to all other progeny cells. Beside the fast and slow cell population, a quiescent long-term cell population marked by Flamingo homologue Celsr1 existed at the apical most end mesenchyme.

In the end, the results of high and low dose tamoxifen injection in *pCAG*^{ERT2Cre}*; R26R mT/mG* mice confirmed the existence of prospective stem cells at the apical end of mouse incisor dental pulp that contribute to the formation of dental pulp tissue. Furthermore, the results also presented an odontoblast formation pattern: a clonal cell cluster consisted of 20-30 cells in the fast cycling cells area that gave rise to a patch of odontoblasts.

In summary, in this chapter we identified a MSCs niche located at the apical end of the mouse inciosr pulp tissue as generally believed.

Chapter 4 : Gene Expression in Dental Stem Cell

4.1 Introduction

It has been suggested by many studies that MSCs at the apical end of mouse incisor dental pulp mesenchyme and the perivascular area, along with epithelium stem cells in the cervical loop contribute to the continuous growth and eruption of mouse incisors which is different from that of molars and all human teeth that lack the ability to grow throughout lifetime (Harada et al., 1999). Results in chapter 3 showed a stem cell population to be located at the apical end of the mesenchyme area between the two cervical loops by series label-retaining and lineage tracing experiments. A gene microarray of previous study in our laboratory has compared gene expression patterns between incisors and molars, the expression of several stem cell genes such as *Crabp1, Hus-1, Ikaros and Thy-1* were identified to be up-regulated in incisors (Mantesso and Sharpe, 2008). Another subsequent microarray compared the gene expression differences between the incisor apical end that contains the stem cells and incisor body dental pulp tissues (Lapthanasupkul and Feng, 2009) (Fig. 4.1). As a result, *Thy-1 gene* showed an obvious up-regulated expression in both microarrays (Fig. 4.2). Since Thy-1 has been used as a marker of stem cells in several tissues such as liver (Petersen et al., 1998), BM (Mayani and Lansdorp, 1994) and epidermis (Nakamura et al., 2006), it was selected as a candidate marker of mesenchymal stem cell of mouse incisors for further investigation.

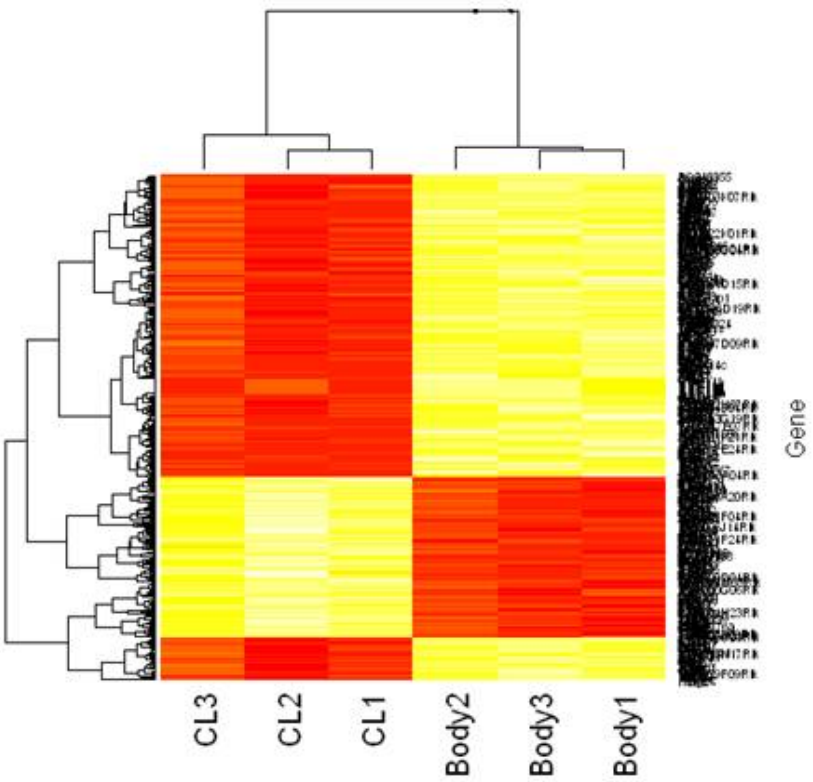

Fig 4. 1: Heatmap of gene expression comparison between the pulp tissues of incisor body (Body) and the cervical loop (CL).

Compared with the expression in the body pulp tissue (Body1-3) (yellow area), genes in the cervical loop area (CL1-3) (red area) were up-regulated. Also fewer genes showed up-regulation in the body samples compared with the cervical loop area. Rows represent genes and columns represent the samples. Genes that fall into one cluster (vertical axis) had a similar behaviour in the experiments. Genes that fall into one cluster (horizontal axis) share the same category. Expression intensities were represented by red and yellow, for high and low intensities, respectively. (Mantesso and Sharpe, 2008.)

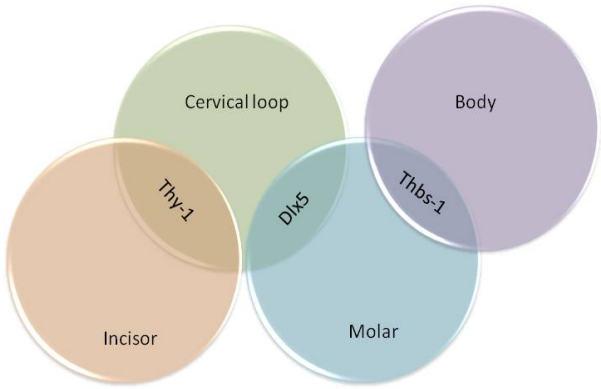

Fig 4. 2: Venn diagram of common genes in stem cell and Body/CL microarrays.

Thy-1 was up-regulated in incisor pulp tissues comparing with molar pulp tissue (Microarray analysis-1 of stem cell genes); Thy-1 was found up-regulated in the cervical loop side pulp when the genetic expression of this area was compared with incisor body areas (Microarray analysis-2**),** while Distal-less homeobox 5 (*Dlx5)* was up-regulated in molar pulp tissues (Microarray analysis-1) and the incisor cervical loop (Microarray analysis-2). Up-regulation of Thrombospondin 1 (*Thbs-1)* in molar pulp tissues (Microarray analysis-1) and the incisor body (Microarray analysis-2) were found.（Lapthanasupkul and Feng, 2009）

Definitive identification of Thy-1 expression in mouse incisor dental pulp stem cells requires lineage tracing. In lineage tracing, a set of labeled progeny cells originate from a single cell carrying marks which can be inherited and thus being traced in the whole tissue (Kretzschmar and Watt, 2012). This method has been widely used to identify adult stem cells (Haegebarth and Clevers, 2009, Joyner and Zervas, 2006, Brumovsky et al., 2014). One of the methods of lineage tracing which is different from exogenous incorporation is genetic recombination, which usually relies on the *Cre-loxP* system, allowing us to trace certain gene expressing cells (Fig. 4.3 a). In our study, two reporter mouse lines (*R26R-Confetti and R26R mT/mG*) were mated with *Thy-1Cre* transgenic mice, where *Cre* is driven by *Thy-1* promoter, to trace Thy-1 expressing cells inside the mouse incisor dental pulp. In *Thy-1Cre* reporter transgenic mice where Cre is expressed, the *loxP*-flanked sequence is deleted and Thy-1+ cells and all their descendants are permanently marked by expression of a specific reporter (Soriano, 1999, Snippert et al., 2010, Muzumdar et al., 2007). By tracing these cell reporters, the location of Thy-1expressing cells and their descendants can be identified.

In order to examine how different cells contribute to the maintenance and repair of a given tissue, multicolor reporter constructs with two or more markers are being used increasingly for lineage tracing (Rinkevich et al., 2011). A widely used reporter system, the ‘‘Brainbow’’ mouse enables combinatorial expression of four different fluorescent proteins in a stochastic manner (Livet, 2007). In the following studies, the Brainbow-2.1 construct was designed to target the Rosa26 locus to make a reporter mouse ubiquitously expressing the construct (Snippert et al., 2010). Researchers have successfully used this reporter mouse to randomly label Lgr5 positive stem cell derived clones within the intestinal crypt with different fluorescence (Fig. 4.3 b). Thus, in addition to mT/mG double-fluorescent reporter mouse line (Fig. 4.3 c) R26R-Confetti reporter mouse line was used to investigate how Thy-1 progeny cells contribute to the

maintenance of a mouse incisor. Not only questions such as how and where Thy-1 cells+ are maintained in mouse dental pulp tissue can be addressed by tracing Thy-1 derived dental pulp cells, but also more importantly, single stem cell clone can be traced as cells in same colour were derived from the same single clone.

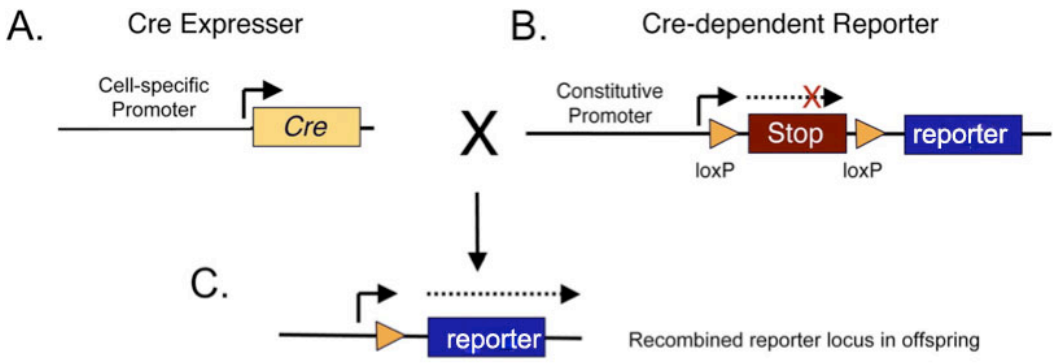

Fig 4.3 (a): Schematic of the Cre/loxp lineage tracing methodology.

(A) Transgenic mice expressing the Cre recombinase under the control of a cell-specific promoter (*Thy1*). (B) Reporter mice with a reporter gene blocked by a constitutively active promoter by transcriptional stop sequences that are flanked by *loxP* sites. (C) Cell specific Cr*e* excise the stop sequences, resulting in transcription of the reporter gene (Lounev et al., 2009).

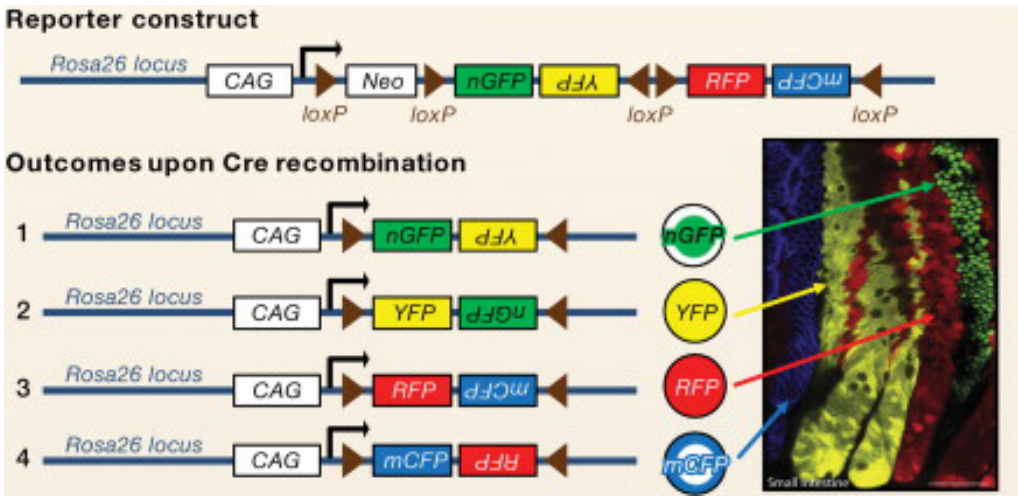

Fig 4.3 (b): Schematic of the possible outcomes of the R26R-Confetti recombination in *Cre/loxp* lineage tracing.

Brainbow-2.1 constructs encoding four fluorescent proteins driven by the strong CAG promoter into the Rosa26 locus (Snippert et al., 2010). Upon Cre recombination, the Neomycin (Neo) cassette is removed and the multicolour construct recombines randomly to result in four possible outcomes with different fluorescent proteins being expressed (image shows clonal expression of the four fluorescent proteins in small intestine, Snippert et al., 2010).

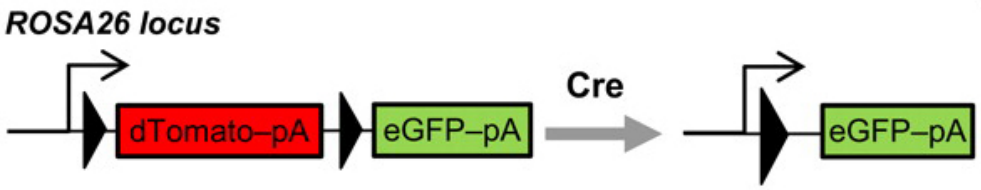

Fig 4. 3 (c): Schematic representation of the effect of Cre recombinase excision on the expression of dTomato and membrane tethered eGFP.

Upon Cre recombination, dTomato is removed and the eGFP fluorescent proteins being expressed.

Besides *Thy-1*, a set of genes that are associated with DPSCs were chosen and detected in the mouse incisor based on a number of criteria to confirm the location of MSC niche. To begin with, targets of major signaling pathways that are active within the putative stem cell niche (Joyner and Zervas, 2006) were investigated. In the mouse incisor, the Hedgehog signaling (Hh) pathway plays an important role in controlling incisor tooth growth. Studies have showed that Hh signaling is required for the continuous generation of ameloblasts in the adult by blocking the Hh pathway *in vivo* using a smoothened inhibitor (Seidel et al., 2010). In a recent study, Gli1 positive Hh-responsive cells were reported as present in both the epithelial stem cell compartment and the dental pulp mesenchyme. More importantly, these Gli1 expressing cells contributes to all mesenchymal derivatives (Zhao et al., 2014). This suggests its function as a stem cell marker in both epithelial and mesenchyme tissue. In addition, Patched, a crucial transmembrane protein in the Hedgehog signaling pathway, was also detected in the incisor dental pulp mesenchyme as it has been strongly suggested that Hedgehog signaling regulates MSCs involved in maintenance and regeneration. Thus, Gli1, Shh and Patched from Hh signaling pathway were selectied for investigation in the study.

The transforming growth factor *beta* (TGF-β) signaling pathway is also involved in the cellular processes of incisor development and growth. TGF-β receptor type I

(Alk5/Tgfbr1) has been reported to regulate tooth initiation in the dental mesenchyme and development of the incisor epithelium since loss of Alk5 in the neural crest tissue resulted in delayed tooth initiation and development (Zhao et al., 2008, Zhao et al., 2011). When Alk5 was deleted specifically in the dental mesenchyme, the expression of Fgf3 and Fgf10 are down-regulated in the mesenchyme, leading to reduced proliferation and fewer LRCs in the cervical loop (Zhao et al., 2011). Next, Dickkopf-related protein 1 (Dkk1), a potent inhibitor of Wnt/β-catenin signaling was investigated. It is known that Wnt/β-catenin signaling in the dental epithelium is critical for dental patterning during multiple stages of early tooth development (Lohi et al., 2010). During embryogenesis, the Dkk1 mediated Wnt inhibition controls the spatio-temporal dynamics of cell fate determination, cell differentiation and cell death. Studies have shown that Axin2 lacZ signal, which reflects the canonical Wnt signaling pathway, was expressed in dental pulp and developing odontoblast cells, but not in ameloblast cells postnatally. This suggested a potential role for canonical Wnt signaling in postnatal tooth formation (Han et al., 2011).

In addition to the important targets of major signaling pathways mentioned previously, Paired box 9 (Pax9) was also chosen to be investigated in the incisor. Pax9 plays an important role in the establishment of the inductive capacity of the tooth mesenchyme. In Pax9-deficient embryos tooth development is arrested at the bud stage, where Pax9 is required for the mesenchymal expression of Bmp4, Msx1 and Lef1 (Peters et al., 1998). In addition to missing teeth, the craniofacial and visceral skeletogenesis is also disturbed in Pax9 deficient mice. This crucial gene is essential for the generation of a pool of taste bud progenitors and to maintain their competence towards prosensory cell fate induction (Kist et al., 2014). Thus it is interesting to locate Pax9 expressing cells in the mouse incisor.

4.2 Results

4.2.1 Investigation of the expression of Thy-1 in the dental pulp of mouse incisors

In chapter 3, the stem cell population was identified to be located at the apical end mesenchyme area between two cervical loops by a series of label-retaining and tracing experiments. Stem cell microarrays by previous studies have also suggested Thy-1 as a candidate stem cell marker for further investigation. To confirm those Thy-1 expressing mesenchymal cells are stem cells of mouse incisor dental pulp, whole mount ISH and immunostaining were performed on PN5 mouse (n=10) incisors, respectively. Results showed that Thy-1 was expressed at the apical end of mouse incisor where the MSC niche is believed to be located. Optical Projection Tomography (OPT) was used to view Thy-1 gene expression patterns in three-dimensions (3D) in which ISH staining was observed in the middle of the cervical loop area of the mouse incisor (movies included in the enclosed DVD). Representative images of the samples from the movie are shown in (Fig. 4.4). In frozen sections of PN5 incisors, immunostaining for Thy-1 showed that individual or small groups of Thy-1 expressing cells were in the mesenchymal tissue between lingual cervical loop and labial cervical loop, while no Thy-1 expressing cells were observed in the mesenchymal tissue close to labial cervical loop or lingual cervical loop. This result suggested a small number of Thy-1+ cells are located in the area between cervical loops (Fig. 4.5 A, B, C, D).

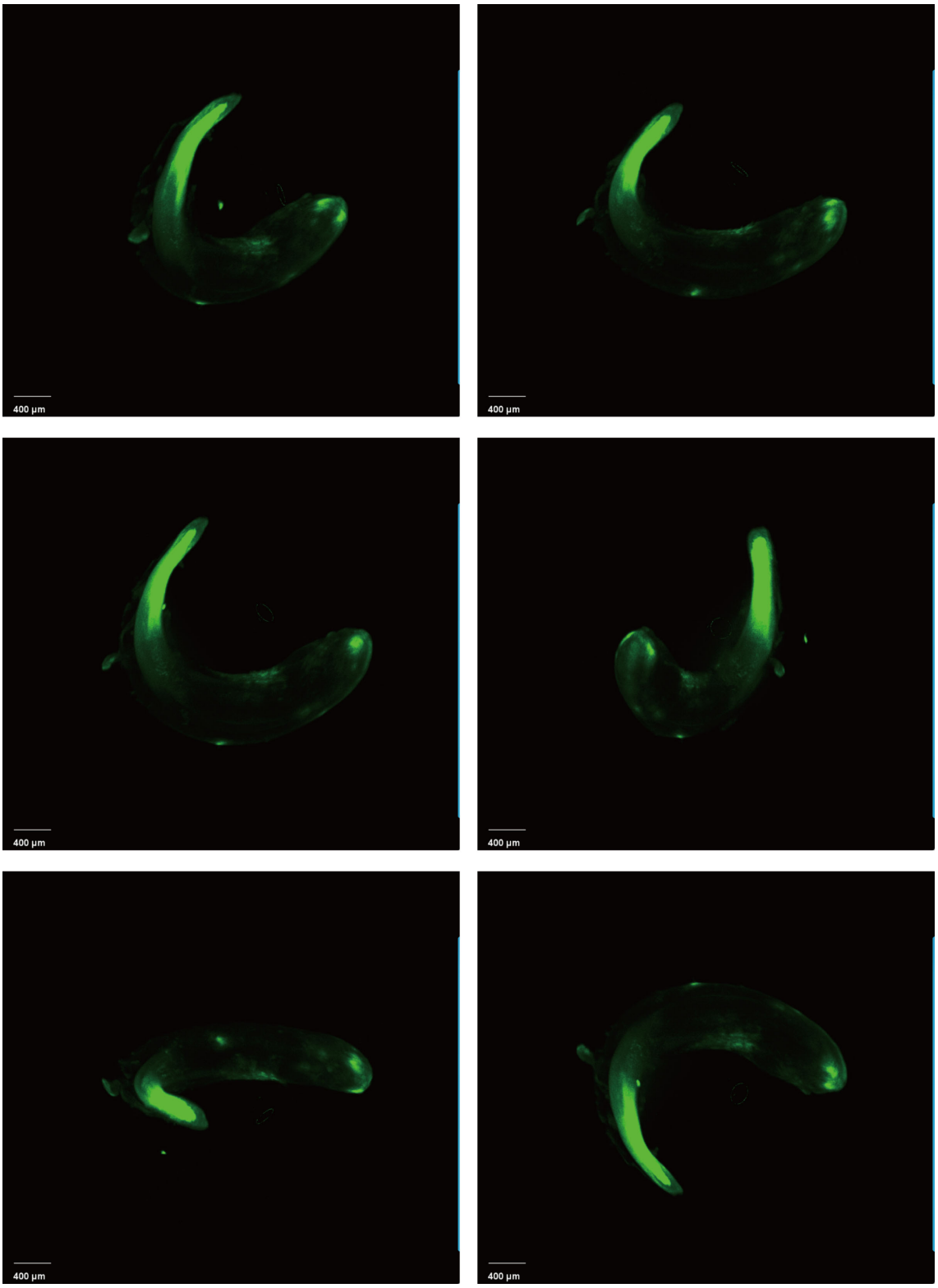

Fig 4. 4: Still images of PN5 mouse mandibular incisor 3D construction after ISH.

Thy-1 was expressed at the apical area of the mouse incisor where the mesenchymal stem cells are located. (Fluorescence in the tip of incisor is due to background and auto-fluorescence).

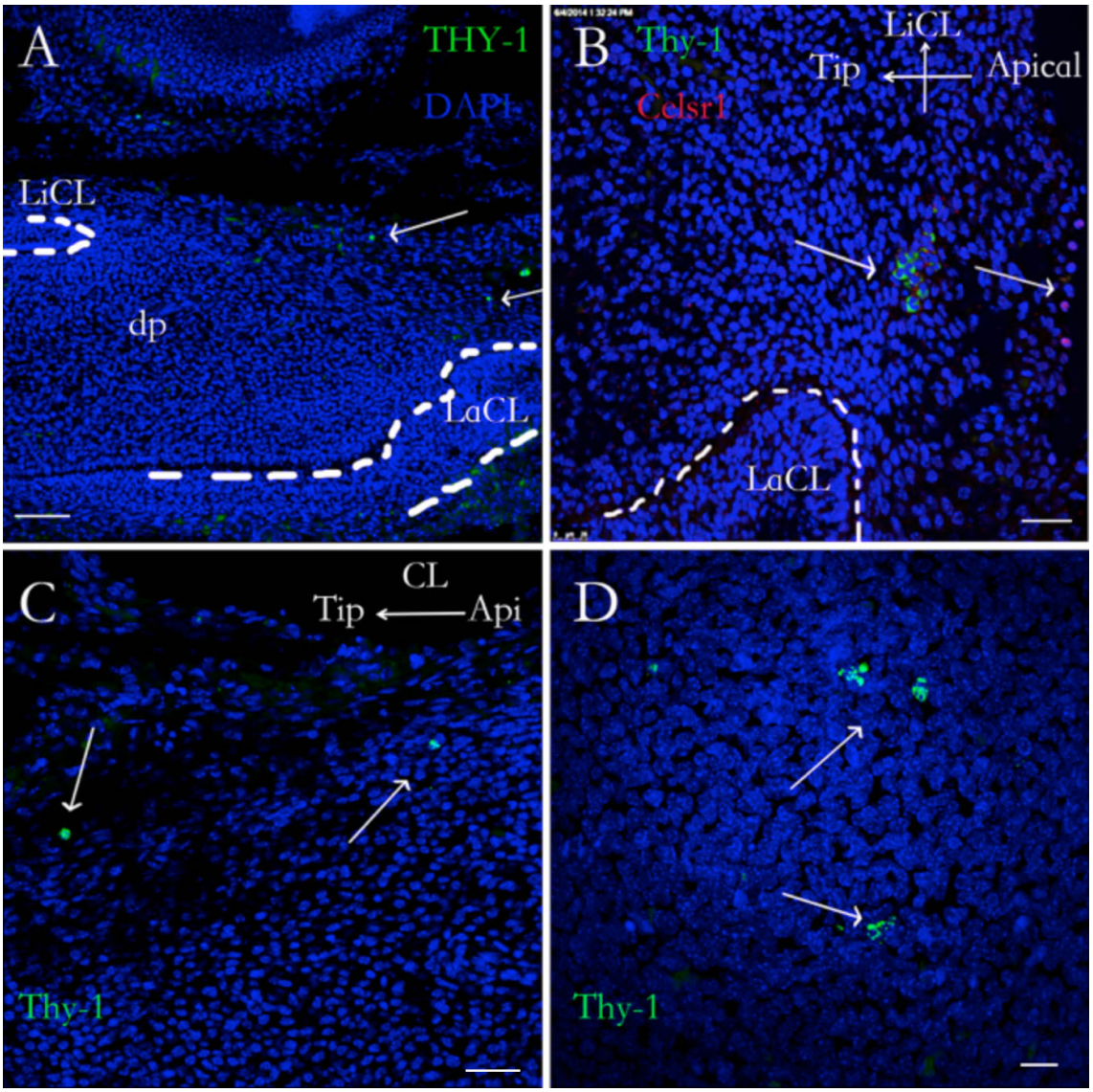

Fig 4. 5: Immunostaining of Thy1+ cells in PN5 mouse mandibular incisor dental pulp (sagittal sections).

(A) Arrows show individual Thy-1+ cells were detected in the area between cervical loops of incisor dental pulp. (B) A Thy-1+ cell cluster (green) was located in the slow cycling cells area next to several quiescent Celsr1+ (red) cells. (C) High magnification of Thy-1+ cells at the apical end incisor dental pulp tissue. (D) Thy-1+ cells were detected to locate at the apical end mesenchyme. Pictures were taken by confocal z-stack from cryosection. Thy-1 antibody was checked in salivary gland tissue (not shown). Abbreviation: dp, dental pulp; CL, cervical loop; Api, apical end; LaCL, labical cervical; LiCL, lingual cervical loop. Scale bar=500 µm in (A). Scale =25 µm in (B, C). Scale bar=10 µm in (D).

4.2.2 Analysis of Thy-1 expressing cells in the dental pulp of mouse incisors

Flow cytometry was used to analyze the proportion of Thy-1 expressing cells in the mouse incisor dental pulp at different postnatal stages. PN5 (n=24) and adult mice (n=6) were used to obtain both upper and lower incisors for this experiment. Incisor dental

pulp mesenchymal cells were dispersed and incubated with anti-CD90 (Thy-1) antibody prior to do flow cytometry. All experiments were repeated three times. The result of flow cytometry showed that 13.2±0.9% of PN5 and 12.4±1.5% of adult incisor pulp mesenchymal cells were Thy-1+ cells, suggesting that a relatively stable number of Thy-1+ cells exist in the incisor dental pulp (Fig 4.6 A, B). Furthermore, to analyze the Thy-1 derived cells from the whole dental pulp at different stages of incisor growth, Thy-1+ derived cells in *Thy-1Cre; R26R mT/mG* were collected and analyzed using flow cytometry with anti-GFP antibody at PN5 (n=24) and adult stage (n=6). Experiments were repeated three times. The results showed that 17.1±1.9% pulp cells were GFP+ in PN5 mouse incisor while 17.9±1.5% cells were GFP+ in adult mouse incisor, (Fig 4.6 C, D) suggesting a constant contribution of Thy-1+ cells in the formation of dental pulp tissue. Taken together, our flow cytometry analyses confirmed that Thy-1 expressing cells constantly contribute to dental pulp formation during different postnatal growth.

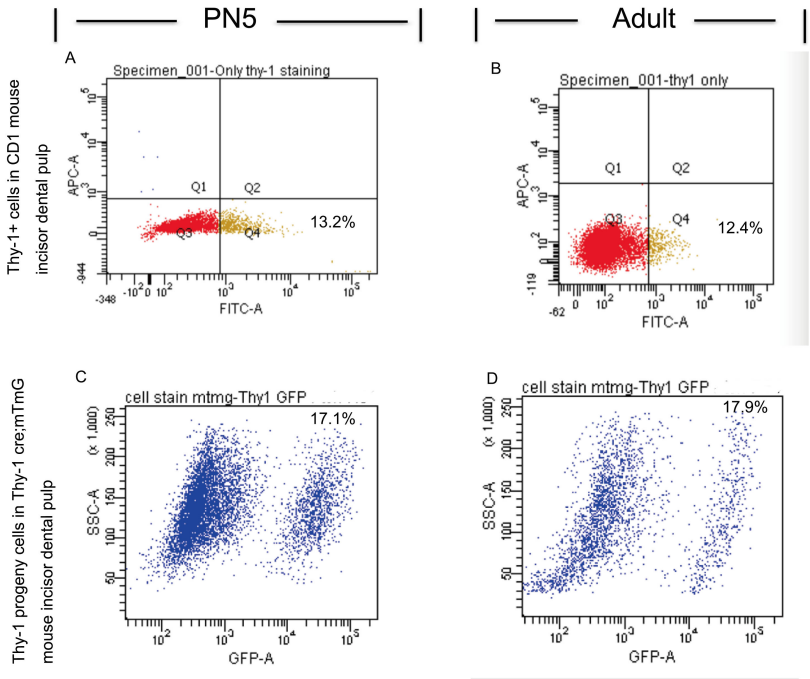

Fig 4. 6: Thy-1+ cells and their progeny cells in mouse incisor dental pulp.

(A) The percentage of Thy-1+ cells in digested adult dental pulp tissue was 12.4% comparing 13.2% in PN5 incisor dental pulp tissue (B). (C) Thy-1 derived GFP+ cells in *Thy-1Cre; R26R mT/mG* incisor was 17.1% at postnatal stage. (D) The percentage of Thy-1 derived GFP+ cells in adult *Thy-1Cre; R26R mT/mG* mouse incisor was 17.9%. The number of gated cells was 10,000.

4.2.3 Analysis of Thy-1 expressing cells in fast and slow cycling cells

To compare the slow cycling cell population, fast cycling cell population and Thy-1+ cells in mouse incisor dental pulp, flow cytometry was performed to analyze the co-localization within these cells. EdU was given to CD1 mice to label slow (n=12) and fast cycling cells (n=12), respectively. Detection of fast cycling cells and slow cycling cells is shown in Fig. 4.7, (A and C). 17.8% of pulp cells were EdU+ 24 hours after EdU injection that were considered as fast cycling cells; 4.3% of pulp cells were still EdU+ after 6 weeks chase time which were defined as slow cycling cells.

In the co-localization analysis of fast cycling cells and Thy-1+ cells (Fig. 4.7 B), flow cytometry analysis results showed that about 20.07% of pulp cells were EdU+ 24 hours after EdU injection. This result was consistent with prior percentage of fast cycling cells. There was 14.8% of pulp cells detected in the whole pulp were Thy-1+ cells. The result also showed that a small proportion of cells were EdU+ (fast cycling cells) and Thy-1+ cells, that accounted for 3.27% of all in the incisor pulp cells. Thus, around 16.3% fast cycling cells were Thy+, which account for 22% of total Thy-1+ cells (Table 4.1). In the colocalization analysis of slow cycling cells and Thy-1+ (Fig. 4.7 D), the result showed that 4.63% of pulp cells were slow cyling cells while 10.28% of pulp cells were Thy-1+ cells, 1.34% of pulp cells were both positive to EdU and Thy antibody which means approximately 30% of slow cycling cells were Thy-1+ cells, suggesting a considerable contribution of Thy-1+ cells to the slow cycling cell population (Table 4.1). All experiments were repeated 3 times and showed similar results.

Table 4. 1: The percentage of cells in each population

29% Slow cycling cells are Thy-1+
13% Thy-1 cells are slow cycling cells
16.3% Fast cycling cells are Thy-1+
22% Thy-1+ cells are fast cycling cells

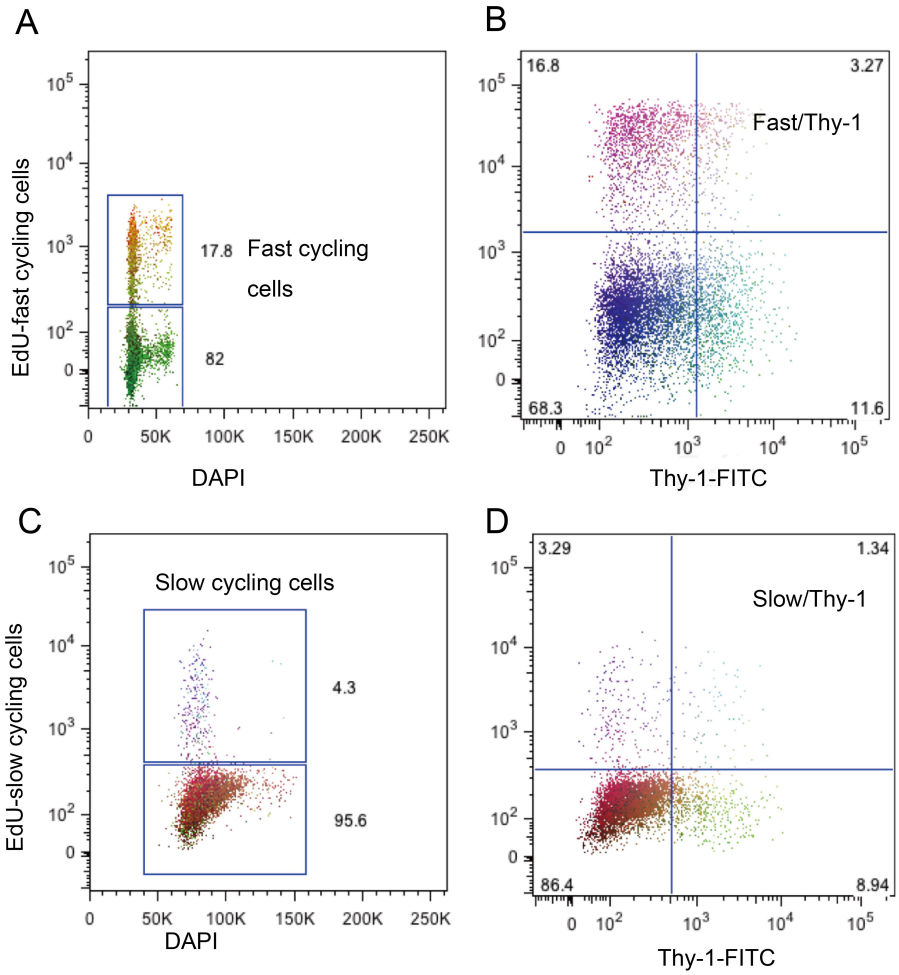

Fig 4. 7: Flow cytometry analysis of Thy-1+ cells in the mouse incisor dental pulp.

(A) The percentage of EdU+ cells in digested adult incisor dental pulp tissue was 17.8% 24 hours after EdU injection. (B) Flowcytometry analysis of fast cycling cells and Thy-1+cells showed that 20.07% pulp cells were fast cycling cells, 3.27% of pulp cells were fast cycling cells and positive to Thy-1antibody, 14.87% pulp cells were Thy-1+. (C) 4.3% of pulp cells were still EdU+ after 6 weeks wash time, suggesting a slow cycling cell population in the mouse incisor dental pulp. (D) 4.63% pulp cells were slow cycling cells and 9.7 % of all pulp cells were Thy-1+ cells. 1.34% pulp cells were slow cycling cells and positive to Thy-1 antibody. The number of gated cells was 10,000 for each analysis.

4.2.4 Analysis of gene expression changes of Thy-1 expressing cells

To analyze the gene expression pattern of Thy-1 expressing cells (Thy-1+) in comparison with Thy-1 negative (Thy-1-) cells in dental pulp tissue, both Thy-1+ cells and Thy-1– cells were collected from adult mice incisors (n=12) by FACS and RNA extracted for gene microarray. The gene expression result of Thy-1+ cells showed that many genes were up-regulated in comparison with Thy-1- cells, including signaling pathway molecules which are important for tooth development such as *Integrinα5, Notch11, Wnt9a, Bmp1b, Pax6, Pax9, Fgf3, Fgf10, Ncam1* and *Vcam1*. Intriguingly, among those up-regulated genes in Thy-1+ cells, several ESC markers were noticed, for example, *Klf4, Sox2, CBX7* and *Zic3* showed 2-5 fold up-regulated expression in Thy-1+ cells, while *Nanog* – a transcription factor critically involved with self-renewal of undifferentiated embryonic stem cells – was dramatically up-regulated, namely 16 fold compared in Thy-1- cells (Fig. 4.8).

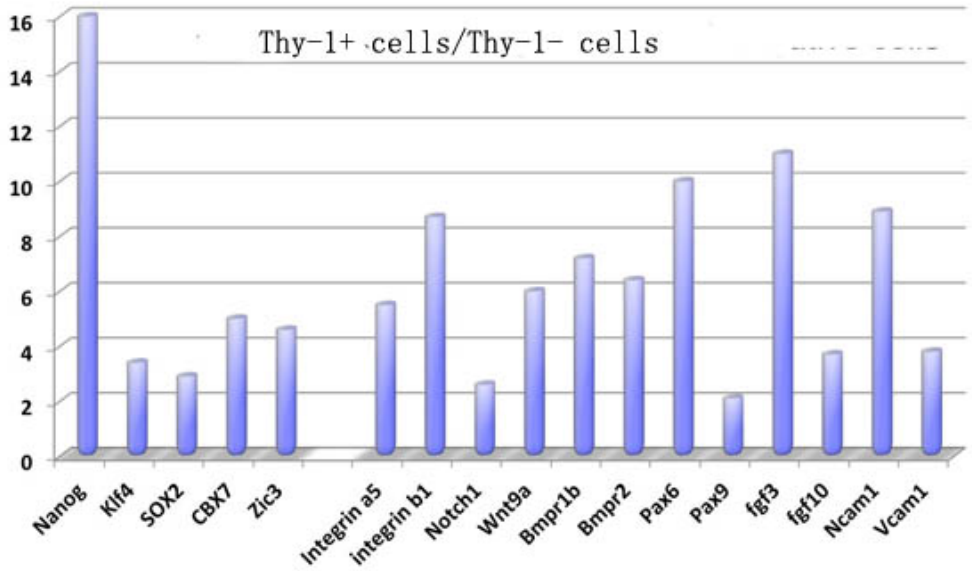

Fig 4. 8: The comparison of up-regulated genes in Thy1 expressing cells with Thy-1 negative cells. (Samples were prepared together with Dr. Zhengwen An who performed this data analysis)

4.2.5 Investigation the properities of Thy-1 expressing cells *in vitro*

To investigate the properties of Thy-1 expressing cells *in vitro*, FACS was used to purify and enrich the population of Thy-1+ cells by labeling cells with fluorescent

antibodies. Incisor dental pulp cells from 10 CD1 mice (PN5) were applied in FACS. In the following experiment, Thy-1– and Thy-1+ cells collected from FACS were cultured in 6-well plate (100,000 per well). The morphology of cells can be important in many contexts, for example the morphology indicates the status of the cells, both in terms of health and differentiation. Thus, sorted Thy-1+ cell cultures were monitored and compared with the sorted Thy-1- cell cultures. In passage 1, after 3 days in culture, Thy-1+ cells were much fewer than Thy-1- cells, which were almost confluent. Thy-1+ cells and Thy-1- cells were both heterogeneous: cells had a round, fibroblastic and neural appearance (Fig. 4.9 A, B). After 14 days in culture, Thy-1+ expressing cells were further reduced in number compared with Thy-1- cells. Individual Thy-1+ cells grew bigger in size with a stretched appearance (Fig. 4.9 A') while most Thy-1- cells still kept a fibroblastic spindle shaped appearance (Fig. 4.9 B'). Taken together, these results showed that the dental pulp stem cells were heterogeneous and Thy-1+ sorted cells grew poorly in culture compared to Thy-1- cells.

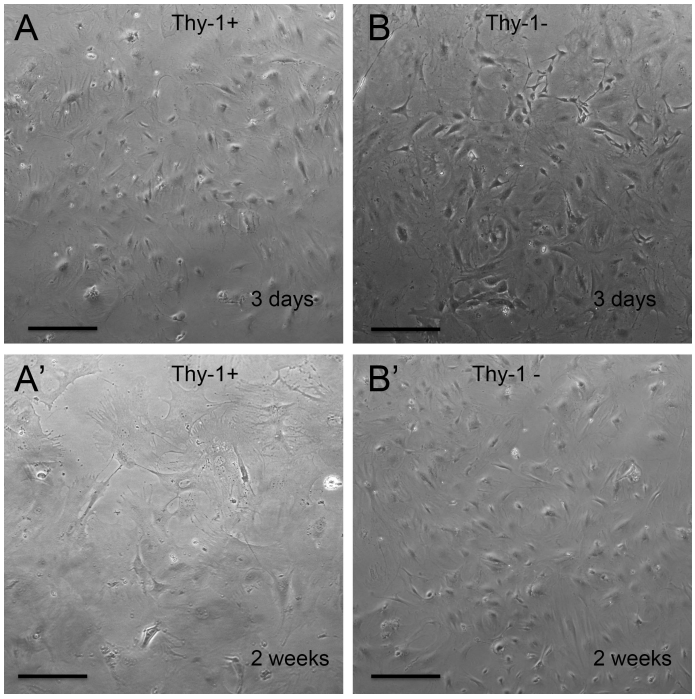

Fig 4. 9: Morphology of Thy-1+ and Thy-1- cells after 3 days, 14 days in culture.

Cell culture showed that Thy-1+ cells (A) were fewer in number and hardly grew in culture (A') when compared with the nearly confluent Thy-1- cells after 3 days culture (B) and 14 days culture (B'). Scale bar = 100μm.

4.2.6 Lineage tracing of Thy-1 expressing cells in mouse incisors dental pulp

To investigate the role of Thy-1+ cells in the mouse incisor dental pulp mesenchymal tissue *in vivo,* lineage tracing of these cells was performed. Two transgenetic mouse lines (*Thy-1Cre; R26R-Confetti* and *Thy-1Cre; R26 mT/mG)* were generated and analyzed. In *Thy-1Cre;R26R mT/mG* mice, Thy-1 derived cells can be identified by detecting GFP expression. In *Thy-1Cre;R26R-Confetti* mice, Cre recombination produced four possible outcomes: red, yellow, blue and green. These colours label all Thy-1 derived cells. One single Thy-1 expressing cell and its progeny were in one of these four colours. Thus, single Thy-1+ cell clone can be identified by examining the colour of cells in *Thy-1Cre;R26R-Confetti* mice incisors.

4.2.6.1 Validation of Cre expression

To confirm that Cre expression was driven by *Thy-1* gene promoter and an effective recombination existed between *Cre* and *loxP* sites, immunostaining for Cre was performed. Cre protein expression was observed mostly at the apical end of mouse incisor between cervical loops. This result was consistent with the immunostaining of Thy-1 in which a small number of Thy-1+ cells were found in the area between the cervical loops (Fig. 4.5). Thus, both Cre+ and Thy-1+ cells were identified in the incisor mesenchyme between cervical loops (Fig. 4.10). These results showed that Cre was successfully activated in Thy-1+ cells. Thy-1+ cells and derived cells can be labeled with fluorescence in the transgenic mouse incisor dental pulp.

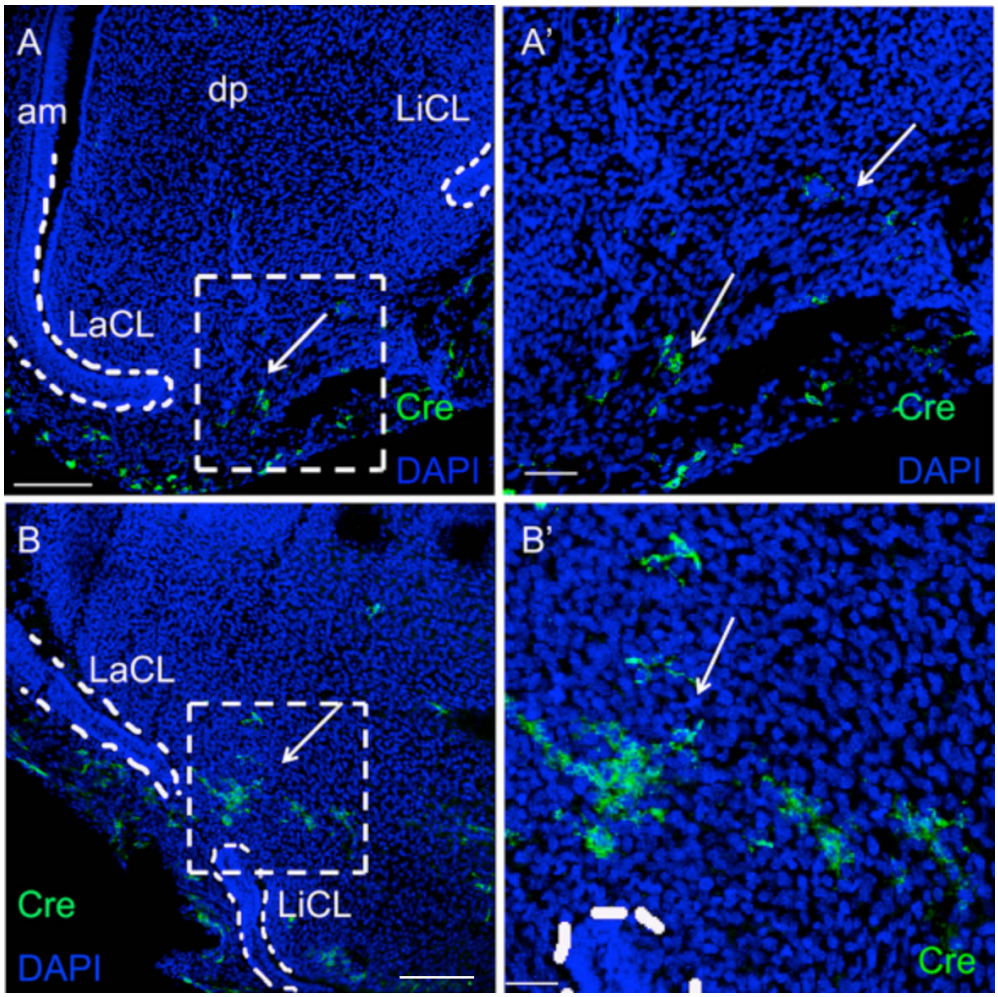

Fig 4. 10: Cre expression in PN5 mouse mandibular incisor (Sagital sections).

Arrows show Cre expressing cells in the *Thy-1Cre* mouse incisor dental pulp tissue. (A) and (B) Cre expressing cells were detected by immunostaining in the area between the cervical loops and adjacent dental follicle. (A') and (B') High magnification of dashed area in (A) and (B). Abbreviation: am, ameloblasts; dp, dental pulp cells; LaCL, labial cervical loop; LiCL, lingual cervical loop. Scale bar=100 µm in (A and B). Scale bar =50 µm in (A'). Scale =25 µm in (B').

4.2.6.2 Investigation of Thy-1 derived cells in the mouse incisor dental pulp

In *Thy-1Cre;R26R mT/mG* mice, GFP+ Thy-1 derived cells originated from the mesenchyme area between the cervical loops where the Thy-1+ cells were located (Fig. 4.11 A-C). GFP+ cells were initially concentrated in the area between the cervical loops and furthermore expanded down to the pulp tissue. This result was consistent with the finding that the Thy-1+ cells were located in the area between the cervical loops. Similar result came from *Thy-1Cre;R26R-Confetti* mice, multiple colour labeled cells were observed in the same area as GPF+ cells, while these multiple colour labeled cells formed their own cell streams from the area between the cervical loops and moved

down to dental pulp tissue (Fig. 4.12 A-C). Since single colour cell stream represent single clone of Thy-1+ cells, this result confirmed that individual Thy-1+ clones formed from cells that existed in the area between the cervical loops.

Results form *Thy-1Cre;R26R mT/mG* mice and *Thy-1Cre;R26R-Confetti* mice also showed that a large number of labeled cells contributed to the dental pulp formation of incisors. Most of the labeled cells were distributed throughout the pulp (Fig. 4.11 C). In *Thy-1Cre;R26R-Confetti* mice, cell streams from the mesenchyme area between cervical loops were found to have moved toward the whole incisor dental pulp (Fig. 4.12 A, B, E). Additionally, more than one colour cell streams were found in one incisor dental pulp, indicating several Thy-1expressing cells together contributed to the formation of dental pulp mesenchyme (Fig. 4.12 E). Taken together, these results suggested that Thy-1+ cells located in the area between cervical loops were able to form cell clone and contributed to the formation of dental pulp cells.

In addition to form dental pulp cells, Thy-1 progeny cells were also found to generate odontoblasts. Labeled cells were detected in *Thy-1Cre;R26R mT/mG* and *Thy-1Cre;R26R-Confetti* mice odontoblasts, respectively. Tracing results showed that labeled cell streams from the area between the cervical loops moved along the direction of tooth growth and contributed to the generation of odontoblasts in addition to dental pulp formation (Fig. 4.11 A', B', D, Fig. 4.12 A, D, F). However, the lineage tracing results showed that the labeled odontoblasts in both reporter mouse lines were presented as cell patches rather than individual cells. Roughly 20-30 cells were found in each patch of odontoblasts (Fig. 4.11 D). In the *Thy-1Cre;R26R-Confetti* mice, these odontoblast patches were all in same colour suggested that they might be from a single stem clone (Fig. 4.13 A, A'). Taken together, all these results suggested that Thy-1+ cells contributed to the formation of odontoblasts and these odontoblasts in one patche were from a single Thy-1+ cell clone.

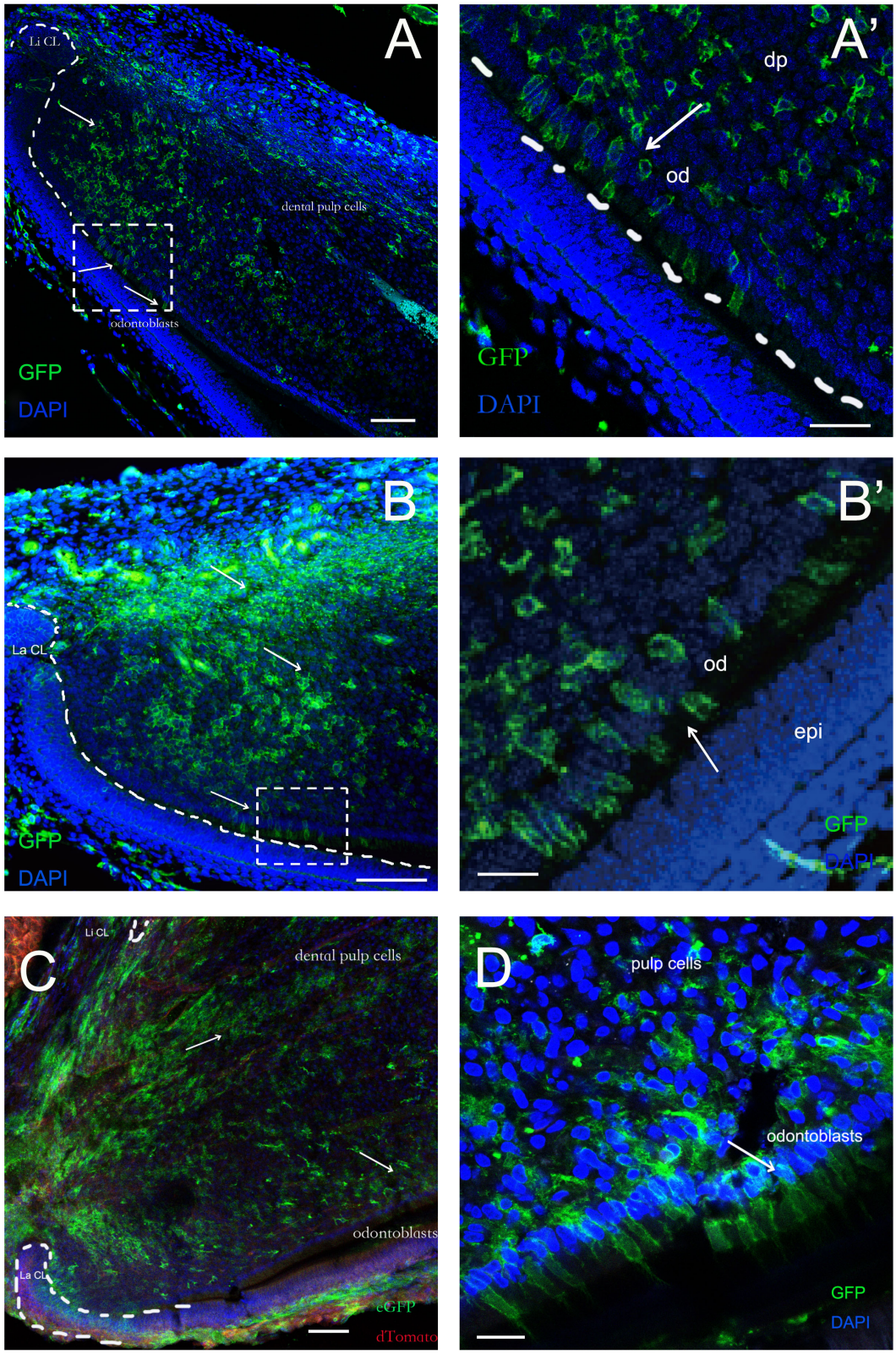

Fig 4. 11: Thy-1 derived cells in mouse incisor dental pulp tissue (sagital sections).

(A, B) Paraffin sections of *Thy-1Cre;R26R mT/mG* mouse incisor showed that GFP+ (arrow) cells originated from slow cycling cells area and contributed to the incisor dental pulp and odontoblast. (A', B') High magnification of GFP+ cells in odontoblasts (arrows). (C) Cryosections of *Thy-1Cre;R26R mT/mG* mouse incisor showed that GFP+ cell (arrows) streams from slow cycling cells area contributed to dental pulp and odontoblast. (D) Arrow shows one patch of Thy-1 derived odontoblasts (approximately 30). Abbreviation: dp, dental pulp cells; od, odontoblasts; LaCL, labial cervical loop; LiCL, lingual cervical loop; epi, epithelia. Scale bar= 250 µm in (A, B, C). Scale bar= 50 µm in (A'). Scale bar= 25 µm in (B'). Scale bar= 10 µm in (D).

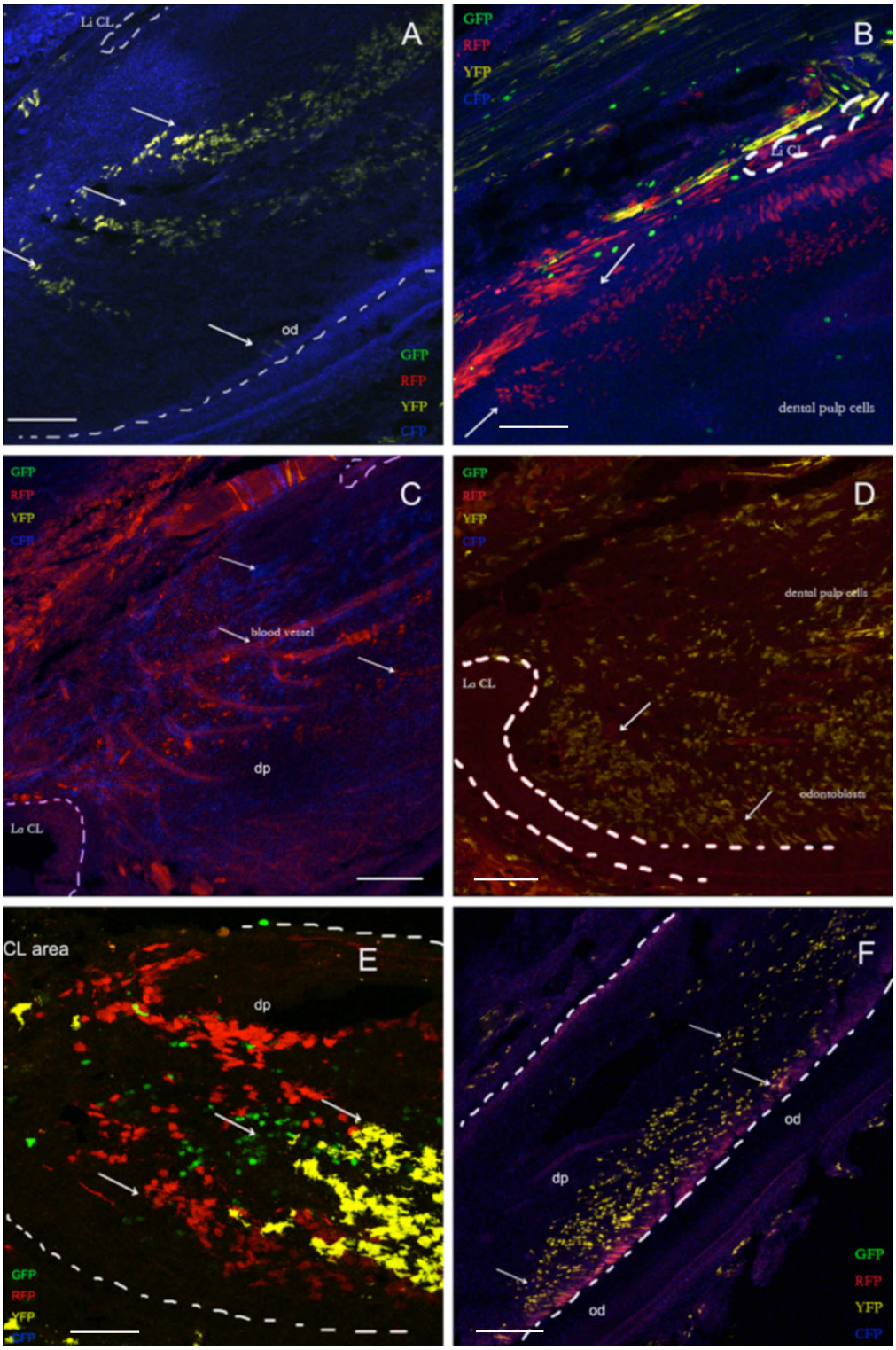

Fig 4. 12: Cryosections of *Thy-1Cre;R26R-Confetti* mouse lower incisor (Sagital sections).

Multiple coloured cells (GFP+, RFP+, YFP+, CFP+) from apical end mesenchyme formed cell stream and contributed to the formation of dental pulp tissue in *Thy-1Cre;R26R-Confetti* mouse incisor. (A) Three cell streams were found originated from the apical end of mouse incisor and moved to form dental pulp tissue including odontoblasts (arrow). (B, C, E) Muliple coloured cell streams were found at the apical end of incisor representing different cell clones in *Thy-1Cre;R26R-Confetti* mouse incisor. (D, F) More odontoblasts (arrow) were formed from coloured cell stream (arrow) in *Thy-1Cre;R26R-Confetti* mouse incisor. Abbreviation: dp, dental pulp cells; od, odontoblasts; LaCL, labial cervical loop; LiCL, lingual cervical loop. Scale bar = 250 µm in (A, B, D, F) and 150 µm in (C, E).

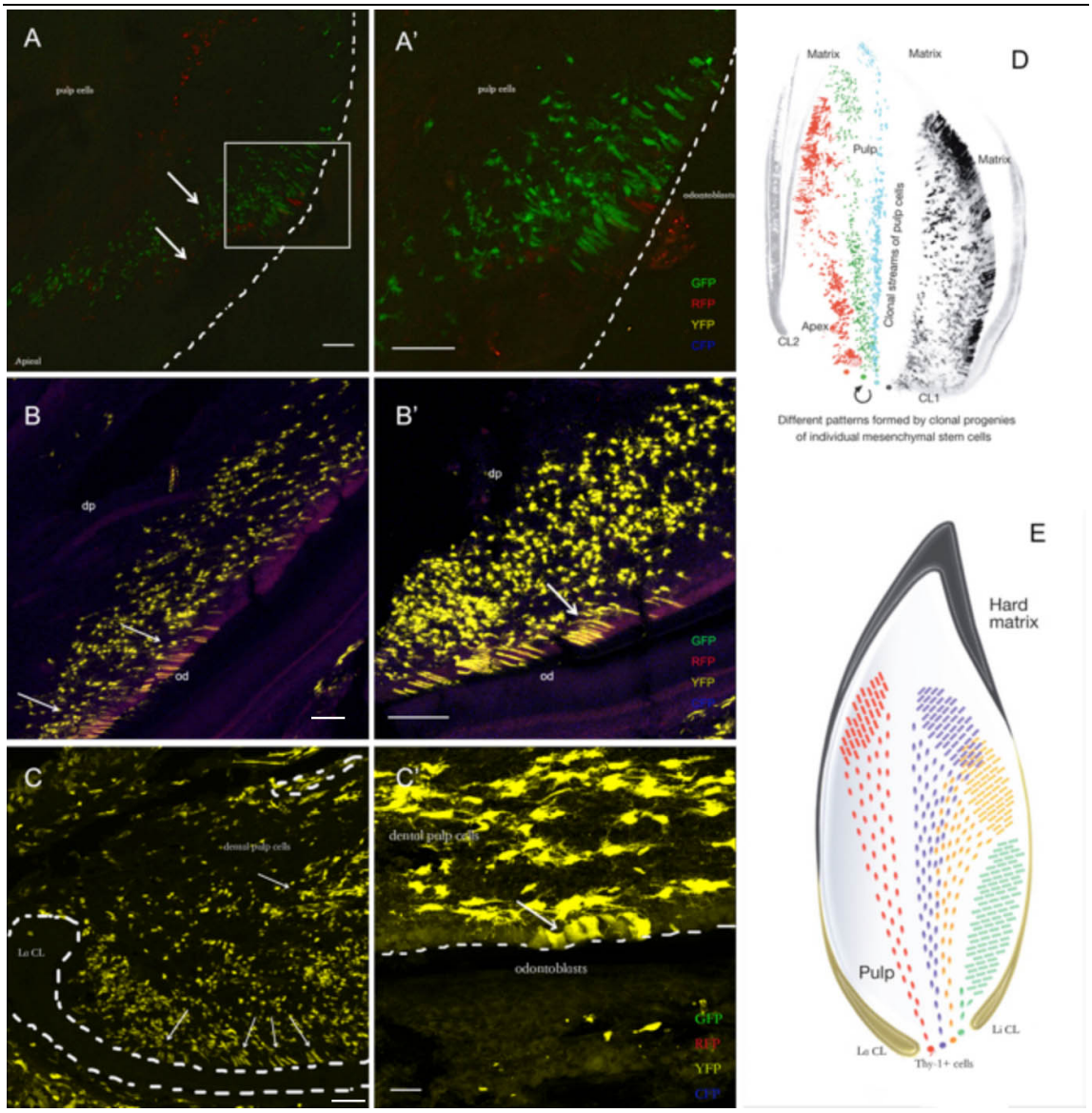

Fig 4. 13: Thy-1 derived odontoblasts in *Thy-1Cre;R26R-Confetti* mouse lower incisor (sagittal sections).

(A, A'-C, C') Streams of traced cells were connected to clusters of odontoblasts (arrows) originating from the same recombination events in Thy-1 cells. (D, E) Illustration of clonally-organized pulp and odontoblasts (Kaukua et al., 2014). Scale bars = 25 µm in (A, B, C, A', B'). Scale bars = 10 µm in (C').

In summary, these lineage tracing results suggested that Thy-1+ cells which were located in the area between the cervical loops were able to form cell clones and contribute to the formation of mouse incisor dental pulp tissue (Fig. 4.13 D, E). However, although a large number of the labeled cells in any of these transgenic mice contributed to dental pulp formation in incisor, not all dental pulp cells were derived from them. In both of the *Thy-1 Cre* reporter mouse lines, labeled odontoblasts in

incisor dental pulp were located in patches alternating with unlabeled cells. The exact percentage of Thy-1+ cell contribution to the whole incisor dental pulp tissue was variable but between 20%-40% which was consistent with the flow cytometry results showed approximately 30% of slow cycling cells were Thy-1+.

4.2.7 Investigation of other sources of cells in the growth of mouse incisor dental pulp

For decades it has been believed that the dental mesenchymal stem cells gave rise to pulp cells and odontoblasts derive from neural crest cells after their migration in the early head and formation of ectomesenchymal tissue (Kaukua et al., 2014, Chai et al., 2000). Studies have shown the connection of sensory nerve and MSCs at the apical end neurovascular bundle area (Zhao et al., 2014), thereby in order to investigate the function of neural cells in the incisor dental pulp, immunostaining of neural markers were performed on the *Thy-1Cre; R26R mT/mG* mouse incisor sections. Interestingly, some odontoblasts and pulp cells were found to be neurofilament+ (an intermediate filament normally found in neurons). This neurofilament+ population was exclusive from the Thy-1 derived cell population (Figure 4,14 B, C'). Once these neurofilament+ cells formed odontoblasts, stained cell bands alternating with non-stained cell bands like the pattern of Thy-1 derived odontoblasts were observed. Most importantly, these vacant bands were perfectly occupied by Thy-1 derived odontoblasts (Fig. 4.14 A, A', B', C). This result may suggest another neural crest originating cell population contributes to the formation of odontoblasts although further investigated is required.

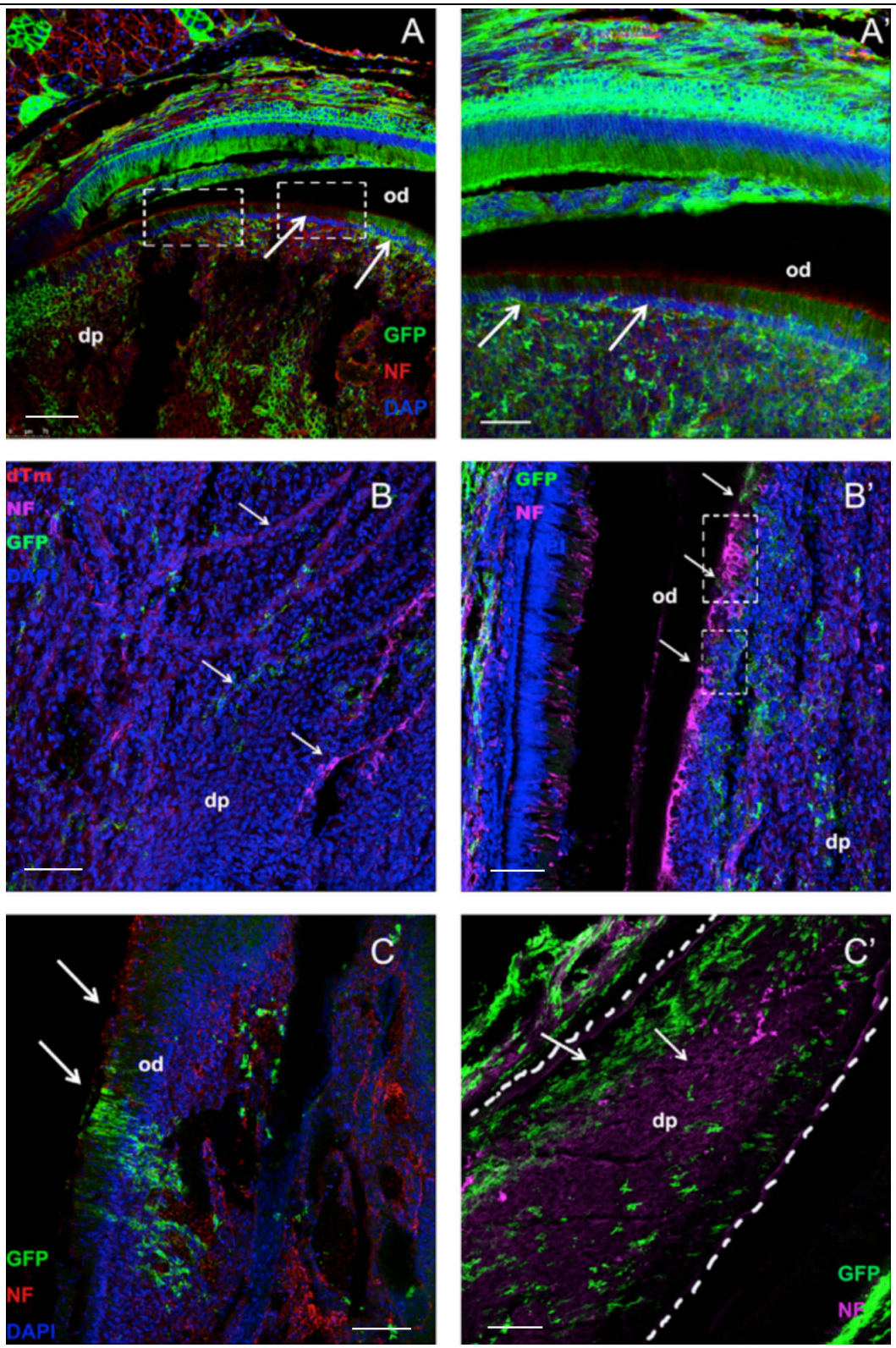

Fig 4. 14: Immunostaining of neurofilament in Thy-1Cre;R26R mT/mG mouse mandibular incisor (sagittal sections).

(A, A', B', C) Arrows show odontoblast patches from Thy-1 derived cell population and neurofilament+ cells respectively. (B) Arrows showed dental pulp cells fromThy-1 derived cell population and immunostaining of neurofilament+ cells respectively. (C') Arrows show dental pulp cell streams from Thy-1 derived cell population and neurofilament+ cells respectively. Abbreviation: dp, dental pulp cells; od, odontoblasts; NF, neurofilament. Scale bars = 50 µm in (A, A', B, B' C, C').

4.2.8 Investigation the expression of genes involved in incisor MSCs regulation

To investigate the gene expression in tooth MCSs, more important genes and proteins involved in the regulation of tooth growth were checked in the PN5 mouse incisor by immunostaining and ISH. These genes were chosen based on a number of criteria as mentioned earlier. These chosen genes include *Shh; Gli1*, the sonic hedgehog (*Shh*) responsive gene (Seidel et al., 2010); Hh receptor gene Patched (*Ptc-1*), a reliable indicator of Hh signaling activity (Ingham and McMahon, 2001); TGF-β receptor type I (Alk5/Tgfbr1), a member of the TGF-β superfamily that regulate craniofacial development; DKK1, a Wnt signaling pathway inhibitor and pax9, a paired box family transcription factor which is involved in craniofacial, tooth and limb development, as well as other sites during mouse embryogenesis.

The results showed that Shh was only expressed in the labial side epithelium, including in the ameloblasts, TA cells and the undifferentiated cells at the end of the labial cervical loop (Fig. 4.15 A, A'). The expression of Gli-1 more restricted in the epithelial tissues and in the labial side mesenchyme, however, this expression was very weak, optimized experiment is required (Fig. 4.15 B, B'). Hh receptor Ptc-1 was expressed both in the epithelial and mesenchyme in the apical end of mouse incisor (Fig. 4.15 C, C'). Alk5 was mainly located in the mesenchyme close to the labial cervical loop where fast cycling cells were located in the mouse incisor corresponding to the report that loss of Alk5 expression in CNC cells resulted in delayed tooth initiation and non-uniform mandible defects (Zhao et al., 2008) (Fig 4.15 D, D'). Immunostaining of Pax9 showed that plenty of Pax9 positive cells were located in the dental follicle and the dental mesenchyme at the apical end of mouse incisor corresponding to the function of Pax9 in regulating the development of the tooth during embryogenesis (Fig 4.15 E, E'). Dkk1 was strictly limited in the odontoblasts that suggested its involvement in Wnt signaling

regulating the formation of odontoblasts (4.15 F, F').

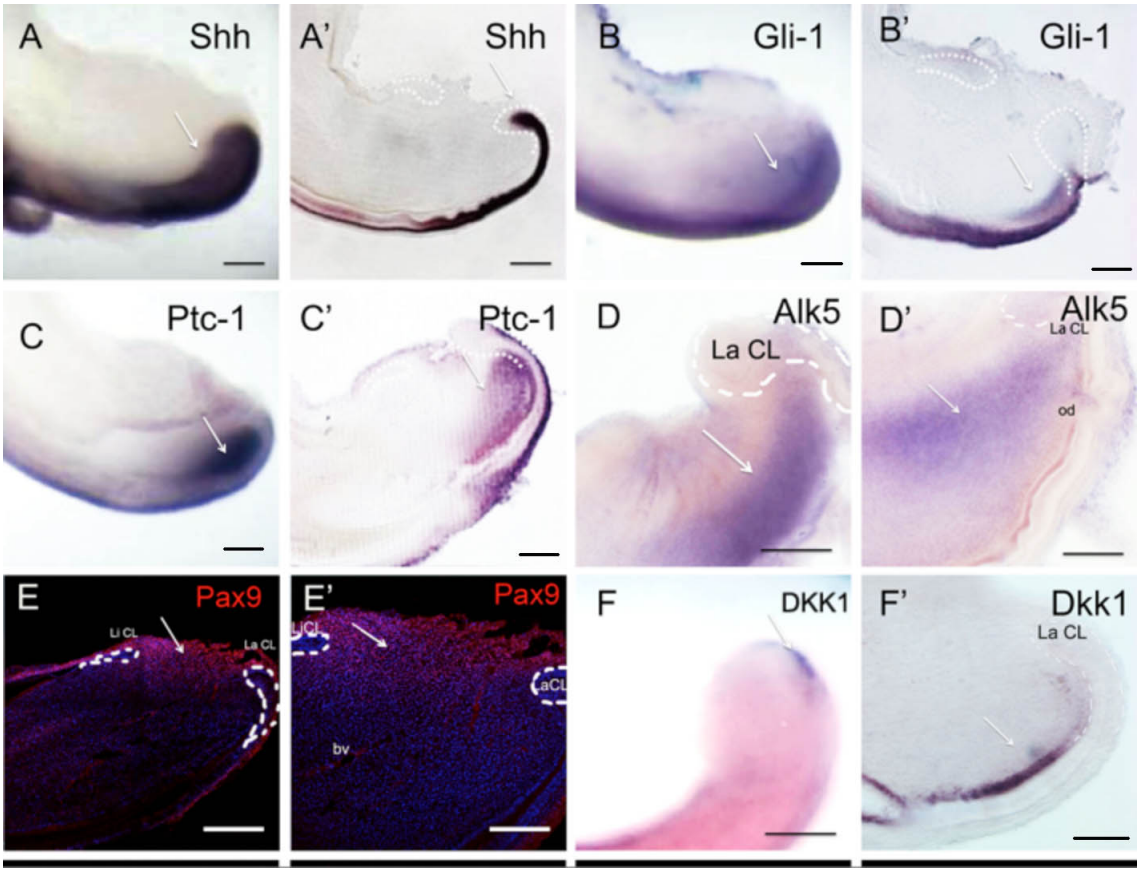

Fig 4. 15: Expression of genes involved in incisor development (sagittal sections).

Shh was strongly expressed in the dental epithelium, including the labial cervical loop and the ameloblasts (A, A'). Gli-1 was expressed in epithelium in addition to a narrow part of the mesenchymal tissue next to the labial cervical loop where fast cycling cells were located (B, B'). Gli-1 expression was carried out together with Dr.Abd-Elmotelb. Ptc-1 was expressed both in dental epithelium, ameloblasts precursor cells and the mesenchymal tissue next to the labial cervical loop; a weakly expression in part of the mesenchymal tissue between the cervical loops was also detected (C, C'). Alk5 located in the mesenchymal tissue next to the labial cervical loop (D, D'). Pax9 positive cells were mainly located in the apical end dental pulp and outside dental follicle (E, E'). Dkk1 was strictly limited in the odontoblasts (F, F'). All the probes and antibodys were checked on other tissues as positive control, samples from the same tissue without probe or antibody were used as negative control (not shown). Scale bar =250 µm in (A, B, C, B'). Scale bar =100 µm in (A', C'). Scale bar =100 µm in (D' F'). Scale bar =100 µm in (D, E, F).

4.3 Discussion

4.3.1 Identification of Thy-1 in the mouse incisor MSCs for further investigation

The continuously growing mouse incisor is an excellent model to study the function and regulation of stem cells. In the mouse incisors, cells constituting the mouse incisor are mostly derived from two embryonic sources: neural crest ectomesenchyme and ectodermal epithelium (Harada et al., 1999). Studies have shown that the epithelial stem cells are located mainly in the labial cervical loop while mesenchymal stem cells dwell in a niche at the tooth apex where they produce two differentiated derivatives. However, the lack of specific surface markers that can distinguish MSCs from their differentiated progeny has hampered the widespread use of MSCs for regenerative dentistry (Kaltz et al., 2010). Fortunately, the microarray methods for large-scale analysis of mRNA gene expression makes it possible to search systematically for key molecules (Duggan et al., 1999). Thus, a microarray performed in our laboratory in a previous study has compared stem cell gene expression between mouse incisor and molar dental pulp tissues (Mantesso and Sharpe, 2008). Since the growth of the mouse incisor begins from the apical end, gene chip microarrays were also carried out to compare the gene expression in the body and cervical loop portions of dental pulp. Subsequently, up-regulated genes in the cervical loop area from this microarray were compared with the up-regulated genes in the former microarrays. Surprisingly, there were only three genes in common. They were *Dlx5* which encodes a member of a homeobox transcription factor gene family similar to the *Drosophila* distal-less gene (Sajan et al., 2011), *Thbs-1*, a matricellular glycoprotein first discovered in activated platelets (Lawler et al., 1978) and *Thy-1*. Previous research has shown that Thy-1 was widely used as a marker for mouse haematopoietic stem cells (Petersen et al., 1998) and human haematopoietic

progenitor cells (Craig et al., 1993). It is also believed to be a general mesenchymal stem cell marker (Horwitz et al., 2005). More importantly, *Thy-1* is expressed in human dental pulp cell lines (Suguro et al., 2008) and was reported to be expressed in the subodontoblastic zone (Hosoya et al., 2012). Due to its up-regulated expression in the cervical loop area, which harbors the mesenchymal stem cells in addition to its role as a general mesenchymal stem cell marker, *Thy-1* was selected for further study.

4.3.2 Investigation of Thy-1 expression in the mouse incisor

Previous studies in the laboratory have identified the expression of Thy-1 in the development of mouse teeth. Therefore, ISH was used to investigate Thy-1 expression in the mouse incisor dental pulp at postnatal stages PN5. The results revealed that the expression of Thy-1 was limited to the apical end mesenchyme where the stem cell niche is located. Immunostaining results showed that Thy-1 and Thy-1 derived Cre expressions were detected in the slow cycling cell area. In addition, evidence form lineage tracing showed that all Thy-1 progeny cells were originated from the apical end of mouse incisor. These results all suggested that Thy-1+ cells existed at the apical end of mouse incisor dental pulp tissue. However, an inducible *Thy-1 Cre* mouse line is required to confirm which population Thy-1+ cells origin from by temporal controlling Thy-1 expression. Collectively, these results suggested that Thy-1 expressing cells in mouse dental pulp were MSCs and existed in a MSC stem cell niche in mouse incisor dental pulp.

4.3.3 Comparion of Thy-1 expression in the mouse incisor between postnatal stage and adult stage

Our flow cytometry analysis revealed that the Thy-1+ cell number was almost same at

adult stage mouse incisor dental pulp in comparision with 5 day-old mice, suggesting a constant contribution of Thy-1+ cells in the growth of mouse incisors. It might be conflict with the idea that Thy-1 expression started to decrease with aging as the MSCs number decreased with age in human bone marrow mesenchymal stem cells (hBMSCs). Studies showed that in the early passages of hBMSCs, Thy-1 was one of the stem cell markers that decreased significantly with age, although it was expressed in all samples regardless of donor age (Stolzing et al., 2008). In addition, a similar decrease of stem cell numbers in their niche along with aging has also been reported in *Drosophila* female germ line stem cells (GSC) (Tseng et al., 2014). However, all these evidences came from other tissue that different frmm continually growing mouse incisor and were collected in in vitro studies. These data may indicate either a tissue specificity of MSCs or an effect of their micro-environment.

4.3.4 Analysis of Thy-1 expressing cells in fast and slow cycling cells

Dental pulp MSCs are heterogeneous cell populations identified based on their *in vitro* characteristics. In our study, a MSC niche was identified comprising fast cycling cells and slow cycling cells by a series of label-retaining experiments. In the following study, the slow cycling cells were compared with Thy-1+ cells by performing flow cytometry analyzes. The results showed that after 6 weeks chase time when odontoblasts and ameloblasts in mouse incisors were turned over (Harada et al., 1999; Smith and Warshawsky, 1975) 4.3% dental pulp cells were considered as slow cycling cells. This result has been verified by a recently study using H2BGFP labeling mice which showed that less than 5% incisor dental pulp cells are slow cycling (Zhao et al., 2014). Our study also revealed that approximately 30 % of slow cycling cells were Thy-1+ cells, which suggested that slow cycling cells possibly are or at least contain stem cells in the

mouse incisoras. Lineage tracing experiment has proved Thy-1+ cells contributed to the growth and development of mouse incisor. Meanwhile, not all slow cycling cells were Thy-1 positive. This suggested a heterogeneity of these label-retaining cells. Evidence from a recent study has revealed that a significant population of mesenchymal stem cells in mouse incisoris derived from peripheral nerve-associated glia (Kaukua et al., 2014). Researchers have pointed that pericytes also contributed to the repair and growth of mouse incisor as MSCs (Feng et al., 2011). In addition, Gli1+ cells at the apical end of mouse incisor have been recently identified as MSCs and contribute to the tooth development and growth (Zhao et al., 2014). Thus, these MSCs probably compose the slow cycling cells together. Beyond that, the possibility that some differentiated cells still keep EdU labeling cannot be excluded.

In the detection of fast cycling cells, 17.8% of pulp cells were EdU+ 24 hours after EdU injection that were considered as fast cycling cells. According to the flow cytometry analysis, these cells have finished one cell cycle within 24 hours. This result was also consistent with our previous time course study suggesting a quick dividing cell population in the mouse incisor. In the co-localization analysis of fast cycling cells and Thy-1+ cells, flow cytometry analysis results showed that a small proportion of fast cycling cells (16.3 %) were Thy-1+. This is probably a result that a population of fast cycling cells from Thy-1+ slow cycling cells were still expressing Thy-1 in the beginning stage. However, in our study, nearly 65% Thy-1 cells were neither slow cycling nor fast cycling cells, this disposition of these cells are still a question. One possibility is that some Thy-1+ cells were derived from slow cycling cells but were not included in our fast cycling cells since the criterion of “fast cycling cell” was only set on 24 hours time point, not all the slow cycling cells or fast cycling cells proliferated at the same time, which led to less number of cells that were counted. In addition, flow

cytometry analysis result was obtained based on its sensitivity, the incubation time of antibody and the antibody itself could both alter the detectable Thy-1+ cells. For example, according to our immunostaining results less Thy-1+ cell were observed in comparison to flow cytometry analysis.

In summary, in the mouse incisor dental pulp, there were approximately 4.3% of slow cycling cells and approximately 20% fast cycling cells detected in the whole pulp cells. This result was consistent with our ICH result, thus roughly described a MSC niche model consisting by two cell polulations with different proliferation rates. In addition, our flow cytometry analysis of results further indicated the heterogeneity of MSCs in the mouse incisor, though more studies are required in the future.

4.3.5 Investigation of Thy-1+ cell population *in vitro*

In cell culture experiments, incisor dental pulp cells were sorted into 2 groups according to the Thy-1 expression as Thy-1- and Thy-1+. These sorted Thy-1+ cell cultures were monitored and compared with the sorted Thy-1- cultured cells. We noticted that Thy-1+ cells were heterogeneous, thereby suggesting their wide origins. Previous work in our laboratory had demonstrated such a heterogeneity: CD146, a transmembrane glycoprotein, with other markers such as Neural/Glial Antigen 2 (NG2) and platelet-derived growth factor receptor-beta (PDGFRβ) used together to locate pericytes; a cell type believed to be MSCs has been shown to co-express with Thy-1 and accounts for 1.7% of pulp tissue cells by flow cytometry analysis. This CD146+/Thy-1+ population probably represents the pericyte MSC population inside the dental pulp. Also, CD133, expressed by hematopoietic progenitors and considered as a cell surface marker of adult stem cells has been shown to be expressed in a Thy-1+ CD133+ subpopulation in dental pulp (Mona Abd-Elmotelb, 2013). Together, these results

suggested that the Thy-1+ population is heterogeneous and Thy-1 is expressed by a wide variety of cells (Craig et al., 1993, Saalbach et al., 1999).

Our study also demonstrated that Thy-1+ sorted cells were few in number and grew poorly in culture compared with Thy-1- cells. This could be due to an unsuitable culture condition. Previous work in our laboratory has shown that in cell culture, with successive passaging, the Thy-1+ population declined to 1.9% in passage 4 from 23% in passage 1. Nevertheless, when cultured with a feeder layer, the Thy-1+ population did not decline (Nakamura et al., 2006). This may suggest an unknown microenvironment role controlling Thy-1 expression *in vivo* (Tseng et al., 2014, Hsu et al., 2014). In chapter 3, the MSC niche in the mouse incisor has been characterized. Thy-1 was confirmed to be expressed in the stem cell niche of the mouse incisor, accordingly, the significantly poor growth of Thy-1+ population compared with the Thy-1- cells could be due to either stem cells maintaining their slow cycling state or a lack of regulation of the signals from the stem cell niche. However, the Thy-1+ population in murine bone marrow increased to 44% in passage 3 (Eslaminejad et al., 2007), which suggested an expression difference in comparison with mouse incisor dental pulp tissue. This difference of Thy-1+ expression could be caused by different tissue properties, as bone marrow is more cellular when compared with the dental pulp (Shi et al., 2001).

4.3.6 Lineage tracing Thy-1 expressing cells in the growth of mouse incisor

In order to identify stem cells in the tissue, label-retaining experiment and lineage tracing are two optimal methods. Lineage tracing is a technique originally developed to study early embryos, but is now used as the most powerful and reliable tool for identifying stem cells and for deciphering other aspects of tissue behavior. In this study, two reporter mouse lines (*R26R-Confetti* and *R26R mT/mG*) were mated with *Thy-1Cre*

transgenic mice, where *Cre* was driven by a *Thy-1* promoter, to trace Thy-1 expressing cells inside the mouse incisor dental pulp. In the *Thy-1Cre;R26R mT/mG* and *Thy-1Cre;R26-Confetti* mice, labeled Thy-1 progeny cells were found in both dental pulp cells and odontoblasts. Labeled cell streams from the slow cycling cell area contributed to the whole dental pulp along the direction of tooth growth in addition to the formation of odontoblast. This result further confirmed that Thy-1+ cells as dental MSCs contribute to the formation of mouse incisors. However, this contribution was limited, while alternative patches of cells in the odontoblast zones and pulp cells not a labeled Thy-1 progeny cell stream indicated a Thy-1- stem cell population(s) also contributed to the dental pulp formation. These findings explained the flow cytometry result that not all slow cycling cells were Thy-1+ and corroborated the results presented in a previous study, namely that the formation of dental pulp tissue results from more than one cell population as they found a limited contribution of pericyte-derived mesenchyme to odontoblast formation (Feng et al., 2011). Recently, a study in mouse incisors has suggested that a MSC population is peripheral nerve-associated, glia-derived. These glia-derived cells contribute to 50% of pulp cells in the mouse incisor, further proving the heterogeneous nature of MSCs located in mouse incisors (Kaukua et al., 2014).

4.3.7 Investigation of participation of neural crest origin stem cells in the development of the mouse ncisor

Studies of tooth development have proved that odontoblasts, dentine matrix, most pulpal tissues and DPSCs are derived from CNC (d'Aquino et al., 2009). During tooth development, CNC-derived ectomesenchyme contributes to the condensed dental ectomesenchyme during the bud stage and subsequently to the formation of the dental

papilla and surrounding dental follicle (Chai et al., 2000). Recent research has demonstrated that adult rat DPSCs contain primitive stem cell subpopulations of neural crest origin, including Nestin+ precursor cells, Tuj1+ neuron cells and S100+ glial cells (Sasaki et al., 2008). Another study has shown that DPSCs express several neural crest-related markers such as S-100, Nestin, CD57, CD271 and GFAP (Yan et al., 2011). Recently, a study confirmed that a significant population of mesenchymal stem cells evident during the development, self-renewal and repair of a tooth are derived from peripheral nerve-associated glia. Glial cells generate multipotent mesenchymal stem cells that produce pulp cells and odontoblasts (Kaukua et al., 2014). Lastly, in our study, the finding concerning the contribution of neurofilament+ cells might provide a potential neural-related MSCs source in the mouse incisor. Taken together, these evidences suggested stem cells of neural crest origin take part in the development of the mouse incisor.

4.3.8 Analysis of the expression of genes involved in the growth of mouse incisors

Besides Thy-1, several signaling molecules reported importantly regulating stem cell population were investigated in PN5 mouse incisor. These molecules include Shh signaling members Shh, Gli-1, Patch-1, TGF-β family member Alk5, Wnt signaling pathway inhibitor Dkk1 and a key molecule in the development of mouse incisors Pax9. Results showed that they were all expressed at the apical end of mouse incisor. Many studies have proposed that Shh plays a number of roles in stem cell biology, including regulation of fate decisions in embryonic stem cells and survival and self-renewal of neural stem cells (Balordi and Fishell, 2007, Machold et al., 2003). In mouse incisor, Gli1 has been proved expressed in the epithelium stem cells suggesting its function as a stem cell marker in tooth epithelium (Seidel et al., 2010). Interestingly, Gli1 positive

Hh-responsive cells were also found in the dental pulp mesenchyme and according to the recent research in MSCs niche, these cells were considered as MSCs (Zhao et al., 2014). However, our ISH only showed a weak signal in the labial side mesenchyme failed to verify this conclusion, an optimized experiment is required in the future. TGF-β signaling is involved in various biological processes including embryonic development, cell proliferation, migration and differentiation, extracellular matrix (ECM) secretion and epithelial-to-mesenchymal transition (Hill et al., 2009). A study has suggested the involvement of the TGF-β family in the growth of mouse incisor (Zhao et al., 2008). When *Alk5* was knockout specifically in the dental mesenchyme, the FGF signaling was down-regulated, leading to a reduced proliferation and fewer LRCs in the cervical loop (Zhao et al., 2011). Our result showed that Alk5 was expressed in TA cell where FGF signaling exists. This result suggested that Alk5 might control incisor growth mainly through regulating FGF signaling in TA cell proliferation. Interestingly, down regulation of FGF signaling in fast cycling cell population has been associated with Shh signaling expresstion and TGF-β family changes. This indicated an elaborated regulating network in the fast cycling cell population (Zhao et al., 2008).

Pax9, a Pax-family member that is expressed in specific anterior region of limbs, neural crest derived mesenchymal cells of the craniofacial region and midbrain (Peters et al., 1998) was also investigated in our study. Studies in homozygote knockouts mice showed that missing *Pax9* leads to secondary cleft palate and other abnormalities in craniofacial bones and cartilages. More importantly, these *Pax9* knockout mice are missing all their teeth (Peters et al., 1998). In humans, tooth loss due to function loss of Pax9 has also been reported widely suggesting a fundamental role of Pax9 in the tooth formation (Stockton et al., 2000, Lammi et al., 2003, Mostowska et al., 2013). Further analysis of the developing tooth has showed that in *Pax9* null allele homozygotes the tooth development is arrested after bud stage while the mesenchyme fails to condense

around the growing epithelial bud suggesting the function of Pax9 mainly focus in the dental mesenchyme (Peters et al., 1998). Our result of showing Pax9+ cells located in the mesenchymal area between the cervical loop where slow cycling cells were located and all development initiated, further supported the importance of incisor apical end as a stem cell niche which provides cell resource for the tooth growth.

4.3.9 Flow diagram of the chapter 4

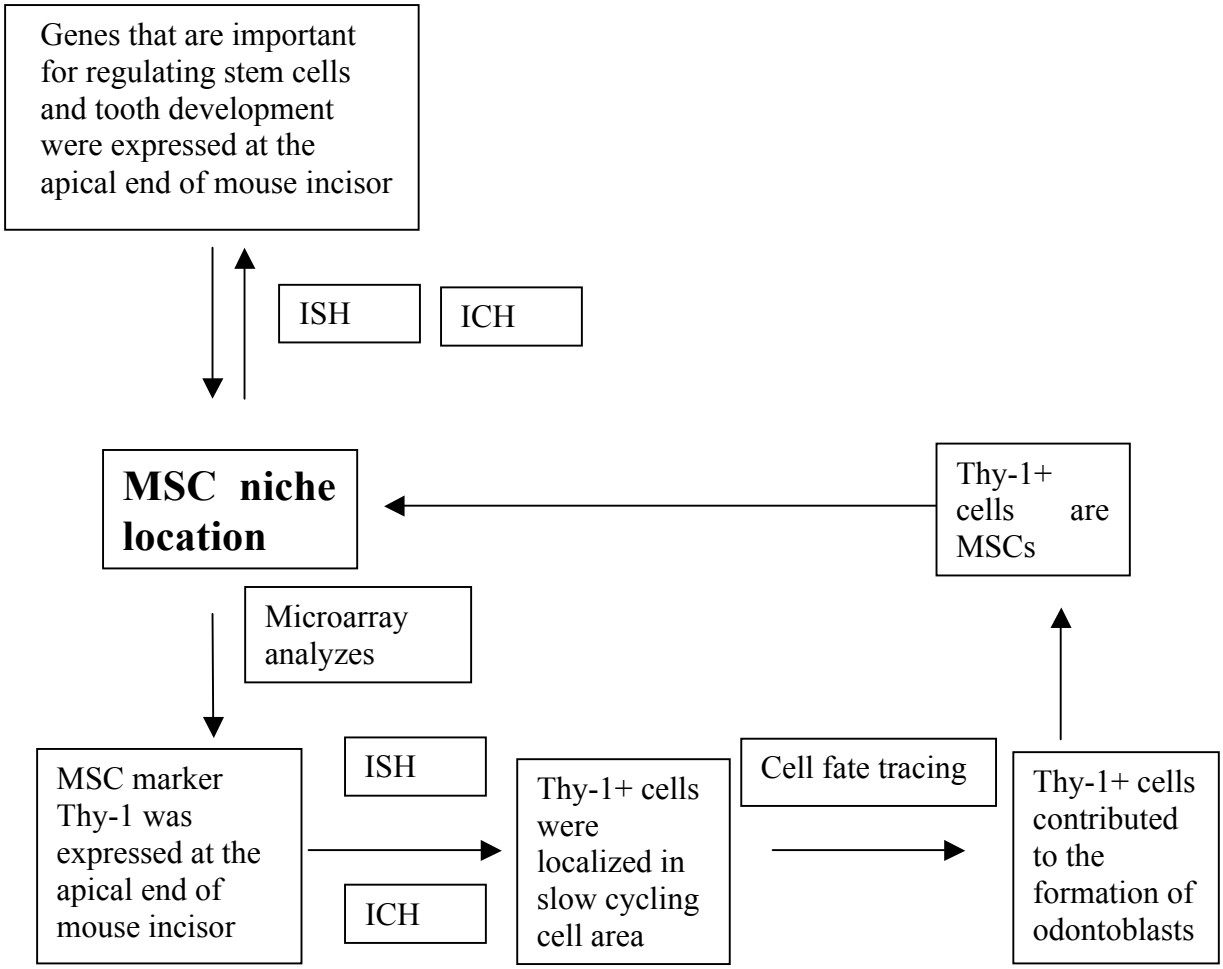

4.4 Conclusion

Mouse incisor is an excellent model to study the function and regulation of stem cells due to its continuously growing property. However, the absence of specific surface markers that can distinguish MSCs from their differentiated progeny always hampers the widespread use of MSCs for regenerative dentistry (Kaltz et al., 2010). Microarray performed in previous studies comparing stem cell gene expression have shown that Thy-1 was up-regulated in the apical end of mouse incisor where MSCs were located. Our ISH and immunostaining results further confirmed that: the expression of Thy-1 was limited to the apical end mesenchyme where the stem cell niche was located.

By tracing Thy-1+ cells in *Thy-1Cre*$^{+/-}$*;R26R mT/mG* and *Thy-1Cre*$^{+/-}$*;R26-Confetti* mice, we found that labeled Thy-1 progeny cells from the stem cell niche contributed to the whole dental pulp along the direction of tooth growth in addition to the formation of odontoblast. This result confirmed that Thy-1+ cells as dental MSCs contributed to the formation of mouse incisors. However, this contribution was limited, alternative patches of Thy-1- progeny cell in the odontoblasts indicated a stem cell population(s) also contributed to dental pulp formation. Interestingly, the finding of non thy-1 derived neurofilament+ cells formed odontoblasts may suggested another cell population that contributed to the formation of odontoblasts although further investigated is required.

In addition, severl molecules reported importantly regulating stem cell population were investigated in PN5 mouse incisor including Shh, Gli-1, Patch-1, Alk5, Dkk1 and Pax9. Results showed that they were all expressed at the apical end of mouse incisor suggesting an elaborated regulating network in this area.

Chapter 5 : The Role of PRC1 Complex in Mouse Incisor Dental Pulp Stem Cells

5.1 Introduction

Dental pulp stem cells are heterogeneous *in vitro* and their *in vivo* identities are still not well understood. A previous study has shown that a perivascular stem cell niche residing within dental pulp provide precursor cells differentiate into odontoblasts in order to repair tooth damage (Feng et al., 2011). However the limited contribution of these cells indicates the existence of another stem cell niche. By performing a series of label-retaining experiments and lineage tracing Thy-1expressing cells in our study, the apical end of mouse incisor was identified as a mesenchymal stem cell niche and was further investigated in this chapter (Fig. 5.1).

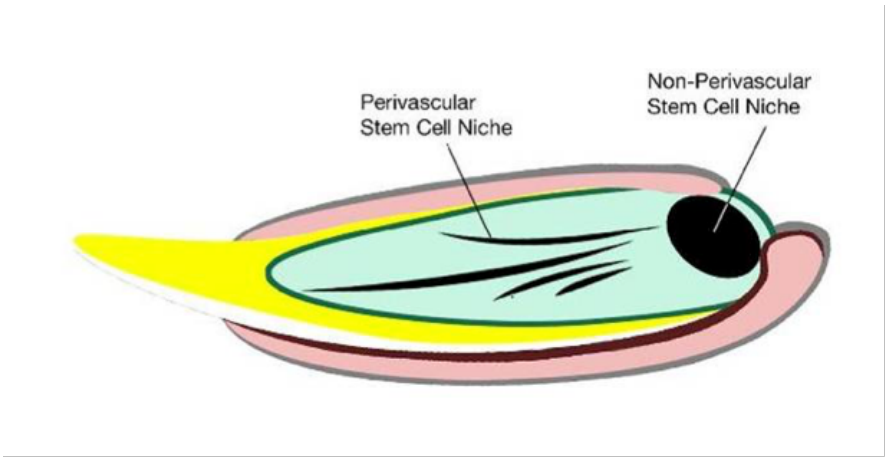

Fig 5. 1: Potential MSCs niches in the mouse incisor.

Studies have shown a perivascular stem cell niche residing within the dental pulp and responded to tooth damage by providing precursor cells that differentiate into odontoblasts (Feng et al., 2011). Non-perivascular stem cell niche located in the epical mesenchyme provided heterogeneous cell population and contributed to the formation of dental pulp tissue and dentin.

In chapter 3, the locations of slow cycling cells, quiescent cells and fast cycling cells (stem cell niche) in the mouse incisor were described. It is crucial to know what genes

are expressed in these cells. Previously, the role of PRC1 complex in the mesenchyme of mouse incisors has been investigated in our laboratory. Whole-mount ISH analysis showed that at postnatal stages all of the genes encoding proteins of the PRC1 complex were expressed in the dental mesenchyme adjacent to the labial and lingual cervical loop epithelium of the mouse incisor (Lapthanasupkul et al., 2012). This indicated that the PRC1 complex genes were expressed in highly proliferative cells (TA cells) in mouse incisors. The PRC1 complex may control the TA cell fate in the development of the mouse incisor.

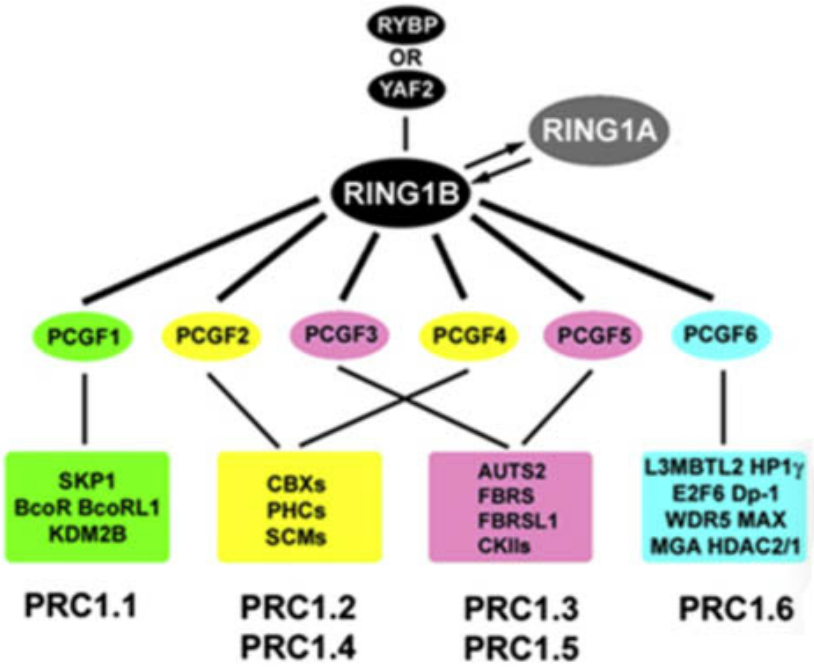

Fig 5. 2: Schematic depiction of PRC1 family complexes.

In *Drosophila*, the core PRC1 complex (Saurin et al., 2001) consists of Polycomb (Pc), a chromo domain containing protein that binds to H3K27me3 (Fischle et al., 2003); dRing, the H2A ubiquitination enzyme (Wang et al., 2004); Posterior sex combs (Psc), which is responsible for *in vitro* chromatin compaction (Francis et al., 2004); and Polyhomeotic (Ph). Additional components such as the PcG protein Sex Comb on Midleg (Scm) are also reported. In mammalian, the PRC1 purified from HeLa cells contains various chromo domain proteins (CBX) homologous to Pc; RING1A and RING1B that similar to dRing; three Ph homologs (PHC1-3); six human Psc homologs that are known collectively as Polycomb group RING fingers (PCGFs); and a Scm homolog, SCMH1 (Levine et al., 2002). Combinatorial association of these different PcG homologs are likely to give rise to functionally distinct PRC1 complexes in humans (Gao et al., 2012). Interestingly, all PRC1 complexes contain RING1A and RING1B (enzymes that catalyze H2AK119ub1 and 2). PRC1 complexes can be divided into six different groups, based on the different PCGF they contain. RING1/YY1-binding protein (RYBP) or its homolog, YAF2, is found in most PRC1 complexes except PRC1.2 and 1.4 which contain CBXs, Ph homologs PHCs and SCMs. Adapted from (Gao et al., 2012).

In the PRC1 complex, Ring1a and Ring1b were considered as core components that play an important role in PcG-mediated silencing by possessing E3 ubiquitin ligase activity for histone H2A (Wang et al., 2004). In ES cells, a group of genes where H2AK119u1 is deposited in a Ring1-dependent manner were identified. These genes are the central targets of Polycomb silencing that are required to maintain ES identity (Endoh et al., 2012). Evidence from ES cells has demonstrated the possible roles of Ring1b in controlling cell proliferation and the maintenance of ES cells. Knockout Ring1a/b in mouse ES cells suggested the role of Ring1a/b for the maintenance of ES cell identity by silencing the genes that govern differentiation of ES cells. In addition, Ring1a/b has been reported to mediate Oct3/4-dependent transcriptional repression. These results indicated the role of Ring1a/b in regulating ES cell self-renewal (Endoh et al., 2008). Furthermore, in order to maintain undifferentiated ES cells, Ring1b is needed to silence a particular subset of genes, which are co-occupied by ES cell regulators including *Oct4* and *Nanog* (van der Stoop et al., 2008). This result further supported the essential role of Ring1b in the stable maintenance of mouse ES cells.

Bcor, another key component in the PRC1 complex, has been found to regulate developmental genes as early as embryonic stem cell differentiation (Wamstad et al., 2008). Bcor was reported to regulate mesenchymal stem cell function through epigenetic mechanisms, which have been identified as important regulators of MSC fate and in the osteogenic and adipogenic differentiation of MSCs (Teven et al., 2011, Cironi et al., 2009). In tooth studies, it has been shown that Bcor mutation increases the proliferation and osteo-dentinogenic potential of MSCs isolated from the dental pulp of a patient with OFCD syndrome, a condition that affects the development of the eyes (oculo-), facial features (facio-), heart (cardio-) and teeth (dental) (Fan et al., 2009). Previous work in our laboratory on *K14-Cre* mediated *Bcor* mutation showed that complete deletion of epithelium-specific *Bcor* can only cause a mild effect on

craniofacial development. However, following study in our laboratory by Dr. Jifan Feng showed that *Pax3-Cre* mediated deletion of the *Bcor* in the craniofacial mesenchyme of neural crest origin resulted in an obvious overgrowth of mouse upper incisors (Fig. 5.3). This suggested the role of *Bcor* in the mesenchyme is more crucial for maintaining craniofacial development; especially tooth development and growth. Therefore more work is required to further understand the role of *Bcor* in dental pulp stem cell homeostasis during development and postnatal growth.

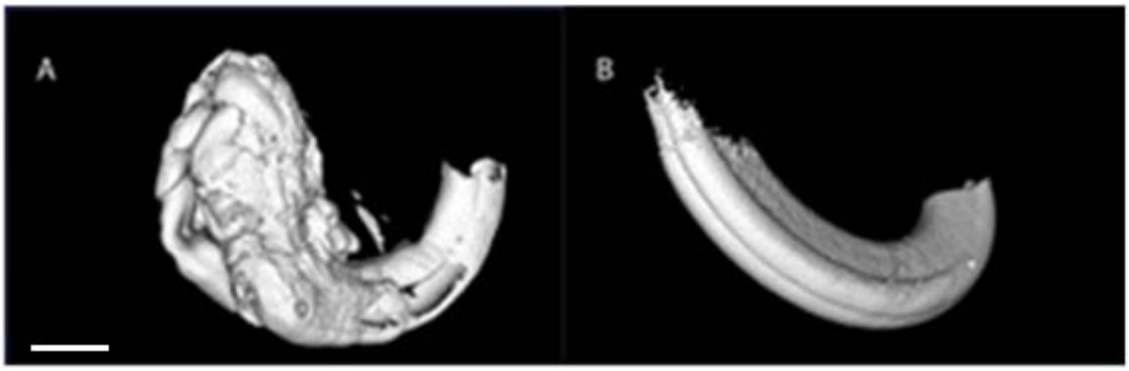

Fig 5. 3: Overview of adult *Bcor*$^{fl/}$*;Pax3 Cre* incisor phenotype by 3D micro-CT reconstruction.

(A) Mutant incisor showed an obvious overgrowth and a bulged cervical loop at the apical end in comparison with the normal mouse incisor (B) (Dr Jifan Feng performed first analysis, more micro-CT were performed by myself afterwards). Scale bar=500μm.

Taken together, both BcoR and Ring proteins in the PRC1 complex are crucial for repressing developmental regulators and maintaining the undifferentiated state of embryonic stem cells. Furthermore, they were expressed in the cells with high proliferative rate in the apical end of mouse incisor. Loss of Bcor led to an obvious overgrowth. Therefore, this chapter will investigate the function of BcoR and Ring1 as key components of the PRC1 complex in controlling the fast cycling cells/TA cells of mouse incisors.

5.2 Results

5.2.1 Identification of Ring1 and BcoR localization in mouse incisor dental pulp

To investigate the location where *Ring1* and *Bcor* genes are expressed, ISH was performed in the postnatal mouse incisor pulp. Whole mount ISH analysis showed that at postnatal stages Ring1 and BcoR were both expressed in the location of highly proliferative cells in mouse incisors (Fig. 5.4 A). In the incisor pulp, Ring1a was predominantly expressed in the whole apical end (Fig. 5.4 B, B') including the fast cycling and slow cycling cell area, while Ring1b was more restricted in the mesenchymal tissue close to the labial cervical loop (Fig. 5.4 C, C') where fast cycling cells are located. The ISH results of BcoR also showed a similar expression area as Ring1b, the fast cycling cell area, but more expression was detected in the preodontoblasts, odontoblasts and dental follicle (Fig. 5.4 D, D') compared with *Ring1b*. Combined with previous work, we have demonstrated that all the gene encoding proteins of the PRC1 complex including *Ring1* and *BcoR* are expressed in the TA cells. This indicated a main role of PRC1 complex in controlling TA cells for the development and growth of the mouse incisor.

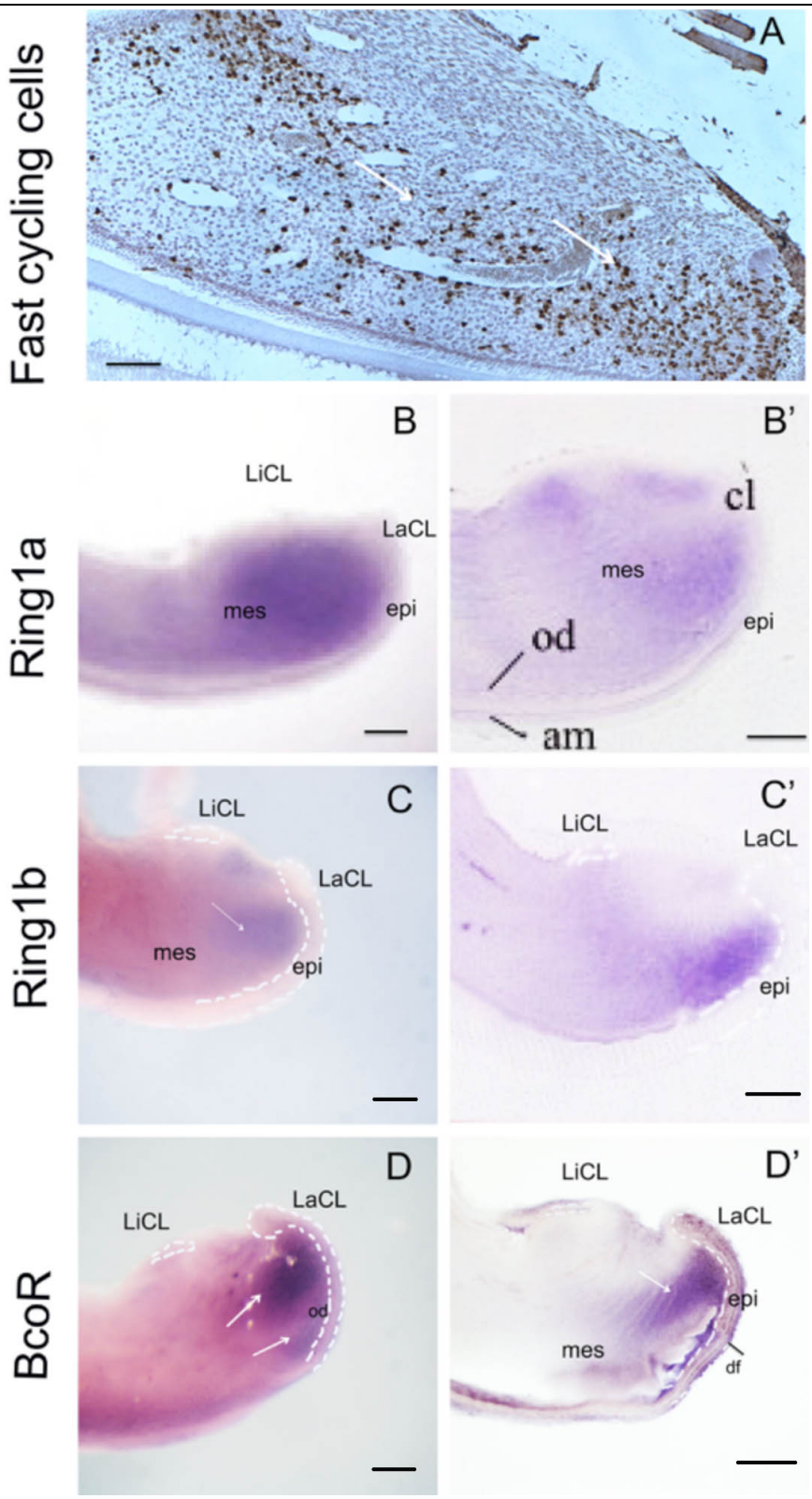

Fig 5. 4: Whole mount ISH of *Ring1* and *BcoR* in the incisor dental pulp of PN5 (sagittal section).

(A) Arrows show BrdU labeled fast cycling cells in the mouse incisor. (B-D) Whole mount ISH on PN5 mice incisors and vibratome sections of ISH results (B'-D'). (B, B') Whole mount ISH and ISH results sections show that Ring1a was expressed in the whole apical end, including the fast cycling cells. (C, C') Ring1b signal was detected mainly in the area close to the cervical loop where the fast cycling cells are located. (D, D') BcoR was expressed mainly in the area close to the labial side cervical loop mesenchyme, odontoblasts epithelium and dental follicle (arrows). Abbreviation: LiCL, lingual cervical; LaCL, labial cervical; am, ameloblasts; od, odontoblasts; mes, mesenchyme; epi, epithelial; df, dental follicle. Scale bar=100µm in (A). Scale bars =500um in (B-D, B'-D').

To detect the Ring1+ and BcoR+ cells, immunostaining was performed both on wax section and cryosection of mouse incisors, unfortunately, immunostaining failed to show any positive reaction, which was possibly due to the quick degradation of Ring1 and Bcor protein during the sample preparation. Thus cells were manually dissected from the apical end of mouse incisor and quickly fixed on section by cytospin before immunostaining was preformed. Immunostaining on these fixed cells (Fig 5.5) showed that around 30% (7/23) pulp cells were Ring1+. Considering only apical end cells were analyzed and Ring1 is expressed in the fast cycling cell area at the apical end of mouse incisor, this number must be higher than the number of Ring1+ cells in the whole dental pulp. Thus result roughly consistent with the percentage of fast cycling cells (15-20%) in the whole dental pulp tissue. However, the detection of Bcor was still unsuccessful. A more effective antibody is required.

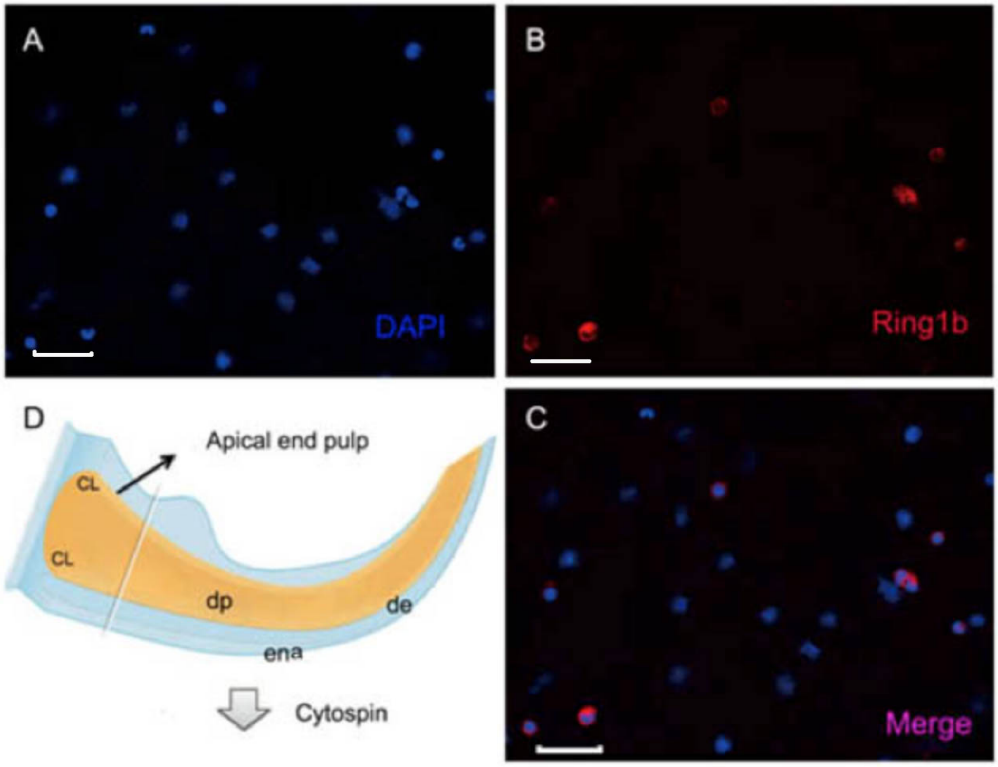

Fig 5. 5: Immunostaining of Ring1b in dental pulp cells from the apical end of mouse incisor.

Apical end dental pulp cells from PN5 mouse incisors were manually dissected and collected for cytospin (D), cells were quickly fixed on slides where immunostaining was performed (A-C). Abbreviation: CL, cervical loop; dp, dental pulp; ena, enamel; de: dentine. Scale bar=50μm in (A, B, C).

5.2.2 Histological analysis of incisor phenotypes of adult *Ring1a*$^{-/-}$; *Ring1b*$^{cko/cko}$ mutants

To investigate the role of Ring1 in the continuously growing mouse incisor, a histological analysis was applied by using mouse lines to genetically knockout the expression of Ring1 complex. *Ring1a*$^{-/-}$;*Ring1b*$^{fl/fl}$ mice were obtained by crossing the *Ring1a*$^{-/-}$ mice with the *Ring1b*$^{fl/fl}$ mice. *R26::CreERT2* transgenic mice were crossed with *Ring1a*$^{-/-}$; *Ring1b*$^{fl/fl}$ mice to generate *Ring1a* $^{-/-}$;*Ring1b*$^{fl/fl}$;*R26::CreERT2* mice to accomplish conditional inactivation of Ring1b *in vivo*. Since an ubiquitous Cre exists in all the cells, by giving tamoxifen injection, Cre recombination would be able to cause Ring1b inactivation in all the animal cells. The conditional deletion of Ring1b was carried out at postnatal stages by injecting OHT at PN9 and PN13 and the *Ring1a*$^{-/-}$;*Ring1b*$^{cko/cko}$ mice were sacrificed at PN17 (n=20). The efficiency of tamoxifen induced Cre expression to inactive Ring1b was confirmed by ISH of PN17 incisors and Ring1 deletion was checked by PCR. The result showed that Cre mRNA was expressed in all the incisor dental pulp cells (Fig. 5.6) and no Ring1b was expressed.

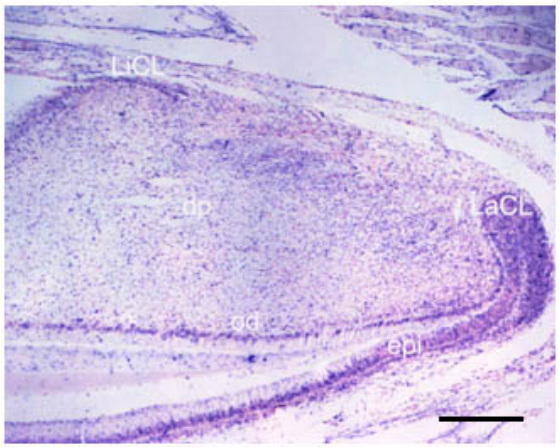

Fig 5. 6: ISH of Cre in PN17 *Ring1a*$^{-/-}$; *Ring1b*$^{cko/cko}$ mouse incisor.

Cre was ubiquitously expressed in the whole incisor dental pulp tissue, including epithelia and mesenchymal tissue. Abbreviation: LiCL, lingual cervical; LaCL, labial cervical, od, odontoblasts, dp, dental pulp cells, epi, epithelial. Scale bar=200μm.

The histology analysis of the Ring1 knockout mouse incisor showed that PN17 *Ring1a*$^{-/-}$*;Ring1b*$^{cko/cko}$ incisors had abnormal cervical loops at their apical ends (Fig. 5.7 A-A5 and Fig. 5.8 B-B5), compared with *Ring1a*$^{-/-}$*;Ring1b*$^{fl/fl}$ *Cre-* incisors (Fig. 5.7 a-a2 and Fig. 5.8 b-b2). Furthermore, differentiation of odontoblasts and ameloblasts was disrupted in *Ring1a*$^{-/-}$*; Ring1b*$^{cko/ck}$ along most of the incisor length (Fig. 5.7 A1-A4 and Fig. 5.8 B1-B4), subsequently leading to disturbances in enamel and dentin formation, compared with *Ring1a*$^{-/-}$*;Ring1b*$^{fl/fl}$ *Cre-* incisors (Fig. 5.7 a2 and Fig. 5.8 b2). Histological analysis further revealed that in *Ring1a*$^{-/-}$*;Ring1b*$^{fl/fl}$ *Cre*-incisors, the odontoblasts and ameloblasts were elongated and highly polarized, while in *Ring1a*$^{-/-}$ *;Ring1b*$^{cko/cko}$ incisors were more round in shape and had no nuclear polarization. Moreover, odontoblast and ameloblast differentiation was rarely observed at the inner side of the labial cervical loop in *Ring1a*$^{-/-}$*;Ring1b*$^{cko/cko}$ incisors, compared with the same region in *Ring1a*$^{-/-}$*;Ring1b*$^{fl/fl}$ *Cre-* incisors. Lastly, the labial cervical loop contained a few cells of stellate reticulum in *Ring1a*$^{-/-}$*;Ring1b*$^{cko/cko}$ mice in comparison with *Ring1a*$^{-/-}$*;Ring1b*$^{fl/fl}$ *Cre-* mice.

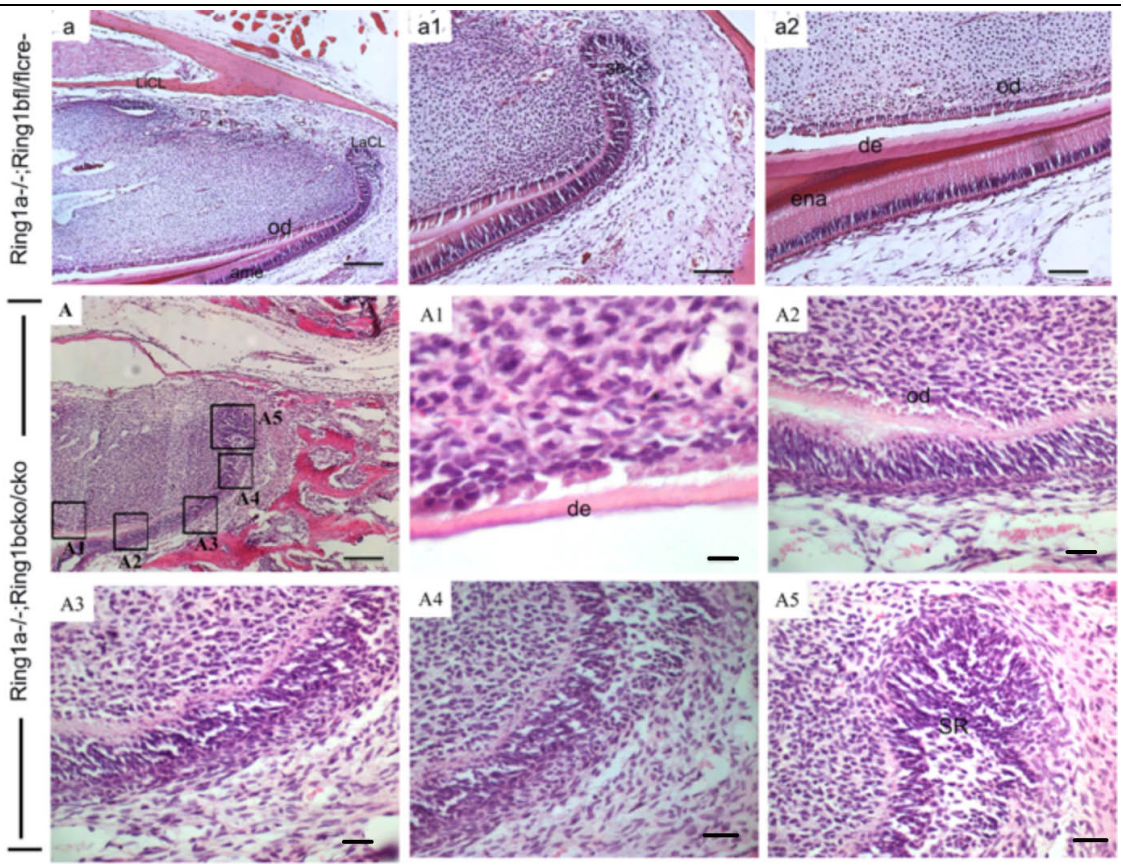

Fig 5. 7: Hematoxylin and eosin stained sagittal sections of a mandible incisor of 17 day-old *Ring1a$^{-/-}$;Ring1b$^{fl/fl}$Cre-* (a-a2) and *Ring1a$^{-/-}$;Ring1b$^{cko/cko}$* mice (A-A5).

(a-a2) *Ring1a$^{-/-}$; Ring1b $^{fl/fl}$Cre-* incisors showed normal incisor development. (a1–a2) Higher power views of boxed regions in (a). In *Ring1a$^{-/-}$;Ring1b$^{fl/fl}$ Cre-* mouse incisor, normal labial cervical loop containing a core of stellate reticulum was shown in (a1); normal odontoblast and ameloblast differentiation was seen in (a2). (A-A5) *Ring1a$^{-/-}$; Ring1b$^{cko/cko}$* incisors showed abnormal incisor development. Differentiation of odontoblasts and ameloblasts was disrupted in Ring1a-/-;*Ring1b$^{cko/cko}$* along most of the incisor length, subsequently leading to disturbances in enamel and dentin formation (A1-A4). Either dentin or enamel was thinner and less mineralized in mutants when compared to the controls (A1, A2). (A5) showed labial cervical loop containing a few cells of SR in *Ring1a$^{-/-}$;Ring1b$^{cko/cko}$* mice. Abbreviation: LiCL, lingual cervical loop；LaCL, labial cervical；od, odontoblasts；de, dentin；ena, enamel；SR, stellate reticulum. Scale bar= 200μm in (a). Scale bars =50μm in (a1, a2). Scale bar =150μm in (A), Scale bars =25μm in (A2-A5), =15μm in (A1).

.

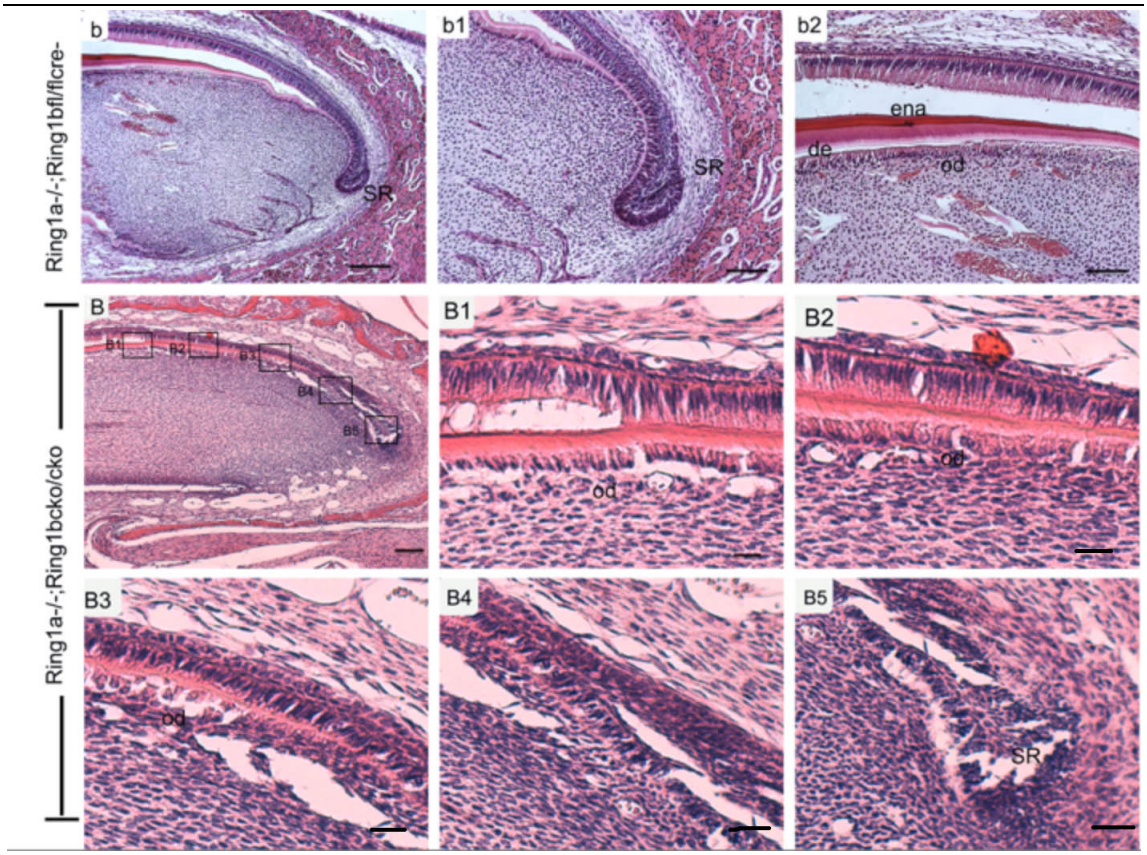

Fig 5. 8: Hematoxylin and eosin stained sagittal sections of a maxillary incisor of 17 day-old *Ring1a$^{-/-}$;Ring1b$^{fl/fl}$ Cre-* (b-b2) and *Ring1a$^{-/-}$;Ring1b$^{cko/cko}$* mice (B-B5).

(b) *Ring1a$^{-/-}$; Ring1b$^{fl/fl}$Cre-* incisors showed normal incisor development, including well formed labial cervical loop (b1) and normal differentiated odontoblasts, ameloblasts (b2). (b1) Higher power views of labial cervical loop that contains a core of SR in *Ring1a$^{-/-}$;Ring1b$^{fl/fl}$ Cre-* mice. (b–b2) Higher power views of differentiation regions in (b). (B1-B4) Odontoblast and ameloblast differentiation failed in *Ring1a$^{-/-}$; Ring1b$^{cko/cko}$* in mice. (B5) showed labial cervical loop containing a few cells of SR in *Ring1a$^{-/-}$;Ring1b$^{cko/cko}$* mice. Abbreviation: od, odontoblasts; de, dentin; ena, enamel; SR, stellate reticulum. Scale bar= 200µmin (b), Scale bars =100µm in (b1, b2). Scale bar =100µm in (B). Scale bars =25µm in (B1-B5).

5.2.3 Investigation of cell proliferation upon *Ring1a$^{-/-}$;Ring1b$^{cko/cko}$* deletion

Histological analysis of *Ring1a$^{-/-}$;Ring1b$^{cko/cko}$* showed a growth arrest in the mouse incisors due to the failure of ameloblast and odontoblast formation. Since Ring1a/b was expressed in the cells with a high proliferative rate, loss of Ring1a/b seems to affect this cell population. Therefore, immunostaining was performed both on *Ring1a$^{-/-}$;Ring1b$^{cko/cko}$* incisors and *Ring1a$^{-/-}$;Ring1b$^{fl/fl}$ Cre-* incisors to investigate cell

proliferation. PH3, a marker of mitotic cells was used to detected proliferation by immunostaining. The result showed a significant decrease in cell proliferation in *Ring1a*$^{-/-}$;*Ring1b*$^{cko/cko}$ incisor (Fig. 5.9) indicating the abnormal development and arrest in growth in the *Ring1b*$^{cko/cko}$ mouse incisor, possibly because of the loss of proliferation in fast cycling cells.

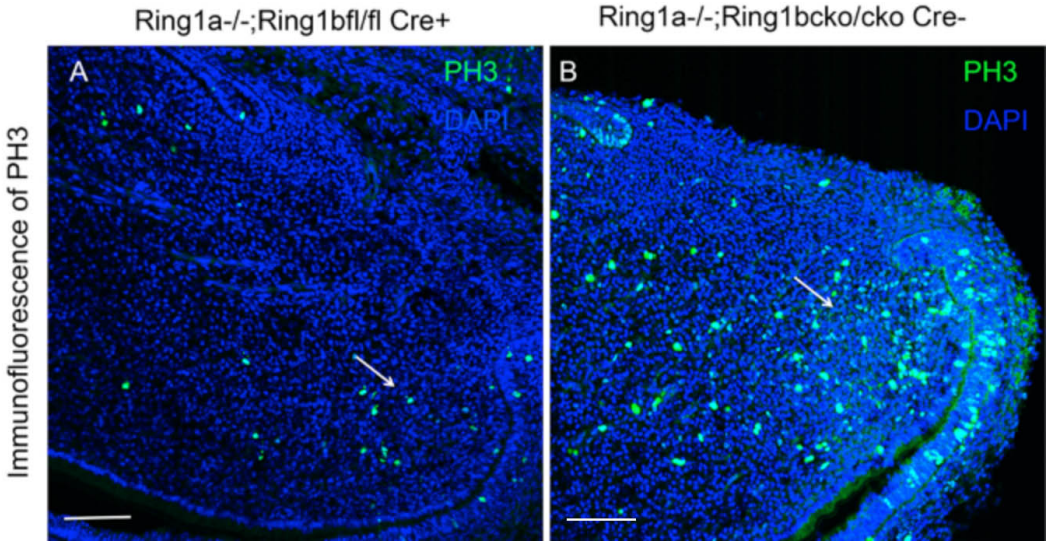

Fig 5. 9: Immunostaining of PH3 on sagittal sections of incisors.

(A) PH3 signal (arrows) was rarely detected in 17 day-old *Ring1a*$^{-/-}$;*Ring1b*$^{cko/cko}$ incisor compared to (B) *Ring1a*$^{-/-}$; *Ring1b*$^{fl/fl}$*Cre-* mice suggesting a decrease in cell proliferation. Scale bars =100 µm in (A B).

5.2.4 Investigation of gene expression changes in *Ring1a*$^{-/-}$;*Ring1b*$^{cko/cko}$ mouse incisor

To investigate gene expression changes upon Ring1 deletion, a microarray comparing *Ring1a*$^{-/-}$;*Ring1b*$^{cko/cko}$ and *Ring1a*$^{-/-}$;*Ring1b*$^{fl/fl}$ *Cre-* mouse incisor dental pulp cells were preformed. *Ring1a*$^{-/-}$;*Ring1b*$^{cko/cko}$ mice were administrated tamoxifen and control mice were given corn oil at PN9 and PN13 and were sacrificed at PN16 followed by RNA extraction and microarray analysis. According to microarray results, about 2000 genes showed significant up-regulation and 980 genes were down-regulated more than a 2-fold change upon Ring1 deletion (Fig. 5.11). Among these, a set of genes of interest

were selected and validated by qPCR (Fig. 5.12).

5.2.4.1 Analysis of down-regulated gene expression in *Ring1a*$^{-/-}$; *Ring1b*$^{cko/cko}$ mouse incisor pulp

Combination of the microarray analysis and qPCR validation showed that loss of Ring1 led to down-regulated pathways that control the cell cycle as well as cell proliferation corresponding to the growth arrest in *Ring1a*$^{-/-}$; *Ring1b*$^{cko/cko}$ mouse incisor. Furthermore, in *Ring1a*$^{-/-}$;*Ring1b*$^{cko/cko}$ incisor, Wnt signaling pathway inhibitor 1 (Dkk1) was down-regulated more than 2 fold. However, this result did not mean an up-regulation of Wnt signaling pathway. Axin2, axis inhibition protein 2, a reporter of Wnt/beta-catenin signaling, showed an obvious down-regulated expression in *Ring1a*$^{-/-}$; *Ring1b*$^{cko/cko}$; *Axin2*^{LacZ} mouse incisor, suggesting a down-regulated Wnt/beta-catenin signaling (Fig. 5.10). The mechanism of down-regulated expression for both Dkk1 and Wnt signaling is not clear, but the loss of cell proliferation might be a main reason since both Dkk1 and Wnt signaling are expressed in the fast cycling cells which greatly reduced their proliferation (Fig. 5.11).

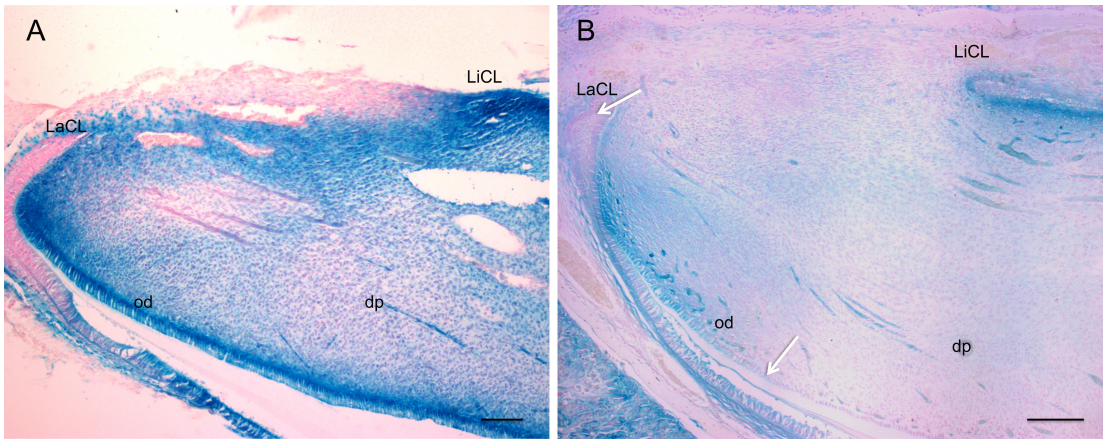

Fig 5. 10: Down-regulation of Wnt/b-catenin signaling in the Ring1 knockdout mouse incisor.

(A) X-gal staining of Wnt/b-catenin reporter mouse incisors showed that Axin2 was strongly expressed in the preodontoblasts, odontoblasts and in the mesenchyme surrounding the cervical loops. In addition, expression was seen throughout lingual epithelium and weakly in labial preameloblasts and ameloblasts. (B) X-gal staining of Ring1 knockout Axin2 reporter mouse incisor showed a weak expression of Axin2 and a failure formation of odontoblast and abnormal labial cervical loop (arrows). Abbreviation: od, odontoblasts; dp, dental pulp; LaCL, labial cervical loop; Li, Lingual cervical loop. Scale bar =100 µm in (A). Scale bar =100 µm in (B).

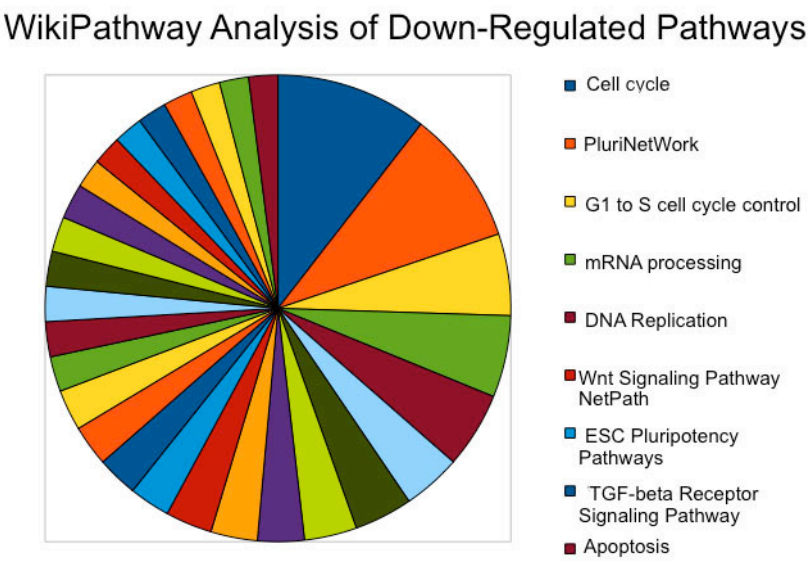

Fig 5. 11: WikiPathway analysis of down-regulated pathways in the *Ring1a/b* knockout mouse incisor pulp.

The result showed that pathways that control cell cycle and proliferation were all down-regulated. Furthermore, Wnt signaling and TGF-β signaling pathways were also down-regulated. In addition, cell differentiation potential and apoptosis were all down-regulated upon Ring1 deletion.

5.2.4.2 Analysis of Notch signaling molecules in *Ring1a*$^{-/-}$; *Ring1b*$^{cko/cko}$ mouse incisor pulp

Among the gene expression changes, about 2000 genes, including Notch pathway genes, had higher expression following the loss of *Ring1* gene (Fig. 5.12). Previous research has shown that polycomb group (PcG) proteins bind to multiple genes in the Notch pathway and control their transcription as well as Notch signaling (Martinez et al., 2009). In a study of *Drosophila melanogaster* eye, PcG protein Polyhomeotic (PH) as a tumour suppressor, controls cellular proliferation by silencing multiple Notch signaling components (Martinez et al., 2009). In the mouse incisor model system, microarray and qPCR analysis showed that Notch signaling molecules including Notch1, Notch 2, Notch 3, Notch 4 and Notch ligands delta-like (Dll) 1, Dll 4, Jagged1, Jagged 2 were all up-regulated following the loss of Ring1. Among these changes, Notch 3 and dll1 were dramatically up-regulated, increasing more than 4 fold. These results further confirmed

the repressive role of PRC1 to the Notch signaling that regulates the renewal and fate decisions of stem cells in the mouse incisor, as well as, other multiple tissues (Hurlbut et al., 2007).

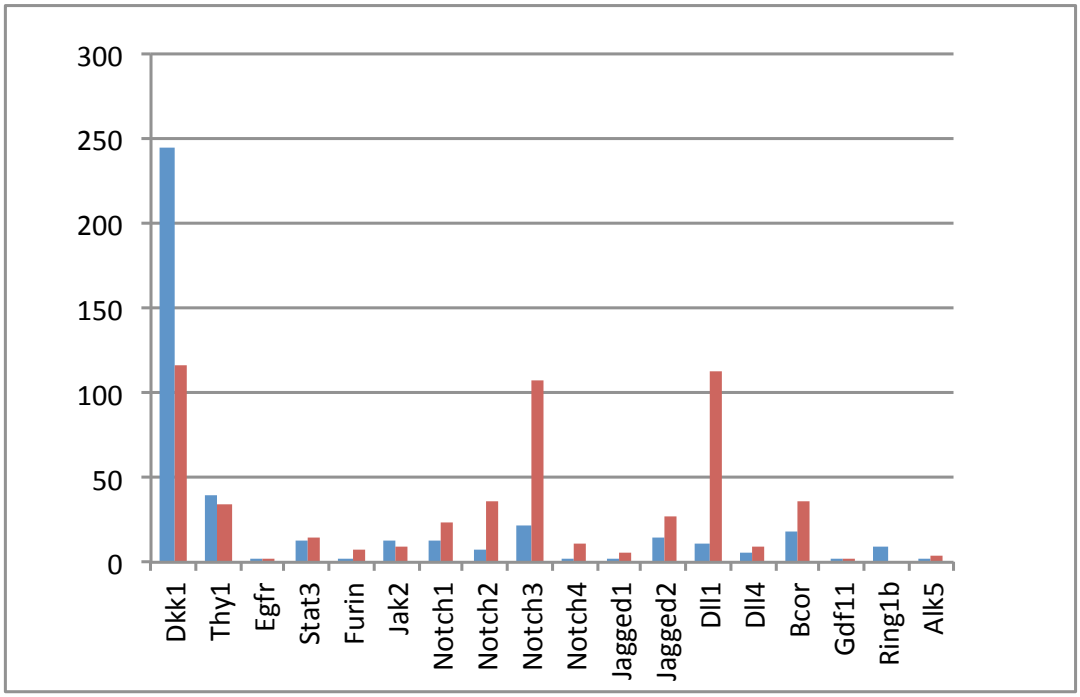

Fig 5. 12: qPCR validation of gene expression changes in *Ring1a*$^{-/-}$;*Ring1b*$^{cko/cko}$ mouse incisor.

Genes were selected according to microarray, *Gdf11* was considered as datum 1, x-axis shows change fold compared to *Gdf11*.

5.2.4.3 Analysis of *Hox* genes in *Ring1a*$^{-/-}$; *Ring1b*$^{cko/cko}$mouse incisor dental pulp cells

Polycomb-group proteins (PcG) are well known for silencing *Hox* genes through modulation of chromatin structure during embryonic development in fruit flies (Di Croce and Helin, 2013). In mammals *Hox* gene expression is important in many aspects of development (Wang et fal., 2002). For example, *Hox* genes play a significant role in controlling cranial neural crest population development in the formation of craniofacial pattern and morphogenesis (Akin and Nazarali, 2005). Studies have demonstrated that another PcG gene *Bmi1*-mediated repression of *Hox* genes preserves the

undifferentiated state of stem cells. Our findings in the mouse incisor further confirmed the repressive role of the PRC1 complex in the regulation of *Hox* genes that are required for the maintenance of adult stem cells and for prevention of inappropriate differentiation. The microarray analysis of mouse incisor dental pulp cells from *Ring1a*$^{-/-}$;*Ring1b*$^{cko/cko}$ and *Ring1a*$^{-/-}$;*Ring1b*$^{fl/fl}$ *Cre-* showed that 19 *Hox* genes from 4 different *Hox* clusters up-regulated following the loss of *Ring1*. To better illustrate the up-regulation of *Hox* genes in *Ring1* null dental pulp tissue, the comparison of *Hox* genes between *Ring1a*$^{-/-}$;*Ring1b*$^{cko/cko}$ and *Ring1a*$^{-/-}$;*Ring1b*$^{fl/fl}$ *Cre-* were shown in Fig. 5.13. This result demonstrated that *Hox a9, b7, c8, c10, c13* and *d13* were up-regulated more than 20 fold, while, *Hox a10, c4, d8, d9, d10* dramatically increased more than 50 fold. Thus, Ring1 suppressed the expression of *Hox* genes in the mouse incisor dental pulp as well as in other tissues.

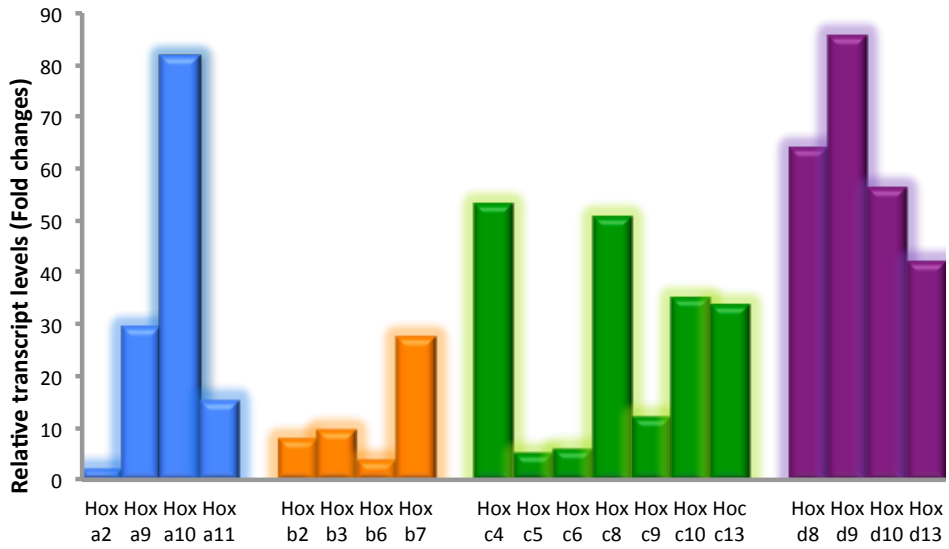

Fig 5. 13: Up-regulation of *Hox* gene family upon *Ring1a/b* inactivation.

Gene changes was compared between *Ring1a*$^{-/-}$;*Ring1b*$^{cko/cko}$ and *Ring1a*$^{-/-}$; *Ring1b*$^{fl/fl}$ *Cre-* mouse incisor dental pulp cells. 19 *Hox* genes from 4 clusters showed at least 2 fold up-regulation. (Samples were prepared together with Dr. Zhengwen An who performed this data analysis)

5.2.5 Comparison of gene expression changes between MSCs of dental pulp and ES cells upon *Ring1a/b* inactivation.

Since the Ring1 was detected as being expressed only at the apical end of the mouse incisor where MSCs were located and where the tooth grows, how the gene expression of these cells in stem cell niche area react to the deletion of the Ring1a/b became of interest. Therefore, we compared the microarray results of *Ring1a*$^{-/-}$; *Ring1b*$^{cko/cko}$ mouse incisor with the ES cell gene changes after *Ring1a/b* deletion (Fig. 5.14). The results showed that gene changes of the cells in the dental pulp stem cell niche area are similar with those of ES cells. Many genes involved in the tooth development showed an obvious up-regulation upon *Ring1a/b* deletion including the *Gata6, Tbx18, Zic1, Barx1, Bmp6, Crlf1* and *Hox* gene families.

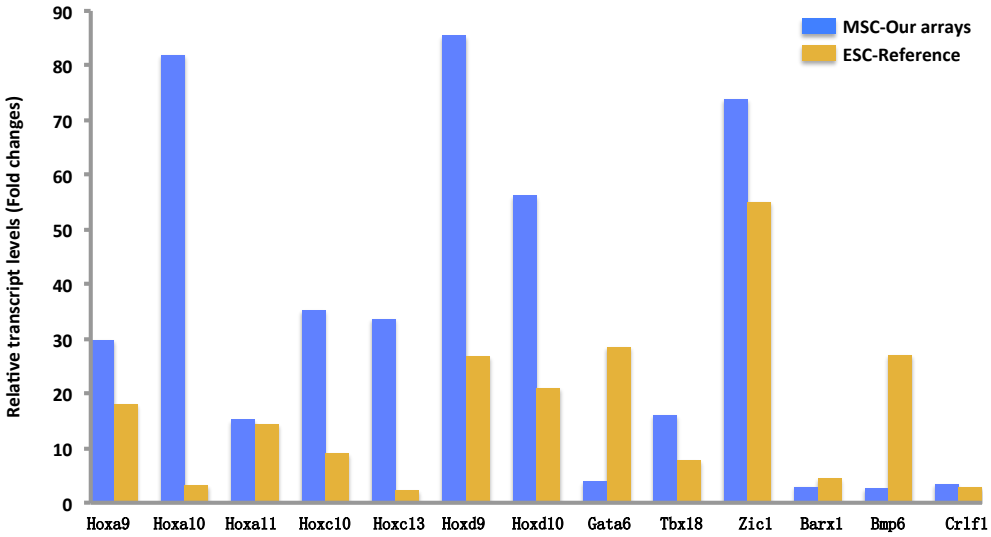

Fig 5. 14: Up-regulation of genes involved in tooth development upon *Ring1a/b* inactivation in both dental pulp MSCs and ESs.

Gene changes were compared between *Ring1a*$^{-/-}$;*Ring1b*$^{cko/cko}$ mouse incisor dental pulp cells and Ring1a/b knockout ESs (Endoh et al., 2008). (Samples were prepared together with Dr Zhengwen An who performed this data analysis)

5.2.6 Tooth phenotype in adult *Pax3-Cre Bcor* conditional knockout mice

Bcor, another component of the PRC1 complex is X-linked, therefore male knockout mice completely lose Bcor in all the Cre-expressing cells and showed more severe phenotpyes than their female counterparts. Previous studies of tooth phenotypes of *Bcor*$^{fl/y}$*;Pax3Cre* mutants by Dr Jifan Feng in our laboratory showed that the lower incisors were significantly smaller with delayed odontoblast and ameloblast differentiation. The cervical loop structures were also abnormal at both lingual and labial sides and the SR were barely distinguishable. The upper incisors of *Bcor*$^{fl/y}$*;Pax3Cre* were generally smaller than their Cre-negative littermates. However, there could be variable phenotypes of individuals such as additional dental epithelial abnormalities.

Since *Bcor*$^{fl/y}$*;Pax3Cre* mutants die at birth due to severe cleft palate, heterozygous *Bcor*$^{fl/+}$*;Pax3Cre* mutants become the only way to further understand the role of Bcor postnatally in the continous tooth growth. However, in our studies, of all the samples (n=40) analyzed in our analyzes, no incisors showed phenotypical changes compared with their littermate controls and both upper and lower incisor appeared relatively normal (Fig. 5.15).

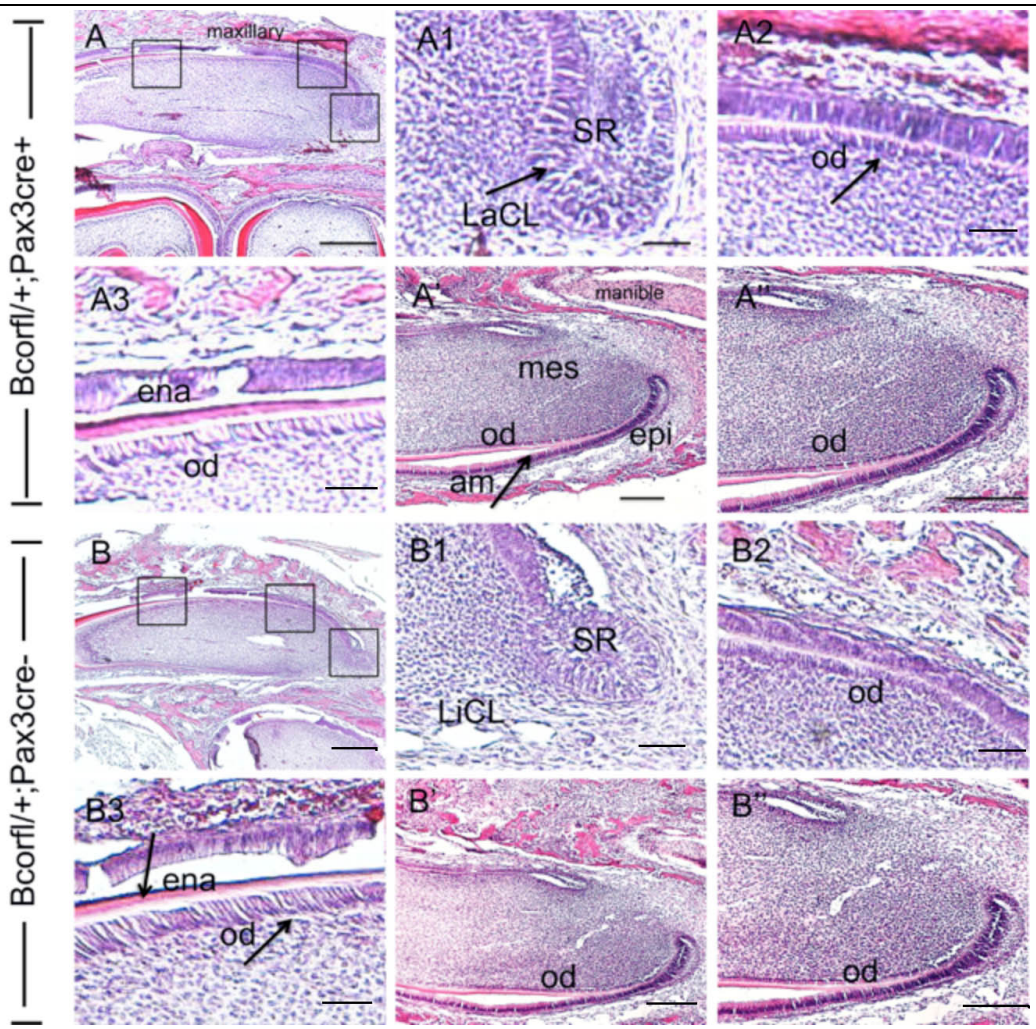

Fig 5. 15: Hematoxylin and eosin stained incisors of 8 day-old *Bcor$^{fl/+}$;Pax3Cre-* (A) and *Bcor$^{fl/+}$;Pax3Cre+* mice (B) (sagittal sections).

Bcor$^{fl/+}$;Pax3Cre+ mouse incisor (A) showed a normal maxillary incisor development in comparison with *Bcor$^{fl/+}$;Pax3Cre-* incisor (B). (A1) Higher power views of labial cervical loop contained a core of SR (arrow) in *Bcor$^{fl/+}$;Pax3 Cre+* mouse incisor. (A2–A3) Higher power views of differentiation regions in (A) showed normal odontoblast and ameloblast differentiation (arrow). (A'-A'') showed a normal mandible incisor development. (B1-B3) Higher power views of boxes in (B) showed a normal labial cervical loop (arrow) and cell differentiation regions (arrow) in *Bcor$^{fl/+}$;Pax3Cre-*. Abbreviation: LiCL, lingual cervical loop; LaCL, labial cervical; od, odontoblasts; ena, enamel; SR, stellate reticulum. Scale bars= 500µmin A, B. Scale bars =25µm in (A1-A3, B1-B3). Scale bars =200µm in (A', B'). Scale bars =250µm in (A'', B'').

To investigate the postnatal phenotypes of *Bcor$^{fl/+}$;Pax3 Cre+* incisors, certain genes which are known to be markers of functional odontoblasts and ameloblasts, including dentin sialophosphoprotein (*Dspp*), *amelogenin* and *shh* were analyzed by ISH. Dspp, normally expressed in odontoblasts and newly differentiated ameloblasts, was found to be expressed normally both in mutant and WT incisors (Fig. 5.16 A, A'). *Amelogenin*, a

gene encoding the major structural protein of enamel matrix and expressed in functional ameloblasts was also detected to be normally expressed in *Bcor*$^{fl/+}$*;Pax3Cre+* incisors (Fig. 5.16 B, B'). Furthermore, Shh, which normally marks pre-ameloblasts, also showed no difference in comparison with WT (Fig. 5.16 C, C').

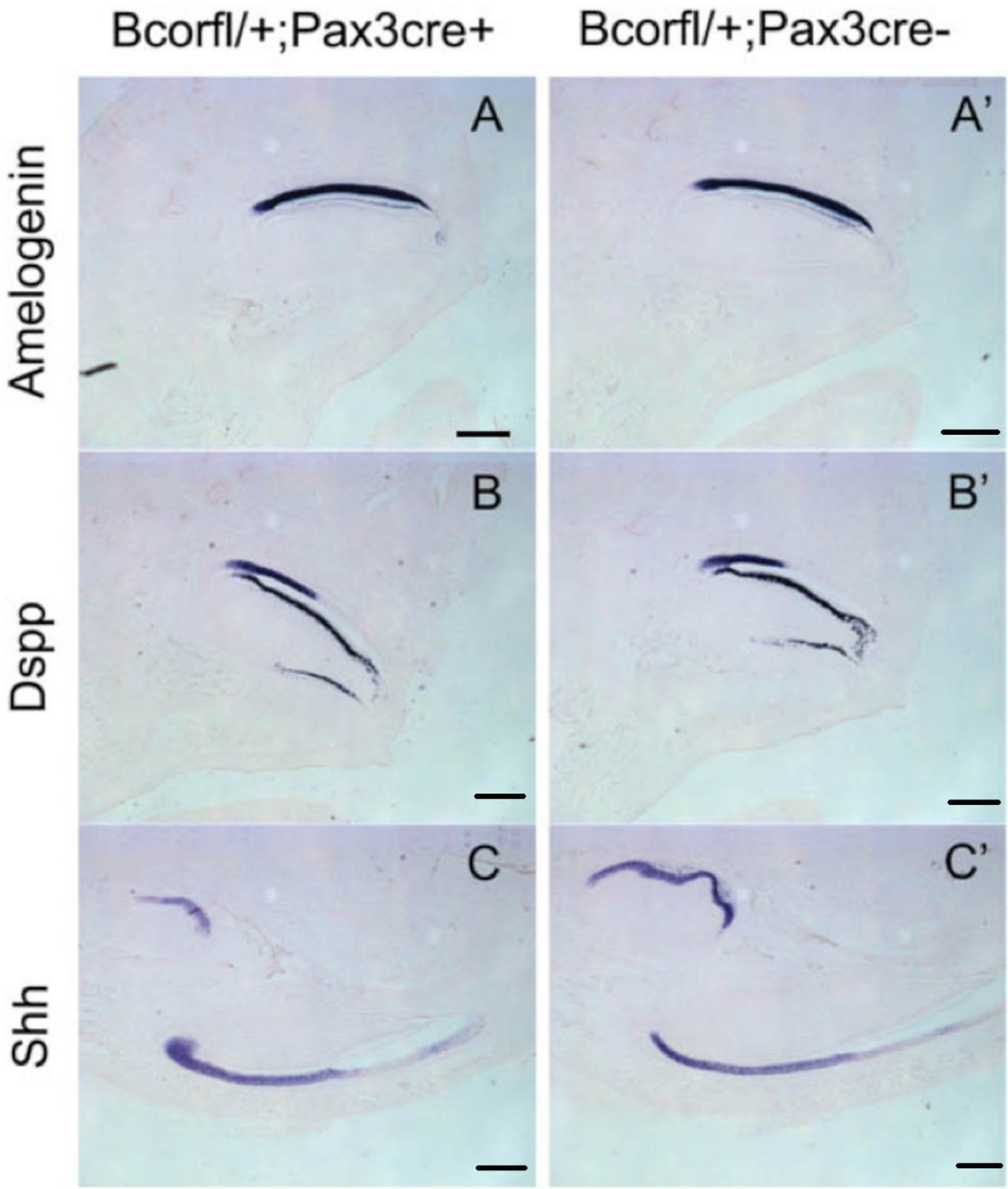

Fig 5. 16: Expression analysis of *Dspp*, *Amelogenin* and *Shh* in 2 day-old incisors of *Bcor*$^{fl/+}$*; Pax3Cre-* and *Bcor*$^{fl/+}$*;Pax3 Cre+* mice (sagittal sections).

(A and A') Expression of Amelogenin in functional ameloblasts in *Bcor*$^{fl/+}$*;Pax3Cre-* and *Bcor*$^{fl/+}$*;Pax3 Cre+* incisor, respectively. (B and B') *Dspp* expression in the odontoblasts (od) and differentiated ameloblasts (am) of *Bcor*$^{fl/+}$*;Pax3Cre-* control and *Bcor*$^{fl/+}$*;Pax3 Cre+* incisors. (C and C') Strong expression of Shh was observed in pre-ameloblasts in *Bcor*$^{fl/+}$*;Pax3Cre-* and *Bcor*$^{fl/+}$*;Pax3 Cre+* incisor, respectively. Scale bars =50µm in (A-C, A'-C')

However, previous work in our laboratory showed an obvious overgrowth phenotype, which varied from a relatively smooth surface to bulges and had a nodular appearance affecting the cervical end. Unfortunately, this phenotype could not be reproduced from our current samples.

5.3 Discussion

5.3.1 Investigation of functions of Ring1a/b in mouse incisor dental pulp stem cells

Rodent incisors are capable of erupting throughout their lifetime to compensate for constant attrition at the incisal edge. Thus, the mouse incisor provides an excellent model for MSC study as tooth-forming cells including enamel-forming ameloblasts and dentin-forming odontoblasts are required and are achieved by stem cells residing at their open proximal (apical) ends (Harada et al., 1999). Our results showed that Ringa/b were expressed in the TA cells (fast cycling cells) that contributed to the formation of whole incisor pulp tissue. Both histology analysis and microarray results revealed that loss of Ring1a/b led to down-regulated proliferation of fast cycling cells and whole incisor growth arrest. This finding was consistent with previous studies showing that the loss of Ring1a/b causes proliferation defects in ES cells (Endoh et al., 2008). The reduced cell proliferation noted in the apical dental mesenchyme fast cycling cells close to both labial and lingual cervical loop epithelium where the differentiation of odontoblast progenitors takes place suggested that Ring1a/b proteins are required, either directly or indirectly, for the proliferation of the dental mesenchymal cells, thereby giving rise to dentin-forming odontoblasts. Apart from the dental mesenchyme, a reduced labial cervical loop with a dramatic decrease in cell proliferation was also noted in *Ring1a/b* gene knockdown mutants. This finding indicated an interaction between dental mesenchyme and cervical loop epithelium, suggesting that Ring1a/b regulates proliferative signals not only within mesenchyme but also in relation to the epithelium.

Under histological analysis, no phenotype of *Ring1a*$^{-/-}$*Ring1b*$^{fl/fl}$Cre- was observed, possibly because of the compensative role of the remaining Ring1b, as a previous study

of *Ring1a*$^{+/-}$; *Ring1b*$^{cko/cko}$ mice did not show any incisor abnormality. That result may indicate a redundancy between Ring1a and Ring1b function during incisor development. A similar result was observed in ES cells: Ring1b single-knockout ES cells appeared normal, whereas Ring1a/b double-knockout ES cells progressively lost ES cell characteristics after tamoxifen treatment to inactivate Ring1b (Endoh et al., 2008).

The mice used in this study became sick shortly after the tamoxifen treatment at PN11, while the inactivation of Ring1b happened as early as several hours after tamoxifen treatment. The total deletion of Ring1b can be confirmed 1 day later by PCR, thus the Ring1b protein level of mice progressively decreased after 24 hours of tamoxifen treatment. These mice got the secondary dose of tamoxifen injection at PN13 and sacrificed at PN17, therefore they were in the presence of tamoxifen for a maximum of 8 days and living in the absence of Ring1b for approximately 7 days. It has been demonstrated that the eruption rate of unimpeded mandibular mouse incisors is approximately 400 μm per day, therefore the phenotype of *Ring1a*$^{-/-}$; *Ring1b*$^{fl/fl}$Cre+ could be reflected as an obvious shorter incisor, however, a measurement analysis in our laboratory showed that the difference of the mean lengths of *Ring1a*$^{-/-}$;*Ring1b*$^{cko/cko}$ was 1500 μm shorter than *Ring1a*$^{-/-}$;*Ring1b*$^{fl/fl}$ *Cre-* mandibular incisors, less than we expected. This suggested that either the *Ring1a*$^{-/-}$;*Ring1b*$^{cko/cko}$ incisors were still capable of growing at a lower rate, or that tamoxifen- induced Cre-mediated excision may only be fully effective for approximately 3 days.

In the microarray analysis, many genes showed expression changes in the *Ring1a/b* null mouse incisor and among these changes the down-regulation of Thy-1 looks interesting since Ring1b was mainly expressed in the fast cycling cells rather than slow cycling cells. One possible explanation is that this down regulation of Thy-1 came from the

Thy-1 and Ring1b co-expressing cells in fast cycling cell population. Knockout of *Ring1a/b* in these cells led to a down-regulation of cell proliferation directly affecting the expression of Thy-1. Another explanation is that down-regulated Thy-1 expression might come from an indirect effect on the slow cycling cell population upon Ring1a/b inactivation. A study in hair follicles has shown that TA cells are an early intermediate in tissue regeneration, whereas emerging TA cells constitute a signaling center that orchestrates tissue growth. Hence primed stem cells (SCs) generate TA cells, while quiescent SCs only proliferate after TA cells form and begin expressing Sonic Hedgehog (Hsu et al., 2014). Therefore, we assumed that loss of Ring1a/b did not affect slow cycling cells (stem cells) directly, but a lower proliferation of fast cycling (TA) cells led to a failed signaling transition from fast cycling cells to slow cycling cells, which indirectly affected the slow cycling cells.

The microarray results also revealed that loss of Ring1b led to down-regulated cell cycle regulators and up-regulation of *Hox* gene family and Notch signaling pathway, indicating a repressive role of Ring1a/b in regulating cell differentiation. A study in neural stem cells (NSCs) has shown that Ring1b may modulate the differentiation potential of NSCs to neurons and glia. Ring1b-deficiency in fetal neural stem cells causes premature neuronal differentiation. In addition, Ring1b mutation can also affect the temporal specification of developing neural progenitors, which showed enhanced neuronal differentiation and reduced gliogenesis (Roman-Trufero et al., 2009). Therefore, in our mouse incisor system, it is possible to argue that Ring1b promotes fast cycling cell proliferation by restricting their differentiation in the stem cell niche. However, Ring1b inactivation in adult stem cell and primitive progenitor cells in the hematopoietic compartment leads to proliferative alterations, rather than differentiation defects. It was suggested that Ring1b might plays an important role in the tight control

of hematopoietic cell turnover via restricting progenitor proliferation and promoting the proliferation of their maturing progeny by selectively altering the expression pattern of cell cycle regulators along hematopoietic differentiation (Cales et al., 2008). These findings possibly indicate that the mechanism of Ring1b in regulating cell proliferation and differentiation might be different among tissues.

When comparing the gene expression changes upon Ring1a/b deletion in dental pulp cells with ES cells, the results were similar. While many gene expressions involved in tooth development were up-regulated, this suggested a similarity between Ring1b expressing fast cycling cells and ES cells. Moreover, among these up-regulations, *Barx1* that is restrictively expressed in the molars, suggesting its role in the differentiation of molars from incisors also was showing an up-regulation upon Ring1a/b inactivation. This result may provide a clue regarding molar and incisor determination.

Taken together we proposed that a regulatory role of Ring1a/b is in the dental mesenchymal stem cell niche in developing and continuously growing mouse incisors. Loss of Ring1a/b therefore leads to a failure of the immediate progeny of mesenchymal stem cells (TA cells) to undergo proliferation and differentiation into odontoblast precursors, resulting in an arrest of the continuous growth of mouse incisors.

5.3.2 Investigation of the downstream targets of Ring1a/b

Mouse incisors require an intricate molecular network to regulate stem cell populations for continuous postnatal growth. In our study, Ring1a/b have been confirmed as expressing in the dental mesenchyme at the apical end of the incisor at the postnatal stage. Also, loss of Ring1a/b caused incisor abnormality, however the downstream targets of PRC1 complex inside dental pulp have not been reported. One candidate that

has been analyzed in this study is Wnt signaling, which is closely associated with stem cell maintenance (Nusse et al., 2008). A recent study has suggested that Wnt activity may play an important role in regulating odontoblast linages, as indicated by the high level expression of Axin2 in developing odontoblasts and the loss of Axin2 in terminal differentiated odontoblasts (Lohi et al., 2010, Suomalainen and Thesleff, 2010). Interestingly, our results showed the expression of Axin2 was up-regulated in this Ring1/Bcor-expressing area and down-regulated following the loss of Ring1a/b. This suggested that Ring1a/b might maintain the differentiation hierarchy of cells in the odontoblast lineage during incisor growth via the modulation of Wnt activity. However, this regulation needs be further investigated through analysis of the Wnt pathway expression changes following alterations in *Ring1a/b* gene expression.

Conditional knockout of *Ring1a/b* and *Bcor* caused morphological changes, not only in the incisor dental mesenchyme, but also in the incisor epithelium, particularly in the cervical loop region, supporting the notion that the maintenance of the cervical loop requires regulatory signals from the dental mesenchyme, such as Fgf10 and Fgf*3* (Harada et al., 1999, Harada et al., 2002). Previous evidence has reported that expression of Fgf*10* and Fgf*3* is restricted to the mesenchyme adjacent to basal epithelial cells and the underlying TA cells expressing their receptors Fgfr1b and Fgfr2b (Harada et al., 1999). FGF signaling has been reported to be essential for proliferation of epithelial stem cells and TA cells in the epithelial stem cell niche residing in the cervical loop (Harada et al., 1999, Harada et al., 2002). Further studies of *Fgf10* null mice also showed that the cervical loop was completely missing at late bell stage (Harada et al., 2002), while *Fgf3* $^{-/-}$*; Fgf10* $^{+/-}$ mice exhibited very thin or no enamel (Wang et al., 2007), confirming that FGF signals from the mesenchyme are required for the development and maintenance of the cervical loop structure. Work in our laboratory has proved that loss of *Ring1a/b* down-regulated the expression of FGF signaling in the

mouse incisor mesenchyme, which is probably the reason why the relative small labial cervical loop was observed in *Ring1a*$^{-/-}$;*Ring1b*$^{cko/cko}$ incisors in comparison with *Ring1a*$^{-/-}$;*Ring1b*$^{fl/fl}$ *Cre-* mouse (Lapthanasupkul et al., 2012). Taken together, knockdown Ring1a/b proteins of the PRC1 complex in postnatal mouse incisors down-regulated *Fgf10* and *Fgf3* gene expression suggested that the mesenchymal PRC1 complex might regulate the epithelium via regulating FGF signaling.

5.3.3 Investigation of functions of *Bcor* in mouse incisor dental pulp stem cells

Bcor has a crucial role in maintaining tooth development in both humans and mice. Dental abnormalitiesare are an important criteria for OFCD syndrome diagnosis (Schulze et al., 1999). ISH for Bcor has found its expression in a specific region in the TA cells and previous work in our laboratory has proved that Bcor is essential to maintain the continuous growth of the mouse incisor. Previous studies using dental-mesenchyme-specific *Bcor*-knockout mice have shown that disruption of Bcor caused obviously abnormal overgrowth of the mouse incisor. We still do not know which cell population plays the important role in this abnormality (slow cycling cells or fast cycling cells) because further investigation is required using molecular markers. However, one possibility is that since Bcor worked as a repressor in controlling TA cells, knockout of Bcor expression in these cells may lead to more cell proliferation to form an overgrowth of the mouse incisor. Therefore, although it is suggested that, in human dental pulp, BCOR inhibits the osteo-dentinogenic potential and proliferation of MSCs, this mechanism might differ within the continuously growing mouse incisor and non-growing human teeth. This difference is supported by our current data. ISH results showed that the Bcor expressing region is a TA cell area. Stem cells from many tissues

are thought to be slow cycling while progenitor/TA cells are known to divide rapidly, therefore, it is very likely that Bcor regulates the mesenchymal component for the incisor growth via mediating progenitor/TA cell fate. In future studies, conditional knock-out mice of the Bcor gene should be used in combination with proliferation and damage-response analysis, to further address the effect of Bcor in regulating the proliferation and differentiation potential of these rapidly dividing cells.

However, one of the big issues in studying Bcor is that *Pax3-Cre Bcor* null mice (*Bcor*$^{fl/y}$*;Pax3Cre*) had obvious abnormalities and did not survive postnatally. We were only able to analyze mice teeth using *Bcor*$^{fl/+}$*;Pax3Cre* adult heterozygotes, in which functional Bcor, although reduced, was still present in part of the mesenchymal cells leading to normal phenotype. Therefore, to clarify the effect of a complete deletion of mesenchymal Bcor in later teeth development, further experiments, such as *in vitro* organ culture or kidney capsule transplantation, needs to be conducted to study the development of *Bcor*$^{fl/y}$*;Pax3Cre* incisors from E18.5 onwards.

5.4 Conclusion

In summary, the results showed that the polycomb group genes *Ring1a/b* and *Bcor* are required for incisor development and growth. Ring1a/b was needed for the maintenance of adult epithelium stem cells in the labial cervical loop and fast cycling mesenchymal cells. Inactivation of Ring1a/b led to impaired cell proliferation and reduced stem cells due to deregulated gene expression. Furthermore, many genes were up-regulated following the deletion of *Ring1a/b gene*, including the *Hox* gene family and Notch signaling pathway and many other genes involved in tooth development further confirmed the repressive role of Ring1a/b protein as a core member of polycomb group protein. Completely Bcor loss leads to birth death, however, heterozygous $Bcor^{fl/+}$*;Pax3Cre* mutants did not show phenotypical changes compared with their littermate controls and both upper and lower incisors appeared to be relatively normal.

Chapter 6: General Discussion and Future Considerations

6.1 *In vivo* identification of dental pulp mesenchymal stem cells

MSCs are heterogeneous cell populations identified based on their *in vitro* characteristics while their *in vivo* identities remain contentious (Zhao et al., 2014). Mouse incisors are capable of continuously growing throughout their lifetime due to the existence of stem cells. The precise location of the mesenchymal stem cells (MSCs) in the incisor has however been clear. The utilization of label-retaining experiments and transgenic reporter mouse lines enabled further understanding of the less established identities and properties of dental pulp stem cells *in vivo*. In this project, a stem cell niche located at the apical end of mouse incisor was described. The work in this thesis also demonstrated that three distinct but connected cell populations exist in this stem cell niche: a slow cycling cell population containing Thy-1+ cells essential for tooth dental pulp and odontoblast formation; a Ring1/Bcor-associated fast cycling cells population crucial for maintaining tissue growth and homeostasis of epithelium stem cells in the labial cervical loop; a quiescent long-term cell population marked by Celsr1 possible provide new stem cells to the stem cell niche.

6.1.1 Identification of MSCs in mouse incisor

Previous studies in our laboratory have demonstrated a limited pericyte contribution to the formation of odontoblasts during dentine repair. Another MSC population must exist in the apical mesenchyme that continuously provides new cells for mouse incisor growth. To clarify the location of MSCs, nucleoside label-retaining experiments were

performed to investigate the cell proliferation rate in the dental pulp cells. This showed that a slow cycling cell population exists in the dental mesenchyme between cervical loops surrounding by a fast cycling cell population more distally. The close proximity of the rapid and slow cycling populations suggested that the rapidly dividing cells might also function as a niche compartment essential for the slow cycling cells maintenance. Unfortunately, gene expression analysis using microarray was not possible since detection of nucleosides for FACs is not compatible with mRNA extraction. The detection of slow cycling cells with nucleosides can be replaced with the use of doxycycline inducible H2B–GFP transgenic mice, which have been suggested as a better labeling approach for this analysis. In these mice, ubiquitous and transient expression of GFP is rapidly activated after doxycycline administration, following washout periods, label-retaining cells can be obtained without damage by FACS. This approach will enable us to investigate slow cycling cells (stem cells) in greater detail, in the future.

6.1.2 Investigation of quiescent long-term cells and noncanonical Wnt signaling

For long-term maintenance of stem cells in adult tissues, a subset of stem cells needs to be kept necessarily in long-term quiescence in a specialized niche (Sugimura et al., 2012). These cells are able to provide a source of new stem cells in the adult tissue. A study in HSCs has shown a quiescent long-term HSC cell population regulated by flamingo mediated noncanonical Wnt signaling in the HSC niche (Sugimura et al., 2012). These quiescent long-term HSCs predominantly express noncanonical Wnt ligands and inhibitors of canonical Wnt signaling under homeostasis. But, under stress, these cells become active and exhibit enhanced canonical Wnt signaling and attenuated noncanonical Wnt signaling (Sugimura et al., 2012). In the mouse, dental pulp stem cells have been reported to date. Since dental pulp stem cells are needed for continuous

tooth growth, an interesting question appeared. Is there a similar quiescent long-term cell population at which noncanonical Wnt signaling functions to in the incisor?

Many Wnts and Wnt pathway mediators are expressed during the development of embryonic teeth. The indispensable role of Wnt signaling in tooth morphogenesis has been demonstrated in mouse and human studies (Dassule and McMahon, 1998, Sarkar and Sharpe, 1999, Kratochwil et al., 2002, Obara et al., 2006, Adaimy et al., 2007). For example, it has been shown that Wnt/β-catenin signaling is observed almost exclusively in mesenchymal tissue of mouse incisor (Suomalainen and Thesleff, 2010). Tooth development in mouse embryos is arrested at an early stage when Wnt signaling is inhibited by expressing the Wnt inhibitor Dkk1 and by inhibiting epithelial β-catenin and when Lef1 (Lymphoid enhancer factor, a nuclear mediator of Wnt signaling) function is deleted (van Genderen et al., 1994, Andl et al., 2002, Liu et al., 2008). Furthermore, Wnt5a, which is often associated with the noncanonical Wnt pathway (Mikels and Nusse, 2006), is intensely expressed in the dental mesenchyme around the cervical loops indicating a negative regulation of the epithelial stem cells in their niche by means of a noncanonical Wnt pathway in the developmental stage (Sarkar and Sharpe, 1999). Therefore, to identify the noncanonical Wnt signaling mediated mesenchymal cells, a long-term label-retaining experiment and immunostaining was performed in the mouse incisor pulp tissue. The result showed that a small number of Celsr1+ (Flamingo homologue) cells were located in the very outer layer of the dental mesenchymal as quiescent cells were, suggesting a long-term quiescent cells population mediated by noncanonical Wnt signaling exists in the stem cell niche of mouse incisor. These long-term quiescent cells might respond to generate new stem cells when the stem cells become depleted.

6.1.3 Lineage tracing of prospective stem cells

To identify prospective stem cell populations in the mouse incisor, a transgenic mouse

line *pCAG*^{ERT2Cre}*; R26R mT/mG* were used in our studies. By temporal control of gene recombination with tamoxifen, a group of labeled cells at the apical end mesenchyme that form patches of odontoblasts were successfully identified. It is reasonable to propose that these labeled cells were from (a) stem cell clones and their location is a stem cell niche, because only stem cell could stay in the mouse incisor and keep producing progeny while all other cells have moved out from the tip of incisor as the tooth growth. However, we still can not answer the questions that how many progeny cells a stem cell can produce, because the group of cells we observed may come from more than one stem cell. Thus, a new four colour labeling transgenic mouse *pCAG*^{ERT2Cre}*; R26R-Confetti* is expected to provide more information by labeling different stem clones with different colours in future studies.

6.2 Thy-1 and MSCs

Dental pulp MSCs are heterogeneous cell populations and are identified based on their *in vitro* characteristics. Their identities *in vivo* are not yet known because of the lack of specific markers (Bianco et al., 2008). In order to identify specific markers for MSCs in mouse incisor, microarray analyzes of mouse incisor and cervical loop area had been done in a previous study. Thy-1, a well known MSCs marker *in vitro* (Horwitz et al., 2005) that is up-regulated in both incisors and the cervical loop areas which contain stem cell niches (Harada et al., 1999), was selected as a candidate to study further.

6.2.1 Analysis of Thy-1 expression in the mouse incisor dental pulp

It has been common practice to use mRNA concentrations to represent the activities of the corresponding proteins, thereby assuming that transcript abundances are the main determinant of protein abundances (Vogel and Marcotte, 2012). Our results of ISH

showed that the expression of Thy-1 was more intense at the apical end of mouse incisor dental pulp tissue where slow cycling cells and fast cycling cells are located. However, at the protein level, Thy-1 was only detected in the slow cycling cell area. A similar result came from the Cre protein expression of *Thy-1 Cre* mouse, immunostaining result showed that *Thy-1* promoter driving *Cre* expression was only detected in the slow cycling cells area. It might argue that this result could be caused by low sensitivity of immunostaining since the flow cytometry, a more sensitive analysis showed more Thy-1 expressing cells in the incisor pulp. According to the flow cytometry result, 12.4% pulp cells were Thy-1 positive, however, that number could change by alternating antibody incubation time and concentration as Thy-1 expression increases progressively. One explanation for this progressive expression of Thy-1 is that Thy-1+ cells are stem cells, which can produce many progeny cells, a small amount of Thy-1 protein could still exist in all these progeny cells.

On the other hand, mRNA concentrations sometime can not truly reflect the corresponding proteins as many post-transcriptional modifications occur once mRNA are synthesized. After the DNA is transcribed and mRNA is formed, protein expression process still needs to be modulated. Besides, cells can rapidly adjust their protein levels through the enzymatic breakdown of existing protein molecules. Lastly, cell division may further dilute the protein concentration, as has been suggested by independent studies (Eden et al., 2011, Vogel and Marcotte, 2012). If this applies to our study, it is not surprising that fast cycling cells in the mouse incisor showed a low Thy-1 protein expression.

The co-localization of Thy-1 and EdU labeling results by flow cytometry seemed to confirmed the ISH result, as it showed that approximately 30 % of 6 weeks chase slow cycling cells were Thy-1+ cells while in the 24 hours EdU label cells, 16.3% cells were also detected positve to Thy-1. It may argue that these Thy-1+; 24 hours EdU label cells

were Thy-1 progeny cells which still have the remaining protein. However, this experiment left a big blank before and after 24 hours chase timing. More data from different time points in the future is required to answer these questions

6.2.2 Lineage tracing of Thy-1+ cells in the mouse incisor dental pulp

One way to identify stem cells in the tissue is linage tracing, thus to trace Thy-1 expressing cells *in vivo*, two transgenic mouse reporter lines: *Thy-1Cre;R26R mT/mG* and *Thy-1Cre;R26R-Confetti* were used in our studies. Our results showed that, in adult stages, Thy-1 expressing cells from the apical end of mouse incisor, contributed to the whole incisor pulp formation. In *Thy-1Cre;R26R-Confetti* mice incisors, cell streams in different colours were found to contribute to the formation of odontoblasts, suggesting different individual Thy-1+ cells and their progeny cells function as stem cell source in the growth of mouse incisor. However, in most *Thy-1Cre;R26R-Confetti* mouse incisors, only a few cell streams of one or two colours were detected. These results were consistent with the finding that only a few Thy-1+ cells were detected by immunostaining, suggesting a limited number of Thy-1 expressing stem cell in the stem cell niche. Interestingly, Thy-1 progeny cells did not form the whole dental pulp tissue suggesting a different stem cell population exists together with the Thy-1+ population, contributing to the formation of dental pulp tissue. This result further confirmed the heterogeneity of dental pulp MSCs and left more questions in the future to fully understand the MSCs in the mouse incisor.

6.2.3 Thy-1+ cells *in vitro*

Thy-1 positive cells from PN5 dental pulp did not grow well *in vitro*. This result may either indicate that the Thy-1+ population cannot be maintained in high numbers, or Thy-1+ cell state changes due to lack of signaling regulation when leaving the stem cell

niche microenvironment. Thus, optimizing the cell culture conditions and mimic *in vivo* environments to support Thy-1+ proliferation and expansion is recommended. Many studies have been performed to test the optimal conditions to maintain MSCs in their undifferentiated state, starting from the usage of different medium to sera concentrations or serum free medium (Lapi et al., 2008, Ayatollahi et al., 2012, Chase et al., 2010). However, these above mentioned studies suggested that, the culture conditions varied in different progenitor cells, as different cells have differential sensitivity to medium, sera and growth factors. This issue may raise questions as to the utility of Thy-1+ dental pulp stem cells in therapeutic transplantation, because transplantation requires a large number of cells. How to produce large number of these Thy-1+ cells *in vitro* is still an obstacle.

6.2.4 Analysis of heterogeneity of slow cycling cells and Thy-1+ cells

In our study, a group of dental pulp MSCs was identified by a series of label-retaining experiments. These slow cycling cells were compared with Thy-1+ cells by performing flow cytometry analysis. The results showed that approximately 30 % of 6 weeks chase slow cycling cells were Thy-1+ cells, suggesting a considerable Thy-1+ cells contribution to the slow cycling cell population. This number could vary if the chase time is altered, however, it still indicated a heterogeneity of both the Thy-1+ cells and slow cycling cells populations. Evidence from a recent study has revealed that a significant population of mesenchymal stem cells during development, self-renewal and repair of a tooth are derived from peripheral nerve-associated glia. Glial cells generate multipotent mesenchymal stem cells that produce pulp cells and odontoblasts (Kaukua et al., 2014). The study also revealed that a population of Schwann-cell-derived dental MSCs are Thy1+. When quantified the amount of schwann-cell-derived progeny in *PLP-CreERT2/R26R-YFP* mice there are approximately 47.28 ±4.02% positive cells

(Kaukua et al., 2014). Hence, including Thy-1+ cells (30%), Schwann cells and SCPs (47.28 ±4.02%) also include other cell populations

One possible candidate is pericytes. Lineage tracing of *NG2Cre;R26R* transgenic mice has demonstrated that there is a pericyte-derived mesenchymal contribution to odontoblast formation (Feng et al., 2011). However, according to their results only around 12% of odontoblasts are possibly derived from pericytes. Recently, new evidence further confirmed this finding. A study suggested that NG2+ pericytes represent an MSC subpopulation that are actively involved in injury repair rather than contribute only a little to homeostasis in mouse incisor (Zhao et al., 2014). These results all indicate that pericytes are part of MSCs in the mouse incisor dental pulp tissue.

In addition, recent studies have revealed that a Gli1 expressing periarterial cell population contributes to mesenchymal derivatives in mouse incisor (Zhao et al., 2014). Previous results have suggested that Gli1 may be a dental epithelial stem cell marker (Seidel et al., 2010). However, a recent study in Gli1 reporter mice showed that Gli1 was expressed both in the dental epithelial cells and at the apical end mesenchyme where the stem cell niche is located. Lineage tracing of Gli1+ cells showed that Gli1+ cells give rise to the entire incisor mesenchyme including NG2+ and CD146+ perivascular cells but not the CD31+ endothelium further supported the idea that Gli1 is a dental mesenchymal marker. FACS analysis of incisors from Gli1-GFP mice suggested that there are around 2300 Gli1+ cells in each lower incisor, comprising about 2% of the entire incisor mesenchyme population (Zhao et al., 2014). This number is less than our label-retaining cell population, which account for about 4.3% of total dental pulp cells suggesting that Gli1+ cells may not contribute all MSCs.

6.3 Ring1, Bcor and fast cycling cells

6.3.1 Analysis of Ring1 and Bcor expression in fast cycling cells

In the MSC niche of mouse incisor, we identified two cell populations with different proliferation rates: slow cycling cell population in the area between the cervical loops and fast cycling cell population located close to the cervical loop. We further presented evidences that the slow cycling cell population, which expressed the stem cell marker Thy-1, contributed to the formation of whole dental pulp tissue, while the population of dental pulp mesenchymal cells with high proliferation rate, expressed PRC1 proteins (Ring1a/b and Bcor) and had characteristics of cell progenitors (TA cells) in tooth growth. Nonetheless, further investigation is required to address the lineage and biology of Ring1a/b expressing cells in the mesenchyme fast cycling cells, as well as the functional roles of Ring1a/b in this population.

6.3.2 Histology analysis of Ring1a/b and Bcor knoctout mouse incisors

In the histology analysis of Ring1a/b knockout mice incisors, the results showed that the morphology of the whole cervical loop was remarkably abnormal in thePN17 *Ring1a*$^{-/-}$; *Ring1b*$^{cko/cko}$ mice, in comparison to the cervical loop of *Ring1a*$^{-/-}$; *Ring1b*$^{fl/fl}$ *Cre-* mice. Upon Ring1a/b deletion, the labial cervical loop that is believed to be the stem cell niche was smaller and holding fewer satellite reticulum cells. While in the dental pulp mesenchyme, fast cycling cells proliferation rate was obviously down-regulated, which further led to a failed odontoblasts formation. All of these indicated an abnormal development and arrest at growth in the *Ring1b*$^{cko/cko}$ mouse incisor. Contrastingly, a previous study using dental-mesenchyme-specific Bcor-knockout mice showed a totally different phenotype. An obviously abnormal overgrowth of the mouse incisor was seen by the disruption of Bcor. It is still not known which cell population plays an important

role in this abnormality (slow cycling cells or fast cycling cells) because further investigation still needs to be done by using molecular markers, however, one reasonable guess is that since Bcor functions as a repressor in controlling TA cells, knockout of Bcor expression in these cells leads to more cell proliferation to form an overgrowth of mouse incisor. This result is very interesting because Ring1a/b and Bcor are both components of the PRC1 complex that is well known for keeping ESs state, however, they play different roles in controlling MSCs of mouse incisor dental pulp. It possibly because of Ring1a/b and Bcor target different downstream signaling. In Ring1a/b knockout mutants, FGF signaling has been shown to be down-regulated expressed which caused a reduced cell proliferation in both epithelium and mesenchymal tissue. While a recent study of Bcor revealed that upon Bcor deletion main effectors of the Shh pathway Gli1 and Gli2 were strongly up-regulated (Tiberi et al., 2014). Since a Gli1+ cell population has been considered as stem cells both in mouse incisor epithelium and mesenchymae (Zhao et al., 2014), up-regulated Gli1expression may activate stem cell proliferation contributing to the overgrowth observed upon Bcor deletion.

6.3.3 Analysis of gene expression changes upon Ring1a/b deletion

Polycomb group proteins including Ring1a/b are well known for silencing *Hox* genes through modulation of chromatin structure during embryonic development in *Drosophila melanogaster* (Di Croce and Helin, 2013). The microarray results showed a significant up-regulation of *Hox* genes along with a stem cell niche phenotype in Ring1a/b deletion mouse incisor. It is reasonable to wonder if *Hox* genes act as downstream targets of PRC complex that are involved in the regulation of TA cells. In a study of Bmi (PCGF4), a component of PRC complex protein, histological analysis showed a similar cervical loop phenotype with an up-regulated *Hox* gene expression. It

has been demonstrated that reducing *Hox* a9/c9 expression reconstituted the incisor epithelial stem cell expression signature. When introducing exogenous *Hox* a9/c9 by lentiviral transduction into cultured control labial cervical cells, over-expression of *Hox* genes caused enlarged cell size (Biehs et al., 2013). Collectively, all these results suggested that *Hox* gene expression was suppressed by PRC complex proteins in the dental pulp tissue and knockout Ring1a/b, a core component of PRC1 complex, would cause an epithelia stem cell phenotype via alteration of *Hox* gene expression.

In addition, our microarray results also showed that gene expression changes in dental pulp stem cells niche area cells are identical with ESs. Many genes involved in tooth development showed an obvious up-regulation upon Ring1a/b deletion including *Gata6*, *Tbx18, Zic1, Barx1, Bmp6* and *Crlf1,* enforcing the idea that Ring1a/b regulated those cells in the dental pulp stem cell niche as a repressor.

6.4 Understanding of MSC niche regulation

Several signaling pathways critical for the formation and maintenance of the incisor stem cells both during development and in adults are found in the mouse incisor apical end mesenchyme where fast and slow cycling cells located. Among the most well studied of these is FGF signaling. Fgf10 is expressed in the mesenchyme neighburing both the lingual and labial cervical loops. Fgf3 expression, in contrast, is only present in the mesenchyme adjacent to the labial cervical loop (Harada et al., 1999, Wang et al., 2007). Our study in Ring1a/b knockout mice showed that FGF signaling was reduced in the fast cycling cell area, which led to a growth arrest of mouse incisor and abnormality of labial cervical loop in epithelia. This result not only suggested that Ring1a/b in fast cycling cells are required for maintaining endogenous levels of FGF expression but is also essential for the regulation of FGF signaling which is import in the formation and

maintenance of epithelial stem cells in the labial cervical loop. This also indicated a mesenchymal-epithelial interaction in regulating the stem cell niche in epithelium tissue.

The ISH results confirmed that Alk5 (Tgfbr1) was expressed at the apical mesenchyme where fast cycling cells are located, suggesting an involvement of TGF-β family in the growth of mouse incisor. Studies in mouse incisor suggested that Alk5 in the dental mesenchyme regulates proper tooth initiation and development of the incisor epithelium (Zhao et al., 2011). When Alk5 was deleted specifically in the dental mesenchyme, FGF signaling was down-regulated, leading to reduced proliferation and fewer LRCs in the cervical loop (Zhao et al., 2011). This result may indicate either a direct or an indirect involvement of TGF-β family to FGF signaling in the growth of mouse incisor.

Interestingly, Pax9, which is required in the establishment of the inductive capacity of the tooth mesenchyme (Peters et al., 1998), was found expressed in the slow cycling cells area. Studies have suggested that the activation of mesenchymal FGF expression occurs at least in part through the transcription factors Msx1 and Pax9, which interact to initiate the expression of Fgf3 and Fgf10 at E12.5 and thus the subsequent formation of the incisors (Kuang-Hsien Hu et al., 2014). Therefore, Pax9 may still work as an up stream regulator in the slow cycling cells, initiating the expression of *Fgf*3 and *Fgf*10 genes in the fast cycling cells during postnatal stage.

It has been proposed that signaling through the Hedgehog (Hh) pathway plays a number of roles in stem cell biology, including regulation of fate decisions in embryonic stem cells (Gaspard et al., 2008) and survival and self-renewal of neural stem cells (Balordi and Fishell, 2007). In addition to FGF and TGF-β/BMP signaling, Hh pathway is also an important regulator of mouse incisor stem cells. As mentioned earlier, Gli1 positive Hh-responsive cells were found in both the epithelial stem cell compartment and the dental pulp mesenchyme. According to the recent research in MSCs niche, these cells

were considered as MSCs in the mesenchymal (Zhao et al., 2014). However, in adult *Ptc-1*$^{fl/fl}$*;CreER*^{Tm} mouse incisor, where Shh signialing was blocked by conditional knockout of the Shh receptor Ptc-1, histological analysis of ameloblasts and odontoblasts did not show any abnormity in the tamoxifen treated mice. Although another study group reported a similar result (Cobourne et al., 2009), it might be due to an inadequate exposure to prolonged increased Shh signaling.

Members of the Notch signaling pathway demonstrate intriguing expression patterns in the incisor. Several studies have pointed to a role for these genes in the regulation of the epithelium stem cells. In mouse incisors, Notch 1 and Notch 2 expression is in the cervical loop (Harada et al., 1999). Notch 3, on the other hand, is reported to be expressed both in the dental mesenchyme (Harada et al., 1999) and cervical loop (Mitsiadis et al., 1998). The genes encoding the Notch ligands, *Dll1* and *Jagged 2* are also expressed in the cervical loop dental epithelium (Mitsiadis et al., 1998). Our microarray analysis upon *Ring1a/b* gene deletion mice showed that Notch signaling was repressed by Ring1a/b. Knockout *Ring1a/b* gene can lead to an up-regulation of Notch signaling members and a reduced stem cell number in the cervical loop. However, when cervical loops dissected from new born mice were cultured with the Notch signaling inhibitor, DAPT, they had reduced proliferation and increased apoptosis, leading to an overall reduction in size (Felszeghy et al., 2010). These conflicting results further suggested a complicated regulation network of stem cells in mouse incisors.

In summary, the continuous growth of the mouse incisor is orchestrated by a fine-tuned dynamic regulatory interaction between the mesenchyme and epithelium. Transforming growth factor beta (TGF*β*), bone morphogenetic protein (BMP), Wnt, fibroblast growth factor (FGF) and Hedgehog pathways are involved in this process. The signals from the underlying mesenchyme are essential for epithelial stem cell and MSCs maintenance in the cervical loop area. Polycomb proteins Ring1a/b from fast cycling cells are required

for maintaining endogenous levels of FGF expression in mesenchyme and repress Hox and Notch pathways.

6.5 MSCs and incisors

Stem cells are found in many adult organs where they respond to provide a source of cells needed for tissue growth or to repair tissue damage. Adult human teeth do not grow and have only a limited ability to repair following damage, however, the incisors of rodents grow continuously to accommodate wear and tear. This is achieved by resident stem cell populations existing in the tooth that provide sources of cells to replace all mesenchymal-forming odontoblasts and epithelium-forming ameloblasts. Our study highlights the incisor as an excellent model for studying MSCs. With the establishment of MSCs niche consist of quiescence cells, slow cycling cells and fast cycling cells and stem cell marker Thy-1, we will be able to target MSCs specifically and precisely to inactivate a specific gene in order to test its *in vivo* function in regulating MSCs. In summary, the dental mesenchymal stem cell niche identified in mouse incisors provides an attractive, easily visualized and manipulated, experimental system to study the characteristics and behaviour of adult stem cells.

6.6 Stem cell niches in molar and incisor

Dental hard tissues are formed particularly by odontoblasts (dentin) and ameloblasts (enamel). In human, however, once the tooth erupts into the oral cavity, the dental epithelial tissue is lost, thus teeth lose the potential to regenerate enamel. The remaining mesenchymal tissues have a limited capacity to regenerate dentin, cementum and pulp which suggests that the MSC populations exist in the adult teeth (Kuang-Hsien Hu et al., 2014). To date, several types of dental stem cells have been isolated from human teeth,

including DPSCs (Gronthos et al., 2000), SHEDs (Miura et al., 2003), PDLSCs (Seo et al., 2004), DFPCs (Morsczeck et al., 2005) and SCAPs (Sonoyama et al., 2006). These stem cells reside in different part of teeth (niches) and were identified according to their MSC-like properties *in vitro* and tissue forming capacity *in vivo*. However, as previously mentioned, human adult teeth lose the potential to regenerate enamel and human epithelial stem cells in adult teeth was never reported (Volponi et al., 2010).

In contrast, mice, which are an important and commonly used model for investigation of tooth development, exhibit two different types of tooth growth. Like human, mouse molar have limited capacity to regenerate dentin. Our BrdU chase experiment did not detect as much BrdU Labelling cells in the molar as in the incisor, while, mouse incisors grow throughout their lifetime and BrdU chase experiment showed a continuous cell proliferation. The continuous formation of enamel and dentin in incisor is made by the presence of active adult epithelial and mesenchymal stem cells respectively. The epithelial stem cells, which have been well studied, reside in a niche called the cervical loop. BrdU chase experiments have confirmed the existence of label-retaining cells in the cervical loop of mouse incisor. Following studies have further elucidated the mechanism about the signaling pathways regulating the stem cell niche such as FGF signaling pathway, SHH signaling pathway and TGFβ-BMP signaling pathway (Harada et al., 1999). Several potential markers for dental stem cells in the cervical loop have been identified such as Sox2, Bmi1 and Gli1. It is possible that these markers mark different stem cell populations. There also appear to be Lgr5 expressing stellate reticulum cells in the cervical loop (Chang et al., 2013) and it is possible that these cells represent yet another subgroup of stem cells as Lgr5 is a stem cell marker in other tissue (Schuijers and Clevers, 2012).

The mesenchymal stem cell niche in the mouse incisor dental pulp has not yet as well characterized as their epithelial counterparts. Numerous experiments have consistently

suggested that MSCs are associated with the vascular niche. In vascular niche pericytes can differentiate into a variety of mesenchymal populations ranging from osteoblasts, chondrocytes and adipocytes to fibroblasts (Doherty et al., 1998, Farrington-Rock et al., 2004). In human, the vascular niche was studied using BrdU chase experiment in immature third molars. One day after deep cavity preparation BrdU labelling was found in blood vessels surrounding the cavity, while after 4 days, the labelling was restricted only to the cavity area suggesting that perivascular progenitor/stem cells can proliferate in response to odontoblast injury and migrate to the injury site (Tecles et al., 2005). In mice, researchers applied an *in vivo* approach by using transgenic mouse lines to genetically label and linage trace pericytes and characterise their properties during development and following tooth damage. Results showed that pericytes had limited contribution to tooth growth, however, upon tooth damage stimuli, they were actively involved in dentin repair via migration, proliferating and differentiating into dentin-producing odontoblasts suggesting pericytes from vascular niche could serve as a MSC population in the dental pulp tissue of mouse incisor (Feng et al., 2011). Besides vascular niche it is generally thought that another MSC niche is located at the apical end of the incisor between the laCL and liCL. This notion was supported by the findings that cells in this area retain BrdU labeling (Seidel et al., 2010) and respond to odontoblast damage in explant cultures (Feng et al., 2011). Interestingly, Bmi1 and Gli1, markers for the cervical loop epithelial stem cells, are also expressed in the BrdU retaining mesenchymal cells in the area between cervical loops (Biehs et al., 2013, Seidel et al., 2010), reinforcing the idea that a MSC niche is located at the apical end of mouse icnsir. In this MSC niche, researchers have reported that sensory nerves secrete Shh protein to activate Gli1 expression in periarterial cells that contribute to all mesenchymal derivatives (Zhao et al., 2014). This suggested an important neurovascular function in the stem cell microenvironment.

To date, several stem cell populations have been reported in this stem cell niche besides Gli1 periarterial cells. For example, a significant population of mesenchymal stem cells during development, self-renewal and repair of a tooth are derived from peripheral nerve-associated glia. Glial cells generate multipotent mesenchymal stem cells that produce pulp cells and odontoblasts. In addition, our lineage tracing experiment of Thy-1 expressing cells showed that Thy-1 progeny contributed odontoblasts with non Thy-1 progeny ones. In summary, in comparison to stem cell niche in the molar, mouse incisor MSCs are mainly located in the niche at the apical end and continuously contribute to the growth of mouse incisor in adulthood while stem cells in the molar localized in several different locations and only limited regenerate dentin, cementum and pulp. Nonetheless, further experiments are required to investigate the architecture of the MSC niche, as well as the functional roles of certain molecules in it. In the future, expression profiling using gene expression microarray or RNA sequencing at the single cell level will be desirable to provide more informations.

6.7 Future work

As discussed above, additional work is needed to be accomplished in terms of elaborating the MSC niche of mouse incisor in the future. Firstly, stem cell identity needs to be further explored. A multi-colour reporter mouse line ($CAG^{ET2}Cre$; R26R-Confetti) is needed to trace single MSC clone in the mouse incisor to better study the stem cells and their progeny cells. In addition, a H2B-GFP mouse line which can activate GFP expression by external control, is needed to collect GFP expressing cells for gene analysis and *in vitro* cell studies. These transgenic mice express the human histone 1, H2bj, protein (HIST1H2BJ) and GFP fusion protein, HIST1H2BJ/GFP, under the control of a tetracycline-responsive promoter element (TRE; tetO). When hemizygotes are bred with another transgenic mouse expressing reverse

tetracycline-controlled trans-activator protein (rtTA) or tetracycline-controlled trans-activator protein (tTA) to create bi-transgenic animals, tissue-specific HIST1H2BJ/GFP transgene expression can be regulated with the tetracycline analog, doxycycline. Pulse-chase administration of doxycycline results in retention of GFP signal in rarely dividing, or infrequently cycling, label-retaining cells. This approach will avoid the damage of cells when cells are sorted with nucleotide labeling. Thus, cells can remain a healty state for microarray analysis to provide more information about the molecular mechanism of the quiescent state of stem cell. Furthermore, both slow cycling cells and fast cycling cells can be acquired without damage and be used for gene expression comparsion. The difference of gene expression between these two populations may provide us a clue of molecular mechanism for stem cell activation. Secondly, more time points need to be selected to trace fast cycling cells and slow cycling cells in the mouse incisor. In our study, these two populations were identified to localize a MSC niche. However, the exact numbers of these two populations is still needed to be determined. Thirdly, a conditional homozygous Bcor knockout mouse line is required to investigate the function of Bcor in the regulation of mouse incisor stem cells in adulthood as homozygotes may show more obvious phenotypes of mouse incisors. By labelling the cells with necloeside markers in this mouse line, the question of which cell population contributes to the overgrowth of mouse incisor can be addressed.

6.8 Summary

In this study, a MSC niche of mouse incisor was identified by 1) detecting the asymmetric division of MSCs through labeling cells with different proliferation rates; 2) detecting the location of stem cell clone through space-time control of GFP expression

in *pCAGERT2;R26R mT/mG* mouse incisor; 3) detecting the location of quiescent cells that are usually located in the stem cell niche through label-retaining experiment and Celsr1 expression; 4) selseting Thy-1 as a MSC marker in the mouse incisor dental pulp and performing cell fate tracing of Thy-1+ cells. In addition, Ring1, that are expressed by the fast cycling cells was investigated.

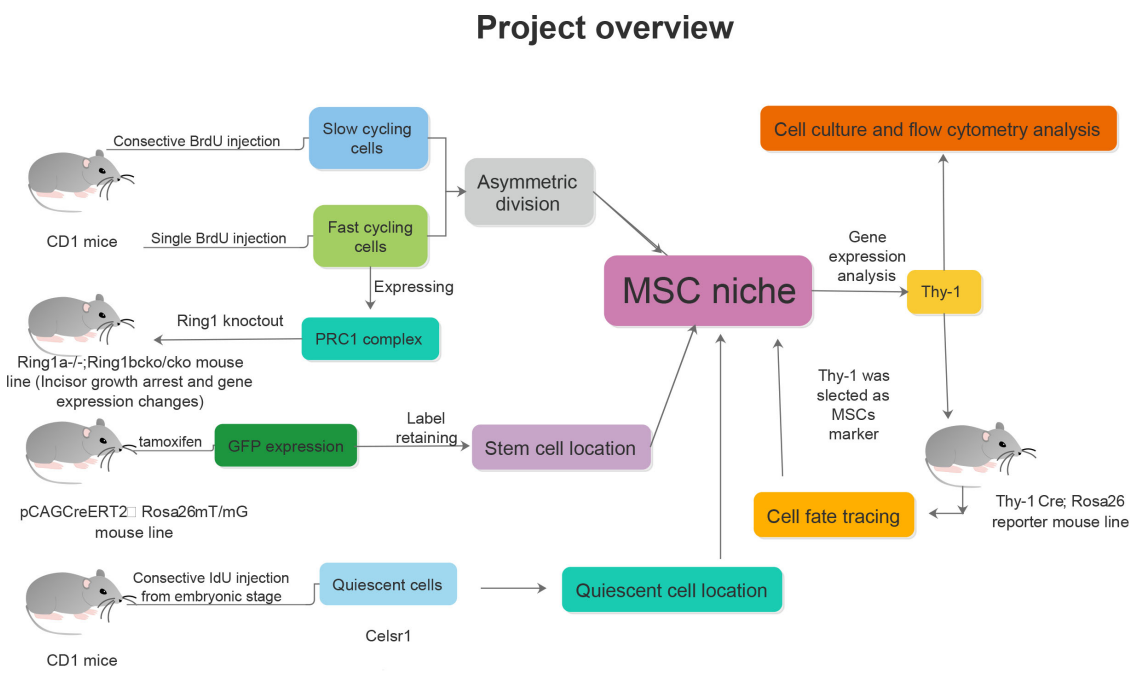

Fig 6.1: Project overview.

In summary, in the continuously growing mouse incisor, three cell populations exist in the apical end: slow cycling cells, fast cycling cells and quiescent cells. The slow cycling cells mainly approach the area between two cervical loops at the apical end of mouse incisor. As MSCs marker, Thy-1 expressing cells in this area contribute to the formation of dental pulp tissue. While fast cycling cells are located distally and regulated by PRC1 complex. Beside the fast and slow cell population, a quiescent long-term cell population marked by Celsr1 exists at the apical most end mesenchyme. All these results suggest a MSCs niche locating at the apical end of the mouse inciosr pulp tissue as generally believed.

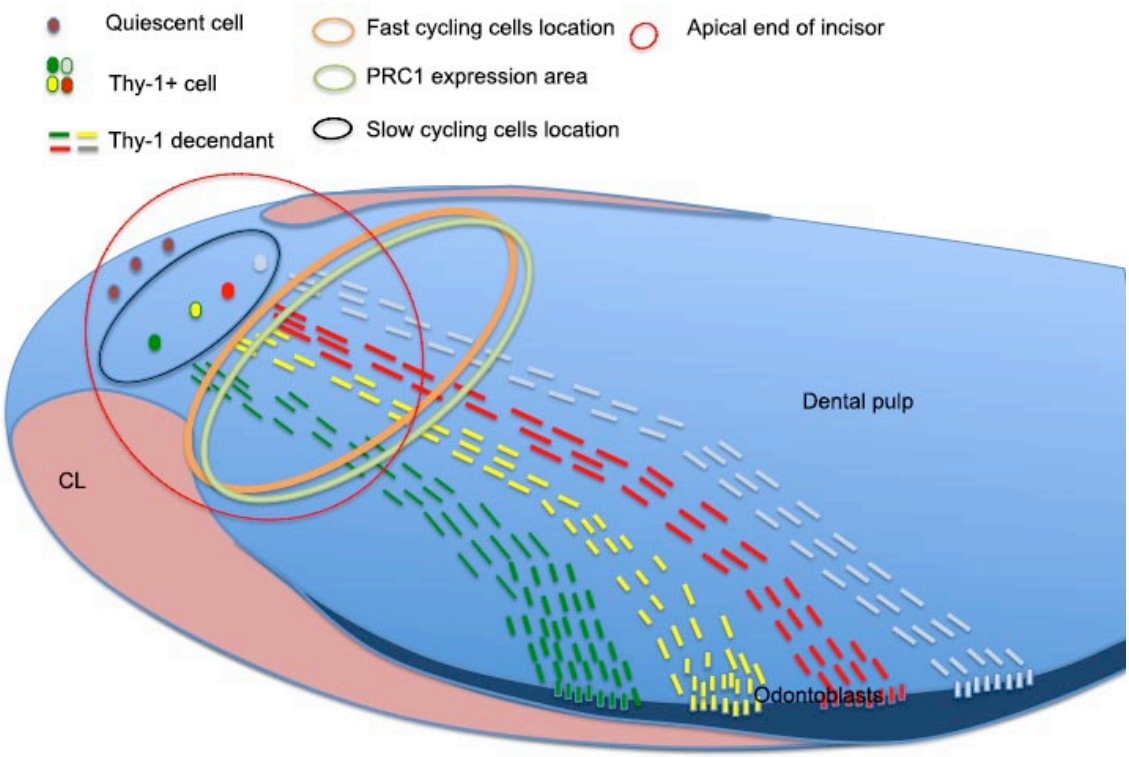

Fig 6. 2: Schematic diagram of project conclusion.

Bibliography

Abeysinghe, H. R., Cao, Q., Xu, J., Pollock, S., Veyberman, Y., Guckert, N. L., Keng, P. & Wang, N. 2003. THY1 expression is associated with tumor suppression of human ovarian cancer. *Cancer Genetics and Cytogenetics,* 143**,** 125-132.

Adaimy, L., Chouery, E., Megarbane, H., Mroueh, S., Delague, V., Nicolas, E., Belguith, H., de Mazancourt, P. & Megarbane, A. 2007. Mutation in WNT10A is associated with an autosomal recessive ectodermal dysplasia: the odonto-onycho-dermal dysplasia. *Am J Hum Genet,* 81**,** 821-8.

Akin, Z. N. & Nazarali, A. J. 2005. Hox genes and their candidate downstream targets in the developing central nervous system. *Cell Mol Neurobiol,* 25**,** 697-741.

Al-Nbaheen, M., Vishnubalaji, R., Ali, D., Bouslimi, A., Al-Jassir, F., Megges, M., Prigione, A., Adjaye, J., Kassem, M. & Aldahmash, A. 2013. Human stromal (mesenchymal) stem cells from bone marrow, adipose tissue and skin exhibit differences in molecular phenotype and differentiation potential. *Stem Cell Rev,* 9**,** 32-43.

Almqvist, P. & Carlsson, S. R. 1988. Characterization of a hydrophilic form of Thy-1 purified from human cerebrospinal fluid. *J Biol Chem,* 263**,** 12709-15.

Andl, T., Reddy, S. T., Gaddapara, T. & Millar, S. E. 2002. WNT signals are required for the initiation of hair follicle development. *Dev Cell,* 2**,** 643-53.

Andreadis, D., Bakopoulou, A., Leyhausen, G., Epivatianos, A., Volk, J., Markopoulos, A. & Geurtsen, W. 2014. Minor salivary glands of the lips: a novel, easily accessible source of potential stem/progenitor cells. *Clin Oral Investig,* 18**,** 847-56.

Arthur, A., Shi, S., Zannettino, A. C., Fujii, N., Gronthos, S. & Koblar, S. A. 2009. Implanted adult human dental pulp stem cells induce endogenous axon guidance. *Stem Cells,* 27**,** 2229-37.

Ayatollahi, M., Salmani, M. K., Geramizadeh, B., Tabei, S. Z., Soleimani, M. & Sanati, M. H. 2012. Conditions to improve expansion of human mesenchymal stem cells based on rat samples. *World J Stem Cells,* 4**,** 1-8.

Bai, Y., Bai, Y., Matsuzaka, K., Hashimoto, S., Fukuyama, T., Wu, L., Miwa, T., Liu, X., Wang, X. & Inoue, T. 2011. Cementum- and periodontal ligament-like tissue formation by dental follicle cell sheets co-cultured with Hertwig's epithelial root sheath cells. *Bone,* 48**,** 1417-26.

Balordi, F. & Fishell, G. 2007. Hedgehog signaling in the subventricular zone is required for both the maintenance of stem cells and the migration of newborn neurons. *J Neurosci,* 27**,** 5936-47.

Beyer Nardi, N. & da Silva Meirelles, L. 2006. Mesenchymal stem cells: isolation, in vitro expansion and characterization. *Handb Exp Pharmacol***,** 249-82.

Bianco, P., Robey, P. G. & Simmons, P. J. 2008. Mesenchymal stem cells: revisiting history, concepts, and assays. *Cell Stem Cell,* 2**,** 313-9.

Biehs, B., Hu, J. K., Strauli, N. B., Sangiorgi, E., Jung, H., Heber, R. P., Ho, S., Goodwin, A. F., Dasen, J. S., Capecchi, M. R. & Klein, O. D. 2013. BMI1 represses Ink4a/Arf and Hox genes to regulate stem cells in the rodent incisor. *Nat Cell Biol,* 15**,** 846-52.

Birbrair, A., Wang, Z. M., Messi, M. L., Enikolopov, G. N. & Delbono, O. 2011. Nestin-GFP transgene reveals neural precursor cells in adult skeletal muscle.

PLoS One, 6**,** e16816.

Bradley, J. E., Ramirez, G. & Hagood, J. S. 2009. Roles and regulation of Thy-1, a context-dependent modulator of cell phenotype. *Biofactors,* 35**,** 258-65.

Brumovsky, P. R., La, J. H. & Gebhart, G. F. 2014. Distribution across tissue layers of extrinsic nerves innervating the mouse colorectum - an in vitro anterograde tracing study. *Neurogastroenterol Motil,* 26**,** 1494-507.

Cahill, D. R. & Marks, S. C., Jr. 1980. Tooth eruption: evidence for the central role of the dental follicle. *J Oral Pathol,* 9**,** 189-200.

Cales, C., Roman-Trufero, M., Pavon, L., Serrano, I., Melgar, T., Endoh, M., Perez, C., Koseki, H. & Vidal, M. 2008. Inactivation of the polycomb group protein Ring1B unveils an antiproliferative role in hematopoietic cell expansion and cooperation with tumorigenesis associated with Ink4a deletion. *Mol Cell Biol,* 28**,** 1018-28.

Cao, R., Wang, L., Wang, H., Xia, L., Erdjument-Bromage, H., Tempst, P., Jones, R. S. & Zhang, Y. 2002. Role of histone H3 lysine 27 methylation in Polycomb-group silencing. *Science,* 298**,** 1039-43.

Chai, Y., Jiang, X., Ito, Y., Bringas, P., Jr., Han, J., Rowitch, D. H., Soriano, P., McMahon, A. P. & Sucov, H. M. 2000. Fate of the mammalian cranial neural crest during tooth and mandibular morphogenesis. *Development,* 127**,** 1671-9.

Chang, J. Y., Wang, C., Jin, C., Yang, C., Huang, Y., Liu, J., McKeehan, W. L., D'Souza, R. N. & Wang, F. 2013. Self-renewal and multilineage differentiation of mouse dental epithelial stem cells. *Stem Cell Res,* 11**,** 990-1002.

Chase, L. G., Lakshmipathy, U., Solchaga, L. A., Rao, M. S. & Vemuri, M. C. 2010. A novel serum-free medium for the expansion of human mesenchymal stem cells. *Stem Cell Res Ther,* 1**,** 8.

Cironi, L., Provero, P., Riggi, N., Janiszewska, M., Suva, D., Suva, M. L., Kindler, V. & Stamenkovic, I. 2009. Epigenetic features of human mesenchymal stem cells determine their permissiveness for induction of relevant transcriptional changes by SYT-SSX1. *PLoS One,* 4**,** e7904.

Coady, J. M., Toto, P. D. & Santangelo, M. V. 1967. Histology of the mouse incisor. *J Dent Res,* 46**,** 384-8.

Cobourne, M. T., Xavier, G. M., Depew, M., Hagan, L., Sealby, J., Webster, Z. & Sharpe, P. T. 2009. Sonic hedgehog signalling inhibits palatogenesis and arrests tooth development in a mouse model of the nevoid basal cell carcinoma syndrome. *Dev Biol,* 331**,** 38-49.

Craig, W., Kay, R., Cutler, R. L. & Lansdorp, P. M. 1993. Expression of Thy-1 on human hematopoietic progenitor cells. *J Exp Med,* 177**,** 1331-42.

Curtin, J. A., Quint, E., Tsipouri, V., Arkell, R. M., Cattanach, B., Copp, A. J., Henderson, D. J., Spurr, N., Stanier, P., Fisher, E. M., Nolan, P. M., Steel, K. P., Brown, S. D., Gray, I. C. & Murdoch, J. N. 2003. Mutation of Celsr1 disrupts planar polarity of inner ear hair cells and causes severe neural tube defects in the mouse. *Curr Biol,* 13**,** 1129-33.

d'Aquino, R., De Rosa, A., Laino, G., Caruso, F., Guida, L., Rullo, R., Checchi, V., Laino, L., Tirino, V. & Papaccio, G. 2009. Human dental pulp stem cells: from biology to clinical applications. *J Exp Zool B Mol Dev Evol,* 312B**,** 408-15.

Daltoe, F. P., Mendonca, P. P., Mantesso, A. & Deboni, M. C. 2014. Can SHED or DPSCs be used to repair/regenerate non-dental tissues? A systematic review of in vivo studies. *Braz Oral Res,* 28.

Dassule, H. R. & McMahon, A. P. 1998. Analysis of epithelial-mesenchymal interactions in the initial morphogenesis of the mammalian tooth. *Dev Biol,*

202, 215-27.

de Napoles, M., Mermoud, J. E., Wakao, R., Tang, Y. A., Endoh, M., Appanah, R., Nesterova, T. B., Silva, J., Otte, A. P., Vidal, M., Koseki, H. & Brockdorff, N. 2004. Polycomb group proteins Ring1A/B link ubiquitylation of histone H2A to heritable gene silencing and X inactivation. *Dev Cell,* 7, 663-76.

Di Croce, L. & Helin, K. 2013. Transcriptional regulation by Polycomb group proteins. *Nat Struct Mol Biol,* 20, 1147-55.

Diaz-Flores, L., Jr., Madrid, J. F., Gutierrez, R., Varela, H., Valladares, F., Alvarez-Arguelles, H. & Diaz-Flores, L. 2006. Adult stem and transit-amplifying cell location. *Histol Histopathol,* 21, 995-1027.

Doherty, M. J., Ashton, B. A., Walsh, S., Beresford, J. N., Grant, M. E. & Canfield, A. E. 1998. Vascular pericytes express osteogenic potential in vitro and in vivo. *J Bone Miner Res,* 13, 828-38.

Dominici, M., Le Blanc, K., Mueller, I., Slaper-Cortenbach, I., Marini, F., Krause, D., Deans, R., Keating, A., Prockop, D. & Horwitz, E. 2006. Minimal criteria for defining multipotent mesenchymal stromal cells. The International Society for Cellular Therapy position statement. *Cytotherapy,* 8, 315-7.

Dowthwaite, G. P., Bishop, J. C., Redman, S. N., Khan, I. M., Rooney, P., Evans, D. J., Haughton, L., Bayram, Z., Boyer, S., Thomson, B., Wolfe, M. S. & Archer, C. W. 2004. The surface of articular cartilage contains a progenitor cell population. *J Cell Sci,* 117, 889-97.

Duggan, D. J., Bittner, M., Chen, Y., Meltzer, P. & Trent, J. M. 1999. Expression profiling using cDNA microarrays. *Nat Genet,* 21, 10-4.

Eden, E., Geva-Zatorsky, N., Issaeva, I., Cohen, A., Dekel, E., Danon, T., Cohen, L., Mayo, A. & Alon, U. 2011. Proteome half-life dynamics in living human cells. *Science,* 331, 764-8.

Endoh, M., Endo, T. A., Endoh, T., Fujimura, Y., Ohara, O., Toyoda, T., Otte, A. P., Okano, M., Brockdorff, N., Vidal, M. & Koseki, H. 2008. Polycomb group proteins Ring1A/B are functionally linked to the core transcriptional regulatory circuitry to maintain ES cell identity. *Development,* 135, 1513-24.

Endoh, M., Endo, T. A., Endoh, T., Isono, K., Sharif, J., Ohara, O., Toyoda, T., Ito, T., Eskeland, R., Bickmore, W. A., Vidal, M., Bernstein, B. E. & Koseki, H. 2012. Histone H2A mono-ubiquitination is a crucial step to mediate PRC1-dependent repression of developmental genes to maintain ES cell identity. *PLoS Genet,* 8, e1002774.

Erices, A., Conget, P. & Minguell, J. J. 2000. Mesenchymal progenitor cells in human umbilical cord blood. *Br J Haematol,* 109, 235-42.

Eslaminejad, M. B., Nadri, S. & Hosseini, R. H. 2007. Expression of Thy 1.2 surface antigen increases significantly during the murine mesenchymal stem cells cultivation period. *Dev Growth Differ,* 49, 351-64.

Evans, M. J. & Kaufman, M. H. 1981. Establishment in culture of pluripotential cells from mouse embryos. *Nature,* 292, 154-6.

Fan, Z., Yamaza, T., Lee, J. S., Yu, J., Wang, S., Fan, G., Shi, S. & Wang, C. Y. 2009. BCOR regulates mesenchymal stem cell function by epigenetic mechanisms. *Nat Cell Biol,* 11, 1002-9.

Farrington-Rock, C., Crofts, N. J., Doherty, M. J., Ashton, B. A., Griffin-Jones, C. & Canfield, A. E. 2004. Chondrogenic and adipogenic potential of microvascular pericytes. *Circulation,* 110, 2226-32.

Feil, S., Valtcheva, N. & Feil, R. 2009. Inducible Cre mice. *Methods Mol Biol,* 530, 343-63.

Felszeghy, S., Suomalainen, M. & Thesleff, I. 2010. Notch signalling is required for the survival of epithelial stem cells in the continuously growing mouse incisor. *Differentiation,* 80**,** 241-8.

Feng, J., Mantesso, A., De Bari, C., Nishiyama, A. & Sharpe, P. T. 2011. Dual origin of mesenchymal stem cells contributing to organ growth and repair. *Proc Natl Acad Sci U S A,* 108**,** 6503-8.

Firth, A. L. & Yuan, J. X. 2012. Identification of functional progenitor cells in the pulmonary vasculature. *Pulm Circ,* 2**,** 84-100.

Fischle, W., Wang, Y., Jacobs, S. A., Kim, Y., Allis, C. D. & Khorasanizadeh, S. 2003. Molecular basis for the discrimination of repressive methyl-lysine marks in histone H3 by Polycomb and HP1 chromodomains. *Genes Dev,* 17**,** 1870-81.

Francis, N. J., Kingston, R. E. & Woodcock, C. L. 2004. Chromatin compaction by a polycomb group protein complex. *Science,* 306**,** 1574-7.

Friedenstein, A. J. 1976. Precursor cells of mechanocytes. *Int Rev Cytol,* 47**,** 327-59.

Fujita, T., Iwata, T., Shiba, H., Igarashi, A., Hirata, R., Takeda, K., Mizuno, N., Tsuji, K., Kawaguchi, H., Kato, Y. & Kurihara, H. 2007. Identification of marker genes distinguishing human periodontal ligament cells from human mesenchymal stem cells and human gingival fibroblasts. *J Periodontal Res,* 42**,** 283-6.

Furutachi, S., Miya, H., Watanabe, T., Kawai, H., Yamasaki, N., Harada, Y., Imayoshi, I., Nelson, M., Nakayama, K. I., Hirabayashi, Y. & Gotoh, Y. 2015. Slowly dividing neural progenitors are an embryonic origin of adult neural stem cells. *Nat Neurosci,* 18**,** 657-65.

Gao, Z., Zhang, J., Bonasio, R., Strino, F., Sawai, A., Parisi, F., Kluger, Y. & Reinberg, D. 2012. PCGF homologs, CBX proteins, and RYBP define functionally distinct PRC1 family complexes. *Mol Cell,* 45**,** 344-56.

Gaspard, N., Bouschet, T., Hourez, R., Dimidschstein, J., Naeije, G., van den Ameele, J., Espuny-Camacho, I., Herpoel, A., Passante, L., Schiffmann, S. N., Gaillard, A. & Vanderhaeghen, P. 2008. An intrinsic mechanism of corticogenesis from embryonic stem cells. *Nature,* 455**,** 351-7.

Gay, I. C., Chen, S. & MacDougall, M. 2007. Isolation and characterization of multipotent human periodontal ligament stem cells. *Orthod Craniofac Res,* 10**,** 149-60.

Greco, V. & Guo, S. 2010. Compartmentalized organization: a common and required feature of stem cell niches? *Development,* 137**,** 1586-94.

Gronthos, S., Mankani, M., Brahim, J., Robey, P. G. & Shi, S. 2000. Postnatal human dental pulp stem cells (DPSCs) in vitro and in vivo. *Proc Natl Acad Sci U S A,* 97**,** 13625-30.

Guo, Z., Li, H., Li, X., Yu, X., Wang, H., Tang, P. & Mao, N. 2006. In vitro characteristics and in vivo immunosuppressive activity of compact bone-derived murine mesenchymal progenitor cells. *Stem Cells,* 24**,** 992-1000.

Haegebarth, A. & Clevers, H. 2009. Wnt signaling, lgr5, and stem cells in the intestine and skin. *Am J Pathol,* 174**,** 715-21.

Han, X. L., Liu, M., Voisey, A., Ren, Y. S., Kurimoto, P., Gao, T., Tefera, L., Dechow, P., Ke, H. Z. & Feng, J. Q. 2011. Post-natal effect of overexpressed DKK1 on mandibular molar formation. *J Dent Res,* 90**,** 1312-7.

Handa, K., Saito, M., Tsunoda, A., Yamauchi, M., Hattori, S., Sato, S., Toyoda, M., Teranaka, T. & Narayanan, A. S. 2002. Progenitor cells from dental follicle are able to form cementum matrix in vivo. *Connect Tissue Res,* 43**,** 406-8.

Harada, H., Kettunen, P., Jung, H. S., Mustonen, T., Wang, Y. A. & Thesleff, I. 1999. Localization of putative stem cells in dental epithelium and their association

with Notch and FGF signaling. *J Cell Biol,* 147**,** 105-20.

Harada, H., Mitsuyasu, T., Toyono, T. & Toyoshima, K. 2002. Epithelial stem cells in teeth. *Odontology,* 90**,** 1-6.

Haug, J. S., He, X. C., Grindley, J. C., Wunderlich, J. P., Gaudenz, K., Ross, J. T., Paulson, A., Wagner, K. P., Xie, Y., Zhu, R., Yin, T., Perry, J. M., Hembree, M. J., Redenbaugh, E. P., Radice, G. L., Seidel, C. & Li, L. 2008. N-cadherin expression level distinguishes reserved versus primed states of hematopoietic stem cells. *Cell Stem Cell,* 2**,** 367-79.

Hill, J. J., Tremblay, T. L., Cantin, C., O'Connor-McCourt, M., Kelly, J. F. & Lenferink, A. E. 2009. Glycoproteomic analysis of two mouse mammary cell lines during transforming growth factor (TGF)-beta induced epithelial to mesenchymal transition. *Proteome Sci,* 7**,** 2.

Horwitz, E. M., Le Blanc, K., Dominici, M., Mueller, I., Slaper-Cortenbach, I., Marini, F. C., Deans, R. J., Krause, D. S., Keating, A. & International Society for Cellular, T. 2005. Clarification of the nomenclature for MSC: The International Society for Cellular Therapy position statement. *Cytotherapy,* 7**,** 393-5.

Hosoya, A., Hiraga, T., Ninomiya, T., Yukita, A., Yoshiba, K., Yoshiba, N., Takahashi, M., Ito, S. & Nakamura, H. 2012. Thy-1-positive cells in the subodontoblastic layer possess high potential to differentiate into hard tissue-forming cells. *Histochem Cell Biol*.

Hsu, Y. C., Li, L. & Fuchs, E. 2014. Transit-amplifying cells orchestrate stem cell activity and tissue regeneration. *Cell,* 157**,** 935-49.

Huang, A. H., Snyder, B. R., Cheng, P. H. & Chan, A. W. 2008a. Putative dental pulp-derived stem/stromal cells promote proliferation and differentiation of endogenous neural cells in the hippocampus of mice. *Stem Cells,* 26**,** 2654-63.

Huang, G. T., Gronthos, S. & Shi, S. 2009. Mesenchymal stem cells derived from dental tissues vs. those from other sources: their biology and role in regenerative medicine. *J Dent Res,* 88**,** 792-806.

Huang, G. T., Sonoyama, W., Liu, Y., Liu, H., Wang, S. & Shi, S. 2008b. The hidden treasure in apical papilla: the potential role in pulp/dentin regeneration and bioroot engineering. *J Endod,* 34**,** 645-51.

Hurlbut, G. D., Kankel, M. W., Lake, R. J. & Artavanis-Tsakonas, S. 2007. Crossing paths with Notch in the hyper-network. *Curr Opin Cell Biol,* 19**,** 166-75.

In 't Anker, P. S., Scherjon, S. A., Kleijburg-van der Keur, C., Noort, W. A., Claas, F. H., Willemze, R., Fibbe, W. E. & Kanhai, H. H. 2003. Amniotic fluid as a novel source of mesenchymal stem cells for therapeutic transplantation. *Blood,* 102**,** 1548-9.

Inagaki, T., Iwasaki, S., Matsumura, Y., Kawamura, T., Tanaka, T., Abe, Y., Yamasaki, A., Tsurutani, Y., Yoshida, A., Chikaoka, Y., Nakamura, K., Magoori, K., Nakaki, R., Osborne, T. F., Fukami, K., Aburatani, H., Kodama, T. & Sakai, J. 2014. The FBXL10/KDM2B scaffolding protein associates with novel polycomb repressive complex-1 to regulate adipogenesis. *J Biol Chem*.

Ingham, P. W. & McMahon, A. P. 2001. Hedgehog signaling in animal development: paradigms and principles. *Genes Dev,* 15**,** 3059-87.

Jernvall, J. & Thesleff, I. 2000. Reiterative signaling and patterning during mammalian tooth morphogenesis. *Mech Dev,* 92**,** 19-29.

Jiang, Y., Jahagirdar, B. N., Reinhardt, R. L., Schwartz, R. E., Keene, C. D., Ortiz-Gonzalez, X. R., Reyes, M., Lenvik, T., Lund, T., Blackstad, M., Du, J., Aldrich, S., Lisberg, A., Low, W. C., Largaespada, D. A. & Verfaillie, C. M. 2002.

Pluripotency of mesenchymal stem cells derived from adult marrow. *Nature,* 418**,** 41-9.

Jones, S., Horwood, N., Cope, A. & Dazzi, F. 2007. The antiproliferative effect of mesenchymal stem cells is a fundamental property shared by all stromal cells. *J Immunol,* 179**,** 2824-31.

Joyner, A. L. & Zervas, M. 2006. Genetic inducible fate mapping in mouse: establishing genetic lineages and defining genetic neuroanatomy in the nervous system. *Dev Dyn,* 235**,** 2376-85.

Kadar, K., Kiraly, M., Porcsalmy, B., Molnar, B., Racz, G. Z., Blazsek, J., Kallo, K., Szabo, E. L., Gera, I., Gerber, G. & Varga, G. 2009. Differentiation potential of stem cells from human dental origin - promise for tissue engineering. *J Physiol Pharmacol,* 60 Suppl 7**,** 167-75.

Kaltz, N., Ringe, J., Holzwarth, C., Charbord, P., Niemeyer, M., Jacobs, V. R., Peschel, C., Haupl, T. & Oostendorp, R. A. 2010. Novel markers of mesenchymal stem cells defined by genome-wide gene expression analysis of stromal cells from different sources. *Exp Cell Res,* 316**,** 2609-17.

Kanafi, M., Majumdar, D., Bhonde, R., Gupta, P. & Datta, I. 2014. Midbrain cues dictate differentiation of human dental pulp stem cells towards functional dopaminergic neurons. *J Cell Physiol,* 229**,** 1369-77.

Kaukua, N., Shahidi, M. K., Konstantinidou, C., Dyachuk, V., Kaucka, M., Furlan, A., An, Z., Wang, L., Hultman, I., Ahrlund-Richter, L., Blom, H., Brismar, H., Lopes, N. A., Pachnis, V., Suter, U., Clevers, H., Thesleff, I., Sharpe, P., Ernfors, P., Fried, K. & Adameyko, I. 2014. Glial origin of mesenchymal stem cells in a tooth model system. *Nature,* 513**,** 551-4.

Kim, S. S., Kwon, D. W., Im, I., Kim, Y. D., Hwang, D. S., Holliday, L. S., Donatelli, R. E., Son, W. S. & Jun, E. S. 2012. Differentiation and characteristics of undifferentiated mesenchymal stem cells originating from adult premolar periodontal ligaments. *Korean J Orthod,* 42**,** 307-17.

Kimura, H., Usui, T., Tsubouchi, A. & Uemura, T. 2006. Potential dual molecular interaction of the Drosophila 7-pass transmembrane cadherin Flamingo in dendritic morphogenesis. *J Cell Sci,* 119**,** 1118-29.

Kist, R., Watson, M., Crosier, M., Robinson, M., Fuchs, J., Reichelt, J. & Peters, H. 2014. The formation of endoderm-derived taste sensory organs requires a Pax9-dependent expansion of embryonic taste bud progenitor cells. *PLoS Genet,* 10**,** e1004709.

Kordes, C. & Haussinger, D. 2013. Hepatic stem cell niches. *J Clin Invest,* 123**,** 1874-80.

Kratochwil, K., Galceran, J., Tontsch, S., Roth, W. & Grosschedl, R. 2002. FGF4, a direct target of LEF1 and Wnt signaling, can rescue the arrest of tooth organogenesis in Lef1(-/-) mice. *Genes Dev,* 16**,** 3173-85.

Kretzschmar, K. & Watt, F. M. 2012. Lineage tracing. *Cell,* 148**,** 33-45.

Ku, M., Koche, R. P., Rheinbay, E., Mendenhall, E. M., Endoh, M., Mikkelsen, T. S., Presser, A., Nusbaum, C., Xie, X., Chi, A. S., Adli, M., Kasif, S., Ptaszek, L. M., Cowan, C. A., Lander, E. S., Koseki, H. & Bernstein, B. E. 2008. Genomewide analysis of PRC1 and PRC2 occupancy identifies two classes of bivalent domains. *PLoS Genet,* 4**,** e1000242.

Kuang-Hsien Hu, J., Mushegyan, V. & Klein, O. D. 2014. On the cutting edge of organ renewal: Identification, regulation, and evolution of incisor stem cells. *Genesis,* 52**,** 79-92.

Lammi, L., Halonen, K., Pirinen, S., Thesleff, I., Arte, S. & Nieminen, P. 2003. A

missense mutation in PAX9 in a family with distinct phenotype of oligodontia. *Eur J Hum Genet,* 11**,** 866-71.

Lapi, S., Nocchi, F., Lamanna, R., Passeri, S., Iorio, M., Paolicchi, A., Urciuoli, P., Coli, A., Abramo, F., Miragliotta, V., Giannessi, E., Stornelli, M. R., Vanacore, R., Stampacchia, G., Pisani, G., Borghetti, L. & Scatena, F. 2008. Different media and supplements modulate the clonogenic and expansion properties of rabbit bone marrow mesenchymal stem cells. *BMC Res Notes,* 1**,** 53.

Lapthanasupkul, P., Feng, J., Mantesso, A., Takada-Horisawa, Y., Vidal, M., Koseki, H., Wang, L., An, Z., Miletich, I. & Sharpe, P. T. 2012. Ring1a/b polycomb proteins regulate the mesenchymal stem cell niche in continuously growing incisors. *Dev Biol,* 367**,** 140-53.

Lawler, J. W., Slayter, H. S. & Coligan, J. E. 1978. Isolation and characterization of a high molecular weight glycoprotein from human blood platelets. *J Biol Chem,* 253**,** 8609-16.

Levine, S. S., Weiss, A., Erdjument-Bromage, H., Shao, Z., Tempst, P. & Kingston, R. E. 2002. The core of the polycomb repressive complex is compositionally and functionally conserved in flies and humans. *Mol Cell Biol,* 22**,** 6070-8.

Liu, D., Yovchev, M. I., Zhang, J., Alfieri, A. A., Tchaikovskaya, T., Laconi, E. & Dabeva, M. D. 2015. Identification and characterization of mesenchymal-epithelial progenitor-like cells in normal and injured rat liver. *Am J Pathol,* 185**,** 110-28.

Liu, F., Chu, E. Y., Watt, B., Zhang, Y., Gallant, N. M., Andl, T., Yang, S. H., Lu, M. M., Piccolo, S., Schmidt-Ullrich, R., Taketo, M. M., Morrisey, E. E., Atit, R., Dlugosz, A. A. & Millar, S. E. 2008. Wnt/beta-catenin signaling directs multiple stages of tooth morphogenesis. *Dev Biol,* 313**,** 210-24.

Livet, J. 2007. [The brain in color: transgenic "Brainbow" mice for visualizing neuronal circuits]. *Med Sci (Paris),* 23**,** 1173-6.

Locatelli, F., Corti, S., Donadoni, C., Guglieri, M., Capra, F., Strazzer, S., Salani, S., Del Bo, R., Fortunato, F., Bordoni, A. & Comi, G. P. 2003. Neuronal differentiation of murine bone marrow Thy-1- and Sca-1-positive cells. *J Hematother Stem Cell Res,* 12**,** 727-34.

Lohi, M., Tucker, A. S. & Sharpe, P. T. 2010. Expression of Axin2 indicates a role for canonical Wnt signaling in development of the crown and root during pre- and postnatal tooth development. *Dev Dyn,* 239**,** 160-7.

Lounev, V. Y., Ramachandran, R., Wosczyna, M. N., Yamamoto, M., Maidment, A. D., Shore, E. M., Glaser, D. L., Goldhamer, D. J. & Kaplan, F. S. 2009. Identification of progenitor cells that contribute to heterotopic skeletogenesis. *J Bone Joint Surg Am,* 91**,** 652-63.

Lv, F. J., Tuan, R. S., Cheung, K. M. & Leung, V. Y. 2014. Concise review: the surface markers and identity of human mesenchymal stem cells. *Stem Cells,* 32**,** 1408-19.

Machold, R., Hayashi, S., Rutlin, M., Muzumdar, M. D., Nery, S., Corbin, J. G., Gritli-Linde, A., Dellovade, T., Porter, J. A., Rubin, L. L., Dudek, H., McMahon, A. P. & Fishell, G. 2003. Sonic hedgehog is required for progenitor cell maintenance in telencephalic stem cell niches. *Neuron,* 39**,** 937-50.

Marion, R. M., Strati, K., Li, H., Murga, M., Blanco, R., Ortega, S., Fernandez-Capetillo, O., Serrano, M. & Blasco, M. A. 2009. A p53-mediated DNA damage response limits reprogramming to ensure iPS cell genomic integrity. *Nature,* 460**,** 1149-53.

Martin, G. R. 1981. Isolation of a pluripotent cell line from early mouse embryos

cultured in medium conditioned by teratocarcinoma stem cells. *Proc Natl Acad Sci U S A,* 78**,** 7634-8.

Martinez, A. M., Schuettengruber, B., Sakr, S., Janic, A., Gonzalez, C. & Cavalli, G. 2009. Polyhomeotic has a tumor suppressor activity mediated by repression of Notch signaling. *Nat Genet,* 41**,** 1076-82.

Masson, N. M., Currie, I. S., Terrace, J. D., Garden, O. J., Parks, R. W. & Ross, J. A. 2006. Hepatic progenitor cells in human fetal liver express the oval cell marker Thy-1. *Am J Physiol Gastrointest Liver Physiol,* 291**,** G45-54.

Mayani, H. & Lansdorp, P. M. 1994. Thy-1 expression is linked to functional properties of primitive hematopoietic progenitor cells from human umbilical cord blood. *Blood,* 83**,** 2410-7.

Miao, Z., Jin, J., Chen, L., Zhu, J., Huang, W., Zhao, J., Qian, H. & Zhang, X. 2006. Isolation of mesenchymal stem cells from human placenta: comparison with human bone marrow mesenchymal stem cells. *Cell Biol Int,* 30**,** 681-7.

Mikels, A. J. & Nusse, R. 2006. Purified Wnt5a protein activates or inhibits beta-catenin-TCF signaling depending on receptor context. *PLoS Biol,* 4**,** e115.

Mitsiadis, T. A. 2009. Horizons in Clinical Nanomedicine. *Horizons in Clinical Nanomedicine.* Pan Stanford Publishing.

Mitsiadis, T. A., Barrandon, O., Rochat, A., Barrandon, Y. & De Bari, C. 2007. Stem cell niches in mammals. *Exp Cell Res,* 313**,** 3377-85.

Mitsiadis, T. A., Hirsinger, E., Lendahl, U. & Goridis, C. 1998. Delta-notch signaling in odontogenesis: correlation with cytodifferentiation and evidence for feedback regulation. *Dev Biol,* 204**,** 420-31.

Miura, M., Gronthos, S., Zhao, M., Lu, B., Fisher, L. W., Robey, P. G. & Shi, S. 2003. SHED: stem cells from human exfoliated deciduous teeth. *Proc Natl Acad Sci U S A,* 100**,** 5807-12.

Morris, R. 1985. Thy-1 in developing nervous tissue. *Dev Neurosci,* 7**,** 133-60.

Morsczeck, C., Gotz, W., Schierholz, J., Zeilhofer, F., Kuhn, U., Mohl, C., Sippel, C. & Hoffmann, K. H. 2005. Isolation of precursor cells (PCs) from human dental follicle of wisdom teeth. *Matrix Biol,* 24**,** 155-65.

Morsczeck, C., Vollner, F., Saugspier, M., Brandl, C., Reichert, T. E., Driemel, O. & Schmalz, G. 2010. Comparison of human dental follicle cells (DFCs) and stem cells from human exfoliated deciduous teeth (SHED) after neural differentiation in vitro. *Clin Oral Investig,* 14**,** 433-40.

Mostowska, A., Zadurska, M., Rakowska, A., Lianeri, M. & Jagodzinski, P. P. 2013. Novel PAX9 mutation associated with syndromic tooth agenesis. *Eur J Oral Sci,* 121**,** 403-11.

Mrozik, K., Gronthos, S., Shi, S. & Bartold, P. M. 2010. A method to isolate, purify, and characterize human periodontal ligament stem cells. *Methods Mol Biol,* 666**,** 269-84.

Muzumdar, M. D., Tasic, B., Miyamichi, K., Li, L. & Luo, L. 2007. A global double-fluorescent Cre reporter mouse. *Genesis,* 45**,** 593-605.

Nakamura, H., Yukita, A., Ninomiya, T., Hosoya, A., Hiraga, T. & Ozawa, H. 2010. Localization of Thy-1-positive cells in the perichondrium during endochondral ossification. *J Histochem Cytochem,* 58**,** 455-62.

Nakamura, Y., Muguruma, Y., Yahata, T., Miyatake, H., Sakai, D., Mochida, J., Hotta, T. & Ando, K. 2006. Expression of CD90 on keratinocyte stem/progenitor cells. *Br J Dermatol,* 154**,** 1062-70.

Nanci, A. 2007. Ten Cate's Oral Histology: Development, Structure, and Function: St.

Louis, Missouri, Mosby.

Neubuser, A., Peters, H., Balling, R. & Martin, G. R. 1997. Antagonistic interactions between FGF and BMP signaling pathways: a mechanism for positioning the sites of tooth formation. *Cell,* 90**,** 247-55.

Nishida, E., Sasaki, T., Ishikawa, S. K., Kosaka, K., Aino, M., Noguchi, T., Teranaka, T., Shimizu, N. & Saito, M. 2007. Transcriptome database KK-Periome for periodontal ligament development: expression profiles of the extracellular matrix genes. *Gene,* 404**,** 70-9.

Nusse, R., Fuerer, C., Ching, W., Harnish, K., Logan, C., Zeng, A., ten Berge, D. & Kalani, Y. 2008. Wnt signaling and stem cell control. *Cold Spring Harb Symp Quant Biol,* 73**,** 59-66.

Obara, N., Suzuki, Y. & Takeda, M. 2006. Gene expression of beta-catenin is up-regulated in inner dental epithelium and enamel knots during molar tooth morphogenesis in the mouse. *Cell Tissue Res,* 325**,** 197-201.

Ohlstein, B., Kai, T., Decotto, E. & Spradling, A. 2004. The stem cell niche: theme and variations. *Curr Opin Cell Biol,* 16**,** 693-9.

Ohshima, H., Nakasone, N., Hashimoto, E., Sakai, H., Nakakura-Ohshima, K. & Harada, H. 2005. The eternal tooth germ is formed at the apical end of continuously growing teeth. *Arch Oral Biol,* 50**,** 153-7.

Papaccio, G., Graziano, A., d'Aquino, R., Graziano, M. F., Pirozzi, G., Menditti, D., De Rosa, A., Carinci, F. & Laino, G. 2006. Long-term cryopreservation of dental pulp stem cells (SBP-DPSCs) and their differentiated osteoblasts: a cell source for tissue repair. *J Cell Physiol,* 208**,** 319-25.

Peters, H., Neubuser, A., Kratochwil, K. & Balling, R. 1998. Pax9-deficient mice lack pharyngeal pouch derivatives and teeth and exhibit craniofacial and limb abnormalities. *Genes Dev,* 12**,** 2735-47.

Petersen, B. E., Goff, J. P., Greenberger, J. S. & Michalopoulos, G. K. 1998. Hepatic oval cells express the hematopoietic stem cell marker Thy-1 in the rat. *Hepatology,* 27**,** 433-45.

Pivoriuunas, A., Surovas, A., Borutinskaite, V., Matuzeviccius, D., Treigyte, G., Savickiene, J., Tunaitis, V., Aldonyte, R., Jarmalavicciuute, A., Suriakaite, K., Liutkeviccius, E., Venalis, A., Navakauskas, D., Navakauskiene, R. & Magnusson, K. E. 2010. Proteomic analysis of stromal cells derived from the dental pulp of human exfoliated deciduous teeth. *Stem Cells Dev,* 19**,** 1081-93.

Pont, S. 1987. Thy-1: a lymphoid cell subset marker capable of delivering an activation signal to mouse T lymphocytes. *Biochimie,* 69**,** 315-20.

Rege, T. A. & Hagood, J. S. 2006. Thy-1 as a regulator of cell-cell and cell-matrix interactions in axon regeneration, apoptosis, adhesion, migration, cancer, and fibrosis. *FASEB J,* 20**,** 1045-54.

Reif, A. E. & Allen, J. M. 1964. The Akr Thymic Antigen and Its Distribution in Leukemias and Nervous Tissues. *J Exp Med,* 120**,** 413-33.

Ringrose, L. & Paro, R. 2004. Epigenetic regulation of cellular memory by the Polycomb and Trithorax group proteins. *Annu Rev Genet,* 38**,** 413-43.

Rinkevich, Y., Lindau, P., Ueno, H., Longaker, M. T. & Weissman, I. L. 2011. Germ-layer and lineage-restricted stem/progenitors regenerate the mouse digit tip. *Nature,* 476**,** 409-13.

Roman-Trufero, M., Mendez-Gomez, H. R., Perez, C., Hijikata, A., Fujimura, Y., Endo, T., Koseki, H., Vicario-Abejon, C. & Vidal, M. 2009. Maintenance of undifferentiated state and self-renewal of embryonic neural stem cells by

Polycomb protein Ring1B. *Stem Cells,* 27**,** 1559-70.

Ruparel, N. B., de Almeida, J. F., Henry, M. A. & Diogenes, A. 2013. Characterization of a stem cell of apical papilla cell line: effect of passage on cellular phenotype. *J Endod,* 39**,** 357-63.

Ryan, J. M., Barry, F. P., Murphy, J. M. & Mahon, B. P. 2005. Mesenchymal stem cells avoid allogeneic rejection. *J Inflamm (Lond),* 2**,** 8.

Saalbach, A., Wetzig, T., Haustein, U. F. & Anderegg, U. 1999. Detection of human soluble Thy-1 in serum by ELISA. Fibroblasts and activated endothelial cells are a possible source of soluble Thy-1 in serum. *Cell Tissue Res,* 298**,** 307-15.

Sajan, S. A., Rubenstein, J. L., Warchol, M. E. & Lovett, M. 2011. Identification of direct downstream targets of Dlx5 during early inner ear development. *Hum Mol Genet,* 20**,** 1262-73.

Salibian, A. A., Widgerow, A. D., Abrouk, M. & Evans, G. R. 2013. Stem cells in plastic surgery: a review of current clinical and translational applications. *Arch Plast Surg,* 40**,** 666-75.

Sarkar, L. & Sharpe, P. T. 1999. Expression of Wnt signalling pathway genes during tooth development. *Mech Dev,* 85**,** 197-200.

Sasaki, R., Aoki, S., Yamato, M., Uchiyama, H., Wada, K., Okano, T. & Ogiuchi, H. 2008. Neurosphere generation from dental pulp of adult rat incisor. *Eur J Neurosci,* 27**,** 538-48.

Saurin, A. J., Shao, Z., Erdjument-Bromage, H., Tempst, P. & Kingston, R. E. 2001. A Drosophila Polycomb group complex includes Zeste and dTAFII proteins. *Nature,* 412**,** 655-60.

Scadden, D. T. 2006. The stem-cell niche as an entity of action. *Nature,* 441**,** 1075-9.

Schofield, R. 1978. The relationship between the spleen colony-forming cell and the haemopoietic stem cell. *Blood Cells,* 4**,** 7-25.

Schuijers, J. & Clevers, H. 2012. Adult mammalian stem cells: the role of Wnt, Lgr5 and R-spondins. *EMBO J,* 31**,** 2685-96.

Schulze, B. R., Horn, D., Kobelt, A., Tariverdian, G. & Stellzig, A. 1999. Rare dental abnormalities seen in oculo-facio-cardio-dental (OFCD) syndrome: three new cases and review of nine patients. *Am J Med Genet,* 82**,** 429-35.

Schwartz, Y. B. & Pirrotta, V. 2007. Polycomb silencing mechanisms and the management of genomic programmes. *Nat Rev Genet,* 8**,** 9-22.

Seidel, K., Ahn, C. P., Lyons, D., Nee, A., Ting, K., Brownell, I., Cao, T., Carano, R. A., Curran, T., Schober, M., Fuchs, E., Joyner, A., Martin, G. R., de Sauvage, F. J. & Klein, O. D. 2010. Hedgehog signaling regulates the generation of ameloblast progenitors in the continuously growing mouse incisor. *Development,* 137**,** 3753-61.

Seki, T., Spurr, N., Obata, F., Goyert, S., Goodfellow, P. & Silver, J. 1985. The human Thy-1 gene: structure and chromosomal location. *Proc Natl Acad Sci U S A,* 82**,** 6657-61.

Selvaraj, V., Plane, J. M., Williams, A. J. & Deng, W. 2010. Switching cell fate: the remarkable rise of induced pluripotent stem cells and lineage reprogramming technologies. *Trends Biotechnol,* 28**,** 214-23.

Seo, B. M., Miura, M., Gronthos, S., Bartold, P. M., Batouli, S., Brahim, J., Young, M., Robey, P. G., Wang, C. Y. & Shi, S. 2004. Investigation of multipotent postnatal stem cells from human periodontal ligament. *Lancet,* 364**,** 149-55.

Shi, S., Robey, P. G. & Gronthos, S. 2001. Comparison of human dental pulp and bone marrow stromal stem cells by cDNA microarray analysis. *Bone,* 29**,** 532-9.

Shi, X., Han, W., Yamamoto, H., Tang, W., Lin, X., Xiu, R., Trune, D. R. & Nuttall, A. L. 2008. The cochlear pericytes. *Microcirculation,* 15**,** 515-29.

Shima, Y., Kengaku, M., Hirano, T., Takeichi, M. & Uemura, T. 2004. Regulation of dendritic maintenance and growth by a mammalian 7-pass transmembrane cadherin. *Dev Cell,* 7**,** 205-16.

Sinclair, K., Yerkovich, S. T. & Chambers, D. C. 2013. Mesenchymal stem cells and the lung. *Respirology,* 18**,** 397-411.

Smith, C. E. & Warshawsky, H. 1975. Cellular renewal in the enamel organ and the odontoblast layer of the rat incisor as followed by radioautography using 3H-thymidine. *Anat Rec,* 183**,** 523-61.

Snippert, H. J., van der Flier, L. G., Sato, T., van Es, J. H., van den Born, M., Kroon-Veenboer, C., Barker, N., Klein, A. M., van Rheenen, J., Simons, B. D. & Clevers, H. 2010. Intestinal crypt homeostasis results from neutral competition between symmetrically dividing Lgr5 stem cells. *Cell,* 143**,** 134-44.

Sonoyama, W., Liu, Y., Fang, D., Yamaza, T., Seo, B.-M., Zhang, C., Liu, H., Gronthos, S., Wang, C.-Y., Wang, S. & Shi, S. 2006. Mesenchymal stem cell-mediated functional tooth regeneration in swine. *PLoS ONE [Electronic Resource],* 1**,** e79.

Sonoyama, W., Liu, Y., Yamaza, T., Tuan, R. S., Wang, S., Shi, S. & Huang, G. T. 2008. Characterization of the apical papilla and its residing stem cells from human immature permanent teeth: a pilot study. *J Endod,* 34**,** 166-71.

Soriano, P. 1999. Generalized lacZ expression with the ROSA26 Cre reporter strain. *Nat Genet,* 21**,** 70-1.

Stockton, D. W., Das, P., Goldenberg, M., D'Souza, R. N. & Patel, P. I. 2000. Mutation of PAX9 is associated with oligodontia. *Nat Genet,* 24**,** 18-9.

Stolzing, A., Jones, E., McGonagle, D. & Scutt, A. 2008. Age-related changes in human bone marrow-derived mesenchymal stem cells: consequences for cell therapies. *Mech Ageing Dev,* 129**,** 163-73.

Sugimura, R., He, X. C., Venkatraman, A., Arai, F., Box, A., Semerad, C., Haug, J. S., Peng, L., Zhong, X. B., Suda, T. & Li, L. 2012. Noncanonical Wnt signaling maintains hematopoietic stem cells in the niche. *Cell,* 150**,** 351-65.

Suguro, H., Asano, M., Kaneko, Y., Omagari, D., Ogiso, B., Moro, I. & Komiyama, K. 2008. Characterization of human dental pulp-derived cell lines. *Int Endod J,* 41**,** 609-16.

Suomalainen, M. & Thesleff, I. 2010. Patterns of Wnt pathway activity in the mouse incisor indicate absence of Wnt/beta-catenin signaling in the epithelial stem cells. *Dev Dyn,* 239**,** 364-72.

Takahashi, K., Tanabe, K., Ohnuki, M., Narita, M., Ichisaka, T., Tomoda, K. & Yamanaka, S. 2007. Induction of pluripotent stem cells from adult human fibroblasts by defined factors. *Cell,* 131**,** 861-72.

Takahashi, K. & Yamanaka, S. 2006. Induction of pluripotent stem cells from mouse embryonic and adult fibroblast cultures by defined factors. *Cell,* 126**,** 663-76.

Tecles, O., Laurent, P., Zygouritsas, S., Burger, A. S., Camps, J., Dejou, J. & About, I. 2005. Activation of human dental pulp progenitor/stem cells in response to odontoblast injury. *Arch Oral Biol,* 50**,** 103-8.

Tepass, U., Truong, K., Godt, D., Ikura, M. & Peifer, M. 2000. Cadherins in embryonic and neural morphogenesis. *Nat Rev Mol Cell Biol,* 1**,** 91-100.

Teven, C. M., Liu, X., Hu, N., Tang, N., Kim, S. H., Huang, E., Yang, K., Li, M., Gao, J. L.,

Liu, H., Natale, R. B., Luther, G., Luo, Q., Wang, L., Rames, R., Bi, Y., Luo, J., Luu, H. H., Haydon, R. C., Reid, R. R. & He, T. C. 2011. Epigenetic regulation of mesenchymal stem cells: a focus on osteogenic and adipogenic differentiation. *Stem Cells Int,* 2011**,** 201371.

Thesleff, I., Wang, X. P. & Suomalainen, M. 2007. Regulation of epithelial stem cells in tooth regeneration. *C R Biol,* 330**,** 561-4.

Thomson, J. A., Itskovitz-Eldor, J., Shapiro, S. S., Waknitz, M. A., Swiergiel, J. J., Marshall, V. S. & Jones, J. M. 1998. Embryonic stem cell lines derived from human blastocysts. *Science,* 282**,** 1145-7.

Tiberi, L., Bonnefont, J., van den Ameele, J., Le Bon, S. D., Herpoel, A., Bilheu, A., Baron, B. W. & Vanderhaeghen, P. 2014. A BCL6/BCOR/SIRT1 complex triggers neurogenesis and suppresses medulloblastoma by repressing Sonic Hedgehog signaling. *Cancer Cell,* 26**,** 797-812.

Tseng, C. Y., Kao, S. H., Wan, C. L., Cho, Y., Tung, S. Y. & Hsu, H. J. 2014. Notch signaling mediates the age-associated decrease in adhesion of germline stem cells to the niche. *PLoS Genet,* 10**,** e1004888.

Tucker, A. & Sharpe, P. 2004. The cutting-edge of mammalian development; how the embryo makes teeth. *Nat Rev Genet,* 5**,** 499-508.

Usui, T., Shima, Y., Shimada, Y., Hirano, S., Burgess, R. W., Schwarz, T. L., Takeichi, M. & Uemura, T. 1999. Flamingo, a seven-pass transmembrane cadherin, regulates planar cell polarity under the control of Frizzled. *Cell,* 98**,** 585-95.

Valk-Lingbeek, M. E., Bruggeman, S. W. & van Lohuizen, M. 2004. Stem cells and cancer; the polycomb connection. *Cell,* 118**,** 409-18.

van der Stoop, P., Boutsma, E. A., Hulsman, D., Noback, S., Heimerikx, M., Kerkhoven, R. M., Voncken, J. W., Wessels, L. F. & van Lohuizen, M. 2008. Ubiquitin E3 ligase Ring1b/Rnf2 of polycomb repressive complex 1 contributes to stable maintenance of mouse embryonic stem cells. *PLoS One,* 3**,** e2235.

van Genderen, C., Okamura, R. M., Farinas, I., Quo, R. G., Parslow, T. G., Bruhn, L. & Grosschedl, R. 1994. Development of several organs that require inductive epithelial-mesenchymal interactions is impaired in LEF-1-deficient mice. *Genes Dev,* 8**,** 2691-703.

Vanacker, J., Viswanath, A., De Berdt, P., Everard, A., Cani, P. D., Bouzin, C., Feron, O., Diogenes, A., Leprince, J. G. & des Rieux, A. 2014. Hypoxia modulates the differentiation potential of stem cells of the apical papilla. *J Endod,* 40**,** 1410-8.

Vincent, J. B., Skaug, J. & Scherer, S. W. 2000. The human homologue of flamingo, EGFL2, encodes a brain-expressed large cadherin-like protein with epidermal growth factor-like domains, and maps to chromosome 1p13.3-p21.1. *DNA Res,* 7**,** 233-5.

Vogel, C. & Marcotte, E. M. 2012. Insights into the regulation of protein abundance from proteomic and transcriptomic analyzes. *Nat Rev Genet,* 13**,** 227-32.

Volponi, A. A., Pang, Y. & Sharpe, P. T. 2010. Stem cell-based biological tooth repair and regeneration. *Trends Cell Biol,* 20**,** 715-22.

Voog, J. & Jones, D. L. 2010. Stem cells and the niche: a dynamic duo. *Cell Stem Cell,* 6**,** 103-15.

Wamstad, J. A., Corcoran, C. M., Keating, A. M. & Bardwell, V. J. 2008. Role of the transcriptional corepressor Bcor in embryonic stem cell differentiation and early embryonic development. *PLoS One,* 3**,** e2814.

Wang, H., Wang, L., Erdjument-Bromage, H., Vidal, M., Tempst, P., Jones, R. S. & Zhang, Y. 2004. Role of histone H2A ubiquitination in Polycomb silencing.

Nature, 431**,** 873-8.

Wang, J., Mager, J., Schnedier, E. & Magnuson, T. 2002. The mouse PcG gene eed is required for Hox gene repression and extraembryonic development. *Mamm Genome,* 13**,** 493-503.

Wang, J., Wang, X., Sun, Z., Wang, X., Yang, H., Shi, S. & Wang, S. 2010. Stem cells from human-exfoliated deciduous teeth can differentiate into dopaminergic neuron-like cells. *Stem Cells Dev,* 19**,** 1375-83.

Wang, X. P., Suomalainen, M., Felszeghy, S., Zelarayan, L. C., Alonso, M. T., Plikus, M. V., Maas, R. L., Chuong, C. M., Schimmang, T. & Thesleff, I. 2007. An integrated gene regulatory network controls stem cell proliferation in teeth. *PLoS Biol,* 5**,** e159.

Williams, A. F. & Gagnon, J. 1982. Neuronal cell Thy-1 glycoprotein: homology with immunoglobulin. *Science,* 216**,** 696-703.

Wobus, A. M. & Boheler, K. R. 2005. Embryonic stem cells: prospects for developmental biology and cell therapy. *Physiol Rev,* 85**,** 635-78.

Wu, Q. & Maniatis, T. 2000. Large exons encoding multiple ectodomains are a characteristic feature of protocadherin genes. *Proc Natl Acad Sci U S A,* 97**,** 3124-9.

Yamanaka, S. 2007. Strategies and new developments in the generation of patient-specific pluripotent stem cells. *Cell Stem Cell,* 1**,** 39-49.

Yamanaka, S., Li, J., Kania, G., Elliott, S., Wersto, R. P., Van Eyk, J., Wobus, A. M. & Boheler, K. R. 2008. Pluripotency of embryonic stem cells. *Cell & Tissue Research,* 331**,** 5-22.

Yao, S., Pan, F., Prpic, V. & Wise, G. E. 2008. Differentiation of stem cells in the dental follicle. *J Dent Res,* 87**,** 767-71.

Yokoi, T., Saito, M., Kiyono, T., Iseki, S., Kosaka, K., Nishida, E., Tsubakimoto, T., Harada, H., Eto, K., Noguchi, T. & Teranaka, T. 2007. Establishment of immortalized dental follicle cells for generating periodontal ligament in vivo. *Cell Tissue Res,* 327**,** 301-11.

Yu, J., Vodyanik, M. A., Smuga-Otto, K., Antosiewicz-Bourget, J., Frane, J. L., Tian, S., Nie, J., Jonsdottir, G. A., Ruotti, V., Stewart, R., Slukvin, II & Thomson, J. A. 2007. Induced pluripotent stem cell lines derived from human somatic cells. *Science,* 318**,** 1917-20.

Zhang, H., Boddupally, K., Kandyba, E., Kobielak, K., Chen, Y., Zu, S., Krishnan, R., Sinha, U. & Kobielak, A. 2014. Defining the localization and molecular characteristic of minor salivary gland label-retaining cells. *Stem Cells,* 32**,** 2267-77.

Zhao, H., Feng, J., Seidel, K., Shi, S., Klein, O., Sharpe, P. & Chai, Y. 2014. Secretion of shh by a neurovascular bundle niche supports mesenchymal stem cell homeostasis in the adult mouse incisor. *Cell Stem Cell,* 14**,** 160-73.

Zhao, H., Li, S., Han, D., Kaartinen, V. & Chai, Y. 2011. Alk5-mediated transforming growth factor beta signaling acts upstream of fibroblast growth factor 10 to regulate the proliferation and maintenance of dental epithelial stem cells. *Mol Cell Biol,* 31**,** 2079-89.

Zhao, H., Oka, K., Bringas, P., Kaartinen, V. & Chai, Y. 2008. TGF-beta type I receptor Alk5 regulates tooth initiation and mandible patterning in a type II receptor-independent manner. *Dev Biol,* 320**,** 19-29.

Zuk, P. A., Zhu, M., Ashjian, P., De Ugarte, D. A., Huang, J. I., Mizuno, H., Alfonso, Z. C., Fraser, J. K., Benhaim, P. & Hedrick, M. H. 2002. Human adipose tissue is a source of multipotent stem cells. *Mol Biol Cell,* 13**,** 4279-95.

Zvaifler, N. J., Marinova-Mutafchieva, L., Adams, G., Edwards, C. J., Moss, J., Burger, J. A. & Maini, R. N. 2000. Mesenchymal precursor cells in the blood of normal individuals. *Arthritis Res,* 2**,** 477-88.

Publication

Lapthanasupkul, P., J. Feng, A. Mantesso, Y. Takada-Horisawa, M. Vidal, H. Koseki, L. Wang, Z. An, I. Miletich and P. T. Sharpe (2012). "Ring1a/b polycomb proteins regulate the mesenchymal stem cell niche in continuously growing incisors." Dev Biol**367**(2): 140-153.

Kaukua, N., M. K. Shahidi, C. Konstantinidou, V. Dyachuk, M. Kaucka, A. Furlan, Z. An, L. Wang, I. Hultman, L. Ahrlund-Richter, H. Blom, H. Brismar, N. A. Lopes, V. Pachnis, U. Suter, H. Clevers, I. Thesleff, P. Sharpe, P. Ernfors, K. Fried and I. Adameyko (2014). "Glial origin of mesenchymal stem cells in a tooth model system." Nature**513**(7519): 551-554.

Developmental Biology 367 (2012) 140–153

Contents lists available at SciVerse ScienceDirect

Developmental Biology

journal homepage: www.elsevier.com/locate/developmentalbiology

Ring1a/b polycomb proteins regulate the mesenchymal stem cell niche in continuously growing incisors

Puangwan Lapthanasupkul [a,1], Jifan Feng [a,1], Andrea Mantesso [a], Yuki Takada-Horisawa [b], Miguel Vidal [c], Haruhiko Koseki [b], Longlong Wang [a], Zhengwen An [a], Isabelle Miletich [a], Paul T. Sharpe [a,*]

[a] Department of Craniofacial Development, Dental Institute, King's College London, London SE1 9RT, United Kingdom
[b] RIKEN Research Center for Allergy and Immunology, 1–7-22 Suehiro, Tsurumi-ku, Yokohama 230-0045, Japan
[c] Centro de Investigaciones Biologicas, Department of Developmental and Cell Biology, Ramiro de Maeztu 9, 28040 Madrid, Spain

ARTICLE INFO

Article history:
Received 7 November 2011
Received in revised form
23 April 2012
Accepted 25 April 2012
Available online 4 May 2012

Keywords:
Ring1a/b
Polycomb
Stem cells
Mouse incisors
Mouse molars

ABSTRACT

Rodent incisors are capable of growing continuously and the renewal of dental epithelium giving rise to enamel-forming ameloblasts and dental mesenchyme giving rise to dentin-forming odontoblasts and pulp cells is achieved by stem cells residing at their proximal ends. Although the dental epithelial stem cell niche (cervical loop) is well characterized, little is known about the dental mesenchymal stem cell niche. Ring1a/b are the core Polycomb repressive complex1 (PRC1) components that have recently also been found in a protein complex with BcoR (Bcl-6 interacting corepressor) and Fbxl10. During mouse incisor development, we found that genes encoding members of the PRC1 complex are strongly expressed in the incisor apical mesenchyme in an area that contains the cells with the highest proliferation rate in the tooth pulp, consistent with a location for transit amplifying cells. Analysis of *Ring1a*$^{-/-}$;*Ring1b*$^{cko/cko}$ mice showed that loss of Ring1a/b postnatally results in defective cervical loops and disturbances of enamel and dentin formation in continuously growing incisors. To further characterize the defect found in *Ring1a*$^{-/-}$;*Ring1b*$^{cko/cko}$ mice, we demonstrated that cell proliferation is dramatically reduced in the apical mesenchyme and cervical loop epithelium of *Ring1a*$^{-/-}$;*Ring1b*$^{cko/cko}$ incisors in comparison to *Ring1a*$^{-/-}$;*Ring1b*$^{fl/fl}$ *cre-* incisors. Fgf signaling and downstream targets that have been previously shown to be important in the maintenance of the dental epithelial stem cell compartment in the cervical loop are downregulated in *Ring1a*$^{-/-}$;*Ring1b*$^{cko/cko}$ incisors. In addition, expression of other genes of the PRC1 complex is also altered. We also identified an essential postnatal requirement for Ring1 proteins in molar root formation. These results show that the PRC1 complex regulates the transit amplifying cell compartment of the dental mesenchymal stem cell niche and cell differentiation in developing mouse incisors and is required for molar root formation.

© 2012 Elsevier Inc. All rights reserved.

Introduction

Rodent incisors including mouse incisors differ from molars as they are capable of continuously growing throughout the lifetime of the animal. These incisors grow and erupt continuously in order to compensate for functional attrition that constantly occurs at their incisal edges as the mouse feeds. Whereas molars have an obvious crown and root axis, mouse incisors have no conventional crown or root, rather the labial, enamel-covered surface is equivalent to a crown and the lingual, enamel-free surface to a root (Ohazama et al., 2010; Tummers and Thesleff, 2008; Tummers et al., 2007). The most proximal end of the incisor is open to provide a channel for blood and nerve supplies. Since the incisors continue grow, the renewal of tooth-forming cells including enamel-forming ameloblasts and dentin-forming odontoblasts is required and is achieved by stem cells residing at their open proximal (apical) ends (Harada et al., 1999; Smith and Warshawsky, 1975). The mouse incisor is therefore an interesting model to study the regulation of dental epithelial and mesenchymal stem cells in the same organ. It has been proposed that stem cells reside in specific compartments called 'stem cell niches' that provide essential signals required for their function and maintenance. Besides the stem cells themselves, components of the niche are thought to include supporting cells, extracellular matrix as well as neurovascular tissue. Communication among the cells inside the niche via signaling molecules is crucial to accomplish the balance between self-renewal and differentiation of stem cells (Jones and Wagers, 2008; Schofield, 1978). Additionally, the stem cell niche also protects stem cells from depletion and protects the host from excessive proliferation of stem cells (Scadden, 2006).

Early stages of mouse incisor embryonic development are similar to those of molars but when the incisor buds reach the cap stage

* Corresponding author.
E-mail address: paul.sharpe@kcl.ac.uk (P.T. Sharpe).
[1] Authors made equal contributions.

0012-1606/$ - see front matter © 2012 Elsevier Inc. All rights reserved.
http://dx.doi.org/10.1016/j.ydbio.2012.04.029

they rotate anteroposteriorly. Subsequently, at the bell stage (E16.5) the epithelial compartments of the apex form a special structure called " the cervical loop". Histologically, the cervical loop comprises a central core of star-shaped cells called stellate reticulum that are surrounded by a layer of epithelial cells (Fig. 1A). The cervical loop at the labial aspect that is responsible for the continuous generation of ameloblast precursors, is larger than the one at the lingual aspect that does not generate ameloblasts and contains a larger number of stellate reticulum cells. It has been shown that these stellate reticulum cells contain slowly dividing stem cells that subsequently undergo asymmetric cell division. As these stem cells proliferate, one daughter cell remains within the niche as an undifferentiated stem cell whereas the other daughter cell is displaced away from the niche, enters a zone of transit-amplifying cells (TA cells) and differentiates into ameloblast (Harada et al., 1999). In addition to molecular signals in the cervical loop epithelium, it has been proposed that mesenchymal signals are also of importance and direct the continuous proliferation of epithelial progenitor cells. Members of Fibroblast growth factors (FGFs) family, *Fgf10* and *Fgf3*, are found to be expressed in the incisor mesenchyme and their receptors, including *Fgfr1b* and *Fgfr2b* are expressed adjacently in the dental epithelium (Harada et al., 1999). The potential role of *Fgf10* in the maintenance of the stem cell compartment is further confirmed by a hypoplastic cervical loop and a decreased growth rate of the dental epithelium in *Fgf10* null mice during late stages of incisor development. Additionally, *in vitro* experiments using an anti-FgF10 neutralizing antibody showed that functional disturbance of Fgf10 results in apoptosis of cervical loop cells (Harada et al., 2002). A similar phenotype was observed by epithelial-specific deletion of Fgfr2 in the cervical loop confirming that Fgf signals from the mesenchyme are required for the development and maintenance of the cervical loop stem cell niche (Lin et al., 2009).

The precise location of the mesenchymal stem cell niche in the incisor is unclear although the mesenchymal stem cells (MSCs) are generally believed to be located in the apical end mesenchyme, close to the cervical loops, since the growth and differentiation of the incisor always initiates at the apical end then extends towards the incisal end. Feng et al. (2011) suggested dual origins of dental pulp mesenchymal stem cells during incisor growth and repair, one of which located in the apical dental mesenchyme tissue (Feng et al., 2011). This was also confirmed by another study, using consecutive 5-bromo-2-deoxyuridine (BrdU) administration followed by a chase period, which showed a label-retaining slow-cycling stem cell population located in the very apical end of the incisor dental pulp mesenchyme (Seidel et al., 2010).

Polycomb Group (PcG) proteins were first described as repressors of *Hox* genes in *Drosophila melanogaster*. Mutations of these proteins in flies result in homeotic transformation of one body segment into the identity of another (Lewis, 1978). A number of studies in flies and mammals demonstrated that most PcG proteins are not classic DNA binding proteins but present as large multimeric protein complexes and exist as heterogeneous complexes of varying compositions. This existence is thought to result from a distinction of target genes for these complexes and also contributes to different functions of each complex (Satijn et al., 1997). It has been shown that the function of PcG complexes is to maintain the transcriptional repression of target genes by binding to the chromatin and inducing higher-order chromatin structure (Ringrose and Paro, 2004; Schuettengruber et al., 2007). Aside from the role in the control of body plan and segmentation, accumulating studies also revealed crucial functions of PcG proteins in the maintenance of embryonic and adult stem cells, control of cell proliferation, cancer development, genomic imprinting and X-chromosme inactivation (Delaval and Feil, 2004; Heard, 2005; Sparmann and van Lohuizen, 2006).

In mammals, two distinct PcG complexes have been extensively studied: Polycomb Repressive Complex (PRC) 1 and PRC2. While the PRC1 is essential for stable maintenance of gene repression by preventing nucleosome remodeling, PRC2 is involved in the initiation of gene repression and functions as a histone methyltransferase that specifically methylates lysine 27 of histone H3 (H3K27) in nucleosomes (Cao et al., 2002; Schwartz and Pirrotta, 2007; Valk-Lingbeek et al., 2004). Mammalian PRC1 consists of orthologs of *Drosophila* Polycomb (Cbx2, Cbx4, Cbx6, Cbx7 and Cbx8), Posterior sex combs (Mel18, Bmi1, Nspc1/Pcgf1 and MBLR), dRing (Ring1a and Ring1b) and Polyhomeotics (Phc1, Phc2 and Phc3). The core PRC2 consists of Suz12, Eed, Ezh1 and Ezh2 (Ringrose and Paro, 2004; Schwartz and Pirrotta, 2007). Among the core PRC1, Ring1a and Ring1b have been shown to possess E3 ubiquitin ligase activity for histone H2A that plays an important role in PcG-mediated silencing (de Napoles et al., 2004; Wang et al., 2004). Apart from the PRC1, Ring1a/b have further been identified in other protein complexes with BCoR and Fbxl10/Kdm2R (Gearhart et al., 2006; Sanchez et al., 2007).

Emerging evidence has demonstrated possible roles of Ring1b in the control of cell proliferation as well as the maintenance of ES cells. Using *Ring1a/b* knockout mouse ES cells, Ring1a/b have been shown to be required for the maintenance of ES cell identity by silencing the genes that govern differentiation of ES cells. It has been demonstrated that transcriptional repression mediated by Ring1a/b is Oct3/4-dependent. Moreover, in the presence of enforced expression of the differentiation inducer, *Gata6*, Ring1a/b target genes become derepressed and the Ring1a/b binding is also significantly reduced. These results indicate that Ring1a/b act downstream of the core transcriptional regulatory circuit to regulate ES cell self-renewal (Endoh et al., 2008). Subsequent studies further supported the essential role of Ring1b in stable maintenance of mouse ES cells. In order to maintain undifferentiated ES cells, Ring1b is needed to silence a particular subset of genes, which are co-occupied by ES cell regulators including Oct4 and Nanog. These Ring1b target genes also possess bivalent histone marks with CpG-rich promoters, and include developmental transcriptional factors, morphogens and cell surface markers (van der Stoop et al., 2008).

We provide here evidence that PRC1 gene expression localizes to a population of cells distal to the predicted location of the mesenchymal stem cells that have characteristics of transit amplifying cells and that the Ring1 components of the PRC1 complex are essential for proliferation and differentiation of these cells.

We show that in addition to providing precursors for the continuous replacement of mesenchymal cells during incisor growth, Ring1 proteins are essential for maintaining expression of Fgfs that act to regulate the adjacent epithelial stem cell niche, the labial cervical loop. In addition we also identify a role for Ring1 proteins in supporting normal molar root development.

Results

Genes encoding proteins of the PRC1 complex are expressed in highly proliferative cells in the apical mesenchyme in continuously growing incisors

Whole-mount *in situ* hybridization analysis showed that at post natal stages all of the genes encoding proteins of the PRC1 complex were expressed in the dental mesenchyme adjacent to the labial and lingual cervical loop epithelium of the mouse mandibular (Figs. 1 and 2) and maxillary (data not shown) incisors. *Ring1a* and its homolog, *Ring1b*, were expressed in the apical mesenchyme of the incisors (Fig. 1B,B′,C,C′; Fig. 2 A,A′, B,B′). Ring1b was also expressed in cells of the dental follicle and some patchy expression was evidence in the epithelial cells in the area of preameloblast formation (Fig. 2 B′). Expression of *Nspc1/Pcgf1* was observed in the apical mesenchyme

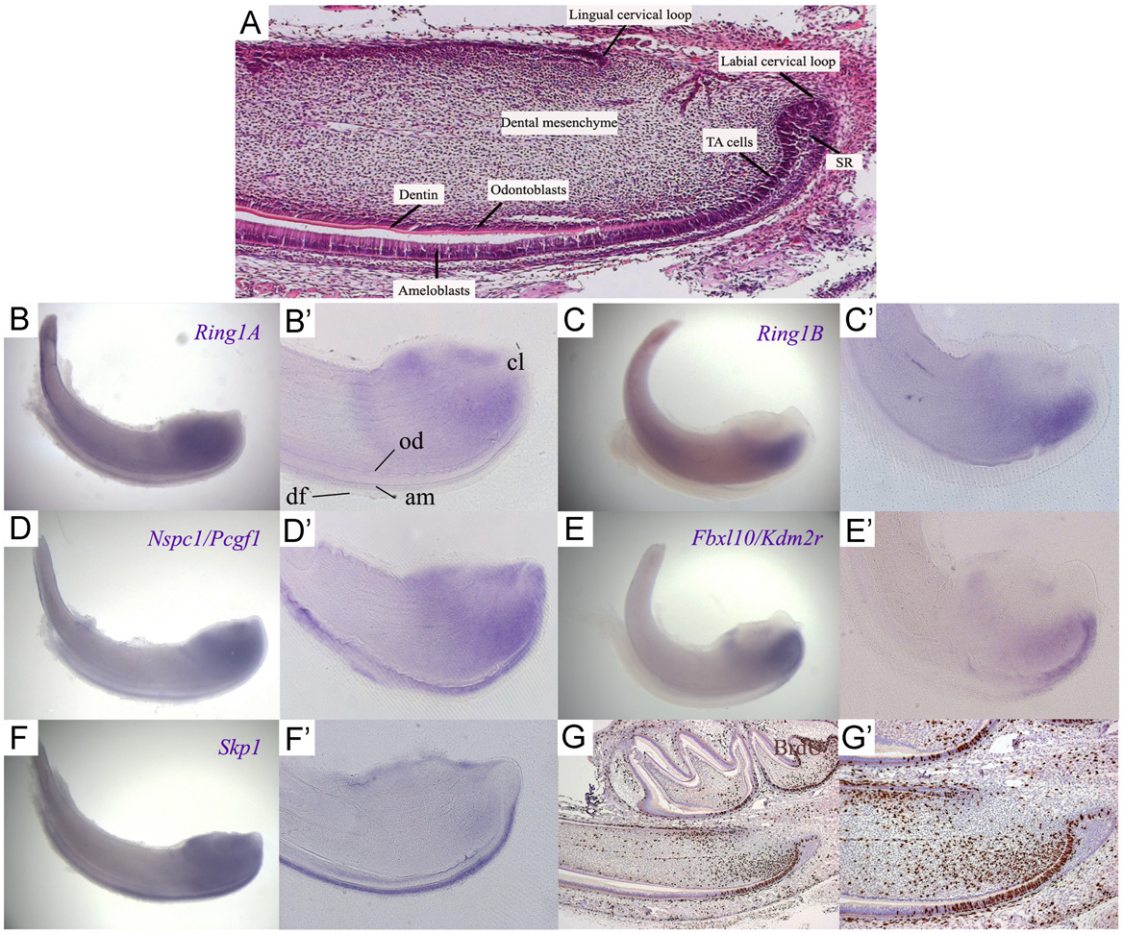

Fig. 1. Co-expression of genes encoding proteins of the PRC1 complex and cell proliferation marker BrdU in 2 day-old mouse mandibular incisor apical mesenchyme. (A) The apical end of incisor consists of cervical loops at both lingual and labial sides surrounding the dental mesenchyme. The labial cervical loop contains a stellate reticulum (SR) core surrounded by dental epithelium. TA, transit-amplifying. (B, B′, C, C′) *Ring1a* and *Ring1b* are strongly expressed in the dental mesenchyme close to both labial and lingual cervical loops of the incisor and in the area of cells with high rates of proliferation (TA cells). (D, D′) *Nspc1* is expressed in the dental mesenchyme near labial and lingual cervical loops, and in the transit-ampifying cells of the dental epithelium. (E, E′) *Fbxl10* expression is notable in the labial mesenchyme and the transit-ampifying cells of the dental epithelium. (F, F′) *Skp1* is weakly expressed in the mesenchyme and more highly expressed in cells of the dental follicle (df) of the incisor germ and the ameloblasts (Am). (G, G′) BrdU expression indicates that highly proliferative cells were located predominantly in the dental mesenchyme near labial and lingual cervical loops, and in also the transit-amplifying cells of the dental epithelium.

and part of the dental epithelium and follicle of the mouse incisor (Fig. 1D,D′; Fig. 2C,C′). *Fbxl10/Kdm2r* showed a similar but weaker expression compared to the expression of *Nspc1* (Fig. 1E,E′). *Skp1* expression was observed weakly in apical mesenchyme and in cells of the dental follicle covering the apical part of the developing incisor as well as the enamel-forming ameloblasts (Fig. 1F,F′; Fig. 2D,D′).

Many stem cell populations contain slow-cycling cells that produce progenitor cells that are rapidly dividing, often called transit-amplifying (TA) cells. We analysed the proliferation characteristics of the apical mesenchymal cells by administration of a single short pulse of synthetic nucleoside analogue, BrdU and located labeled cells using immunohistochemistry. BrdU+ve rapid-dividing cells were located in mesenchymal cells at the apical end as previously shown in a position that closely matched the location of PRC1 expressing cells, distal to label retaining cells (Fig. 1G,G′), suggesting that these cells are transit amplifying cells (Harada et al., 1999; 2002;Seidel et al., 2010).

Ring1a$^{-/-}$;Ring1b$^{cko/cko}$ mice display incisors with defective cervical loops and abnormal enamel and dentin formation

In order to determine the roles of Ring1 proteins in incisors, postnatal conditional inactivation using tamoxifen-inducible Cre was used. Since *Ring1a$^{-/-}$* mice survive and are fertile, *Ring1b$^{fl/fl}$* mice were crossed with *Ring1a$^{-/-}$* and double homozygotes then crossed with *Rosa26::CreERT2* transgenic mice. Administration of tamoxifen between postnatal days 9 to 13 created double *Ring1a/b* loss of function animals that were analysed at P17.

Morphology of mouse maxillary and mandibular incisors was examined using microCT scanning and analysis revealed that P17 *Ring1a$^{-/-}$;Ring1b$^{cko/cko}$* incisors (Fig. 3B) had a similar gross morphology to *Ring1a$^{-/-}$;Ring1b$^{fl/fl}$cre-* incisors but were obviously shorter (Fig. 3A). In order to evaluate the incisor length, measurement analysis of incisor length (indicated by dotted lines in Fig. 3A and B) was carried out as described in the Materials and Methods section. The mean lengths of mandibular incisors of *Ring1a$^{-/-}$;Ring1b$^{cko/cko}$* mice were 6576 μm (Fig. 3B), whereas those of *Ring1a$^{-/-}$;Ring1b$^{fl/fl}$cre-* mice were 8085 μm (Fig. 3A). Statistical analysis by *t*-test additionally revealed that mandibular incisors (asterisks in Fig. 3C; $P<0.01$) of *Ring1a$^{-/-}$;Ring1b$^{cko/cko}$* mice ($n=8$) were significantly shorter than those of *Ring1a$^{-/-}$; Ring1b$^{fl/fl}$ cre-* incisors ($n=6$).

Histological examination revealed that P17 *Ring1a$^{-/-}$;Ring1b$^{cko/cko}$* incisors had abnormal cervical loops at their apical ends (Fig. 4B5, Fig. 2S), compared to *Ring1a$^{-/-}$;Ring1b$^{fl/fl}$ cre-* incisors (Fig. 4D5, Fig. 2S). Differentiation of odontoblasts and ameloblasts

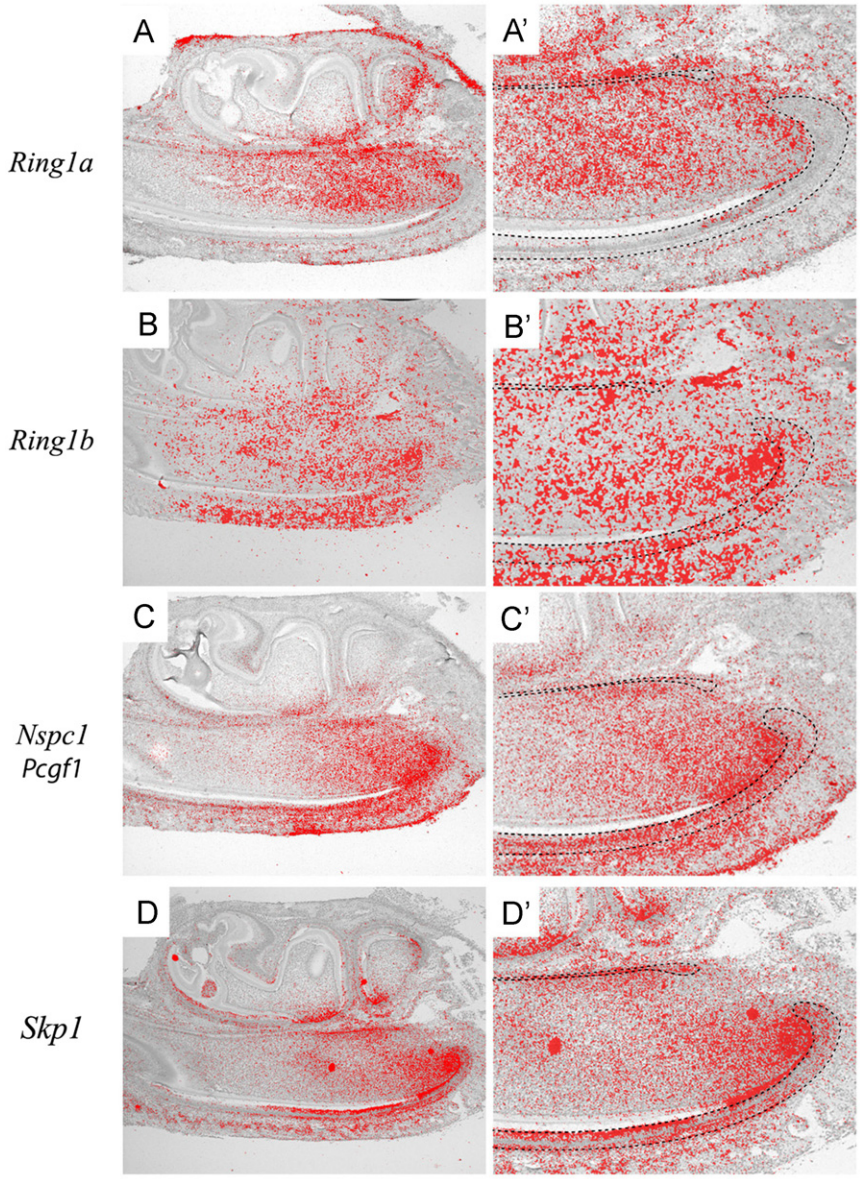

Fig. 2. Radioactive *in situ* hybridisation of PRC1 complex genes. Radioactive *in situ* hybridisation for *Ring1* (*A, A′*), *Ring1b B, B′*), *Nspc1/Pcgf1*(*C, C′*) and *Skp1* (*D, D′*) on sagittal sections of P5 mandibular incisors (A, A′). Silver grains were false coloured in red cervical loop outlined by black dashes. All four genes are expressed in mesenchymal cells between the lingual and labial aspects of the epithelial cervical loop. (For interpretation of the references to color in this figure legend, the reader is reffered to the web version of this article.)

was disrupted in *Ring1a*$^{-/-}$;*Ring1b*$^{cko/cko}$ along most of the incisor length (Fig. 4D1–D4), subsequently leading to disturbances in enamel and dentin formation, compared to *Ring1a*$^{-/-}$;*Ring1b*$^{fl/fl}$*cre-* incisors (Fig. 4B1–B4). While in *Ring1a*$^{-/-}$;*Ring1b*$^{fl/fl}$*cre-* incisors the odontoblasts and ameloblasts were elongated and highly polarized (Fig. 4B1–B4), in *Ring1a*$^{-/-}$;*Ring1b*$^{cko/cko}$ incisors they were more round in shape and had no nuclear polarization (Fig. 4D1–D4). No evidence of any odontoblast and ameloblast differentiation was observed at the inner side of the labial cervical loop in *Ring1a*$^{-/-}$;*Ring1b*$^{cko/cko}$ incisors (Fig. 4D4), compared to the same region of *Ring1a*$^{-/-}$;*Ring1b*$^{fl/fl}$*cre-* incisors (Fig. 4B4). Furthermore, in *Ring1a*$^{-/-}$;*Ring1b*$^{cko/cko}$ incisors, the tips of labial cervical loop were still present but they appeared smaller (Fig. 4D5) than those of *Ring1a*$^{-/-}$;*Ring1b*$^{fl/fl}$ *cre-* incisors (Fig. 4B5). MicroCT and histological examination of *Ring1a*$^{-/-}$;*Ring1b*$^{fl/fl}$*cre-* incisors showed them to be indistinguishable from wild type (data not shown).

Loss of Ring1a and Ring1b leads to down-regulation of genes important for enamel and dentin formation

Abnormal odontoblasts and ameloblasts observed in *Ring1a*$^{-/-}$; *Ring1b*$^{cko/cko}$ incisors were further analysed by *in situ* hybridization analysis of genes known to be markers of functional odontoblasts and ameloblasts, including *Dentin sialophosphoprotein* (*Dspp*), *Amelogenin* and *Shh*. *Dspp*, normally expressed in odontoblasts and newly differentiated ameloblasts (Begue-Kirn et al., 1998), was found to be down-regulated in *Ring1a*$^{-/-}$;*Ring1b*$^{cko/cko}$ incisors (Fig. 5C), compared to wild type (WT) incisors (Fig. 5A) and *Ring1a*$^{-/-}$;*Ring1b*$^{fl/fl}$*cre-* incisors (Fig. 5B). *Amelogenin*, a gene encoding the major structural protein of enamel matrix and expressed in functional ameloblasts (Zeichner-David et al., 1995), was absent in *Ring1a*$^{-/-}$;*Ring1b*$^{cko/cko}$ incisors (Fig. 5F), in comparison to WT (Fig. 5D) and *Ring1a*$^{-/-}$;*Ring1b*$^{fl/fl}$*cre-* incisors (Fig. 4E). Furthermore, *Shh* which normally marks pre-ameloblasts (Bitgood and McMahon,

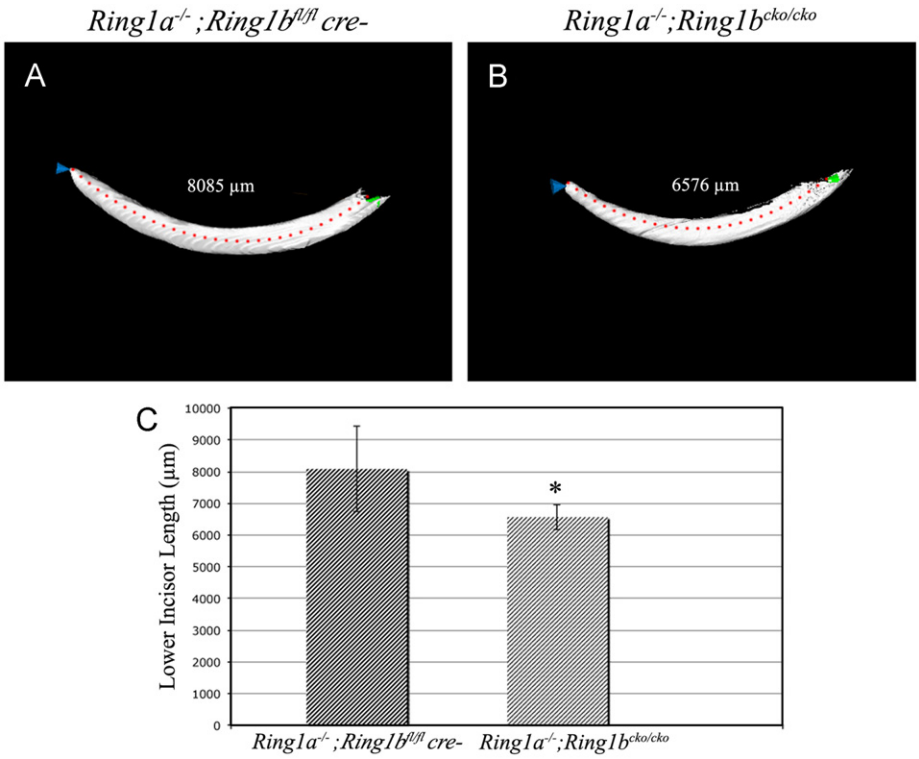

Fig. 3. MicroCT anaylsis of P17 *Ring1a*$^{-/-}$;*Ring1b*$^{fl/fl}$*cre-* and *Ring1a*$^{-/-}$;*Ring1b*$^{cko/}$*cko* incisors. (A) *Ring1a*$^{-/-}$;*Ring1b*$^{fl/fl}$*cre-* shows a normal shape of mouse incisor. (B) Incisor of *Ring1a*$^{-/-}$;*Ring1b*$^{cko/cko}$ mouse is shorter than that of *Ring1a*$^{-/-}$;*Ring1b* $^{fl/fl}$*cre-*. Red dots in (A) and (B) indicate the measurement points used to determine the incisor length in MicorCT scans. (C) Mean incisor length ± standard deviation (SD) of mandibular (lower) incisors of *Ring1a*$^{-/-}$;*Ring1b*$^{fl/fl}$*cre-* mice (n=6) and *Ring1a*$^{-/-}$; *Ring1b*$^{cko/cko}$ mice (n=8). Asterisk (*) indicates values significantly different between incisor length of *Ring1a*$^{-/-}$;*Ring1b*$^{cko/cko}$ mice and that of *Ring1a*$^{-/-}$;*Ring1b* $^{fl/fl}$*cre-* mice according to Student's t test ($P<$ 0.01). (For interpretation of the references to color in this figure legend, the reader is reffered to the web version of this article.)

1995), was also downregulated in *Ring1a*$^{-/-}$;*Ring1b*$^{cko/cko}$ incisors (Fig. 5I), compared to WT (Fig. 5G) and *Ring1a*$^{-/-}$;*Ring1b*$^{fl/f}$*cre-* incisors (Fig. 5H). In all these cases, gene expression was maintained in the most distally-located cells at a reduced level and was significantly reduced or absent from proximal cells (Fig. 5C, F, I). These results additionally confirmed the defects previously observed in odontoblasts and ameloblasts in histological sections.

Absence of Ring1a and Ring1b results in reduced cell proliferation in the apical mesenchyme and cervical loop epithelium of the continuously growing mouse incisor

To further investigate the defects found in *Ring1a*$^{-/-}$;*Ring1b*$^{cko/cko}$ incisors, cell proliferation analysis was carried out. Cell proliferation was analysed by immunohistochemistry with an antibody that detects mitosis, Phospho-histone H3(PH3). Immunohistochemical staining showed that mitotically active cells were markedly reduced in the apical mesenchyme adjacent to labial and lingual cervical loops and in the epithelial cells of the labial cervical loops of *Ring1a*$^{-/-}$; *Ring1b*$^{cko/cko}$ incisors (Fig. 5L) in comparison to WT (Fig. 5J) and *Ring1a*$^{-/-}$;*Ring1b*$^{fl/fl}$*cre-* incisor (Fig. 5K). This suggests that Ring1a and Ring1b, either directly or indirectly (possibly by an affect on the mesenchymal stem cells) are required for mitosis of the dental mesenchymal stem/progenitor cells that constantly give rise to dentin-forming odontoblasts and also the cervical loop epithelium, giving rise to enamel-forming ameloblasts.

Loss of Ring1a and Ring1b results in down-regulation of Fgf signaling in the apical end of continuously growing incisors

Fgf signaling has previously been shown to be important for the maintenance of the epithelial stem cell compartment in the cervical loop of continuously growing mouse incisors. Among members of the Fgf family, several Fgfs including *Fgf3*, *Fgf10* and *Fgf9* have been found to be involved in the development of mouse incisors. The cervical loop has been found to be absent in *Fgf10* null mice (Harada et al., 2002) while expression of *Fgf3* in the dental mesenchyme was shown to stimulate epithelial stem cell proliferation (Wang et al., 2007). Radioactive *in situ* hybridization revealed that *Fgf10*, normally expressed in both labial and lingual mesenchyme, was down-regulated in both *Ring1a*$^{-/-}$;*Ring1b*$^{fl/fl}$ *cre-* (Fig. 6B) and *Ring1a*$^{-/-}$;*Ring1b*$^{cko/cko}$ (Fig. 6C) incisors in comparison to WT incisors (Fig. 6A). *Fgf3*, which is restrictedly expressed in the labial mesenchyme was down-regulated in *Ring1a*$^{-/-}$;*Ring1b*$^{fl/fl}$*cre-* (Fig. 6E) and completely absent in *Ring1a*$^{-/-}$;*Ring1b*$^{cko/cko}$ (Fig. 6F) incisors in comparison to WT incisors (Fig. 6D). Analysis of direct downstream targets of Fgf signaling including *Pea3* and *Erm* (also known as *Etv4* and *Etv5*, respectively) (Raible and Brand, 2001; Roehl and Nusslein-Volhard, 2001) was also performed. Expression of *Pea3* and *Erm*, normally detected in the epithelial cervical loops and adjacent mesenchyme (Fig. 6G and J), were markedly down-regulated in *Ring1a*$^{-/-}$;*Ring1b*$^{fl/fl}$*cre-* (Fig. 6H and K) and completely absent in *Ring1a*$^{-/-}$;*Ring1b*$^{cko/cko}$ (Fig. 6I and L) incisors in comparison to WT incisors (Fig. 6G and J). This suggests that *Ring1a* and *Ring1b* regulate Fgf signaling in developing mouse incisors.

Loss of Ring1a and Ring1b leads to alterations of expression of genes encoding the PRC1 complex

Expression analysis of genes encoding members of the PRC1 complex including *Nspc1/Pegf1* and *Fbxl10/Kdm2r*, was further examined in the absence of *Ring1a* and *Ring1b*. Interestingly, *Nspc1/Pcgf1* *m*RNA was shown to be unaffected in both

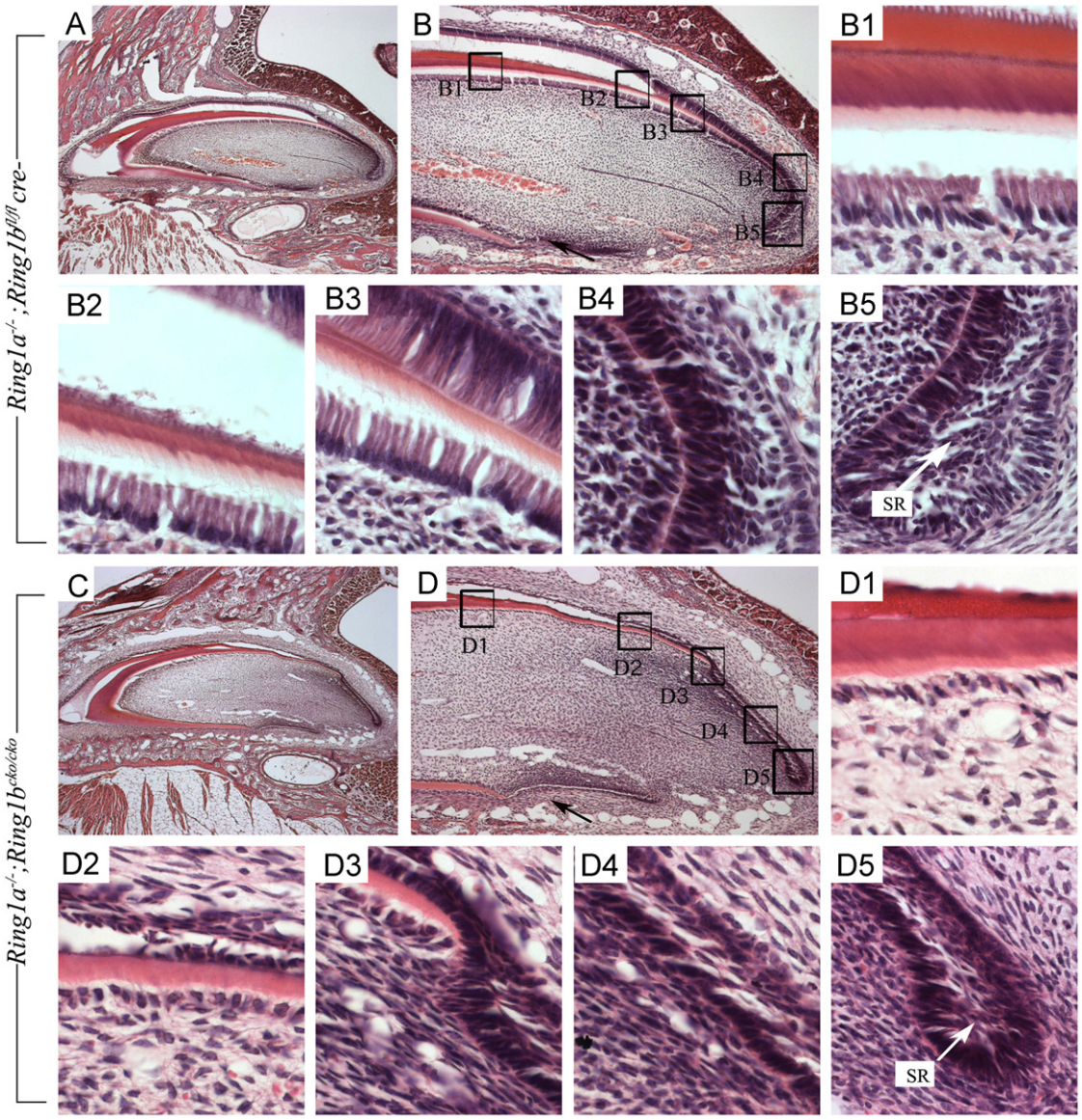

Fig. 4. Hematoxylin and eosin stained sagittal sections of a maxillary incisor of 17 day-old *Ring1a*$^{-/-}$;*Ring1b*$^{cko/cko}$ and *Ring1a*$^{-/-}$;*Ring1b*$^{fl/fl}$*cre-* mice. (A, B) *Ring1a*$^{-/-}$;*Ring1b*$^{fl/fl}$ *cre-* incisors show normal incisor development. (B1–B5) Higher power views of boxed regions in (B) showing normal odontoblast and ameloblast differentiation (B4), labial cervical loop containing a core of stellate reticulum (SR) in *Ring1a*$^{-/-}$;*Ring1b*$^{fl/fl}$ *cre-* mice (B5). (C, D) *Ring1a*$^{-/-}$;*Ring1b*$^{cko/cko}$ incisors show abnormal development. (D1–D4) Higher power views of regions boxed in (D) showing abnormal morphology of odontoblasts and ameloblasts. (D5) Higher magnification of the black box in (D) shows small labial cervical loop containing a few cells of stellate reticulum (SR) in *Ring1a*$^{-/-}$;*Ring1b*$^{cko/cko}$ mice.

Ring1a$^{-/-}$;*Ring1b*$^{fl/fl}$*cre-* (Fig. 6N) and *Ring1a*$^{-/-}$;*Ring1b*$^{cko/cko}$ (Fig. 6O) incisors compared to WT incisors (Fig. 6M), while *Fbxl10/Kdmr2* expression appeared to be down-regulated only in *Ring1a*$^{-/-}$;*Ring1b*$^{cko/cko}$ (Fig. 6R) but not in *Ring1a*$^{-/-}$;*Ring1b*$^{fl/fl}$*cre-* (Fig. 6Q) incisors compared to WT incisors (Fig. 6P). These data show that Ring1a and Ring1b possibly regulate transcription of members of the PRC1 complex including Fbxl10/Kdmr2.

Ring1a and Ring1b are required for the development of molar roots

The apical incisor phenotype observed in *Ring1a*$^{-/-}$;*Ring1b*$^{cko/cko}$ mice prompted us to examine PRC1 gene expression and postnatal development of molars. The key postnatal developmental event is the formation of tooth roots. Expression of *Ring1a, Ring1b, Nspc1, Fbxl10 and Skp1* were all found to be localized in postnatal molars in apical areas at the early stages of root formation, particularly in root odontoblasts (Fig. 7). Micro CT analysis of first molars in P17 postnatal *Ring1a*$^{-/-}$;*Ring1b*$^{cko/cko}$ mice (Fig. 8 B and D) revealed a lack of root formation compared to cre- controls (Fig. 8 A and C). Histological sections of the developing roots identified abnormal root odontoblasts that were small and non-polarised in the *Ring1a*$^{-/-}$;*Ring1b*$^{cko/cko}$ molars (Fig. 9 B′) in comparison to the *cre-* molars (Fig. 9 A′).

In order to begin to understand the molecular consequences of loss of Ring proteins on root formation we investigated the expression of *Bmp4* since this has been linked to the formation of Hertwigs epithelial root sheath formation during root development (Hosoya et al., 2008; Yamashrio et al., 2003). Expression of *Bmp4* was highly restricted to developing root odontoblasts in wild type molars but was more widely distributed in mesenchymal cells in the area of arrested root formation in *Ring1a*$^{-/-}$;*Ring1b*$^{cko/cko}$ (Fig. 9C and D, respectively). This suggests that restriction of BMP signaling to specific areas of root formation involves Ring proteins and in their absence expression becomes more widespread and as a result interferes with the normal development of root odontoblasts.

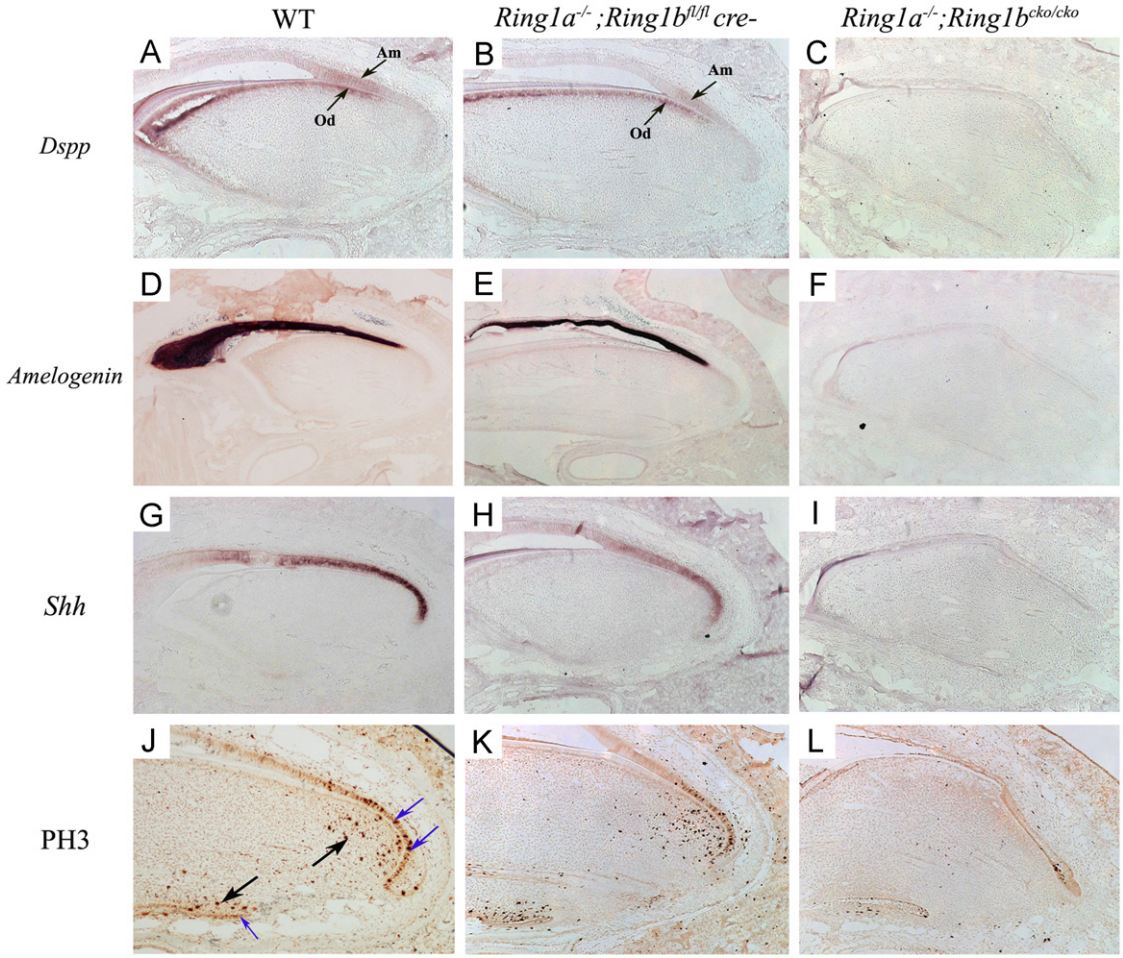

Fig. 5. Expression analysis of *Dspp*, *Amelogenin* and *Shh* and Phopho-histone H3 (PH3) in 17 day-old maxillary incisors of wild-type, *Ring1a*$^{-/-}$;*Ring1b*$^{fl/fl}$*cre-* and *Ring1a*$^{-/-}$;*Ring1b*$^{cko/cko}$ mice (sagittal sections). (A and B) *Dspp* expression in the odontoblasts (od) and differentiated ameloblasts (am) of WT control and *Ring1a*$^{-/-}$;*Ring1b*$^{fl/fl}$*cre-* incisors. (C) Down-regulation of *Dspp* in *Ring1a*$^{-/-}$;*Ring1b*$^{cko/cko}$ incisor. (D and E) Expression of *Amelogenin* in functional ameloblasts in WT and *Ring1a*$^{-/-}$;*Ring1b*$^{fl/fl}$*cre-* incisor, respectively. (F) *Amelogenin* expression is down-regulated in *Ring1a*$^{-/-}$;*Ring1b*$^{cko/cko}$ incisor. (G and H) Strong expression of *Shh* is observed in pre-ameloblasts in WT and *Ring1a*$^{-/-}$;*Ring1b*$^{fl/fl}$*cre-* incisor, respectively. (I) *Shh* transcript is absent in *Ring1a*$^{-/-}$;*Ring1b*$^{cko/cko}$ incisor. Immunohistochemistry against Phopho-histone H3 (PH3) shows a significant decrease of cell proliferation in 17 day-old *Ring1a*$^{-/-}$;*Ring1b*$^{cko/cko}$ incisor (L). A number of mitotic cells are identified in the apical mesenchyme (black arrows) and inside the cervical loop epithelium (blue arrows) in WT (J) and *Ring1a*$^{-/-}$;*Ring1b*$^{fl/fl}$*cre-* incisor (K). (L) A minimal staining of mitotic cells is noted in the apical end of *Ring1a*$^{-/-}$;*Ring1b*$^{cko/cko}$ incisor. (For interpretation of the references to color in this figure legend, the reader is reffered to the web version of this article.)

Discussion

Ring1a/b regulate a mesenchymal stem cell niche in developing incisors

Whilst *Ring1a*$^{-/-}$;*Ring1b*$^{fl/fl}$*cre-* mice do not exhibit any incisor phenotype, mice lacking both *Ring1a* and *Ring1b* postnatally display abnormal incisor development with an impairment of continuous growth. Furthermore, the lack of any incisor abnormalities in Ring1a$^{+/-}$;*Ring1b*$^{cko/cko}$, indicates a redundancy between Ring1a and Ring1b function during incisor development. However this redundancy is not complete since although *Ring1a*$^{-/-}$;*Ring1b*$^{fl/fl}$*cre-* incisors show no phenotypic abnormalities, they do show molecular changes in FGF activity. It has been shown that on the inactive X chromosome, the ubiquitination of histone H2A was retained in cells lacking Ring1a or Ring1b but not in cells lacking both (de Napoles et al., 2004). In addition, *Ring1b* single-knockout ES cells appeared normal whereas *Ring1a/b* double-knockout ES cells progressively lost ES cell characteristics after tamoxifen treatment to inactivate *Ring1b* (Endoh et al., 2008). It is possible that the absence of a tooth phenotype in *Ring1a*$^{+/-}$;*Ring1b*$^{cko/cko}$ is due to a compensatory role of the remaining copy of *Ring1a* for *Ring1b*. The compensatory role of Ring1a for Ring1b has previously been suggested owing to an increased expression of Ring1a protein in *Ring1b*-null ES cells (Endoh et al. 2008).

Rodent incisors are capable of erupting throughout their lifetime since the constant attrition at the incisal edge is compensated by the renewal of tooth-forming tissues at the apex of incisors deeply embedded in the jawbone. Our results show that the morphology of the whole cervical loop is remarkably abnormal in the P17 *Ring1a*$^{-/-}$;*Ring1b*$^{cko/cko}$ mice, in comparison to the cervical loop of *Ring1a*$^{-/-}$;*Ring1b*$^{fl/fl}$*cre-* mice. The mice used in this study exhibited a level of Ring1b protein that progressively decreased after 48 h of tamoxifen treatment. These mice were injected with treated tamoxifen at P9 and P13 and sacrificed at P17, therefore they were in the presence of tamoxifen for a maximum of 8 day. Since there would likely be a delay of around 24h for the drug to start working, the maximum period during which Ring1b inactivation could take place in postnatal tissues was thus approximately 7 day. Our measurement analysis showed that the growth of *Ring1a*$^{-/-}$;*Ring1b*$^{cko/cko}$ incisors was arrested and the incisor lengths of *Ring1a*$^{-/-}$;*Ring1b*$^{cko/cko}$ mice were significantly shorter than those of *Ring1a*$^{-/-}$;*Ring1b*$^{fl/fl}$*cre-* mice. It has

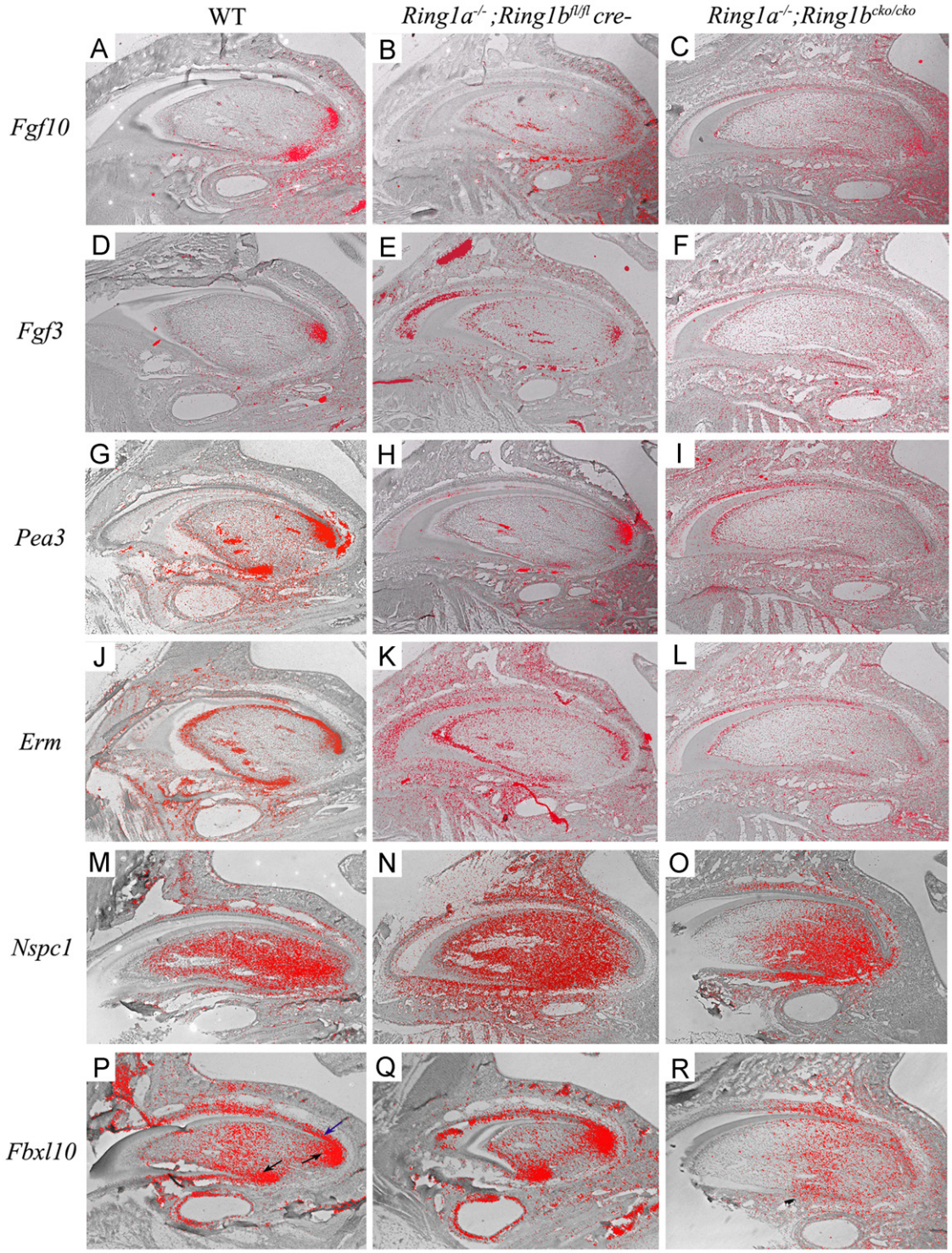

Fig. 6. Fgf signaling and transcripts encoding proteins of the PRC1complex are down-regulated in the apical end of *Ring1a*$^{-/-}$;*Ring1b*$^{fl/fl}$ *cre-* and completely absent in *Ring1a*$^{-/-}$;*Ring1b*$^{cko/cko}$ incisors. (A-R) *In situ* hybridization analysis using 35^{S} probes on paraffin sections of P17 WT, *Ring1a*$^{-/-}$;*Ring1b*$^{fl/fl}$*cre-* and *Ring1a*$^{-/-}$;*Ring1b*$^{cko/cko}$ incisors (red color represents expression). (A) *Fgf10* expression is noted in both labial and lingual mesenchyme in a WT mouse incisor. (D) *Fgf3* is expressed only in the labial mesenchyme in a WT mouse incisor. *Fgf10* (B) and *Fgf3* (E) are down-regulated in *Ring1a*$^{-/-}$;*Ring1b*$^{fl/fl}$*cre-* and absent in *Ring1a*$^{-/-}$;*Ring1b*$^{cko/cko}$ incisors (C and F). Expression of *Erm* (G) and *Pea3* (J) in WT incisors. (H, K) *Erm* and *Pea3* transcript is decreased in *Ring1a*$^{-/-}$;*Ring1b*$^{fl/fl}$*cre-* (H and K) and missing in *Ring1a*$^{-/-}$;*Ring1b*$^{cko/cko}$ incisors (I and L). (M) High expression of *BCoR* is noticed in the labial and lingual mesenchyme (arrows) in WT mouse incisors. (N, O) (M) Expression of *Nspc1* is widespread in the dental mesenchyme of WT incisors. (N, O) Expression pattern of *Nspc1* is unchanged in *Ring1a*$^{-/-}$;*Ring1b*$^{fl/fl}$*cre-* (N) and *Ring1a*$^{-/-}$;*Ring1b*$^{cko/cko}$ (O) incisors. (P) Strong *Fbxl10* expression is noted in the labial and lingual dental mesenchyme (black arrows) as well as part of the dental epithelium (blue arrow) in WT incisors. (Q) *Fbxl10* expression is unaffected in *Ring1a*$^{-/-}$;*Ring1b*$^{fl/fl}$*cre-* incisors. (R) Down-regulation of *Fbxl10* is clearly recognized in *Ring1a*$^{-/-}$;*Ring1b*$^{cko/cko}$ incisors. (For interpretation of the references to color in this figure legend, the reader is reffered to the web version of this article.)

been demonstrated that the eruption rate of unimpeded mandibular mouse incisors is approximately 400 μm per day (Ness, 1965) and the difference of the mean lengths of *Ring1a*$^{-/-}$;*Ring1b*$^{cko/cko}$ and cre- mandibular incisors was 1500 μm, thus they were slightly longer than what we expected if the growth of these incisors was halted for 7 day. This suggests that either the *Ring1a*$^{-/-}$;*Ring1b*$^{cko/cko}$ incisors

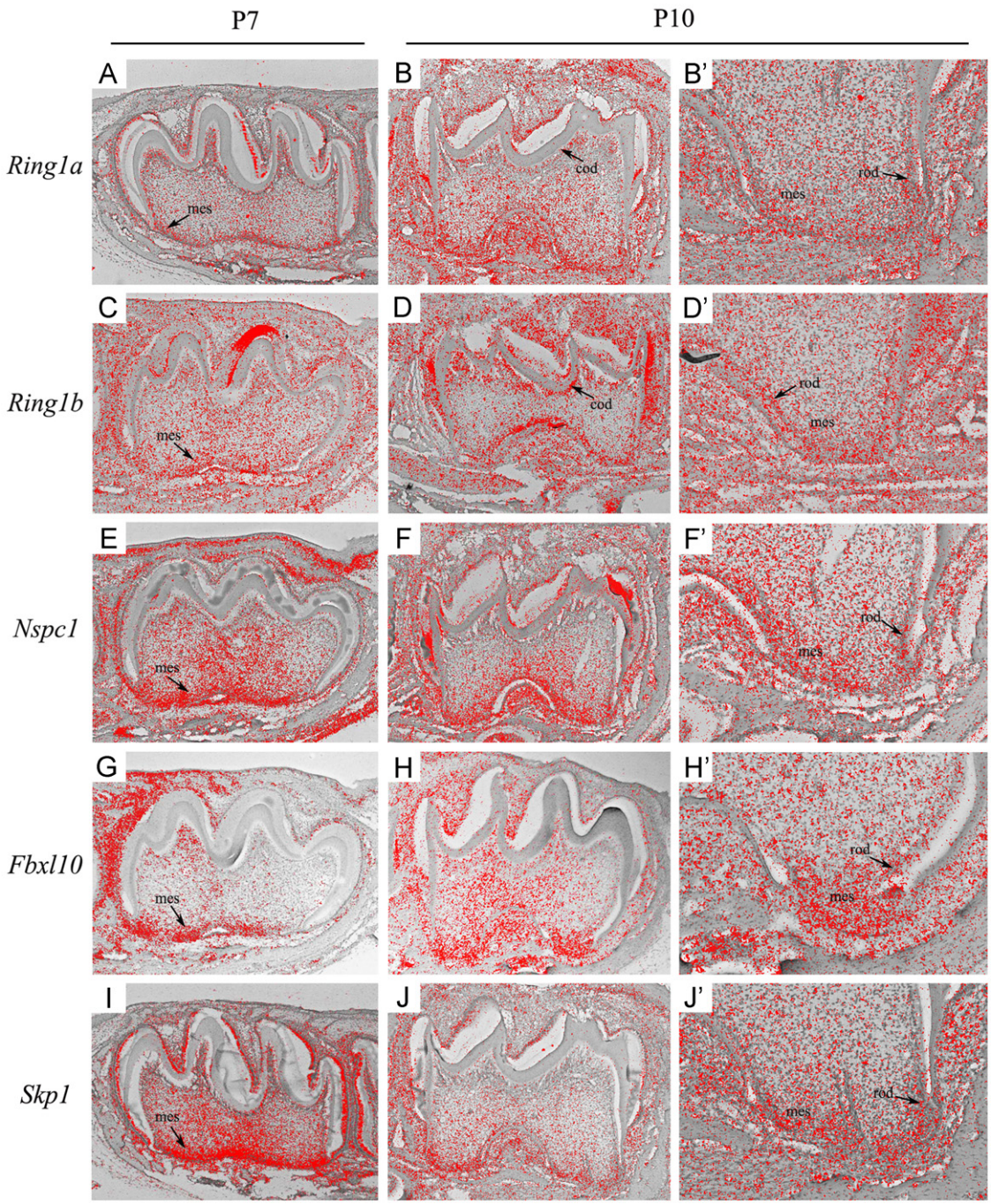

Fig. 7. Expression of genes encoding proteins of the PRC1 complex during postnatal molar development. (A, C, E, G, I) At P7, *Ring1a*, *Ring1b*, *Nspc1*, *Fbxl10* and *Skp1* are all expressed in the dental mesenchyme (mes) at the cervical area of developing molar roots (B, D, F, H, J) At P10, their expression is still maintained in the apical mesenchyme with a weaker expression in the mesenchyme of the coronal pulp. (B′, D′, F′, H′, J′) High magnification views of the apical region of one of the developing molar roots as shown in B, D, F, H and J, respectively. Expression of genes encoding members of the PRC1 complex is present in the apical mesenchyme (mes) and in the root odontoblasts (rod).

were still capable of growing at a lower rate, or that tamoxifen-induced cre-mediated excision may only be fully effective for approximately 4 day.

When comparing the cervical loops of *Ring1a*$^{-/-}$;*Ring1b*$^{cko/cko}$ and *Ring1a*$^{-/-}$;*Ring1b*$^{fl/fl}$*cre-* mice, the secretion of enamel and dentin as well as the differentiation of ameloblasts and odontoblasts that normally appear as an increasing gradient from the apical end towards the incisal end were absent in the double-knockout mice. It is interesting to note that further in the incisal area, the odontoblasts facing the dentin matrix and the ameloblasts facing an empty space of enamel left by histological processing also appeared abnormal. These ameloblasts and odontoblasts were round in shape and had lost their nuclear polarization, suggesting that disruption may have occurred when these cells were differentiating and that they could not achieve terminal differentiation. Other possibilities are that soon after Ring1b was depleted, these cells became atrophic, suggesting an additional maintenance role or were unable to complete their normal rounds of cell division. It is known from tissue recombination experiments that functional differentiation of ameloblasts relies

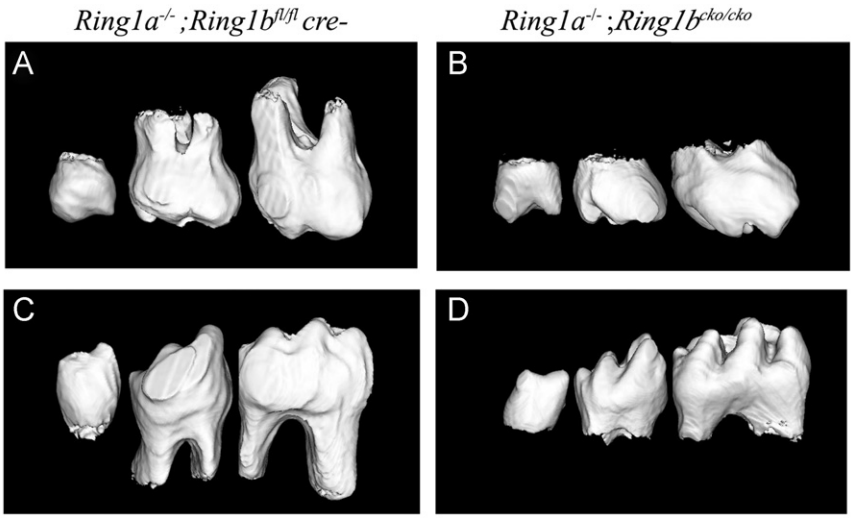

Fig. 8. MicroCT analysis of 17 day-old *Ring1a*$^{-/-}$;*Ring1b*$^{fl/fl}$*cre-* and *Ring1a*$^{-/-}$;*Ring1b*$^{cko/cko}$ molars. (A, C) *Ring1a*$^{-/-}$;*Ring1b*$^{fl/fl}$*cre-* mice show normal maxillary (A) and mandibular (C) molar root development. (B, D) *Ring1a*$^{-/-}$;*Ring1b*$^{cko/cko}$ incisor mice exhibit very short maxillary (B) and mandibular (D) molar roots.

on epithelial-mesenchymal interactions and requires a contact with dentin matrix to trigger differentiation (Karcher-Djuricic et al., 1985; Zeichner-David et al., 1995). The disruption of enamel-forming ameloblasts in *Ring1a*$^{-/-}$;*Ring1b*$^{cko/cko}$ incisors could be due to a lack of dentin matrix secretion that results from aberrant odontoblasts in these double mutant mice. It is therefore possible that that the inability of mesenchymal cells to differentiate into odontoblasts is a cause of the odontoblast defects observed in *Ring1a*$^{-/-}$;*Ring1b*$^{cko/cko}$ mice and that the abnormal ameloblast differentiation is a secondary consequence of this. Alternatively, ameloblast differentiation may be impaired as a consequence of a requirement for Ring proteins in mesenchymal transit amplifying cells for maintenance of the epithelial stem cell niche (see below) or the patchy expression of Ring1b in pre-ameloblasts may have a functional role. The aberrancy of odontoblasts and ameloblasts observed in *Ring1a*$^{-/-}$;*Ring1b*$^{cko/cko}$ incisors was further confirmed by down-regulation of functional molecular markers of these cells, including *Dspp* in odontoblasts (D'Souza et al., 1997) and *Amelogenin* in ameloblasts (Zeichner-David et al., 1995). In addition, *Shh* which is expressed in early ameloblasts (Bitgood and McMahon, 1995) was also reduced from the dental epithelium of *Ring1a*$^{-/-}$;*Ring1b*$^{cko/cko}$ incisors. The reduced expression of these genes in the mutant incisors correlated with abnormal cell morphology and since cells were more abnormal closer to the proximal (cervical loop) end, this would indicate that temporal effects of tamoxifen administration leading to incomplete recombination at early time points. Thus abnormal cell differentiation was thus more extensive that reduction of growth rate. An alternative explanation that cannot be excluded is that loss of Ring proteins has more long-range effects on cell differentiation.

The reduced cell proliferation noted in the apical dental mesenchyme close to both labial and lingual cervical loop epithelium where the differentiation of odontoblast progenitors takes place suggests that *Ring1a/b* proteins are required either directly or indirectly) for proliferation of the dental mesenchymal cells giving rise to dentin-forming odontoblasts. This finding is in agreement with previous studies that have shown that loss of Ring1a/b causes proliferation defects in ES cells (Endoh et al., 2008). Apart from the dental mesenchyme, a dramatically decrease in cell proliferation was also noted in the transit-amplifying cells of the cervical loop epithelium. This finding suggests that *Ring1a/b* regulates proliferative signals not only within the dental mesenchyme but also from the dental mesenchyme to the cervical loop epithelium. The most likely explanation for this is that *Ring1a/b* directly regulates a signaling molecule in the dental epithelium that controls epithelial cell proliferation (see below).

All these findings indicate that *Ring1a/b* double-knockout mutant incisors have lost the ability to grow continuously, highlighting the essential role of *Ring1a/b* in the regulation of the continuous growth of mouse incisors. We propose that *Ring1a*/b act in the dental mesenchymal stem cell micoenvironment (niche) in developing mouse incisors and that the loss of *Ring1a/b* therefore leads to a failure of the immediate progeny of mesenchymal stem cells (TA cells) to undergo proliferation and differentiation into odontoblast precursors, subsequently resulting in an arrest of the continuous growth of mouse incisors.

Ring1a/b regulate Fgf signaling in continuously growing mouse incisors

The importance of *Ring1a/b* during incisor development was further illustrated by a down-regulation of Fgf signaling in *Ring1a*$^{-/-}$;*Ring1b*$^{fl/fl}$*cre-* and *Ring1a*$^{-/-}$;*Ring1b*$^{cko/cko}$ incisors. Notably, Fgf signaling appeared to be reduced in both *Ring1a*$^{-/-}$; *Ring1b*$^{fl/fl}$*cre-* and *Ring1a*$^{-/-}$;*Ring1b*$^{cko/cko}$ incisors, with a bigger decrease in the latter. Prior evidence has revealed that Fgf signaling plays essential roles during the development of mouse incisors, in particular *Fgf3* and *Fgf10*, which are restrictedly expressed in the dental mesenchyme underlying the rapidly proliferating cells of the inner enamel epithelium. Fgf10 has been shown to be a signal necessary for the maintenance of the epithelial stem cell niche residing in the cervical loop, owing to the hypoplastic cervical loops observed in *Fgf10*$^{-/-}$ mice (Harada et al., 2002). *Fgf3*$^{-/-}$ mice display abnormal enamel and *Fgf3*$^{-/-}$; *Fgf10*$^{+/-}$ mice exhibit very thin or no enamel (Wang et al., 2007). It is interesting to note that despite the down-regulation of *Fgf10* in *Ring1a*$^{-/-}$;*Ring1b*$^{cko/cko}$ incisors, the tips of cervical loops, containing putative epithelial stem cells, do not become hypoplastic as seen in *Fgf10*$^{-/-}$ mice. They only appear slightly smaller than those in *Ring1a*$^{-/-}$;*Ring1b*$^{fl/fl}$*cre-* incisors. This may be explained by the fact that *Fgf10* was not completely absent in the dental mesenchyme surrounding the entire tip of cervical loops and that this residual *Fgf10* expression is sufficient to sustain the tips of cervical loops. Another possibility might be that *Ring1b* in these double-knockout mice was conditionally

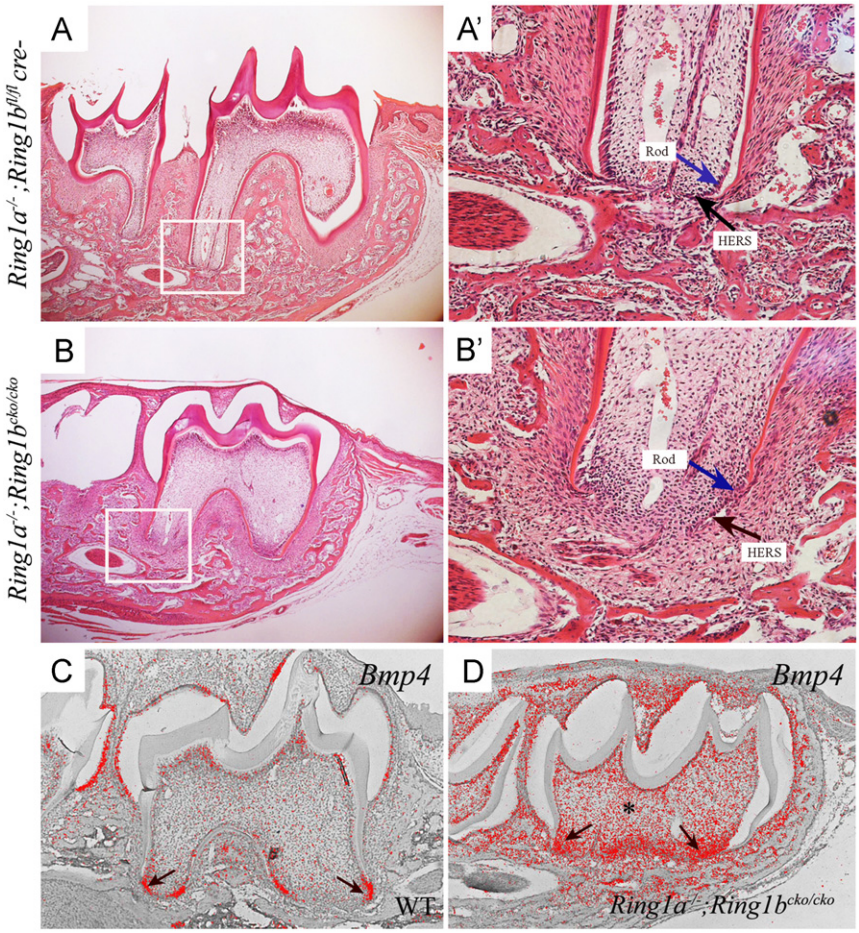

Fig. 9. Histology characteristics and Bmp signaling is altered in the mandibluar molar of *Ring1a*$^{-/-}$;*Ring1b*$^{cko/cko}$ mice. (A-B′) Hematoxylin and eosin stained sections of a P17 mandibular molar of and *Ring1a*$^{-/-}$;*Ring1b*$^{fl/fl}$*cre-* and *Ring1a*$^{-/-}$;*Ring1b*$^{cko/cko}$ mice. (A and B) *Ring1a*$^{-/-}$;*Ring1b*$^{fl/fl}$*cre-* maxillary mandibular (A, box) molars show normal root development whereas very short roots are observed in *Ring1a*$^{-/-}$;*Ring1b*$^{cko/cko}$ mandibular (B, box) molars. (A′) Higher magnification of the white box in (A) shows normal root odontoblasts (Rod) differentiating adjacent to Hertwig's epithelial root sheath (HERS) in *Ring1a*$^{-/-}$;*Ring1b*$^{fl/fl}$*cre-* molar. (B′) Higher magnification of the white box in (B) shows aberrant odontoblast differentiation (blue arrow) close to Hertwig's epithelial root sheath (HERS). (C, D) *In situ* hybridization analysis of *Bmp4* expression using 35^{S} probes on paraffin sections of P11 WT and cre+ developing first molars (red color represents expression). (C) Normal expression of *Bmp4* in early odontoblasts (arrows) in WT developing first molars. (D) Expression of *Bmp4* is upregulated in *Ring1a*$^{-/-}$;*Ring1b*$^{cko/cko}$ developing molars with ectopic expression in the dental pulp (asterisk). (For interpretation of the references to color in this figure legend, the reader is reffered to the web version of this article.)

inactivated for a short period of time that perhaps was not sufficient to cause an overt phenotype on the tips of cervical loops. Since the asymmetric expression of *Fgf3* on the labial aspect has been shown to stimulate epithelial stem cell proliferation and since enamel defects are observed in both *Fgf3*$^{-/-}$ and *Fgf3*$^{-/-}$;*Fgf10*$^{+/-}$ mice (Wang et al., 2007), it is possible that the down-regulation of both *Fgf3* and *Fgf10* in *Ring1a*$^{-/-}$;*Ring1b*$^{cko/cko}$ incisors is likely to be a cause of reduced cell proliferation in the dental epithelium of the cervical loop, leading to the disruption of ameloblast formation. Among the members of Fgf ligands known to be present at the apex of mouse incisors, *Fgf9*, which is normally expressed in the limited area of TA cells or pre-ameloblasts in the labial epithelium was not investigated. However, it has been shown that mesenchymal *Fgf3* and *Fgf10* are targets of epithelial *Fgf9* (Klein et al., 2008; Yokohama-Tamaki et al., 2007).

The impairment of Fgf activity in *Ring1a*$^{-/-}$;*Ring1b*$^{cko/cko}$ incisors was confirmed by the down-regulation of *Pea3* and *Erm*. *Pea3* and *Erm* belong to the Erythroblastoma Twenty-Six (ETS) family of transcription factors that are involved in a variety of transcriptional regulation events during growth and development, including proliferation, differentiation and oncogenic transformation (Monte et al., 1994; Wasylyk et al., 1998; Xin et al., 1992). Both genes have been demonstrated to be direct targets of Fgf signaling, based upon the closely related expression domains and the susceptibility to Fgf signaling interference (O'Hagan and Hassell, 1998; Roehl and Nusslein-Volhard, 2001). Besides being downstream targets of Fgf signaling, particular functions of these genes have not been described, however, it has been suggested that the close connection of *Erm* and *Pea3* transcription to Fgf signaling may serve to integrate Fgf signaling with other signals (Raible and Brand, 2001). Whether this is the case for the continuous growth of mouse incisors is an interesting issue for future research. Reduced Fgf signaling in *Ring1a*$^{-/-}$;*Ring1b*$^{fl/fl}$*cre-* incisors did not result in an obvious phenotype but does suggest that both Ring1a and Ring1b are required for maintaining endogenous levels of FGF expression indicates that these mice have a molecular abnormality and that *Ring1a* itself is essential for the regulation of Fgf signaling.

Ring1a/b regulate genes encoding proteins of the PRC1 complex

The transcriptional alteration of protein members of the PRC1 complex observed in *Ring1a*$^{-/-}$;*Ring1b*$^{fl/fl}$*cre-* and *Ring1a*$^{-/-}$;*Ring1b*$^{cko/cko}$ incisors provides evidence that members of the

PCR1 complex including *Fbxl10* are targets of the complex during the continuous growth of mouse incisors. The importance of *Ring1*, particularly *Ring1b*, on the transcription levels of other members of the same protein complex has previously been demonstrated in PRC1. Loss of Ring1b in ES cells leads to a down-regulation of *Phc1*/*Mph1* and an up-regulation of *Bmi1*, *Mpc2*, *Rypb* and *Phc2*. However, these altered transcription levels do not seem to be entirely reflected in the protein levels, suggesting a distinct post-translation regulation of PRC1 members by Ring1b (Leeb and Wutz, 2007; van der Stoop et al., 2008).

Transcription of *Fbxl10* appears to be regulated by Ring1b but not Ring1a during mouse incisor development, indicating distinct interactions within this complex. *Nspc1/Pcgf1* expression was not altered in the absence of either *Ring1a* or *Ring1a/b*. The down-regulation of *Fbxl10/Kdm2r* expression observed only in *Ring1a*$^{-/-}$;*Ring1b*$^{cko/cko}$ incisors but not in cre- incisors suggests that only *Ring1b* may regulate *Fbxl10/Kdm2r* during the development of mouse incisors. It is likely that this is a direct interaction since *in vitro* protein binding assay has shown that Ring1b protein is able to directly interact with Fbxl10/Kdm2r (Gearhart et al., 2006; Sanchez et al., 2007).

The evidence we present here identifies a population of dental pulp mesenchymal cells that are highly proliferative, express PRC1 proteins and have characteristics of cell progenitors (TA cells) in normal tooth growth and in response to tooth damage. The dental mesenchymal stem cell niche in rodent incisors thus provides an attractive, easily visualized and manipulated, experimental system to study the molecular characteristics and behaviour of mesenchymal and epithelial stem cells in an adult organ.

Ring1a/b also regulate molar root formation

The severely impaired development of molar roots following postnatal loss of Ring1 proteins is consistent with aspects of the changes observed in incisors in these mutants. Molar root odontoblasts were very small, non-polarised and unorganized in the developing roots of *Ring1a*$^{-/-}$;*Ring1b*$^{cko/cko}$ mice, similar features to those in the incisors. A molecular downstream consequence of loss of Ring proteins is a change in the spatial expression of Bmp4 from being restricted to developing root odontoblasts to being widely expressed in undifferentiated root mesenchyme cells. Repression of BMP4 expression in cells other than root odontoblasts may thus be one possible function of PRC1 complex in regulating molar root formation.

Materials and methods

Production of mouse lines

Mutant Ring1a and Ring1b floxed alleles were generated as described previously (Cales et al., 2008; del Mar Lorente et al., 2000). Compound *Ring1a*$^{-/-}$;*Ring1b*$^{fl/fl}$ mice were obtained by crossing the *Ring1a*$^{-/-}$ mice with the *Ring1b*$^{fl/fl}$ mice. To accomplish conditional inactivation of *Ring1b in vivo*, the *Ring1a*$^{-/-}$;*Ring1b*$^{fl/fl}$ compound mice were crossed with *Rosa26::CreERT2* transgenic mice to generate *Ring1a*$^{-/-}$;*Ring1b*$^{fl/fl}$;*Rosa26::CreERT2* mice. The *Rosa26::CreERT2* transgenic mice were produced by inserting a tamoxifen-inducible CreER fusion protein gene into the ubiquitously expressed *Rosa26* gene (Seibler et al., 2003). Conditional deletion of *Ring1b* was carried out at the desired stage of postnatal life by 4-hydroxy tamoxifen (OHT) treatment (40 mg/kg body weight). *Ring1a*$^{-/-}$; *Ring1b*$^{cko/cko}$ mice were obtained by injecting OHT at P9 and P13 to inactivate Ring1b and the *Ring1a*$^{-/-}$;*Ring1b*$^{cko/cko}$ sacrificed at P17. The efficiency of tamoxifen-induced Cre expression to delete Ring1b was confirmed by *in situ* hybridisation of P17 incisors (Fig. 1S).

BrdU administration

To detect rapidly dividing cells, 50 mg/kg body weight BrdU was administered intraperitoneally to wild type postnatal day 2 (P2) pups. Pups were subsequently sacrificed 2 h later and processed through histology and immunohistochemistry analysis.

Gene expression analysis

Whole-mount digoxigenin-labelled *in situ* hybridization was carried out according to Shamim et al. (1998). Digoxigenin-labelled section *in situ* hybridization was carried as previously described (Nakatomi et al., 2006). Radioactive section *in situ* hybridization using ^{35}S UTP radiolabelled riboprobes was performed on 8-μm sections as described previously (Wilkinson, 1982).

MicroCT analysis

Mouse heads were scanned using a GE Locus SP microCT scanner to produce 14 μm voxel size volumes. After scanning, Explore Microview software program (GE) was used for visualization and analysis. Mouse teeth were characterised by generating three dimensional reconstructions and three dimensional isosurfaces of mouse teeth were then produced. For measurement of mouse incisor length, the locations of the centre points of incisors were identified on every 5 cross-sections from the most incisal to apical end. The position of each centre point was identified on the micro CT planes as three co-ordinates (x,y,z). The distance between every two points ((x_1,y_1,z_1) and (x_2,y_2,z_2)), was then calculated using the formula derived from the three dimensional version of the Pythgorean theorem (Distance$=\sqrt{(x_2-x_1)^2+(y_2-y_1)^2+(z_2-z_1)^2}$). The length of the curved incisor was calculated from the sum of all the distances between each dot.

Immunohistochemistry

Sections were incubated with antibody to Phospho-Histone H3 (Upstate, 06–570) or BrdU (Abcam, ab6326) following heat-based antigen retrieval. To perform peroxidase visualization for the biotin conjugated antibody, the sections were incubated in ABC solution (Vectastain kit, Vector, PK-6101). The colour reaction was then developed by applying DAB solution (0.5 mg/ml DAB and 0.1% H_2O_2) onto the sections or using a DAB peroxidase substrate kit (Vector, SK-4100).

Summary

Stem cells are found in many adult organs where they provide a source of cells needed for tissue growth or to replace cells lost as a result of tissue damage. Adult human teeth do not grow and have only a limited ability to repair following damage, however, the incisors of rodents grow continuously to accommodate wear and all the specialised cells of the tooth must be continuously replaced. This is achieved by stem cell populations at the base of the tooth that provide sources of cells to replace all mesenchymal and epithelium-derived tooth cells. Whereas the incisor epithelial stem cell niche is well characterised, the mesenchymal stem cell niche is poorly understood. We have identified genes that are required for incisor tooth growth and cell differentiation that belong the PRC1 complex that is known to be essential for maintenance of embryonic stem cells. We how that PRC1 genes are expressed in the mesenchymal transit amplifying cells and are essential for mesenchymal cell proliferation and also for

expression of signals from the mesenchyme that regulate the epithelial stem cell niche.

Acknowledgements

This project was supported by an MRC grant G0600041) to PTS. PL was supported by a PhD studentship award from the Government of Thailand.

Appendix A. Supporting information

Supplementary data associated with this article can be found in the online version at http://dx.doi.org/10.1016/j.ydbio.2012.04.029.

References

Begue-Kirn, C., Krebsbach, P.H., Bartlett, J.D., Butler, W.T., 1998. Dentin sialoprotein, dentin phosphoprotein, enamelysin and ameloblastin: tooth-specific molecules that are distinctively expressed during murine dental differentiation. Eur. J. Oral. Sci. 106, 963–970.

Bitgood, M.J., McMahon, A.P., 1995. Hedgehog and Bmp genes are coexpressed at many diverse sites of cell-cell interaction in the mouse embryo. Dev. Biol. 172, 126–138.

Cales, C., Roman-Trufero, M., Pavon, L., Serrano, I., Melgar, T., Endoh, M., Perez, C., Koseki, H., Vidal, M., 2008. Inactivation of the Polycomb group protein Ring1B unveils an antiproliferative role in hematopoietic cell expansion and cooperation with tumorigenesis associated with Ink4a deletion. Mol. Cell Biol. 28, 1018–1028.

Cao, R., Wang, L., Wang, H., Xia, L., Erdjument-Bromage, H., Tempst, P., Jones, R.S., Zhang, Y., 2002. Role of histone H3 lysine 27 methylation in Polycomb-group silencing. Science 298, 1039–1043.

D'Souza, R.N., Cavender, A., Sunavala, G., Alvarez, J., Ohshima, T., Kulkarni, A.B., MacDougall, M., 1997. Gene expression patterns of murine dentin matrix protein 1 (Dmp1) and dentin sialophosphoprotein (DSPP) suggest distinct developmental functions *in vivo*. J. Bone Miner. Res. 12, 2040–2049.

de Napoles, M., Mermoud, J.E., Wakao, R., Tang, Y.A., Endoh, M., Appanah, R., Nesterova, T.B., Silva, J., Otte, A.P., Vidal, M., Koseki, H., Brockdorff, N., 2004. Polycomb group proteins Ring1A/B link ubiquitylation of histone H2A to heritable gene silencing and X inactivation. Dev. Cell. 7, 663–676.

del Mar Lorente, M., Marcos-Gutierrez, C., Perez, C., Schoorlemmer, J., Ramirez, A., Magin, T., Vidal, M., 2000. Loss- and gain-of-function mutations show a polycomb group function for Ring1A in mice. Development 127, 5093–5100.

Delaval, K., Feil, R., 2004. Epigenetic regulation of mammalian genomic imprinting. Curr. Opin. Genet. Dev. 14, 188–195.

Endoh, M., Endo, T.A., Endoh, T., Fujimura, Y., Ohara, O., Toyoda, T., Otte, A.P., Okano, M., Brockdorff, N., Vidal, M., Koseki, H., 2008. Polycomb group proteins Ring1A/B are functionally linked to the core transcriptional regulatory circuitry to maintain ES cell identity. Development 135, 1513–1524.

Feng, J., Mantesso, A., De Bari, C., Nishiyama, A., Sharpe, P.T., 2011. Dual origin of mesenchymal stem cells contributing to organ growth and repair. Proc. Nat. Acad. Sci. USA 108, 6503–6508.

Gearhart, M.D., Corcoran, C.M., Wamstad, J.A., Bardwell, V.J., 2006. Polycomb group and SCF ubiquitin ligases are found in a novel BCOR complex that is recruited to BCL6 targets. Mol. Cell Biol. 26, 6880–6889.

Harada, H., Kettunen, P., Jung, H.S., Mustonen, T., Wang, Y.A., Thesleff, I., 1999. Localization of putative stem cells in dental epithelium and their association with Notch and FGF signaling. J. Cell Biol. 147, 105–120.

Harada, H., Toyono, T., Toyoshima, K., Yamasaki, M., Itoh, N., Kato, S., Sekine, K., Ohuchi, H., 2002. FGF10 maintains stem cell compartment in developing mouse incisors. Development 129, 1533–1541.

Heard, E., 2005. Delving into the diversity of facultative heterochromatin: the epigenetics of the inactive X chromosome. Curr. Opin. Genet. Dev. 15, 482–489.

Hosoya, A., Kim, J.Y., Cho, S.W., Jung, H.S., 2008. BMP4 signaling regulates formation of Hertwig's epithelial root sheath during tooth root development. Cell Tissue Res. 333, 503–509.

Jones, D.L., Wagers, A.J., 2008. No place like home: anatomy and function of the stem cell niche. Nat. Rev. Mol. Cell Biol. 9, 11–21.

Karcher-Djuricic, V., Staubli, A., Meyer, J.M., Ruch, J.V., 1985. Acellular dental matrices promote functional differentiation of ameloblasts. Differentiation 29, 169–175.

Klein, O.D., Lyons, D.B., Balooch, G., Marshall, G.W., Basson, M.A., Peterka, M., Boran, T., Peterkova, R., Martin, G.R., 2008. An FGF signaling loop sustains the generation of differentiated progeny from stem cells in mouse incisors. Development 135, 377–385.

Leeb, M., Wutz, A., 2007. Ring1B is crucial for the regulation of developmental control genes and PRC1 proteins but not X inactivation in embryonic cells. J. Cell Biol. 178, 219–229.

Lewis, E.B., 1978. A gene complex controlling segmentation in Drosophila. Nature 276, 565–570.

Lin, Y., Cheng, Y.S., Qin, C., Lin, C., D'Souza, R., Wang, F., 2009. FGFR2 in the dental epithelium is essential for development and maintenance of the maxillary cervical loop, a stem cell niche in mouse incisors. Dev. Dyn. 238, 324–330.

Monte, D., Baert, J.L., Defossez, P.A., de Launoit, Y., Stehelin, D., 1994. Molecular cloning and characterization of human ERM, a new member of the Ets family closely related to mouse PEA3 and ER81 transcription factors. Oncogene 9, 1397–1406.

Nakatomi, M., Morita, I., Eto, K., Ota, M.S., 2006. Sonic hedgehog signaling is important in tooth root development. J. Dent. Res. 85, 427–431.

Ness, A.R., 1965. Eruption rates of impeded and unimpeded mandibular incisors of the adult laboratory mouse. Arch. Oral. Biol. 10, 439–451.

O'Hagan, R.C., Hassell, J.A., 1998. The PEA3 Ets transcription factor is a downstream target of the HER2/Neu receptor tyrosine kinase. Oncogene 16, 301–310.

Ohazama, A., Blackburn, J., Porntaveetus, T., Ota, M.S., Choi, H.Y., Johnson, E.B., Myers, P., Oommen, S., Eto, K., Kessler, J.A., Kondo, T., Fraser, G.J., Streelman, J.T., Pardiñas, U.F.J., Tucker, A.S., Ortiz, P.E., Charles, C., Viriot, L., Herz, J., Sharpe, P.T., 2010. A role for suppressed incisor cuspal morphogenesis in the evolution of mammalian heterodont dentition. Proc. Nat. Acad. Sci. USA 107, 92–97.

Raible, F., Brand, M., 2001. Tight transcriptional control of the ETS domain factors Erm and Pea3 by Fgf signaling during early zebrafish development. Mech. Dev. 107, 105–117.

Ringrose, L., Paro, R., 2004. Epigenetic regulation of cellular memory by the Polycomb and Trithorax group proteins. Annu. Rev. Genet. 38, 413–443.

Roehl, H., Nusslein-Volhard, C., 2001. Zebrafish pea3 and erm are general targets of FGF8 signaling. Curr. Biol. 11, 503–507.

Sanchez, C., Sanchez, I., Demmers, J.A., Rodriguez, P., Strouboulis, J., Vidal, M., 2007. Proteomics analysis of Ring1B/Rnf2 interactors identifies a novel complex with the Fbxl10/Jhdm1B histone demethylase and the Bcl6 interacting corepressor. Mol. Cell Proteomics 6, 820–834.

Satijn, D.P., Gunster, M.J., van der Vlag, J., Hamer, K.M., Schul, W., Alkema, M.J., Saurin, A.J., Freemont, P.S., van Driel, R., Otte, A.P., 1997. RING1 is associated with the polycomb group protein complex and acts as a transcriptional repressor. Mol. Cell Biol. 17, 4105–4113.

Scadden, D.T., 2006. The stem-cell niche as an entity of action. Nature 441, 1075–1079.

Schofield, R., 1978. The relationship between the spleen colony-forming cell and the haemopoietic stem cell. Blood Cells 4, 7–25.

Schuettengruber, B., Chourrout, D., Vervoort, M., Leblanc, B., Cavalli, G., 2007. Genome regulation by polycomb and trithorax proteins. Cell 128, 735–745.

Schwartz, Y.B., Pirrotta, V., 2007. Polycomb silencing mechanisms and the management of genomic programmes. Nat. Rev. Genet. 8, 9–22.

Seibler, J., Zevnik, B., Kuter-Luks, B., Andreas, S., Kern, H., Hennek, T., Rode, A., Heimann, C., Faust, N., Kauselmann, G., Schoor, M., Jaenisch, R., Rajewsky, K., Kuhn, R., Schwenk, F., 2003. Rapid generation of inducible mouse mutants. Nucleic Acids Res. 31, e12.

Seidel, K., Ahn, C.P., Lyons, D., Nee, A., Ting, K., Brownell, I., Cao, T., Carano, R.A., Curran, T., Schober, M., Fuchs, E., Joyner, A., Martin, G.R., de Sauvage, F.J., Klein, O.D., 2010. Hedgehog signaling regulates the generation of ameloblast progenitors in the continuously growing mouse incisor. Development 137, 3753–3761.

Shamim, H., Mahmood, R., Mason, I., 1998. *In Situ* Hybridization to RNA in whole embryos. In molecular embryology. In: Sharpe, P.T., Mason, I. (Eds.), Methods and Protocols. Humana Press, New Jersey.

Smith, C.E., Warshawsky, H., 1975. Cellular renewal in the enamel organ and the odontoblast layer of the rat incisor as followed by radioautography using 3H-thymidine. Anat. Rec. 183, 523–561.

Sparmann, A., van Lohuizen, M., 2006. Polycomb silencers control cell fate, development and cancer. Nat. Rev. Cancer 6, 846–856.

Tummers, M., Thesleff, I., 2008. Observations on continuously growing roots of the sloth and the K14-Eda transgenic mice indicate that epithelial stem cells can give rise to both the ameloblast and root epithelium cell lineage creating distinct tooth patterns. Evol. Dev. 10, 187–195.

Tummers, M., Yamashiro, T., Thesleff, I., 2007. Modulation of epithelial cell fate of the root *in vitro*. J. Dent. Res. 86, 1063–1067.

Valk-Lingbeek, M.E., Bruggeman, S.W., van Lohuizen, M., 2004. Stem cells and cancer; the polycomb connection. Cell 118, 409–418.

van der Stoop, P., Boutsma, E.A., Hulsman, D., Noback, S., Heimerikx, M., Kerkhoven, R.M., Voncken, J.W., Wessels, L.F., van Lohuizen, M., 2008. Ubiquitin E3 ligase Ring1b/Rnf2 of polycomb repressive complex 1 contributes to stable maintenance of mouse embryonic stem cells. PLoS One 3, e2235.

Wang, H., Wang, L., Erdjument-Bromage, H., Vidal, M., Tempst, P., Jones, R.S., Zhang, Y., 2004. Role of histone H2A ubiquitination in Polycomb silencing. Nature 431, 873–878.

Wang, X.P., Suomalainen, M., Felszeghy, S., Zelarayan, L.C., Alonso, M.T., Plikus, M.V., Maas, R.L., Chuong, C.M., Schimmang, T., Thesleff, I., 2007. An integrated gene regulatory network controls stem cell proliferation in teeth. PLoS Biol. 5, e159.

Wasylyk, B., Hagman, J., Gutierrez-Hartmann, A., 1998. Ets transcription factors: nuclear effectors of the Ras-MAP-kinase signaling pathway. Trends Biochem. Sci. 23, 213–216.

Wilkinson, D., 1982. *In Situ* Hybridization: A Practical Approach. Oxford University Press, Oxford, UK.
Xin, J.H., Cowie, A., Lachance, P., Hassell, J.A., 1992. Molecular cloning and characterization of PEA3, a new member of the Ets oncogene family that is differentially expressed in mouse embryonic cells. Genes. Dev. 6, 481–496.
Yamashrio, T., Tummers, M., Thesleff, I., 2003. Expression of bone morphogenetic proteins and Msx genes during root formation. J. Dent. Res. 82, 172–176.
Yokohama-Tamaki, T., Shibata, S., Wakisaka, S., Harada, H., 2007. Fgf-9 play a role for the maintenance of stem cell niche via Fgf-10 expression in the mouse incisors. Eur. Cell Mater. 14, 141.
Zeichner-David, M., Diekwisch, T., Fincham, A., Lau, E., MacDougall, M., Moradian-Oldak, J., Simmer, J., Snead, M., Slavkin, H.C., 1995. Control of ameloblast differentiation. Int. J. Dev. Biol. 39, 69–92.

LETTER

doi:10.1038/nature13536

Glial origin of mesenchymal stem cells in a tooth model system

Nina Kaukua[1]*, Maryam Khatibi Shahidi[2]*, Chrysoula Konstantinidou[3], Vyacheslav Dyachuk[4,5], Marketa Kaucka[4], Alessandro Furlan[6], Zhengwen An[7], Longlong Wang[7], Isabell Hultman[8], Lars Ährlund-Richter[8], Hans Blom[9], Hjalmar Brismar[9], Natalia Assaife Lopes[6], Vassilis Pachnis[3], Ueli Suter[10], Hans Clevers[11,12], Irma Thesleff[13], Paul Sharpe[7], Patrik Ernfors[6], Kaj Fried[1] & Igor Adameyko[4]

Mesenchymal stem cells occupy niches in stromal tissues where they provide sources of cells for specialized mesenchymal derivatives during growth and repair[1]. The origins of mesenchymal stem cells have been the subject of considerable discussion, and current consensus holds that perivascular cells form mesenchymal stem cells in most tissues. The continuously growing mouse incisor tooth offers an excellent model to address the origin of mesenchymal stem cells. These stem cells dwell in a niche at the tooth apex where they produce a variety of differentiated derivatives. Cells constituting the tooth are mostly derived from two embryonic sources: neural crest ectomesenchyme and ectodermal epithelium[2]. It has been thought for decades that the dental mesenchymal stem cells[3] giving rise to pulp cells and odontoblasts derive from neural crest cells after their migration in the early head and formation of ectomesenchymal tissue[4,5]. Here we show that a significant population of mesenchymal stem cells during development, self-renewal and repair of a tooth are derived from peripheral nerve-associated glia. Glial cells generate multipotent mesenchymal stem cells that produce pulp cells and odontoblasts. By combining a clonal colour-coding technique[6] with tracing of peripheral glia, we provide new insights into the dynamics of tooth organogenesis and growth.

Shortly after the dental placode is induced, nerves intimately associate with the developing tooth[7]. To address whether glia-derived cells contribute to dental mesenchymal stem cells (MSCs) during tooth organogenesis, we used mouse strains allowing for permanent genetic labelling of multipotent[8,9] Schwann cell precursors (SCPs) and Schwann cells.

Proteolipid protein 1 (PLP1) and sex-determining region Y-box 10 (Sox10) are expressed in cranial neural crest, but after migration around embryonic days (E)9–10, they are retained in SCPs and not in mesenchyme[10,11]. SCPs at E11.5–12.5 express typical markers of Schwann cell lineage (Supplementary Information and Extended Data Fig. 1). *PLP-CreERT2* and *Sox10-CreERT2* mice[8,12] were therefore used for lineage tracing of SCPs. We controlled the specificity of PLP1 expression at E12.5 (Fig. 1a, b) and confirmed SCP-selective recombination in *PLP-CreERT2/R26YFP* mice by injecting tamoxifen at E12.5. Twenty-four hours later, traced cells expressing yellow fluorescent protein (YFP^+) were located along nerves (Fig. 1c, Supplementary Information and Extended Data Fig. 1m–p). CreERT2 protein was confined to $Sox10^+$ SCPs (Supplementary Information and Extended Data Fig. 1q–t). After tracing for 36 h, mesenchymal YFP^+/$CreERT2^-$ cells appeared close to nerves at the tooth site (Supplementary Information and Extended Data Fig. 2a–d). Induction of recombination at E12.5 and harvesting at E15.5–17.5 resulted in numerous traced cells along peripheral nerves and inside developing incisors (Fig. 1d–f, Supplementary Information and Extended Data Fig. 3a–g). YFP^+ cells formed streams towards the odontoblast layer in spatial coordination with YFP^+ odontoblasts (Fig. 1d). This was independently confirmed in *Sox10-CreERT2* embryos (Fig. 1i–k and Supplementary Information and Extended Data Fig. 3h–k). Sox10 is expressed in SCPs and not in mesenchyme at E12.5 and at E15.5 (Fig. 1g–h, Supplementary Information and Extended Data Figs 1a–c, g–k, q–s, 2e–o and 3l–n). YFP^+ pulp cells and odontoblasts formed the same pattern as seen with *PLP-CreERT2* tracing (Fig. 1i–k). Therefore, SCPs must contribute to pulp and odontoblasts since CreERT2 protein in *Sox10-CreERT2* and *PLP-CreERT2* embryos was confined to SCPs (Supplementary Information and Extended Data Figs 2a–d, m–p and 3c–k).

To examine if patches of SCP-derived odontoblasts and pulp cells have clonal structure, we crossed the *PLP-CreERT2* mice to the *R26RConfetti* reporter strain that allows for colour-encoded identification of clones[6]. This experiment revealed an organized clonal relationship between SCPs, pulp cells and odontoblasts (Supplementary Information and Extended Data Fig. 4a–d) and demonstrated that SCP-derived single MSCs produce pulpal and odontoblast fates (Supplementary Information and Extended Data Fig. 4e). We next examined whether ectomesenchyme-derived MSCs generate the same fates and patterns as SCP-derived MSCs. We induced recombination in neural crest at E8.5 in *PLP-CreERT2/R26RConfetti* strain, before segregation of CreERT2 expression into glial lineage. Recombination in both nerve-associated cells and ectomesenchyme was confirmed at E9.5 (Fig. 2a). When embryos were analysed at E17.5, it became apparent that ectomesenchyme- and SCP-derived MSCs generate the same fates and patterns in pulp and odontoblast layer (Fig. 2b–f).

To address whether Schwann cells generate MSCs also in adult growing incisors, we first confirmed that all $Sox10^+$ cells in the apical proliferative zone were nerve-associated (Supplementary Information and Extended Data Fig. 5) and expressed Schwann cell markers (Supplementary Information and Extended Data Fig. 6a–g). CreERT2 protein was found in the apex at nerve sites in *Sox10-CreERT2* and *PLP-CreERT2* teeth (Supplementary Information and Extended Data Fig. 6h–q). Additionally, expression of CreERT2 protein driven by the PLP-promoter was identified exclusively in a subpopulation of $Sox10^+$ Schwann cells (Supplementary Information and Extended Data Fig. 6j–q). Next, we used *PLP-CreERT2* and *Sox10-CreERT2* animals to analyse the progeny in growing incisors. We injected tamoxifen at postnatal day 60–85 and analysed the teeth 2–3 days later. Small numbers of YFP^+ cells appeared

[1]Department of Neuroscience, Karolinska Institutet, Stockholm 17177, Sweden. [2]Department of Dental Medicine, Karolinska Institutet, Stockholm 17177, Sweden. [3]Division of Molecular Neurobiology, MRC National Institute for Medical Research, London NW7 1AA, UK. [4]Department of Physiology and Pharmacology, Karolinska Institutet, Stockholm 17177, Sweden. [5]A.V. Zhirmunsky Institute of Marine Biology of the Far Eastern Branch of the Russian Academy of Sciences, Vladivostok 690041, Russia. [6]Unit of Molecular Neurobiology, Department of Medical Biochemistry and Biophysics, Karolinska Institutet, Stockholm 17177, Sweden. [7]Department of Craniofacial Development and Stem Cell Biology, King's College London Dental Institute, Guy's Hospital, London SE1 3QD, UK. [8]Department of Women's and Children's Health, Karolinska Institutet, Stockholm 17177, Sweden. [9]Science for Life Laboratory, Royal Institute of Technology, Stockholm 17177, Sweden. [10]Department of Biology, Institute of Molecular Health Sciences, ETH Zurich CH-8093, Switzerland. [11]Hubrecht Institute, Koninklijke Nederlandse Akademie van Wetenschappen (KNAW), PO Box 85164, 3508 AD Utrecht, the Netherlands. [12]Department of Molecular Genetics, University Medical Center Utrecht, Utrecht 3508 GA, the Netherlands. [13]Institute of Biotechnology, Developmental Biology Program, University of Helsinki, Helsinki FI-00014, Finland.

*These authors contributed equally to this work.

©2014 Macmillan Publishers Limited. All rights reserved

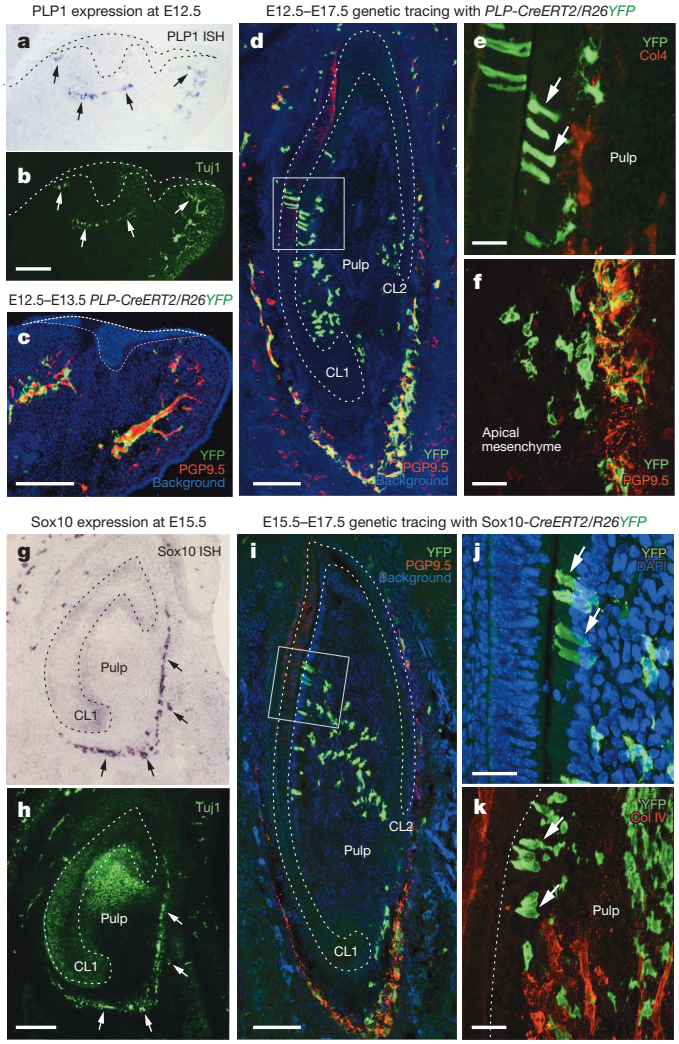

Figure 1 | SCPs give rise to pulp cells and odontoblasts in the developing tooth. **a**, **b**, *In situ* hybridization with PLP1 riboprobe (**a**) on a section of developing mandibular incisor at E12.5 post-stained for Tuj1 (β-III-tubulin)$^+$ nerves (**b**). Arrows indicate identical locations. **c**, Mandible of *PLP-CreERT2/R26YFP* embryo traced from E12.5 to E13.5. See Extended Fig. 2 for details. **d**–**f**, Incisor (**d**) traced from E12.5 to E17.5, *PLP-CreERT2/R26YFP* embryo. **e**, Magnified region from **d**. **f**, Nerve and apical mesenchyme, confocal stack. In **e**, arrows indicate odontoblasts. **g**, **h**, *In situ* hybridization with Sox10 riboprobe (**g**) on an E15.5 mandible post-stained for Tuj1$^+$ fibres (**h**). Arrows point at identical locations. **i**, **j**, Incisor at E17.5 (**i**) from *Sox10-CreERT2/R26YFP* embryo traced from E15.5. **j**, The area outlined in **i**; arrows indicate odontoblasts. **k**, E17.5 incisor from *Sox10-CreERT2/R26YFP* embryo traced from E15.5, confocal stack. Collagen IV labelling: blood vessels; YFP$^+$: pulp cells and odontoblasts (arrows). **a**–**k**, Dotted line: enamel organ. Scale bars, 100 μm (**a**–**d**, **g**–**i**); 25 μm (**e**, **f**, **j**, **k**). CL1 and CL2 indicate labial and lingual aspects of cervical loop.

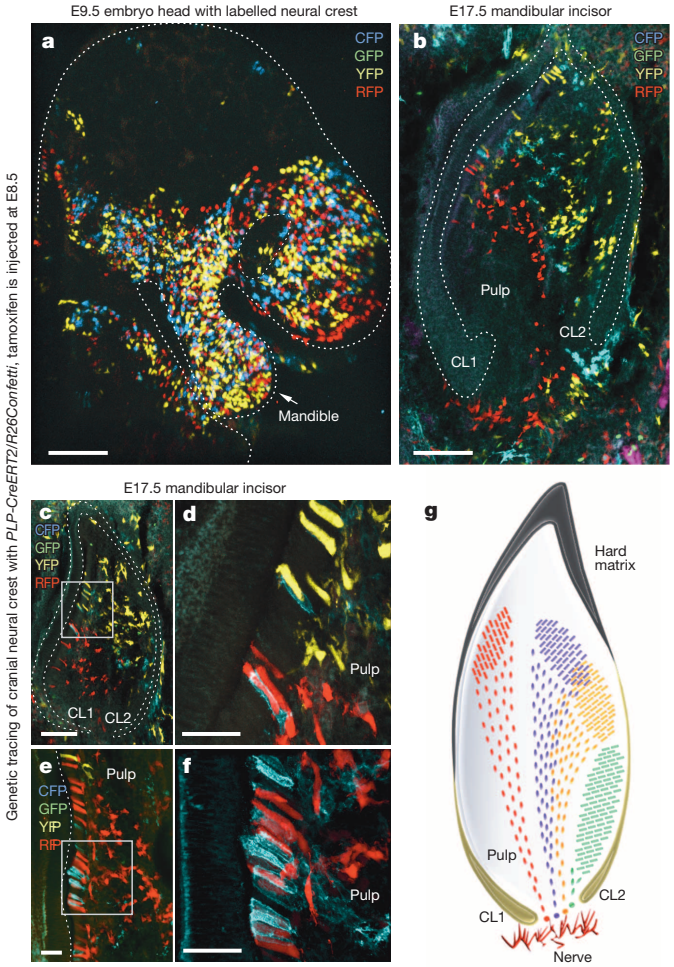

Figure 2 | Clonal contribution of neural crest to tooth development. **a**–**f**, Tracing of neural-crest-derived cells in *PLP-CreERT2/R26Confetti* embryos. **a**, Embryo traced from E8.5 to E9.5, projection of confocal stack. Dotted line demarcates developing head. Arrow: mandible. **b**–**f**, Sections of incisor traced from E8.5 to E17.5. **d**, **f**, Projections of stacks corresponding to areas outlined in **c** and **e**. Note correlation between colours of odontoblasts and adjacent pulp cells. **g**, Illustration of clonally organized pulp and odontoblasts. **b**, **c**, **e**, Dotted line: enamel organ. Scale bars, 100 μm (**a**–**c**); 25 μm (**d**–**f**). CL1 and CL2 indicate labial and lingual aspects of cervical loop.

adjacent to nerves in the apical incisor (Fig. 3a–c, Supplementary Information and Extended Data Fig. 7a–e). After 5 days YFP$^+$ cells at the apex increased in numbers (Supplementary Information and Extended Data Fig. 7f–h). The fates of the progeny were examined at times exceeding the incisor self-renewal (from 30 days after tamoxifen injection). We found that Schwann cells give rise to dental MSCs producing pulp cells and odontoblasts in adult teeth (Fig. 3d–f, Supplementary Information and Extended Data Fig. 7i–k).

Tracing in *PLP-CreERT2/R26RConfetti* mice demonstrated that streams of traced cells were connected to clusters of odontoblasts originating from same recombination events in Schwann cells (Fig. 3g–r, Supplementary Information and Extended Data Fig. 7i–k). The streams appeared increasingly dispersed as they approached odontoblasts labelled by the same colour (Fig. 3m). Clonal streams of pulp cells and odontoblasts intermingled at borders with non-labelled or different-coloured cells (Fig. 3l–p). MSCs produced high numbers of offspring, only a part of which was localized proximally to the dental epithelium and later became pre-odontoblasts. The majority of the progeny acquired a pulpal fate and formed organized streams, with earlier cells progressively displaced distally. Consequently, pulp cells and odontoblasts from the same clone remained associated during growth. These data suggest that progenies of several clones compete for the limited space at the inner surface of the cervical loop and, thus, for the odontoblast fate and final contribution. Indeed, the proportion of odontoblasts within the progeny of a single stem cell varied widely (Fig. 3s). Accordingly, the proximity of an MSC to the cervical loop correlated with the amount of odontoblast-fated progeny and may thus regulate the balance between odontoblast and pulp fates within a single clone (Fig. 3t). Additionally, streams originating closer to the cervical loop contained more cells and connected to larger clusters of odontoblasts than more central streams (Fig. 3q, t–v, Supplementary Information and Extended Data Fig. 8). Lastly, we found no support for a hypothesis that odontoblasts and pulp cells are generated from different pools of MSCs.

©2014 Macmillan Publishers Limited. All rights reserved

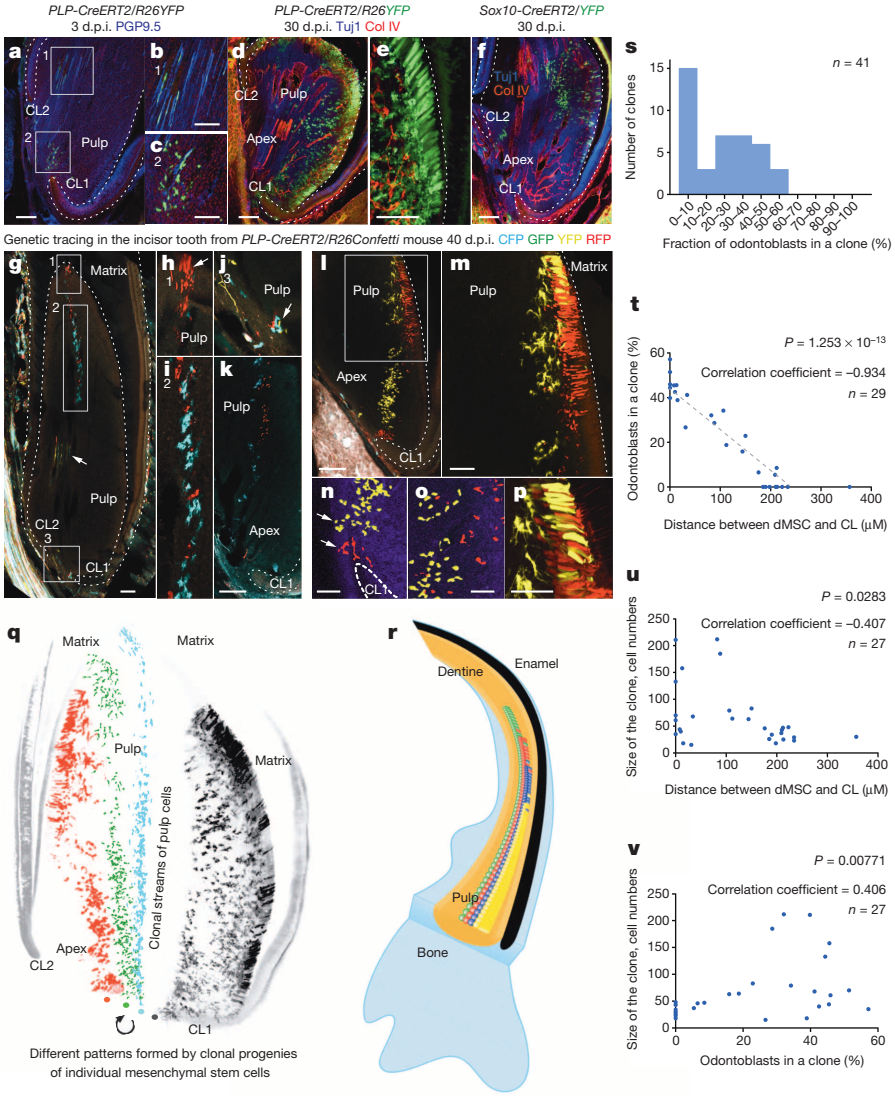

Figure 3 | Schwann cells give rise to dental MSCs in the adult incisor. **a**–**c**, Incisor traced for 3 days from adult *PLP-CreERT2/R26YFP* mouse. Note protein gene product 9.5 (PGP9.5)$^+$ nerve fibres (**a**). **b**, **c**, Magnified areas from **a**. **d**, **e**, Incisor traced for 30 days from adult *PLP-CreERT2/R26YFP* mouse. Note collagen IV$^+$ blood vessels (**d**). **e**, YFP$^+$ odontoblasts and adjacent pulp cells. **f**, Incisor traced for 30 days from *Sox10-CreERT2/R26YFP* mouse. **g**–**k**, Incisor traced for 40 days from *PLP-CreERT2/R26Confetti* incisor. **h**–**j**, Magnified areas from **g**. Arrow in **h** indicates a cluster of odontoblasts; arrow in **j** points at CFP$^+$ and RFP$^+$ cells in proximity to a cervical loop at the base of CFP$^+$ and RFP$^+$ streams shown in **g** and **i**. **k**, Streams of CFP$^+$ and RFP$^+$ pulp cells next to **i** and **j**. **l**, **m**, Incisor traced for 40 days from *PLP-CreERT2/R26Confetti* mouse with YFP$^+$ and RFP$^+$ pulp cells adjacent to clusters of odontoblasts with corresponding colours. **m**, Magnified region from **l**. **n**, Stream of pulp cells (arrows) in proximity to the cervical loop; yellow and red isosurfaces mark YFP$^+$ and RFP$^+$ cells. **o**, **p**, Progenies of individual MSCs intermingle with neighbouring clones in pulp (**o**) and odontoblast layer (**p**), projections of confocal stacks. **q**, **r**, Clonal organization of mesenchymal compartment in adult incisor. **a**–**n**, Dotted line, enamel organ and mineralized matrix. Scale bars, 100 μm (**a**, **d**, **f**, **g**, **k**, **l**); 50 μm (**b**, **c**, **e**, **m**–**p**). CL1 and CL2 indicate labial and lingual aspects of cervical loop. d.p.i., days post-injection. **s**, Incidence of mesenchymal clones depending on fraction of odontoblasts within the clone. **t**–**v**, Proximity of dental MSCs (dMSCs) to cervical loop (CL) correlates with clonal size and proportion of odontoblasts in clone.

To prove the importance of the innervation for tooth growth, we denervated incisors 24 h after tamoxifen injection in *PLP-CreERT2/R26YFP* mice. After 10 days we found almost no progeny in denervated teeth, while contralateral control teeth contained abundant YFP$^+$ odontoblasts and pulp cells (Supplementary Information and Extended Data Fig. 8j–p). Thus, generation of a progeny from PLP$^+$ cells is impaired without innervation.

We quantified the amount of Schwann-cell-derived progeny in *PLP-CreERT2/R26YFP* mice (Supplementary Information and Extended Data Figs 7l and 9a) and found that it varied from 8.23 ± 3.3% (single tamoxifen injection) to 47.28 ± 4.02% (multiple injections) (Supplementary Information and Extended Data Fig. 7m–o). Hence, in addition to Schwann cells and SCPs, there are other sources of dental MSCs, possibly pericytes, which generate odontoblasts in injured teeth[13]. We addressed whether pericytes could be derived from peripheral glia, using NG2 staining[14] on sections from traced mice. However, NG2$^+$ pericytes in teeth were never YFP$^+$. Similar results were obtained in adult incisors (Supplementary Information and Extended Data Fig. 10). Thus, we exclude pericytes as an intermediate for the Schwann-cell- and SCP-derived pulp cells and odontoblasts.

Next we searched for stem cell markers in Schwann-cell-derived dental MSCs. Results from an array of methods strongly suggest that a population of Schwann-cell-derived dental MSCs are Thy1 (CD90)$^+$ (Supplementary Information, Extended Data Fig. 9 and Supplementary Video 1).

Finally, we examined if Schwann-cell-derived cells produce regenerative dentine after trauma. We induced recombination in adult *PLP-CreERT2/R26YFP* mice, and allowed Schwann cells to generate progeny for 1 month. We then inflicted a confined damage to the tooth (Fig. 4a). Six days later, numerous traced cells were observed at the injury site, including odontoblast-like alizarin-red-positive cells adjacent to matrix fragments (Fig. 4b–f). Such features were not seen in intact teeth (Fig. 4g–h) or other controls (Fig. 4i). To confirm that *PLP-CreERT2*-traced cells produce mineralized matrix, we cultured dissociated traced tooth pulp explants for 1 week. YFP$^+$ cells were then sorted by fluorescence-activated cell sorting (FACS) for cultivation in an osteogenic assay (Fig. 4j). Under these conditions, YFP$^+$ cells deposited mineralized matrix (Fig. 4k–l). Thus, Schwann-cell-derived cells exhibit MSC-like characteristics and participate in the regeneration of dentine after damage.

To conclude, SCPs and Schwann cells contribute to development, growth and regeneration of teeth. The concept of glia-to-MSC transition expands the borders of the multipotency of SCPs[15] and suggests that Schwann cells and SCPs are dormant neural-crest-like cells that can be recruited from nerves and contribute to peripheral tissues. On the basis of our results, Schwann cells and SCP might be the *in vivo* origin of neural-crest-derived multipotent stem cells identified in cultures of dissociated embryonic and adult tissues and designated as postmigratory cranial neural crest cells[16] and skin-derived precursors[17].

©2014 Macmillan Publishers Limited. All rights reserved

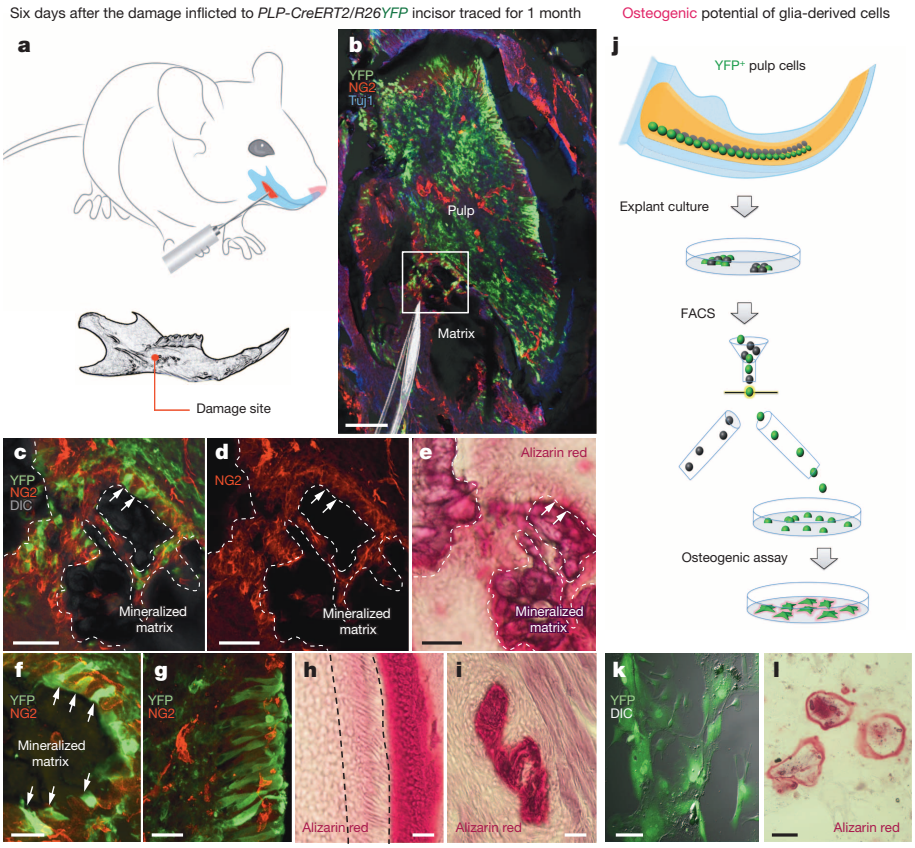

Figure 4 | Schwann-cell-derived cells participate in regeneration of incisors after damage. **a**, Damage to 1-month traced *PLP-CreERT2/R26YFP* adult incisor. Red highlights the injured region. **b**–**e**, YFP$^+$ cells at the injury site, after recovery for 6 days. Needle silhouette shows direction of damage. **c**, **d**, Magnified area from **b**, confocal stack. **e**, Alizarin red staining of damaged region outlined in **b**. Note stained area around ectopic matrix. Arrows in **c**–**e** point at YFP$^+$ cells adjacent to ectopic matrix; dotted line indicates mineralized matrix. **f**, Ectopic matrix in damaged area with YFP$^+$ odontoblast-like cells (arrows). **g**, YFP$^+$ odontoblasts and NG2$^+$ pericytes in intact control incisor. **h**, Alizarin red staining of the odontoblast layer in control. **i**, Matrix fragment from damaged incisor displaced into facial muscle. Note absence of alizarin red staining around matrix fragment compared with ectopic matrix within the pulp (**e**). **j**, Experimental design for addressing mineralizing potential of Schwann-cell-derived cells. **k**, **l**, Mineralization assay. Schwann-cell-derived YFP$^+$ cells (**k**) produce alizarin red$^+$ matrix (**l**) *in vitro* after 1 week in osteogenic media. **k**, DIC, differential interference contrast. Scale bars, 100 μm (**b**); 50 μm (**c**–**e**); 25 μm (**f**–**l**).

METHODS SUMMARY

We used *PLP-CreERT2/R26YFP*[9,12], *Sox10-CreERT2/R26YFP*[8], *Thy1-Cre/R26YFP*[18] and *R26Confetti*[6] mouse strains. Immunohistochemistry and *in situ* hybridization used standard protocols on frozen sections of embryos or adult teeth. Multispectral imaging used Zeiss LSM700 and Zeiss LSM780 confocal systems[11].

Online Content Methods, along with any additional Extended Data display items and Source Data, are available in the online version of the paper; references unique to these sections appear only in the online paper.

Received 22 August 2013; accepted 28 May 2014.
Published online 27 July 2014.

1. Keating, A. Mesenchymal stromal cells: new directions. *Cell Stem Cell* **10,** 709–716 (2012).
2. Koussoulakou, D. S., Margaritis, L. H. & Koussoulakos, S. L. A curriculum vitae of teeth: evolution, generation, regeneration. *Int. J. Biol. Sci.* **5,** 226–243 (2009).
3. Zhao, H. *et al.* Secretion of shh by a neurovascular bundle niche supports mesenchymal stem cell homeostasis in the adult mouse incisor. *Cell Stem Cell* **14,** 160–173 (2014).
4. Caton, J. & Tucker, A. S. Current knowledge of tooth development: patterning and mineralization of the murine dentition. *J. Anat.* **214,** 502–515 (2009).
5. Miletich, I. & Sharpe, P. T. Neural crest contribution to mammalian tooth formation. *Birth Defect Res C* **72,** 200–212 (2004).
6. Snippert, H. J. *et al.* Intestinal crypt homeostasis results from neutral competition between symmetrically dividing Lgr5 stem cells. *Cell* **143,** 134–144 (2010).
7. Luukko, K. *et al.* Secondary induction and the development of tooth nerve supply. *Ann. Anat.* **190,** 178–187 (2008).
8. Laranjeira, C. *et al.* Glial cells in the mouse enteric nervous system can undergo neurogenesis in response to injury. *J. Clin. Invest.* **121,** 3412–3424 (2011).
9. Adameyko, I. *et al.* Schwann cell precursors from nerve innervation are a cellular origin of melanocytes in skin. *Cell* **139,** 366–379 (2009).
10. Hari, L. *et al.* Temporal control of neural crest lineage generation by Wnt/beta-catenin signaling. *Development* **139,** 2107–2117 (2012).
11. Adameyko, I. *et al.* Sox2 and Mitf cross-regulatory interactions consolidate progenitor and melanocyte lineages in the cranial neural crest. *Development* **139,** 397–410 (2012).
12. Leone, D. P. *et al.* Tamoxifen-inducible glia-specific Cre mice for somatic mutagenesis in oligodendrocytes and Schwann cells. *Mol. Cell. Neurosci.* **22,** 430–440 (2003).
13. Feng, J., Mantesso, A., De Bari, C., Nishiyama, A. & Sharpe, P. T. Dual origin of mesenchymal stem cells contributing to organ growth and repair. *Proc. Natl Acad. Sci. USA* **108,** 6503–6508 (2011).
14. Crisan, M., Corselli, M., Chen, W. C. & Peault, B. Perivascular cells for regenerative medicine. *J. Cell. Mol. Med.* **16,** 2851–2860 (2012).
15. Adameyko, I. & Lallemend, F. Glial versus melanocyte cell fate choice: Schwann cell precursors as a cellular origin of melanocytes. *Cell. Mol. Life Sci.* **67,** 3037–3055 (2010).
16. Chung, I. H. *et al.* Stem cell property of postmigratory cranial neural crest cells and their utility in alveolar bone regeneration and tooth development. *Stem Cells* **27,** 866–877 (2009).
17. Jinno, H. *et al.* Convergent genesis of an adult neural crest-like dermal stem cell from distinct developmental origins. *Stem Cells* **28,** 2027–2040 (2010).
18. Dewachter, I. *et al.* Neuronal deficiency of presenilin 1 inhibits amyloid plaque formation and corrects hippocampal long-term potentiation but not a cognitive defect of amyloid precursor protein [V717I] transgenic mice. *J Neurosci.* **22,** 3445–3453 (2002).

Supplementary Information is available in the online version of the paper.

Acknowledgements P. Kovaleva and O. Rogachevskaya helped with illustrations. This study was supported by the Swedish Research Council (I.A., K.F., P.E.), The Bertil Hållsten Research Foundation (I.A.), StratRegen and the Wallenberg Foundation (CLICK, I.A.), the Swiss National Science Foundation (U.S.), Medical Research Council (G0901599; P.S.), a Wallenberg Scholar and European Research Council advanced grant (P.E.), National Graduate School in Odontological Science (M.K.S.), the Swedish Dental Association (N.K., M.K.S.), an EMBO Long-Term Fellowship (M.K.) and Stockholm County Council (N.K.) and Developmental Studies Hybridoma Bank.

Author Contributions N.K., M.K.S., C.K., V.D., M.K., A.F., Z.A., L.W., P.S., I.H., I.A. and K.F. performed experiments, analysed data and wrote the paper. L.A.-R., H.B., H.B., N.A.L., V.P., U.S., H.C., P.S., I.T. and P.E. analysed data and wrote the paper. All authors read and approved the paper.

Author Information Reprints and permissions information is available at www.nature.com/reprints. The authors declare no competing financial interests. Readers are welcome to comment on the online version of the paper. Correspondence and requests for materials should be addressed to I.A. (Igor.Adameyko@ki.se) or K.F. (Kaj.Fried@ki.se).

©2014 Macmillan Publishers Limited. All rights reserved

METHODS

Mouse strains and animal information. All animal work was permitted by the Ethical Committee on Animal Experiments (Stockholm North Committee) and conducted according to The Swedish Animal Agency's Provisions and Guidelines for Animal Experimentation recommendations. Glia-specific genetic tracing mouse strains *PLP-CreERT2/R26YFP*[12], *Sox10-CreERT2/R26YFP*[8] and *Thy1-Cre/R26YFP*[18] (Jackson Laboratory stock number 006143) were used in this study. *R26Confetti*[6] mice were received from the laboratory of H. Clevers. To induce genetic recombination, pregnant females were injected intraperitoneally with tamoxifen (Sigma T5648) dissolved in corn oil (Sigma C8267). A range of tamoxifen concentrations (1.5–5 mg per animal) was used to gain different efficiency of genetic tracing. Mice were killed with isoflurane (Baxter KDG9623) overdose and perfused with PBS and then with 4% paraformaldehyde (Merck 818715) before collection of adult teeth. The tissue was additionally fixed for 3 h in 4% paraformaldehyde at 4 °C on a rocking table, cryopreserved in 30% sucrose (VWR C27480) overnight at 4 °C, embedded in OCT media (HistoLab 45830) and cut into 14 μm or 30 μm sections on a cryostat (Microm). All animal work was done according to the high international ethical standards applied in Sweden and approved by the ethical committee at Stockholm Norra Djurförsöksetiska Nämd.

Staining procedures and *In situ* hybridization. Immunohistochemistry used standard protocol on 14 μm sagittal frozen sections of the embryonic heads, and 30 μm sections of the adult teeth. Antigen retrieval with Dako solution (Dako S1699) and quenching by peroxidase treatment (Merck 1072090500) were done before application of primary antibodies to reduce background fluorescence. Primary antibodies were applied to the tissue and incubated at room temperature (21 °C) overnight. Primary antibodies were CD13 (BD Pharmingen 558745, 1:300), PECAM-1/CD31 (BD Pharmingen 553370, 1:200), collagen IV (AbD Serotec 2150-1470, 1:500), NG2 (Millipore AB5320, 1:200), PGP9.5 (Cederlane CL95101, 1:500), SOX10 (Santa Cruz sc-17342, 1:500), CRE (Novagen 69050, 1:500), green fluorescent protein (GFP; Abcam ab6662, 1:500), 2H3 (generated by Developmental Studies Hybridoma Bank, provided by F. Lallemend, 1:100), BFABP (generated by T. Müller, 1:1,000), Krox20 (Nordic Biosite AB, 1:500), Tuj1 (Promega G712A, 1:1,000), S100β (DAKO A5110, 1:1,000), p-c-Jun (Santa Cruz sc-822, 1:200), Ki67 (Thermo Scientific RM-9106-S1, 1:1,000), GFAP (Abcam ab7260, 1:300), Thy1 (Abcam ab3105, 1:500), P75 (Promega G323A, 1:500), P0 (Abcam 134439, 1:1,000), MBP (Abcam ab7349, 1:200) and ErbB3 (R&D AF4518, 1:500). Alexa secondary antibodies (Invitrogen, 1:800–1:1,000) were used and slides were mounted with glycerol mounting media (Merck 1040942500). Additional stainings were done with 4′,6-diamidino-2-phenylindole (DAPI; Invitrogen D1306, 300 nM applied for 1–5 min at room temperature) and Alizarin red (Sigma A5533, 2% in distilled H_2O applied for 30 s to 3 min).

In situ hybridization on sections was done as previously described[9]. *Plp1* probe corresponded to the open reading frame of PLP1 protein with National Center for Biotechnology Information (NCBI) accession number NM_011123. *Sox10* probe was a gift from T. Müller. Embryo heads were fixed in 4% paraformaldehyde for 2 h and then rinsed in 30% sucrose overnight at 4 °C. Subsequently, the samples were immersed in OCT and kept at −20 °C until sectioning. Images were taken with Carl Zeiss Axioplan 2 light microscope.

Thy1 antisense probes were generated from 2.3 kilobase complementary DNA fragment sequences cloned into pCMV-SPORT6 vector and transcribed in the presence of digoxigenin-labelled UTP, using Kpn1/T7 DIG RNA labelling kit (Roche). Whole-mount digoxigenin-labelled *in situ* hybridization was performed on 5-day postnatal CD1 pups. Incisor samples after whole-mount *in situ* hybridization were embedded in 1% low-melting-point agarose, dehydrated in methanol and cleared in BABB (two parts benzyl benzoate to one part benzyl alcohol) before optical projection tomography scanning. Optical projection tomography scanning was performed using a Bioptonics 3001 OPT scanner (Bioptonics). Reconstructed images were generated using NRecon version 1.6.1.0 (Skyscan) software and further assessed using a Bioptonics viewer version 2.0 (Bioptonics).

Tooth damage. Tamoxifen (5 mg) was administered once a day for two consecutive days to the adult *PLP-CreERT2/R26YFP* animals before a tracing period of 4 weeks, which allowed tracing of both the glia-derived progenitor cells and their progeny forming streams in the dental pulp. Traced mice were anaesthetized by intraperitoneal injection of a combinational drug consisting of 75 mg per kg ketamine (Ketaminol, Intervet 511485) and 1 mg per kg medetomidinhydrochlorid (DormitorVet, OrionPharma 015602) prepared in sterile water for injection (Braun 12250031). The fine damage to the mandibular incisor was done with a syringe needle (BD Microlance 3, 25 gauge × 5/8, 0.5 mm × 16 mm) on the left side by inserting the needle from the outside through the masseter muscle while the contralateral side was kept untouched and used as an internal control. To prevent or minimize postoperative pain, 0.08 mg per kg Tamgesic (Tamgesic 086188) dissolved in sterile saline was injected intramuscularly before the animal was given the antidote (AntisedanVet, OrionPharma 471953) by subcutaneous injection. Six days after the operation, mandibular teeth were collected from the damaged and the contralateral sites.

Explant culture, cell sorting and osteogenic culture. *PLP-CreERT2/R26YFP* mice were injected with 5 mg tamoxifen and traced for 1 month before being killed with an overdose of isoflurane. All incisor teeth were harvested and the tooth pulps were extracted, cut into pieces and seeded as explants in 24-well plates (BD Falcon) at 37 °C with 5% CO_2. The culture medium was composed of Gibco MEM α culture medium with GlutaMAX, 20% fetal bovine serum (FBS, Gibco), 55 nM 2-β-mercaptoethanol (Gibco) and 1× penicillin/streptomycin solution (Gibco), which was changed two or three times during a week. After 1 week of explant culture, cells were harvested for cell sorting. Cells were washed with Dulbecco's phosphate buffered saline (DPBS, Gibco), treated with TrypLE Express (Gibco), centrifuged to obtain cell pellets which were re-suspended in DPBS with 1% FBS and passed through 40 μm cell strainers (BD Falcon). The cells were then sorted with gating for enhanced YFP in a BD FACSAria II cell sorter. YFP^+ cells were then further propagated up to 60% of confluency and consequently directed into osteogenic lineage with the application of a StemPro Osteogenesis differentiation kit and protocol (Gibco). Osteogenic cultures were analysed after 7 days. Cells were fixed with 4% paraformaldehyde for 10 min, washed with distilled H_2O and stained with DAPI nucleic acid stain (Invitrogen). Thereafter, cultures were stained with 40 mM Alizarin R solution (Sigma-Aldrich) following several intensive washes with distilled H_2O.

Denervation. Adult male and female *PLP-CreERT2/R26YFP* mice (weighing 25–30 g) were injected with 5 mg tamoxifen and traced for 24 h before unilateral denervation. The contralateral undamaged mandibular site was used as control. Traced mice were anaesthetized by intraperitoneal injection of a combinational drug consisting of 75 mg per kg ketamine and 1 mg per kg medetomidinhydrochlorid prepared in sterile water for injection. Then 0.08 mg per kg Tamgesic dissolved in sterile saline solution was injected intramuscularly. When anaesthetized and sedated, the eyes of the animals were covered with eye gel (Oculentum simplex APL 336164). The operation site was sterilized with ethanol, and a 15 mm incision of the facial skin over the right masseter muscle was made. The mandibular bone surface was then exposed through a careful blunt dissection of the muscle. Care was taken not to damage the superficial muscle branches of the facial (VII) nerve. The thin bone layer covering the mandibular canal cranial to the incisor apex was carefully removed and the inferior alveolar nerve was exposed and transected with microscissors. Finally, muscle and cutaneous tissue were sutured. To awaken the animals, AntisedanVet (OrionPharma 471953) was given by subcutaneous injection. Wet food was administered to the animals during the survival period. The mice were monitored twice a day and given Tamgesic for pain relief every 12 h for the first 3 days and then once a day thereafter until they were fully recovered. Subsequently, they were continuously monitored. After 10 days, 4% paraformaldehyde perfusion was performed, and both mandibular incisors were then dissected out and processed for microscopy.

Flow cytometry. Dental pulps were obtained from the incisors of *PLP-CreERT2/R26YFP* animals, where the genetic tracing was induced during adulthood for a period of 4 weeks or longer. For each experiment, eight dental pulps were incubated by shaking at 225 r.p.m. in a mixture of collagenase/dispase (2.5 mg ml^{-1}; Roche 11097113001) dissolved in 1× TrypLE Express (Gibco) for 1 h at 37 °C. After the enzymatic dissociation, cells were sorted using a cell strainer and washed in PBS. For subsequent staining, cells were used either live or fixed in cold methanol (45 min on ice followed by wash with PBS) depending on the applied antibody. Cell suspension was first incubated with primary antibodies in PBS at a concentration of 4 μg ml^{-1} (anti-Thy1, anti-Ki67, anti-GFP) for 45–60 min on ice and washed with PBS afterwards. Secondary antibodies diluted 1:1,000 in PBS (Alexa Fluor 405, 488 and 647; Life Technologies) were applied to the cell suspension for 45 min on ice, protected from light and then washed with PBS. Flow-cytometry analysis used FACSCantoII and BD FACSDiva 6.1.3 software. Each experiment with a given staining combination was performed in triplicate and controlled by using unstained sample and corresponding unspecific IgG-stained (4 μg $m1^{-1}$, Santa Cruz) sample.

BrdU and EdU incorporation analysis. BrdU was injected once or every day for 3 weeks at a concentration of 200 μg per g body weight. Mice were then killed after different periods (8 h, 24 h, 32 days, 64 days) and the tissue was sampled. Immunostaining and detection of BrdU was done according to a standard protocol (Abcam BrdU Immunohistochemistry Kit ab125306). Genetic tracing with label-retaining assay (Supplementary Fig. 13e–j): *PLP-CreERT2/R26YFP* mice were injected with 5 mg tamoxifen twice within two sequential days. After 7 months of genetic tracing, five injections of EdU (65 μg per g body weight, every 48 h) were performed. Seventy-one days after the last EdU-injection, the animals were killed and tissue was harvested. EdU flow cytometry assay for the slow cycling cells labelling *in vivo* (Supplementary Fig. 13k–m): 5-day postnatal CD1 pups were continually given EdU injections (3.3 μg per g body weight) for 3 weeks and washed out for another 3 weeks before collection. The incisor pulp cells were freshly collected and EdU staining for flow cytometry was performed according to the manual (Invitrogen).

©2014 Macmillan Publishers Limited. All rights reserved

Thy1-FITC antibody (Ebioscience) was incubated with cells for 10 min at room temperature before cell fixation and EdU detection. A BD Fortessa cell analyser (BD Biosciences) was used with FACSDIVA software for acquisition and Flowjo software for analysis. EdU-Alexa647, Thy1-FITC and DAPI were detected with laser 633 nm, 488 nm and 351 nm excitation and with emission filter 670/30 nm, 530/30 nm and 450/50 nm respectively.

Cell counting and statistics. Statistical data are represented as mean ± s.e.m. Unpaired and paired versions of Student's *t*-test were used to calculate the statistics (*P* value). Pearson's product-moment correlation coefficient (*r*) was calculated to investigate the association of variables in Fig. 3t–v ($n = 29$ for Fig. 3t–u and $n = 27$ for Fig. 3v). Every value corresponding to a dot refers to a single clone; in total, clones were analysed from 11 different animals. Linear regression was used to build an approximation line in Fig. 3t. To analyse the position of dental MSCs in relation to the cervical loop (Fig. 3t–u), multiple sequential sections were analysed. Generally, we devoted several (always more than three) animals to every experiment to accomplish at least a biological triplicate. This was valid for all non-quantitative analyses including work done on sections or in a whole mount. For the genetic tracing experiments reported as graphical panels, at least six embryos derived from at least two females were analysed; in most cases 15–20 embryos were used before conclusions and supporting graphics were generated. During our study more than 100 genetically traced animals of different strains were analysed before concluding final results. The animals were selected and distributed into groups in all experiments randomly. The control for the denervation experiment was an internal control coming from the same animal: the non-operated contralateral side (biological (number of individual animals) $n = 5$, while technical (number of sections analysed) $n = 15$). To quantify the contribution from Schwann-cell-derived MSCs, we analysed three animals per condition counting three sections in every animal (technical $n = 9$). YFP^+ cells and $DAPI^+$ cell nuclei inside the tooth were identified on confocal images, segmented in IMARIS software and counted in a semi-automated way.

Microscopy and imaging. Confocal microscopy used Zeiss LSM700 CLSM and Zeiss LSM780 CLSM instruments. Image processing and analysis used ZEN2010 and Imaris software. The settings for the imaging of Confetti fluorescent proteins were previously described[6]. For Fig. 2a the imaging of the confocal stack was done with a Zeiss LSM780 CLSM, Plan-Apochromat ×10/0.45 M27 Zeiss air objective, 23 optical slices of 12 μm each with the *z*-axis shift of 12 μm for every step. For Supplementary Fig. 1a–c the whole-mount staining, imaging and reconstruction of an embryo were done with instruments, objectives and software according to a published protocol[11].

©2014 Macmillan Publishers Limited. All rights reserved

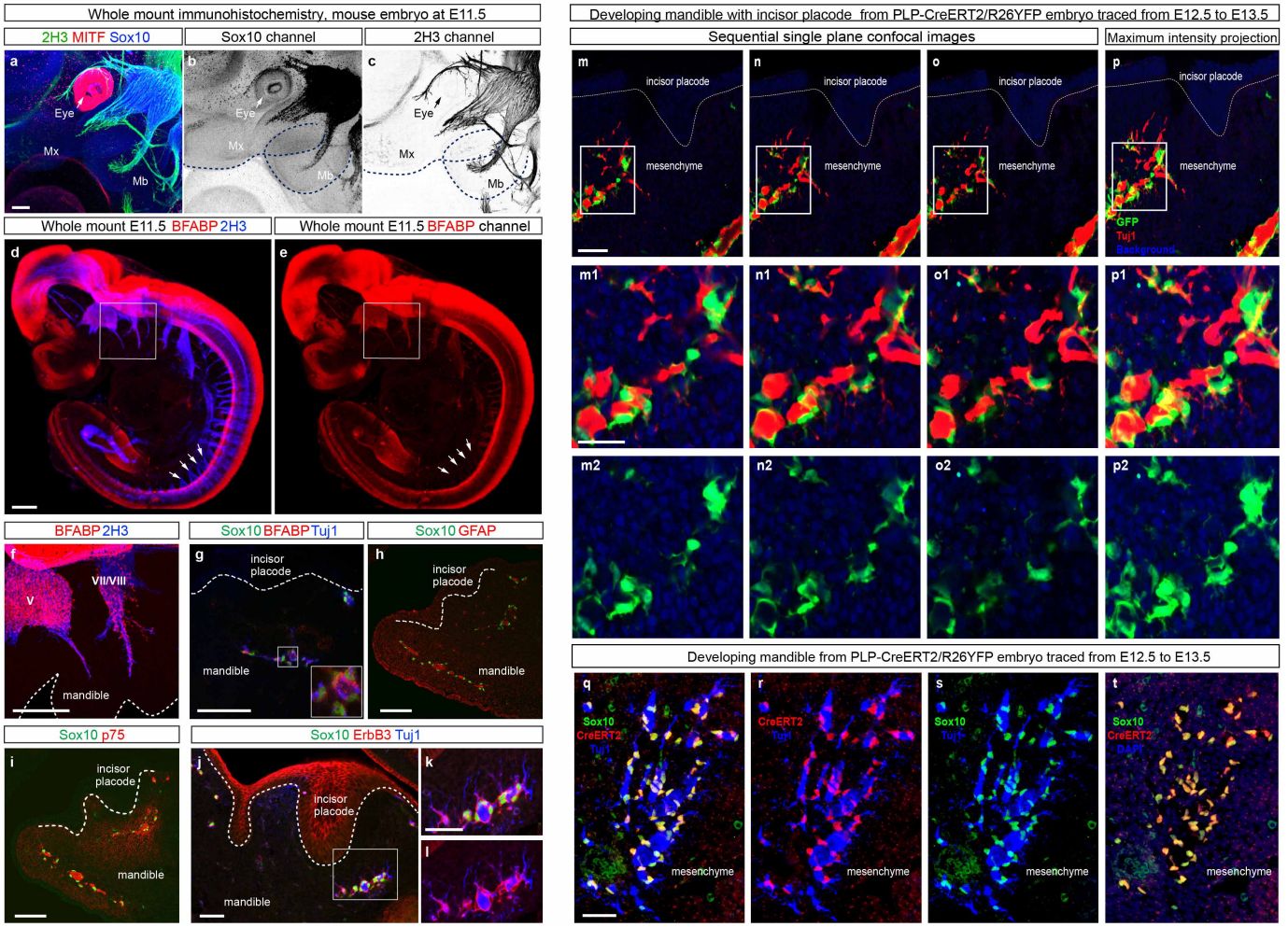

Extended Data Figure 1 | Expression of SCP markers and genetic tracing in nerves of E11.5–13.5 embryos. **a**–**c**, Whole-mount immunohistochemistry performed on an E11.5 mouse embryo with antibodies against 155 kDa neurofilaments (2H3), MITF and Sox10. Note that Sox10$^+$ cells are localized at the nerves in maxillary and mandibular regions. **d**–**f**, Whole-mount immunohistochemistry performed on an E11.5 mouse embryo with antibodies against 155 kDa neurofilaments (2H3) and BFABP. **d**–**e**, Arrows point at posterior ventral spinal nerves hosting immature embryonic glial cells that lack BFABP expression. **f**, Magnified area outlined in **d** by white rectangle. Roman digits show corresponding numbers of cranial ganglia. Dotted line follows the contour of an embryo. **g**–**l**, Sagittal section through E12.5 mandible stained for Sox10 (**g**–**l**), Tuj1 and BFABP (**g**), GFAP (**h**) and p75 (**i**). **j**–**l**, ErbB3 is expressed in all Sox10$^+$ nerve-adjacent SCPs. **k**–**l**, Magnified area outlined by white rectangle in **j**. Dotted line indicates epithelial organ. **m**–**o2**, Sagittal section through E13.5 mandible, sequential single plane optical slices 2 μm in *z*-axis. $\mathbf{m_1}$–$\mathbf{m_2}$, Magnified area outlined in **m**; $\mathbf{n_1}$, $\mathbf{n_2}$, magnified area from **n**; $\mathbf{o_1}$–$\mathbf{o_2}$, respectively, show an area from **o**. **p**–$\mathbf{p_2}$, Region on a section shown in **m**–**o**, maximum intensity projection image. $\mathbf{p_1}$, $\mathbf{p_2}$, Magnified area that is outlined by white rectangle in **p**. **m**–**p**, White dotted line indicates incisor placode. **q**–**t**, Expression of CreERT2, Sox10 and Tuj1 in a mandible traced from E12.5 to E13.5 in *PLP-CreERT2* embryo. Note the full co-localization of Sox10 and CreERT2. Sox10$^+$/CreERT2$^+$ cells are adjacent to the innervation. Scale bars, 100 μm (**a**–**c**, **g**–**i**); 500 μm (**d**–**f**); 50 μm (**j**–**l**); 50 μm (**m**–**t**).

©2014 Macmillan Publishers Limited. All rights reserved

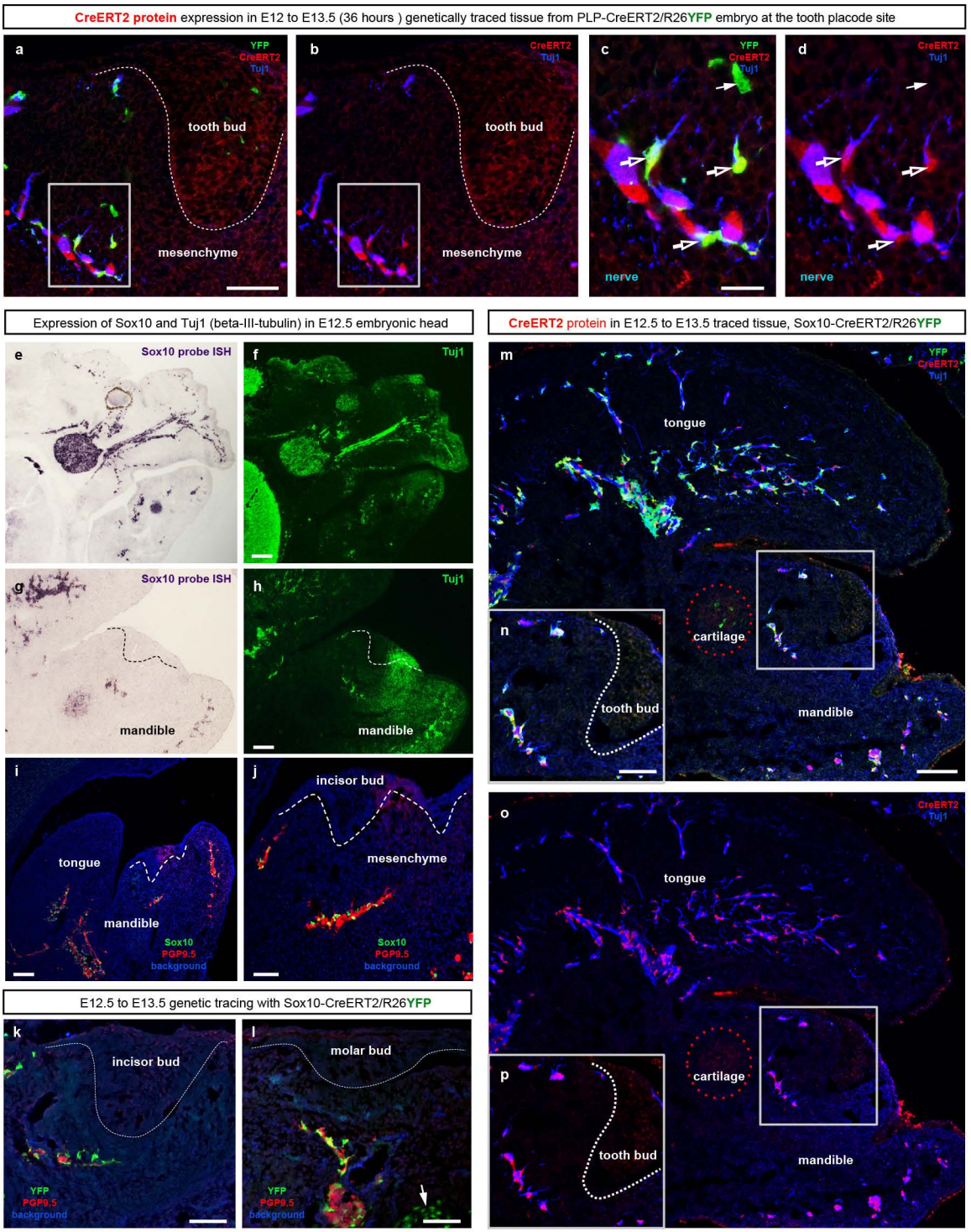

Extended Data Figure 2 | Expression of Sox10, YFP and CreERT2 in a genetically traced mouse embryonic head. **a**–**d**, Expression of CreERT2 protein in a 36 h genetically traced *PLP-CreERT2/R26YFP* embryo at E13.5. **c**, **d**, Magnified areas outlined in **a** and **b**. Open arrows point at CreERT2^{+}/YFP^{+} cells attached to the nerve whereas filled arrow points at CreERT2^{-}/YFP^{+} cell proximal to the nerve. **e**, **f**, *In situ* hybridization with Sox10 riboprobe (**e**) on a section of a mouse embryonic E12.5 head post-stained with Tuj1 (β-III-tubulin, neuronal marker) antibody (**f**). **g**–**h**, *In situ* with Sox10 probe on a section of E12.5 developing mandible (**g**) with incisor tooth bud (outlined by dotted line) post-stained with Tuj1 antibody (**h**). **i**–**j**, Sox10 and PGP9.5 (marker for neurites) are visualized by immunohistochemistry on a section of an embryonic mandible at E12.5. Dotted line outlines incisor bud. **k**–**l**, Sections of developing mandible with incisor (**k**) and molar (**l**) buds from a *Sox10-CreERT2/R26YFP* embryo genetically traced from E12.5 to E13.5 and stained with antibody against the neuronal marker PGP9.5. Arrow in **l** points at developing cartilage. **m**–**p**, Expression of CreERT2 protein in a 24 h genetically traced *Sox10-CreERT2/R26YFP* embryo at E13.5. The developing Meckel's cartilage is outlined by the red dotted circle in **m** and **o**. **n**, **p**, Magnified areas outlined in **m** and **o**. White dotted line shows the borders of tooth bud. Scale bars, 200 μm (**e**–**h**); 100 μm (**i**, **m**, **o**); 50 μm (**a**, **b**, **j**–**l**, **n**–**p**); 10 μm (**c**–**d**).

©2014 Macmillan Publishers Limited. All rights reserved

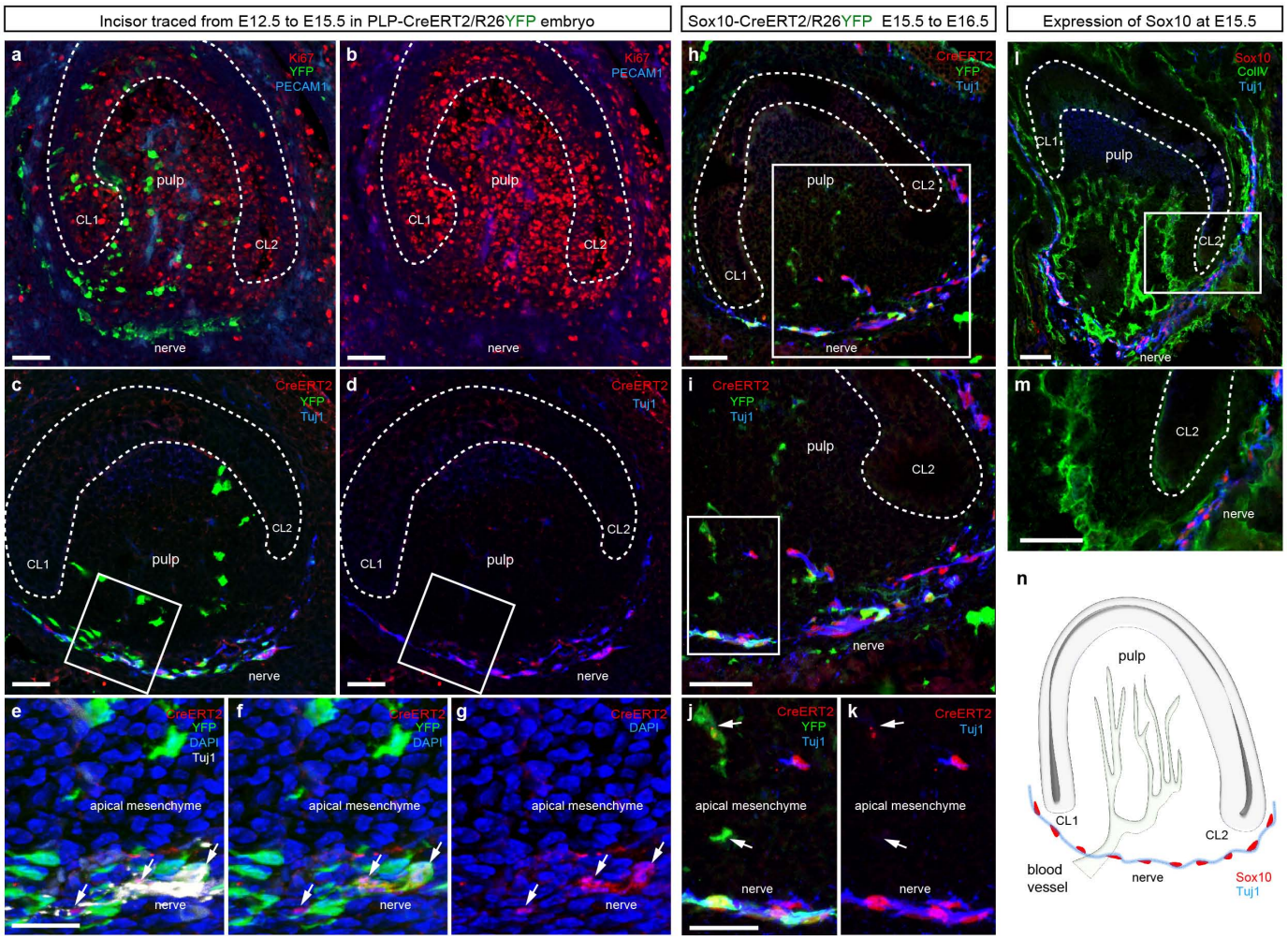

Extended Data Figure 3 | Expression of Sox10 and CreERT2 at intermediate stages of incisor development. **a**–**g**, Incisor traced from E12.5 to E15.5 in *PLP-CreERT2/R26YFP* animals. Enamel organ is outlined by dotted line. **a**, **b**, YFP^+ cells in the nerve and in the pulp are shown together with Ki67 staining. **c**–**g**, Note that the expression of CreERT2 is confined to nerve sites only, as shown in low (**c**, **d**) and high (**e**–**g**) magnification images of developing incisor. **e**–**g**, Area from **c**, **d** shown at high magnification. $YFP^+/CreERT2^+$ cells are indicated by arrows in **e**–**g**. Note the presence of $CreERT2^-/YFP^+$ proximally to the nerve and in the apical mesenchyme. **h**–**k**, Incisor traced from E15.5 to E16.5 in *Sox10-CreERT2/R26YFP* animals. Panel **i** represents a magnified area from **h**. **j**, **k**, Magnified area outlined by white rectangle in **i**. Arrows in **j** and **k** point at $CreERT2^-/YFP^+$ cells in the apical mesenchyme; note that the expression of CreERT2 is confined to the nerve sites only. **l**–**m**, Developing incisor at E15.5 stained with antibodies against Sox10 to show SCPs, Tuj1 to visualize nerves and Col IV to outline the position of vessels. Note that all $Sox10^+$ cells are nerve adjacent. **n**, Schematic drawing showing the position of $Sox10^+$ cells during early bell stage of tooth development. Scale bars, 50 μm (**a**–**d**, **h**, **i**, **l**, **m**); 25 μm (**e**–**g**, **j**, **k**). CL1 and CL2 are the labial and lingual aspects of the cervical loop respectively.

©2014 Macmillan Publishers Limited. All rights reserved

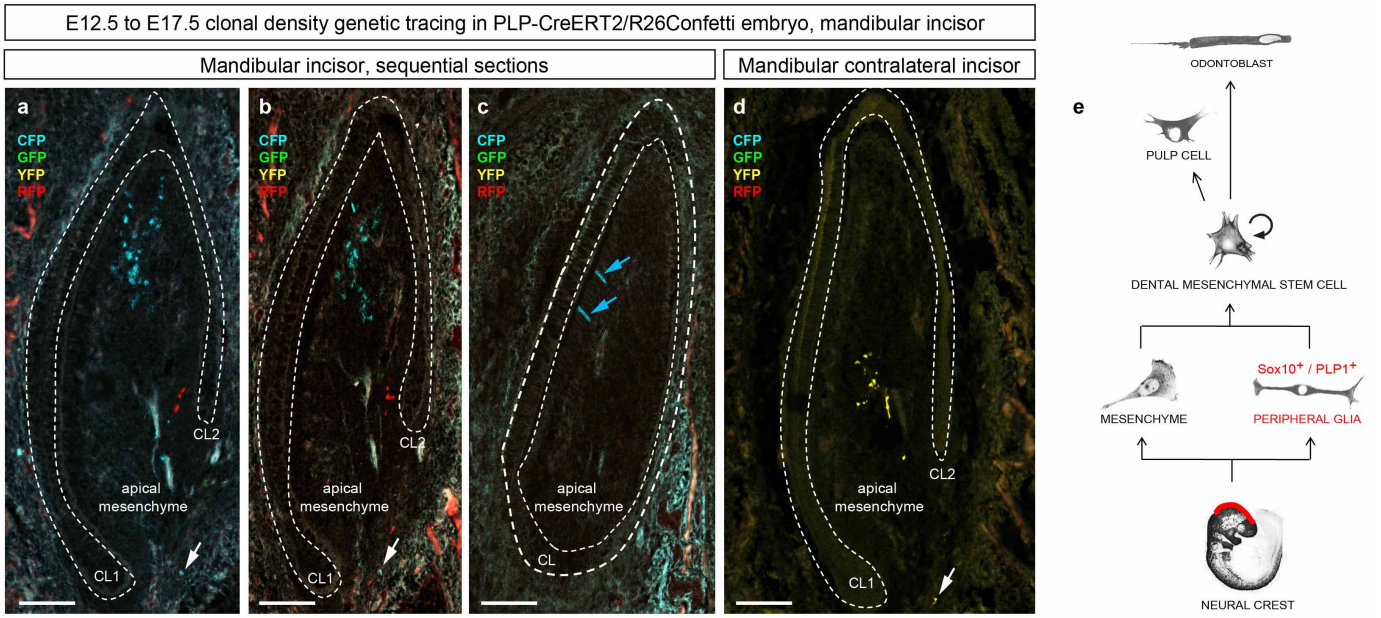

Extended Data Figure 4 | Sub-optimal genetic recombination highlights clonal relationships between pulp cells and odontoblasts during tooth organogenesis. **a**–**c**, Consecutive sections through the incisor from *PLP-CreERT2/R26Confetti* mouse embryo traced from E12.5 to E17.5 (sub-optimal recombination). Note the pulp and odontoblasts progenies of CFP^+ SCPs (white arrows in **a** and **b**). **c**, Section throughout the same tooth where cyan arrows point at columnar CFP^+ odontoblasts. **d**, Section through another clonally traced (sub-optimal recombination) incisor. Note the presence of YFP^+ clone in the pulp. Arrow points at a single YFP^+ cell positioned at the innervation site. **e**, Reconstructed lineage tree of the neural-crest-derived compartment in the tooth. **a**–**d**, Scale bars, 100 μm. CL1 and CL2 are the labial and lingual aspects of the cervical loop respectively.

©2014 Macmillan Publishers Limited. All rights reserved

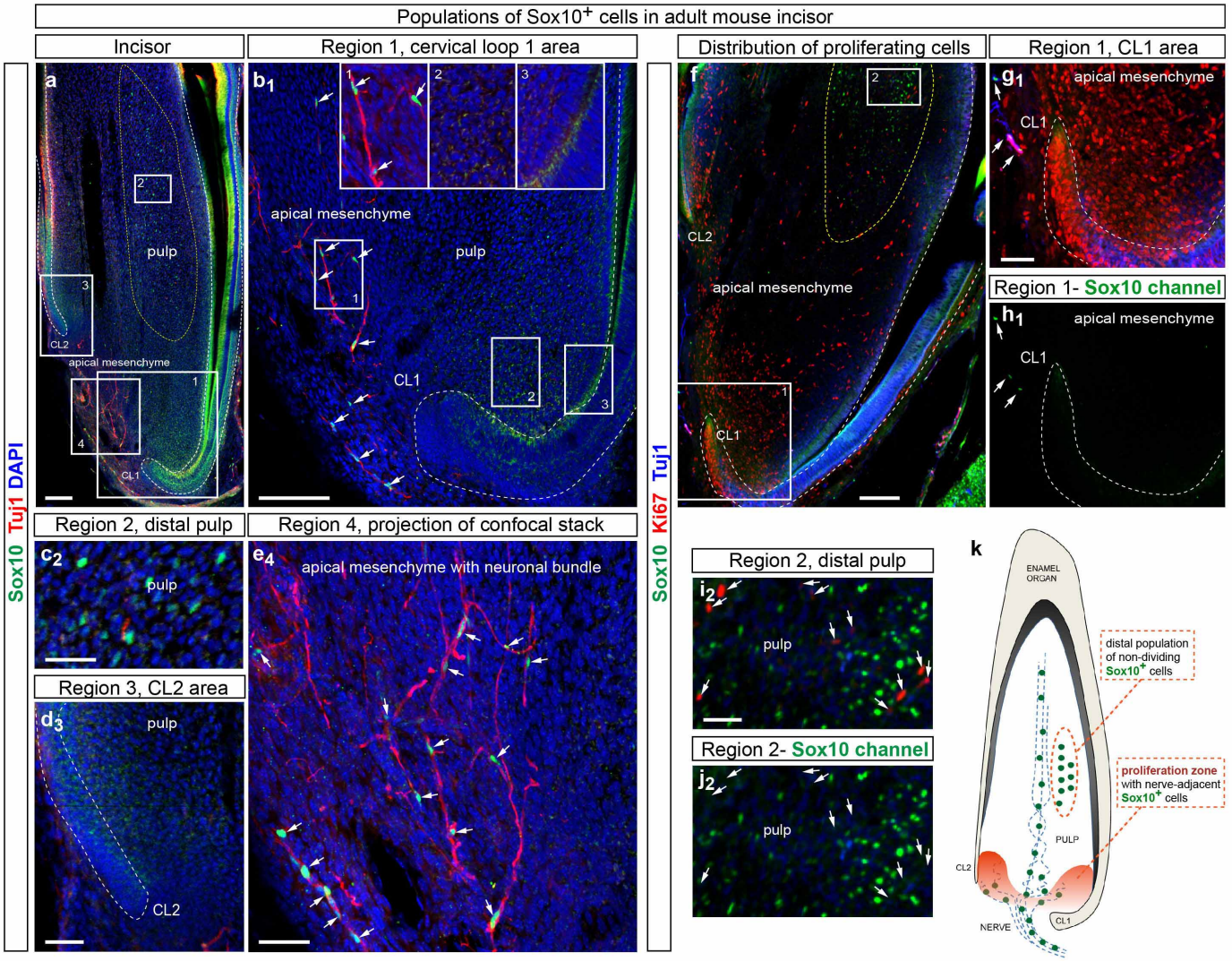

Extended Data Figure 5 | Distribution of Sox10$^+$ cells in adult incisor. **a**, Localization of Sox10$^+$ cells and Tuj1$^+$ nerve fibres in the pulp of adult incisor. Note that apical mesenchyme between the aspects of a cervical loop contains a population of nerve-adjacent Sox10$^+$ cells while the distal pulp harbours an additional population of Sox10$^+$ cells (outlined by a yellow dotted line) that are not adjacent to the nerves. **b**–**e**, Magnified areas from **a** where they are outlined by numbered white rectangles. **b**, Magnified image of apical mesenchyme and cervical loop area with nerve-adjacent Sox10$^+$ cells pointed out by arrows. **c**, Region in the distal pulp showing scattered Sox10$^+$ cells. Note that these cells are not in contact with Tuj1$^+$ fibres. **d**, Cervical loop area including a region of proximal pulp and apical mesenchyme. **e**, Neural bundle in the apical mesenchyme with nerve-adjacent Sox10$^+$ cells pointed out by arrows (projection of a stack). **f**–**k**, Localization of Sox10$^+$ cells in relation to the proliferative growth zone outlined by the expression of Ki67. **g**–**h**, Magnified cervical loop area outlined in **f** by white rectangle 1. Arrows point at detected Sox10$^+$ cells. **i**–**j**, Magnified area shown in **f** by white rectangle 2. Arrows point at Ki67$^+$ cells in the distal pulp. Note that Ki67 does not label the distal population of Sox10$^+$ cells outlined by yellow dotted line in **f**. **k**, Schematic drawing showing two separated populations of Sox10$^+$ cells in the pulp: one population is represented by nerve-adjacent cells and located in proliferative apical mesenchyme while another population is scattered in distal pulp at a significant distance from a cervical loop. Scale bars, 100 µm (**a**, **b**, **f**); 50 µm (**c**–**e**, **g**–**j**). CL1 and CL2 are the labial and lingual aspects of the cervical loop respectively. White dotted line shows enamel organ epithelium.

©2014 Macmillan Publishers Limited. All rights reserved

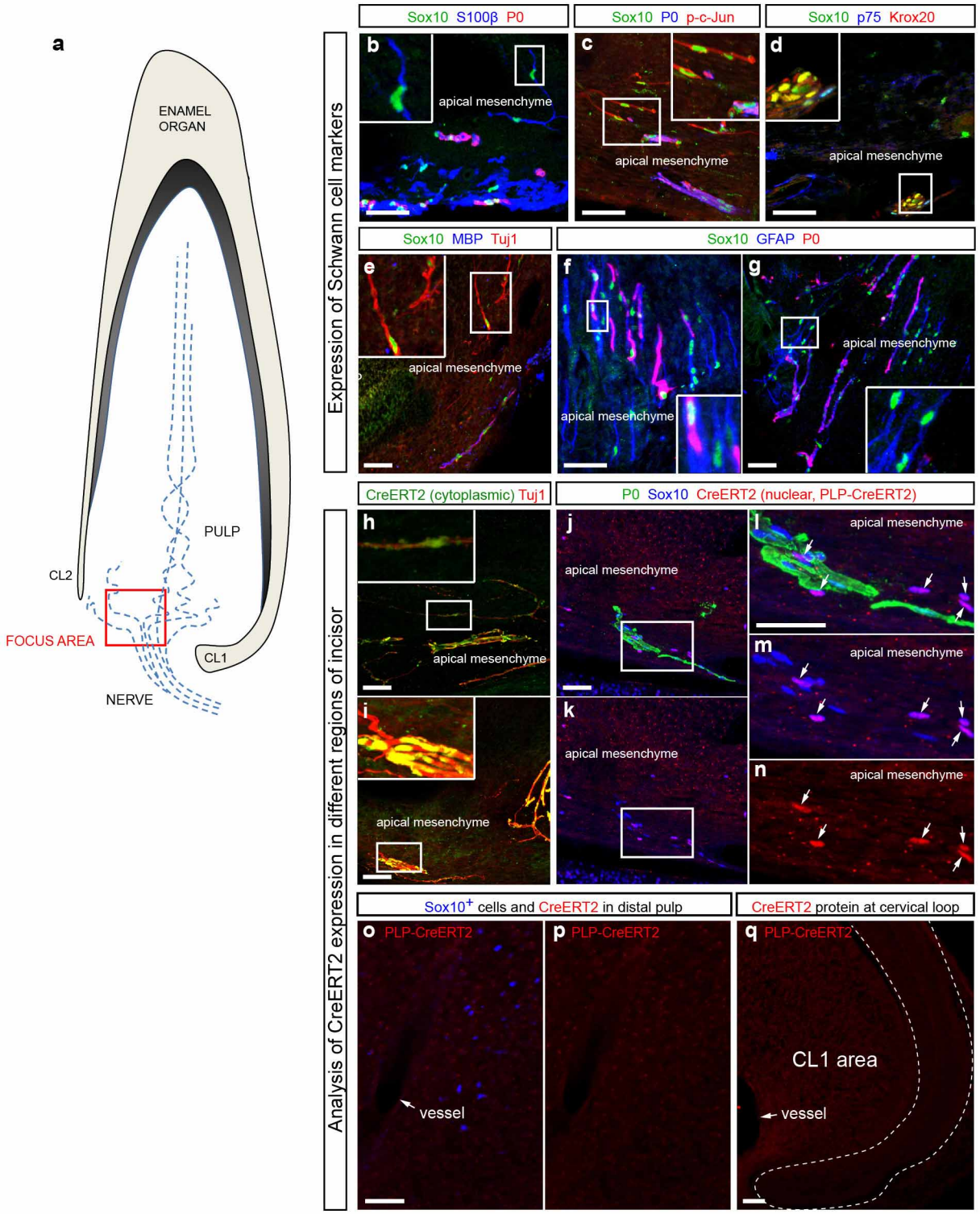

Extended Data Figure 6 | Expression of Schwann cell markers and CreERT2 in adult incisor. **a**, Schematic drawing showing the position of a focus area (red frame) selected for demonstration of Schwann cell markers in **b**–**g**. Schwann cell markers are expressed in Sox10$^+$ nerve-adjacent cells located in apical mesenchyme: S100β and P0 in **b**, P0 and p-c-Jun in **c**, p75 and Krox20 in **d**, MBP in **e** and GFAP and P0 in **f**–**g**. **h**–**q**, Expression of CreERT2 under the control of Sox10- (**o**, **p**) and PLP1- (**q**–**u**) promoters in adult incisor. **h**, **i**, Note that CreERT2 protein is found in cells adjacent to the Tuj1$^+$ nerve fibres in the apical mesenchyme of 30-day traced *Sox10-CreERT2/R26YFP* animals. **j**–**q**, CreERT2 protein is detected in the nuclei of Sox10$^+$ cells (58 ± 7.9% of nerve-adjacent Sox10$^+$ cells are CreERT2$^+$, $n = 5$) in the apical mesenchyme of 20-h traced *PLP-CreERT2/R26YFP* animals. **l**–**n**, Magnified area outlined in **j**, **k**. Arrows point at CreERT2$^+$ nuclei. **o**, **p**, Expression of CreERT2 is not detected in a population of Sox10$^+$ non-glial cells in distal pulp. **q**, Expression of CreERT2 is not found in a cervical loop area. Scale bars, 50 μm. CL1 and CL2 are the labial and lingual aspects of the cervical loop respectively. Dotted line shows enamel organ epithelium.

©2014 Macmillan Publishers Limited. All rights reserved

Two days traced Sox10-CreERT2/R26YFP adult incisor

Five days traced PLP-CreERT2/YFP adult incisor

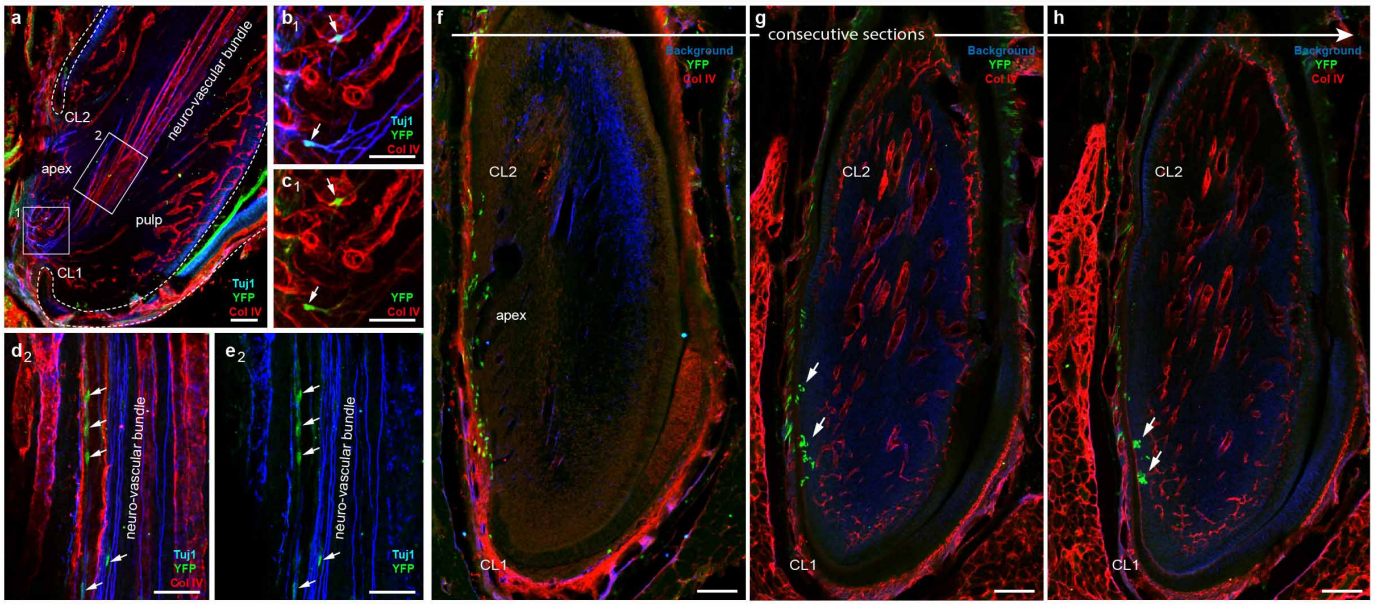

Six months traced PLP-CreERT2/R26YFP adult incisor

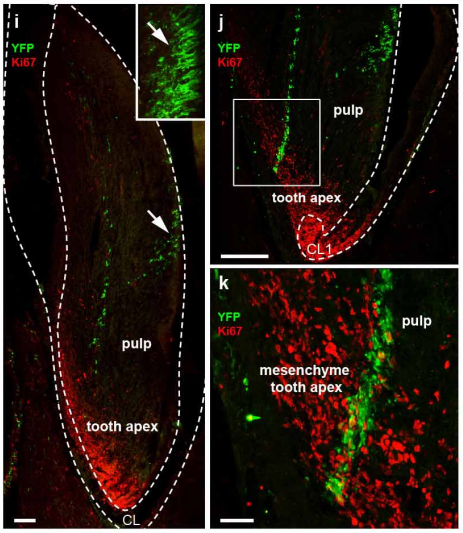

Scheme of tamoxifen injections in PLP-CreERT2/R26YFP animals

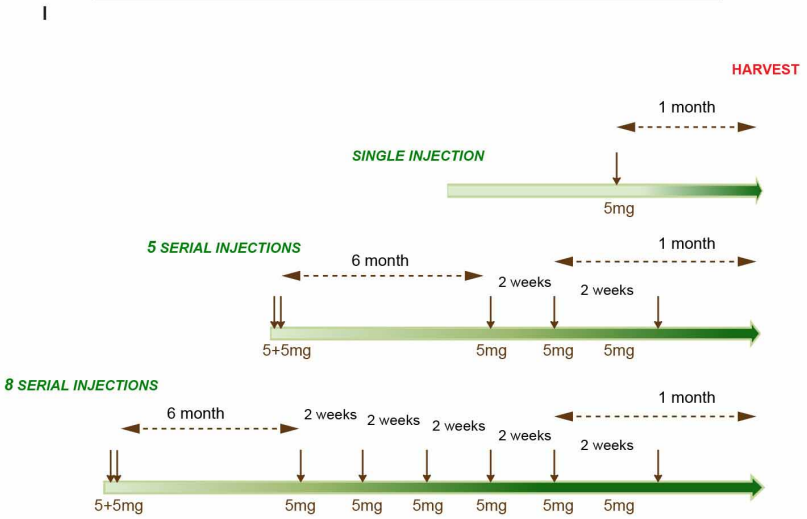

Segmentation of image in IMARIS, PLP-CreERT2/R26YFP incisor, traced ›1 mpi

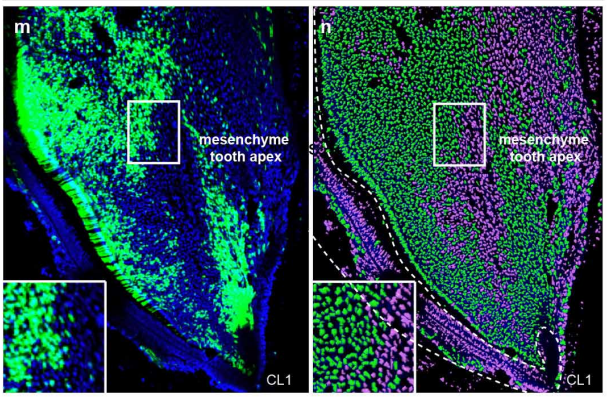

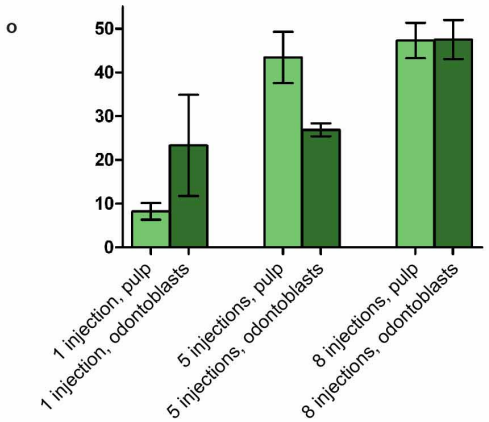

©2014 Macmillan Publishers Limited. All rights reserved

Extended Data Figure 7 | Short and long tracing intervals reveal YFP$^+$ cells at initial positions and uncover the later contribution of Schwann-cell-derived cells to the growing incisor. **a**–**e**, Section through adult incisor traced for 2 days from a *Sox10-CreERT2/R26YFP* mouse stained for collagen IV and Tuj1 to visualize blood vessels and nerves, respectively. **b**, **c**, Magnified area outlined by rectangle 1 in **a**. Arrows point at YFP$^+$ cells adjacent to the innervation of a vascular bundle between cervical loops. **d**, **e**, YFP$^+$ cells (arrows) also appear adjacent to the nerve fibres of vascular bundle distally from cervical loop (position is outlined by rectangle 2 in **a**). Images represent maximum intensity projections of confocal stacks. **e**, **f**, Incisor after 5 days of genetic tracing in a *PLP-CreERT2/R26YFP* animal, sequential sections. Note that YFP$^+$ progeny is located at the apex as indicated by the arrows; YFP$^+$ cells are not detected in the distal pulp. Dotted line outlines enamel epithelium and mineralized matrix. **i**–**k**, Ki67 labelling of a section of an incisor traced for 6 months from an adult *PLP-CreERT2/R26YFP* mouse, single tamoxifen injection at sub-optimal concentration. **i**, Arrows point at a cluster of YFP$^+$ odontoblasts (magnified in inset). Note the presence of YFP$^+$ streams of cells in the pulp after 6 months of genetic tracing. **j**, **k**, YFP$^+$ genetically traced pulp cells are positive for Ki67 only in proximity to the cervical loops. **k**, Magnified area outlined by white rectangle in **j**. Note the absence of Ki67$^+$ cells in the odontoblast layer and in pulp cells at a distance from the cervical loop (CL). **l**, Scheme of genetic tracing experiments involving single and serial tamoxifen injections. **m**, **n**, Segmentation of odontoblast and pulp cell nuclei in the adult genetically traced incisor (**m**) injected eight times with subsequent identification of YFP$^+$ nuclei (**n**) for semi-automated counting in IMARIS. Magnified areas outlined by rectangles are shown in the insets; m.p.i., months post-injection. **i**–**n**, CL1 is a labial cervical loop; dotted line outlines enamel epithelium with adjacent hard matrix. **o**, Contribution of Schwann-cell-derived cells to the incisors from single and multiple injected *PLP-CreERT2/R26YFP* animals ($n = 3$ for each type of experiment). For the quantification of contribution to the odontoblast lineage, only labial odontoblasts were analysed. **a**–**k**, Scale bars, 100 μm (**a**, **f**–**j**); 50 μm (**b**–**e**, **k**); 100 μm (**i**–**j**); 25 μm (**k**). CL1 and CL2 are the labial and lingual aspects of the cervical loop respectively.

©2014 Macmillan Publishers Limited. All rights reserved

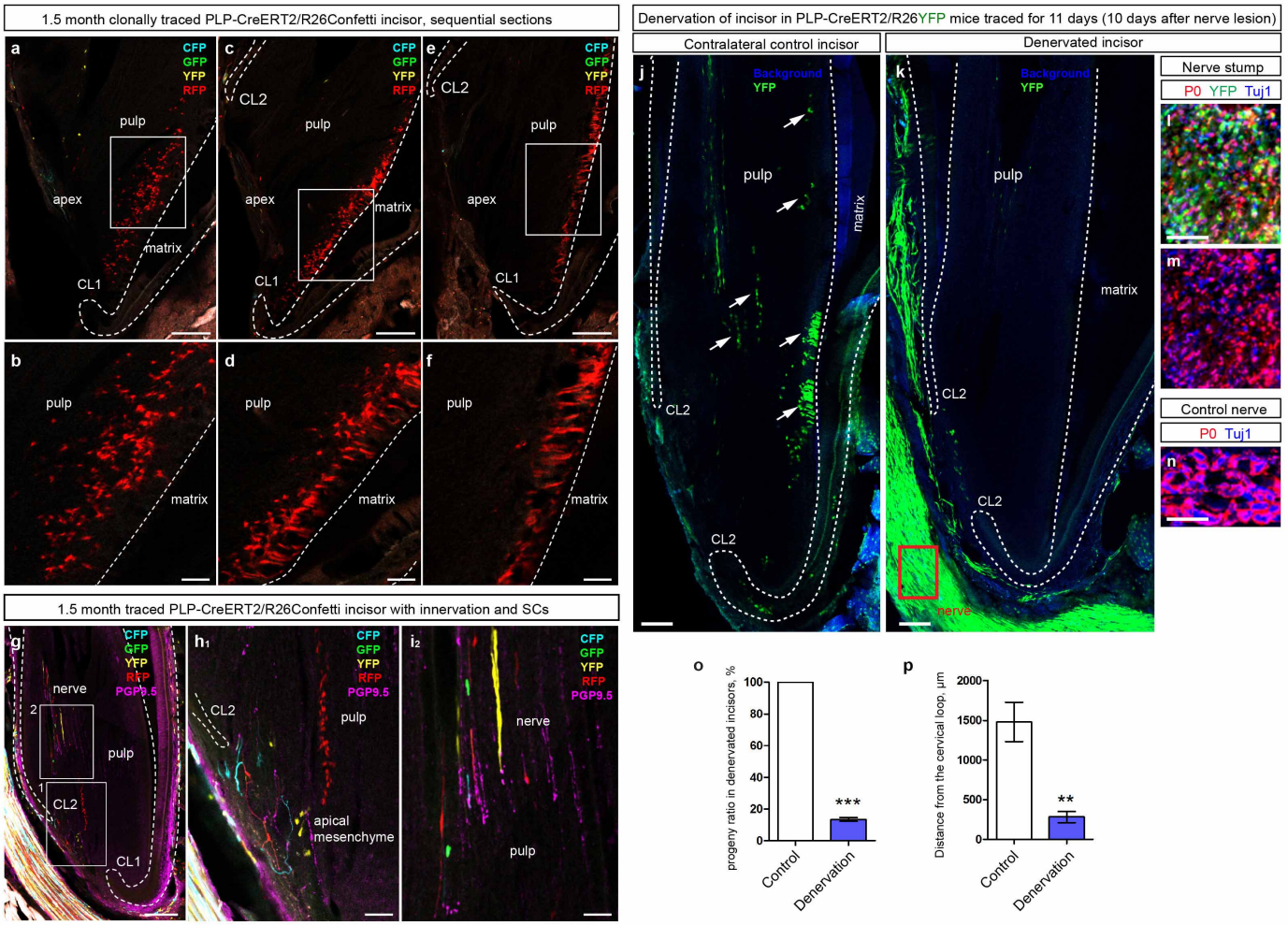

Extended Data Figure 8 | Clonal analysis reveals diversity of progeny originating from different Schwann-cell-derived MSCs that are nerve dependent. **a**–**f**, Consecutive sections of an incisor traced for 1.5 months from a *PLP-CreERT2/R26Confetti* mouse (sub-optimal recombination). **b**, **d**, **f**, Magnified areas from **a**, **c** and **e** respectively. Note numerous dispersed RFP^+ pulp cells in **a**–**d** and large amounts of adjacent RFP^+ odontoblasts in **c**–**f**. **g**–**i**, Another example of an incisor traced for 1.5 months (**g**) from a *PLP-CreERT2/R26Confetti* mouse also stained for PGP9.5 to visualize nerve fibres. **h**, **i**, Magnified areas from **g**. Note the narrow stream of RFP^+ cells in the middle of the dental pulp in **g** and **h**. **j**, **k**, Contralateral control (**j**) and denervated (**k**) incisor teeth 10 days after inferior alveolar nerve transection surgery and 11 days after initiation of genetic tracing by single tamoxifen injection (*PLP-CreERT2/R26YFP* animals). Arrows in **j** point at abundant clusters of YFP^+ odontoblasts and pulp cells. White dotted line indicates enamel organ and hard matrix. **l**–**m**, Wallerian degeneration within the distal stump of the inferior alveolar nerve after the surgery, an area outlined by red rectangle in **k**. **n**, Control nerve. **o**, Quantification of YFP^+ progeny in denervated and contralateral control teeth 10 days after surgery (paired *t*-test $P < 0.0001$, mean difference 86.6; 95% confidence interval 83.58–89.63; $n = 5$). **p**, Quantification of distances between a cervical loop and most distal YFP^+ progeny in control (1,479 ± 246.5 µm) and denervated (282.4 ± 71.52 µm) teeth 10 days after the surgery (unpaired *t*-test $P = 0.0016$, $n = 5$). **a**–**i**, Scale bars, 100 µm (**a**, **c**, **e**, **g**); 25 µm (**b**, **d**, **f**, **h**, **i**); 100 µm (**j**, **k**); 50 µm (**l**–**n**). CL1 and CL2 are the labial and lingual aspects of the cervical loop respectively.

©2014 Macmillan Publishers Limited. All rights reserved

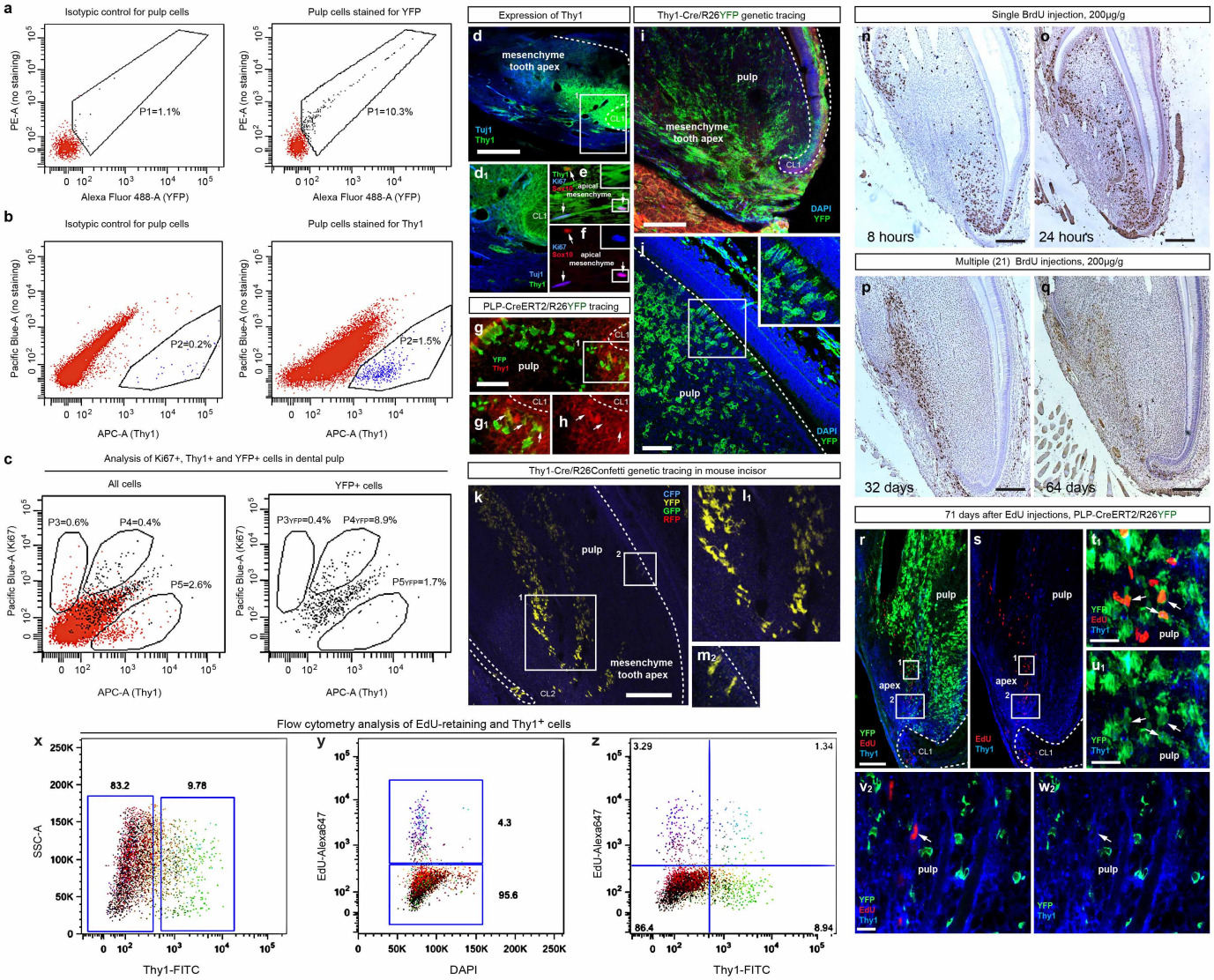

Extended Data Figure 9 | Schwann-cell-derived MSCs express stem cell marker Thy1. **a**–**c**, Flow cytometry analysis of cell populations from dissociated incisor pulp cells. Incisors were isolated from two *PLP-CreERT2/R26YFP* animals that were traced for 5 months after a single tamoxifen injection (5 mg). **a**, Dot plots of isotypic control and immunostaining of non-fixed dissociated pulp cells on the basis of expression of YFP. A region, P1, has been drawn around the YFP^+ cells (also shown in black). **b**, Dot plots of isotypic control and immunostaining of non-fixed dissociated pulp cells on the basis of Thy1 expression. A region, P2, has been drawn around the $Thy1^+$ cells (shown in blue). **c**, Dot plots of selected sub-populations on the basis of expression of proliferative marker Ki67 and Thy1, staining on fixed cells. YFP^+ cells are shown in black. Right panel shows population of YFP^+ cells only. A region, P3, has been drawn around $Thy1^-/Ki67^+$ cells. P4 has been drawn around $Thy1^+/Ki67^+$ cells and P5 around $Thy1^+/Ki67^-$ cells. **d**, $\mathbf{d_1}$, Immunostaining for Thy1 and Tuj1 in an adult incisor. $\mathbf{d_1}$ Magnified area outlined by white rectangle in **d**. **e**, **f**, Ki67, Sox10 and Thy1 in dental MSC niche between labial and lingual aspects of a cervical loop. Arrows point at $Sox10^+$ nuclei of Schwann cells. Note that some Schwann cells are $Ki67^+$. Inset in **e** shows only the Thy1 staining channel from area outlined by white rectangle; inset in **f** shows only the Ki67 staining channel from the same area. **g**–**h**, Incisor from a *PLP-CreERT2/R26YFP* mouse genetically traced for 8 months. Note $Thy1^+/YFP^+$ cells located proximally to the cervical loop CL1 in the low-magnification image (**g**) and indicated by arrows in magnified images ($\mathbf{g_1}$–**h**). Magnified area is highlighted by white rectangle in **g**. **i**, **j**, Genetically traced incisor from a *Thy1-Cre/R26YFP* mouse. Note abundant progeny in the pulp (**i**, **j**) and odontoblast layer specifically shown in inset in **j**. **k**–$\mathbf{m_2}$, Genetically traced incisor from a *Thy1-Cre/R26Confetti* mouse. Note streams of YFP^+ cells in the pulp (**k**–$\mathbf{l_1}$) and a few odontoblasts ($\mathbf{m_2}$). $\mathbf{l_1}$, $\mathbf{m_2}$, Magnified area outlined by white rectangle in **k**. Dotted line marks enamel epithelium and mineralized matrix. **n**–**q**, BrdU incorporation analysis of fast and slowly cycling cells in the incisor. **r**, **s**, EdU^+ slowly cycling cells 71 days after the last EdU injection in Thy1-stained and genetically traced incisor (9 months after last tamoxifen injection). $\mathbf{t_1}$, $\mathbf{u_1}$, Magnified area from **r** and **s** outlined by white rectangle 1. EdU^+/YFP^+ cells are marked by arrows. Note numerous EdU^+ cells in the $Thy1^+$ zone proximal to the cervical loop (CL1) in **s**. $\mathbf{v_2}$, $\mathbf{w_2}$, Magnified area from **r** and **s** outlined by white rectangle 2. Arrows indicate $Thy1^+/EdU^+$ cell. **x**–**z**, Flow cytometry analysis of EdU-retaining (21 days after last the injection) and $Thy1^+$ cells from dental pulp. **x**, Dot plot showing the gating for Thy1-expressing cells. **y**, Dot plot showing the gating of EdU^+ cells among total $DAPI^+$ population. Note that EdU^+ cells represent 4.3% of total cell numbers. **z**, Dot plot of subpopulations on the basis of expression of Thy1 and incorporation of EdU. $EdU^+/Thy1^+$ cells are in the upper right square, constituting 1.34% of total population. Scale bars, 100 μm (**d**, **i**, **k**); 50 μm (**g**, **j**); 100 μm (**n**–**s**); 25 μm ($\mathbf{t_1}$–$\mathbf{w_2}$). CL1 and CL2 are the labial and lingual aspects of the cervical loop respectively.

©2014 Macmillan Publishers Limited. All rights reserved

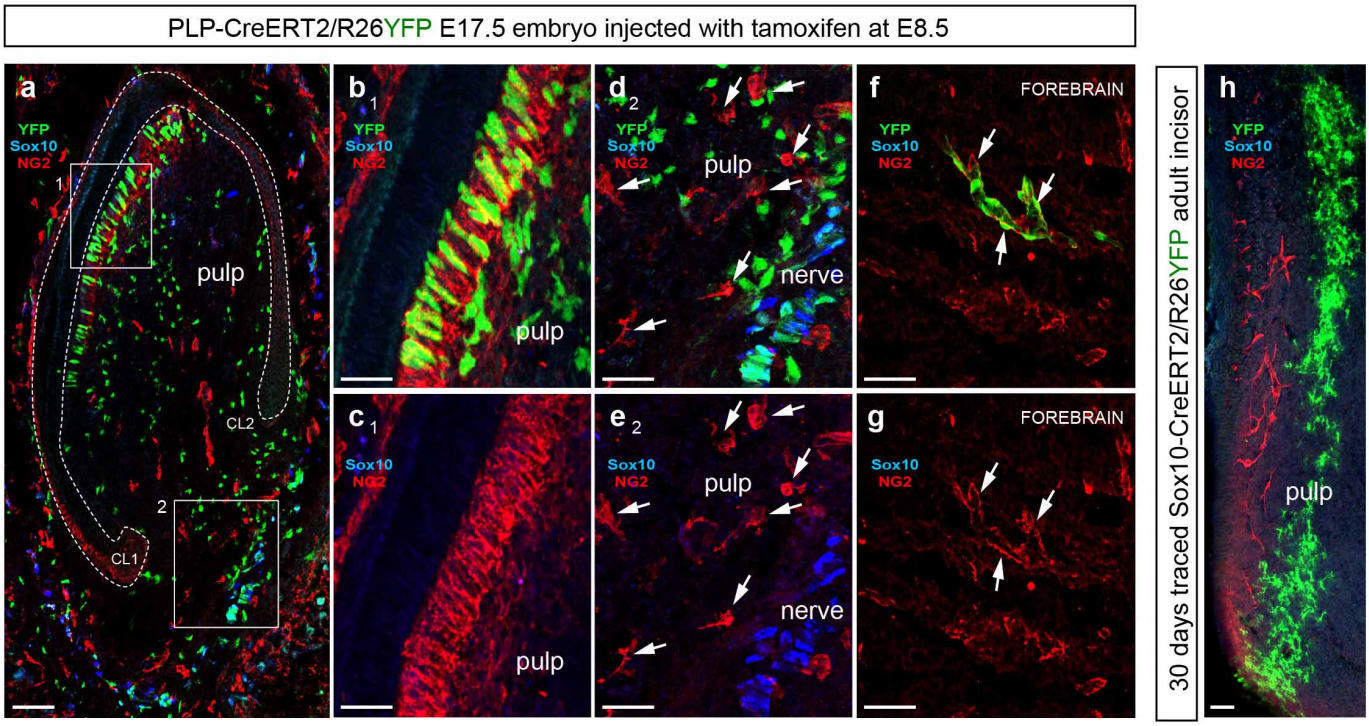

Extended Data Figure 10 | Populations of pericytes and glia-derived cells do not overlap in the tooth. **a**–**e**, Sox10 and NG2 immunohistochemistry on a section of mandibular incisor from a *PLP-CreERT2/R26YFP* embryo genetically traced from E8.5 to E17.5. **a**, Dotted line outlines enamel organ. **b**, **c**, and **d**, **e**, Magnified areas from **a** outlined by white rectangles. Arrows in **d**, **e** show $NG2^+/YFP^-$ pericytes. **f**, **g**, $YFP^+/NG2^+$ pericytes (arrows) in the forebrain of an E8.5 to E17.5 genetically traced *PLP-CreERT2/R26YFP* embryo. **h**, Immunohistochemistry with Sox10 and NG2 antibodies on a section of mandibular incisor traced for 30 days in a *PLP-CreERT2/R26YFP* adult mouse. Note the stream of $YFP^+/NG2^-$ cells in the pulp of the incisor and numerous $YFP^-/NG2^+$ pericytes on the same section. **a**–**h**, Scale bars, 50 μm (**a**); 25 μm (**b**–**h**). CL1 and CL2 are the labial and lingual aspects of the cervical loop respectively.

©2014 Macmillan Publishers Limited. All rights reserved